Doctoral theses at NTNU, 2019:336

Thanh Pierre Doan

Extrinsic connectivity of principal neurons in layer II of the entorhinal cortex

Doctoral thesis

Thanh Pierre Doan

ISBN 978-82-326-4330-1 (printed ver.)
ISBN 978-82-326-4331-8 (electronic ver.)
ISSN 1503-8181

NTNU
Norwegian University of
Science and Technology

NTNU
Norwegian University of Science and Technology
Thesis for the Degree of
Philosophiae Doctor
Faculty of Medicine and Health Sciences
Kavli Institute for Systems Neuroscience

Doctoral theses at NTNU, 2019:2019:336

NTNU
Norwegian University of
Science and Technology

Thanh Pierre Doan

Extrinsic connectivity of principal neurons in layer II of the entorhinal cortex

Thesis for the Degree of Philosophiae Doctor

Trondheim, December 2019

Norwegian University of Science and Technology
Faculty of Medicine and Health Sciences
Kavli Institute for Systems Neuroscience

NTNU
Norwegian University of
Science and Technology

NTNU
Norwegian University of Science and Technology

Thesis for the Degree of Philosophiae Doctor

Faculty of Medicine and Health Sciences
Kavli Institute for Systems Neuroscience

ISBN 978-82-326-4330-1 (printed ver.)
ISBN 978-82-326-4331-8 (electronic ver.)
ISSN 1503-8181

Doctoral theses at NTNU, 2019:336

Printed by NTNU Grafisk senter

Ekstrinsik konnektivitet av prinsipielle nevroner i lag II av entorhinal korteks

Episodisk hukommelse dreier seg om enkelthendelser (i.e. enkle episoder som befinner seg i bestemte tid og sted) og er avhengig av hjernestrukturer som ligger i medial temporallappen. Medial temporallappen inneholder hippocampus og parahippocampale regionen som består av perirhinal, parahippocampal samt lateral og medial entorhinal korteks. Den nåværende modellen av hukommelsessystemet i medial temporallappen hevder at to funksjonelle forskjellige nervebaner går inn i parahippocampal regionen som parallelle 'romlige' parahippocampal - mediale entorhinal ('hvor') og 'ikke-romlige' perirhinal - lateral entorhinal ('hva') strømninger. Begge nervebaner konvergerer innenfor hippocampus som samler etter hvert disse to komplementære informasjoner ('hvor' og 'hva') til en enkel minneopplevelse.

I denne avhandlingen starter vi med å oppsummere publisert litteratur for å legge vekt på integrering av disse strømningene på tvers av parahippocampal regionen. Videre utfordrer vi den rådende modellen sitt anatomisk kjerneprinsipp ved å skaffe gnagerdata som viser at postrhinal korteks (homolog til primat parahippocampal korteks) er først og fremst forbundet med lateral, fremfor medial, entorhinal korteks. Deretter argumenterer vi for at en lignende organisasjon også gjelder i primathjernen. Til sammen peker dette på at lateral entorhinal korteks er den enheten i parahippocampale regionen som mottar mest mangfoldig sensorisk informasjon. Vi tar dette videre på enkeltcelle-nivå med å vise frem at informasjon fra et utvalg av kortikale områder som er forbundet med lateral entorhinal korteks, dvs. medial entorhinal, perirhinal, piriform og kontralateral lateral entorhinal korteks, konvergerer i enkeltceller i lag II som er koblet til hippocampus. Disse nervecellene er lokalisert i lag II sammen med nerveceller som uttrykker calbindin. Vi demonstrerer at disse calbindin-positive nerveceller har forgreininger hovedsakelig innad i entorhinal korteks, men er også forbundet til nerveceller i flere områder av hippocampus og telencephalon.

Til slutt argumenterer vi for at en omvurdering av den rådende modellen er nødvendig og at det er passende å betrakte entorhinal korteks som et funksjonelt kontinuum, hvor dets funksjonelle egenskaper hovedsakelig reflekterer den kombinerte informasjonen som mottas fra andre hjerneområder. Til slutt påpeker vi at konseptet med to funksjonelle distinkte

inndelinger av entorhinal korteks angivelig stammer fra selektiviteten av en liten nabostruktur som heter presubiculum, og fremhever noen bemerkelsesverdige funksjoner av det entorhinale nettverket for å legge grunnlag til en ny modell av episodisk hukommelsessystemet vårt.

Navn kandidat: Thanh P. Doan
Institutt: Kavli Institute for Systems Neuroscience / Centre for Neural Computation
Veileder: Prof. Menno P. Witter
Finansieringskilde: Fakultet for medisin og helsevitenskap NTNU, Forskningsrådet, Kavlistiftelsen

Ovennevnte avhandling er funnet verdig til å forsvares offentlig for graden PhD i Nevrovitenskap
Disputas finner sted i audoritoriet KA12 Kunnskapssenteret, St. Olavs Hospital
Onsdag 11. desember 2019, kl.12.15

Contents

- III. Convergence of cortical inputs to layer II neurons in lateral entorhinal cortex.
- IV. Entorhinal layer II calbindin-expressing neurons originate widespread telencephalic and intrinsic projections.

Acknowledgement

First of all, I would like to express my gratitude to my supervisor Menno Witter for his outstanding supervision, incredible availability and never-ending support in my scientific and clinical aspirations. It has been an immense privilege to learn with him about the beauty and complexity of neuroanatomy from the depths of the medial temporal lobe.

I would also like to thank all my colleagues from the Witter lab, Kavli Institute for Systems Neuroscience and NTNU who made this journey possible, in particular my co-authors Maria Jose Lagartos, Eirik Nilssen, Shinya Ohara and Max Nigro but also Bente Jacobsen and Asgeir Kobro-Flatmoen for stimulating discussions and constructive feedbacks. I am also grateful for extraordinary technical assistance from Grethe Olsen, Hanne Soligard, Bruno Monterotti and Paulo Girao. Jørgen Sugar also deserves a special mention for his scientific dedication, humility and patience to all my ludicrous questions.

Thanks also to my colleagues at St.Olavs hospital who offered me enough flexibility to do my first clinical steps while still intensely working in the lab.

It should also be emphasized that this adventure would not have been possible without the unconditional support from my loving family and dear Andrea.

At last, a particular thought to honor the memory of laboratory rodents, whose invaluable sacrifice make them the true heroes in our quest to understand the mammalian brain.

Preface

The basis for this research originally stemmed in a genuine desire to gain knowledge in fundamental science which represents the invisible bulk part of an iceberg whereas medicine constitutes its emerged tip. With an early interest for the brain, undeniably the most complex and fascinating organ of the human body, pursuing a PhD in functional neuroanatomy after medical school offered a most ideal combination to study how concrete structures and abstract functions relate. Neurons form structural and functional networks which underpin all physiological and pathological nervous system processes. The powerful interdisciplinary approach of Systems Neuroscience bringing together functional anatomy, computation science, genetics and electrophysiology into the study of networks offer the possibility to glance above today's clinical walls that segregate nervous system dysfunctions into neurological, psychiatric or neurosurgical conditions.

In order to illustrate the importance of neural networks, I invite you to take a look at the checkerboard on the next page (**fig.1**) for you to determine which one of the two squares marked "A" and "B" appears darker before proceeding further.

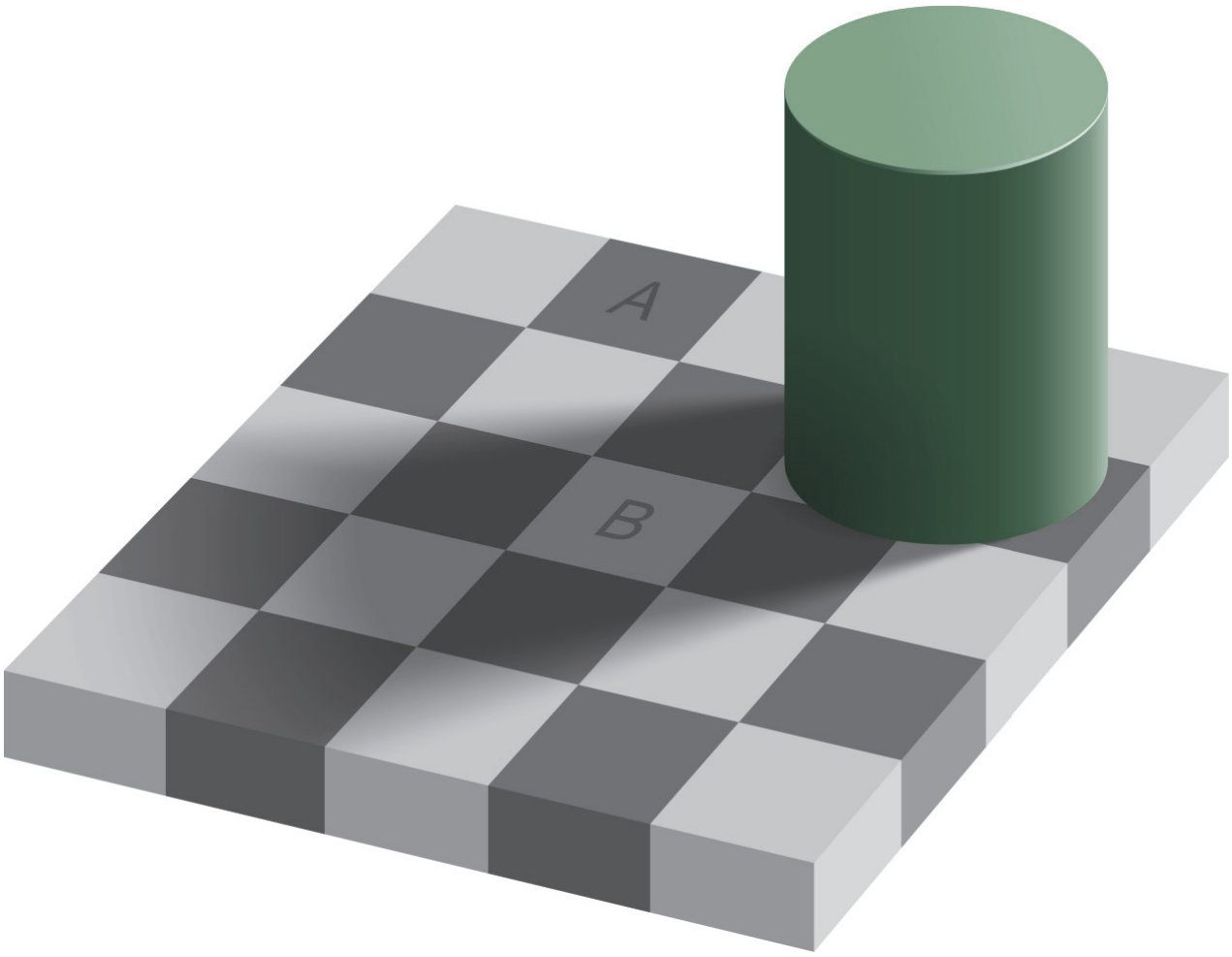

Figure 1. Checker shadow illusion. Courtesy of Edward H. Adelson (1995).

Indeed, the “A” square appears darker than the “B” one. Nevertheless, both squares contain exactly the same shade of grey. You can easily appreciate this by covering the space between these two squares with an opaque item.

How come do we perceive squares “A” and “B” differently then?

This can be explained by the functional organization of the neurons forming the entry point of our visual system, i.e. the retina. When a discrete light stimulus hits neighboring photoreceptors cells in our retina, their connectivity dominated by “lateral inhibition” governs the network such that the ones located at the center of the stimulus will inhibit their neighboring cells. Consequently, the photoreceptors in the center of the light stimulus will transduce a “lighter” signal to the brain, whereas their immediate neighboring cells on the edge of the stimulus will send a “darker” one. This simple universal connectivity pattern increases in fact the contrast and sharpness in neuronal tuning response at many levels of our brain. The present case demonstrates how we can be tricked even at the very first level of stimulus processing and how essential it is to decipher these mechanistic principles if we intend to appreciate the complexity of higher cognitive processes. Functional Neuroanatomy aims to dissect neuronal circuits and understand wiring patterns at any level of the nervous system.

In this thesis, we will take a look at the functional neuroanatomy of the medial temporal lobe (MTL) system which mediates encoding of our personal episodic memory. Among other structures, MTL contains the entorhinal cortex and hippocampus which are high hierarchical cortical areas located many synapses away from our primary sensory organs (**fig. 10**, p.34).

Studying the functional connectivity of the entorhinal cortex, i.e. the nodal point between our senses and the hippocampus where autobiographical memories are formed, offers a glimpse to the fundamental biophysical processes that have shaped our culture throughout the millenia and the very essence of what makes us humans.

Summary

The current model of the medial temporal lobe memory system assumes that two functionally different pathways enter the parahippocampal region as parallel spatial parahippocampal/postrhinal – medial entorhinal ('where') and non-spatial perirhinal – lateral entorhinal ('what') streams that eventually converge within the hippocampus which assembles these complementary information into a memory experience.

In the present thesis, we start by reviewing published literature to emphasize integration of these streams within the parahippocampal region and suggest elements for an alternative model. We further explore the anatomical core principle of the prevailing model by providing rodent data demonstrating that postrhinal cortex (homologous to primate parahippocampal cortex) projects in fact primarily to the lateral, instead of medial, entorhinal cortex. We further argue that a similar organization likely exists in the primate brain pointing to lateral entorhinal cortex as the main multisensory integrative unit of the parahippocampal region. Next, we show that a subset of cortical inputs to lateral entorhinal cortex, i.e. medial entorhinal, perirhinal, piriform and commissural lateral entorhinal cortices, converge at the level of single cells in layer II which project to the hippocampus. Moreover, we study the connectivity of the other main type of entorhinal layer II principal neurons, i.e. the immunochemical calbindin positive cells, which primarily participate to dense intrinsic entorhinal connectivity but also emit projections to hippocampal and telencephalic areas.

At last, we argue that a reappraisal of the prevailing model is necessary and might well benefit of considering the entorhinal cortex as a generalist circuit organized as a functional continuum whose output signal depends primarily on its extrinsic inputs. Finally, we point out that the concept of two functionally distinct entorhinal subdivisions comes from the presubiculum input selectivity and finish by emphasizing certain remarkable features of the overall entorhinal network to lay ground for prospective studies.

Abbreviations

- A35 – area 35 (i.e. ventral perirhinal cortex)
- A36 – area 36 (i.e. dorsal perirhinal cortex)
- AG – Anterograde
- ATN – Anterior thalamic nuclei
- (r)AAV – (recombinant) Adeno associated virus
- (B)DA – (Biotinylated) Dextran amine
- CA – Cornu ammonis field
- ChR2 – Channelrhodopsin-2
- Cb – Calbindin
- CE – Caudal entorhinal area (MEC subdivision)
- CS – Collateral sulcus
- CTB – Cholera toxin subunit B
- DIE – Dorsal intermediate entorhinal area (LEC subdivision)
- DLE – Dorsolateral entorhinal area (LEC subdivision)
- DG – Dentate gyrus
- e.g. – for example *("exampli gratia")*
- EC – Entorhinal cortex
- EPSPs – excitatory postsynaptic potential(s)
- IPSPs – inhibitory postsynaptic potential(s)
- FB – Fast blue
- FG - Flurogold
- GABA – Gamma aminobutyric acid
- HD – Head direction
- HF – Hippocampal formation
- i.e. – that is *("id est")*
- IN – Interneuron
- ME – Medial entorhinal area (MEC subdivision)
- MEC – Medial entorhinal cortex
- L - Layer

- (c)LEC – (commissural) Lateral entorhinal cortex
- PaS – Parasubiculum
- PER – Perirhinal cortex
- PHA-L – Phaseolus vulgaris lectin
- PHC – Parahippocampal cortex
- PHR – Parahippocampal region
- p – postpartum age (in days)
- POR – Postrhinal cortex
- PORd – dorsal postrhinal cortex
- PORv – ventral postrhinal cortex
- PrS – Presubiculum
- PV - Parvalbumin
- Re – Reelin
- RF – Rhinal fissure
- RG - Retrograde
- RSC – Retrosplenial cortex
- SOM – Somatostatin
- TTX - Tetrodotoxin
- Sub – Subiculum
- VIE - Ventral intermediate entorhinal area (LEC subdivision)
- WHS – Waxholm space

List of Articles

Article I

Neurons & Networks in the Entorhinal Cortex: A reappraisal of the lateral and medial entorhinal subdivisions mediating parallel cortical pathways.

Eirik S. Nilssen, Thanh P. Doan, Maximiliano J. Nigro, Shinya Ohara and Menno P. Witter.

Hippocampus, 2019 Aug 13. doi: 10.1002/hipo.23145.

Article II

Convergent projections from perirhinal and postrhinal cortices suggest a multisensory nature of lateral but not medial entorhinal cortex.

Thanh P. Doan, Maria J. Donate Lagartos, Eirik S. Nilssen, Shinya Ohara and Menno P. Witter.

Cell reports, 2019 Oct 15;29(3):617-627.e7. doi: 10.1016/j.celrep.2019.09.005.

Article III

Convergence of cortical inputs to layer II neurons in lateral entorhinal cortex.

Eirik S. Nilssen, Thanh P. Doan and Menno P. Witter.

Manuscript.

Article IV

Entorhinal layer II calbindin-expressing neurons originate widespread telencephalic and intrinsic projections.

Shinya Ohara, Michele Gianatti, K. Itou, Christin Berndtsson, Thanh P. Doan, Takuma Kitanishi, Kenji Mizuseki, Toshio Iijima, Ken-Ishiro Tsutsui, Menno P. Witter.

Frontiers in Systems Neuroscience, 2019 Oct 15;13:54. doi: 10.3389/fnsys.2019.00054.

1. Introduction

Learning and memory are essential attributes for an individual to develop skills and knowledge in order to adapt to any new environment. Memory can be divided into non-declarative (implicit) processes such as procedural memory and habit formation as well as declarative (explicit) processes such as semantic and episodic memory, all depending on distinct brain structures. Episodic memory is the memory for autobiographical events, i.e. collection of past personal experiences that occurred at a particular time and place, and heavily depends on the hippocampus and surrounding medial temporal lobe (MTL).
Initial insights about localization came in the early 1950s following the study of patient H.M. today known as Henry Molaison (1926-2008), who developed total anterograde amnesia following surgical bilateral ablation of his rostromedial temporal lobes in a desperate attempt to treat his refractory epilepsy. The resection included a large part of the hippocampal formation (HF) and surrounding parahippocampal region (PHR) enclosing the entorhinal cortex (EC) among other structures [1-3]. Initially, HF crystallized most attention in light of discoveries of long-term potentiation [4] and spatially modulated 'place cells' [5] culminating into the very influential theory of hippocampal 'cognitive map' [6]. However, PHR eventually received comparable attention in view of the unique nodal connectional position of EC between HF and all major cortical areas in addition to the presence of multiple spatially modulated cells [7]. Cortical information enters MTL by way of PHR before it gets further forwarded by EC to HF across a clear neuroanatomical axis. Today, it is well established that the MTL memory system and its PHR-HF axis contains the neural substrates necessary for episodic memory processes formation.

1.1 General organization of the medial temporal lobe memory system

The PHR and HF are brain structures well-conserved across the entire mammalian kingdom with comparable cytoarchitectural, chemoarchitectural and hodological characteristics [8]. These structures are located caudally in the rodent forebrain, and progressively move ventrally and medially following the process of phylogenetic encephalization resulting in their medial position within the temporal lobe of the primate (**fig.2**) [9].

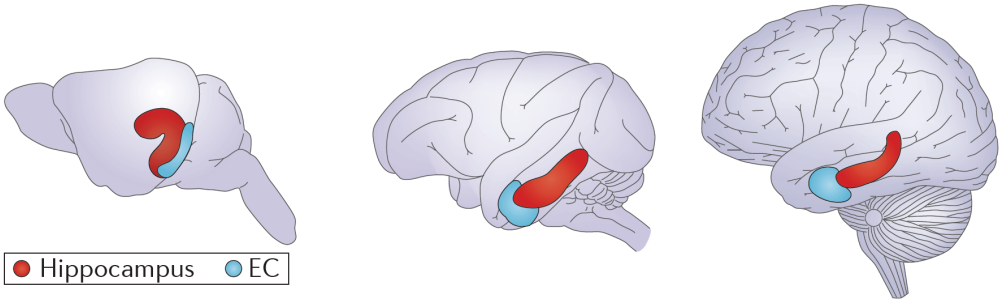

Figure 2. The full long axis of the hippocampal formation (HF, red) can be seen in brains of rats, monkeys and humans from left to right, with the entorhinal cortex (EC, blue). From Strange et al., 2014 [9].

The hippocampus long and curved form is present across all mammalian orders and runs along a posteroanterior axis in primates. In the rodent, HF long axis extends from the rostral septal nuclei of the basal forebrain, stretches dorsally and caudally over the diencephalon, into the caudoventral portion of the hemisphere abutting the adjacent amygdaloid complex and is thus referred as the septotemporal axis (**fig.2-4**).

HF is a three-layered cortex composed of the dentate gyrus (DG) and hippocampus proper which is further divided into Cornu Ammonis fields (CA1, CA2 and CA3) and Subiculum (Sub). PHR is a six-layered cortical mantle wrapping HF comprising not only EC, but also presubiculum (PrS) and parasubiculum (PaS) as well as entorhinal (EC), perirhinal (PER) and postrhinal cortices (POR; homologous to the primate parahippocampal cortex PHC) [10]. EC is divided into lateral (LEC) and medial (MEC) subdivisions and POR and PER are divided into dorsal (PORd and A36 respectively) and ventral (PORv and A35 respectively) parts (**fig.3-4**) [11-14].

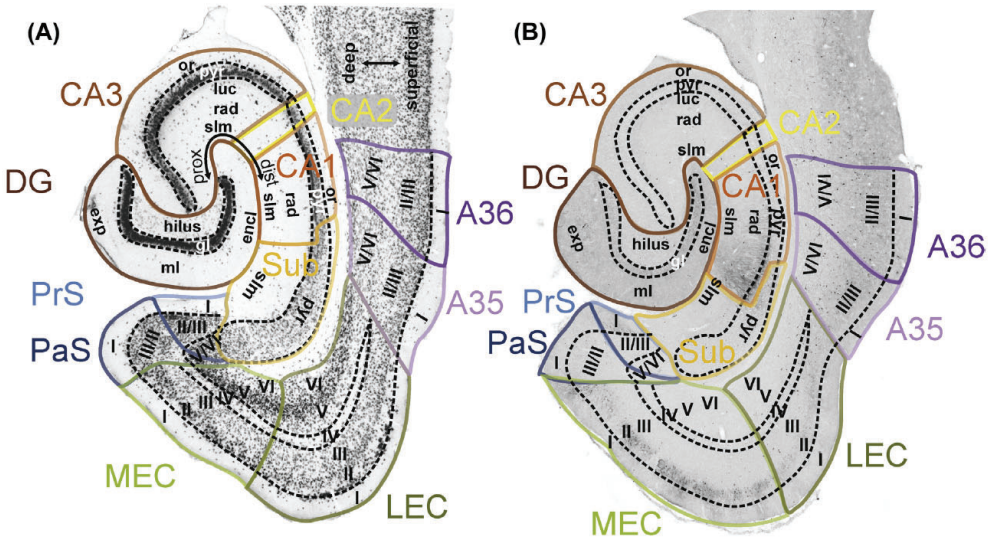

Figure 3. NeuN-stained (A) and calbindin-stained (B) adjacent horizontal sections illustrating histological features of the dentate gyrus (DG; dark brown), CA3 (medium brown), CA2 (yellow), CA1 (orange) and the subiculum (Sub; yellow), the presubiculum (PrS; medium blue), parasubiculum (PaS; dark blue), lateral entorhinal cortex (LEC; dark green), medial entorhinal cortex (MEC; light green) and perirhinal cortex areas 35 (A35; pink) and area 36 (A36; purple). The cortical layers (indicated by Roman numerals). CA, cornu ammonis; dist, distal; encl, enclosed blade of the DG; exp, exposed blade of the DG; gl, granule cell layer; luc, stratum lucidum; ml, molecular layer; or, stratum oriens; prox, proximal; pyr, pyramidal cell layer; rad, stratum radiatum; slm, stratum lacunosum-moleculare. With permission from Cappaert et al., 2015 [14].

In rodents, MEC and LEC have been further subdivided into areas CE and ME in MEC and areas DLE, DIE and VIE in LEC, according to subtle cytoarchitectural and hodological criteria related to monkey EC subdivisions (**fig.4**) [11, 15, 16].

EC constitutes the major cortico-hippocampal nodal point since it receives a myriad of inputs from almost all cortical as well as many subcortical areas and projects in turn massively to the entire longitudinal extent of HF with a clear topology, i.e., dorsolateral EC projects predominantly to septal HF whereas more ventral and medial entorhinal parts gradually project toward more temporal levels of HF (**fig.5**) [14, 17, 18].

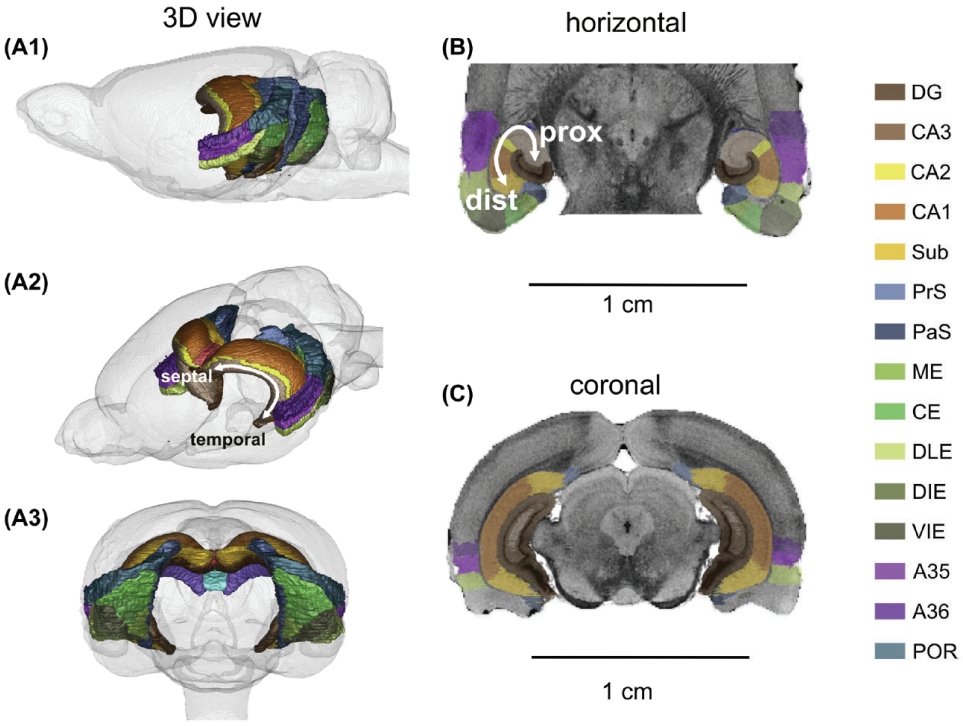

Figure 4. The position of the rat hippocampal formation (HF) and parahippocampal region (PHR). Left column: The Waxholm Rat Brain [19, 20]in a lateral (A1), rostro-dorsolateral (A2) and caudal (A3) view, showing the structures of the HF and PHR inside. The middle column provides examples of horizontal (B) and coronal (C) sections. Sections are taken from the online NeuN atlas (www.rbwb.org) and a color-coded segmentation of the HF and PHR is overlayed [13]. With permission from Cappaert et al., 2015 [14].

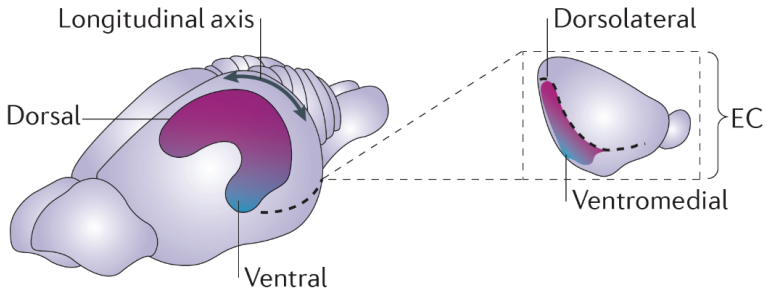

Figure 5. Topographical arrangement of entorhinal–hippocampal connections in rodents. A dorsolateral band of the entorhinal cortex (EC) (magenta) is preferentially connected to the septal/dorsal hippocampus. Increasingly more ventral and medial bands of the EC (purple to blue) are connected to increasingly more ventral levels of the hippocampus. With permission from Strange et al., 2014 [9].

A simplified, yet conceptually important model of the overall PHR-HF intrinsic connectivity relies on its articulation around a relatively unidirectional 'trisynaptic pathway' with superficial EC projecting to DG (i.e. part of the perforant path as EC axons "perforate" Sub on their way to DG), DG to CA3 (i.e. mossy fibers) and CA3 to CA1 (i.e. Schaffer collaterals) (**fig.6**). Nevertheless, one should add an important level of complexity since superficial layers of MEC and LEC project to all fields of HF with clear patterns. In rodents, layer II neurons in LEC project to the outer one-third of the molecular layer of DG and CA3 stratum lacunosum-moleculare and the ones in MEC project to the middle one-third of these layers (**fig.3**). Layer III neurons in LEC project to the CA1/Sub border whereas the ones in MEC project to proximal CA1 and distal Sub [14]. These projections originating from superficial LEC and MEC are collectively called lateral and medial perforant paths respectively. Following intrinsic hippocampal processing of inputs from both entorhinal perforant paths, CA1 and Sub project back to the deep layer V (LVb) [21, 22] whose neurons project to superficial layer V (LVa) as well as layers II and III closing the PHR-HF loop [14, 22]. Neurons in EC LV emit in turn widespread projections to cortical and subcortical domains, constituting thus one of the major HF output pathway to the rest of the brain [11, 23-26]. This latter projection har recently been reported to selectively finds its origin in layer Va [21, 22].

Since the same basic intrinsic PHR-HF circuitry is maintained across mammals [9, 27] and that our data has been obtained in rats and mice, I will be using primarily the rodent nomenclature but occasional comparative remarks will be mentioned. However, it should be noted that direct comparisons with other species are not unambiguous. Different criteria such as location, neuronal chemoarchitecture and overall connectivity should be considered all together to define comparable cortical areas [27]. Recently, alignment of the distribution of EC neuronal markers along a comparable coordinate system has suggested possible distinctive connectivity patterns between caudomedial and rostrolateral primate EC, reminiscent of rodent MEC and LEC respectively [28]. In all non-primate mammalian species studied so far, the binary entorhinal distribution to DG exquisitely coincides with cyto- and chemoarchitectonically defined MEC and LEC and has thus been used as clear-cut hodological criterion [27, 29, 30]. However, the primate entorhinal-hippocampal projection pattern evolves along a gradient between extremes located at its caudomedial and rostrolateral poles [31]. Presubicular inputs have also been proposed as a defining hodological criterion in rats, guinea pigs and cats since it projects selectively to the well-

defined cyto- and chemoarchitectonally entorhinal area whose superficial layers emit a clear medial perforant path hippocampal-projecting pattern, i.e. MEC [32-34]. Finally, seminal studies have also argued that rodent MEC and LEC as well as primate caudomedial and rostrolateral EC seemingly receive most of their respective inputs from the neighboring POR/PHC and PER respectively (**fig.6**) [35-41].

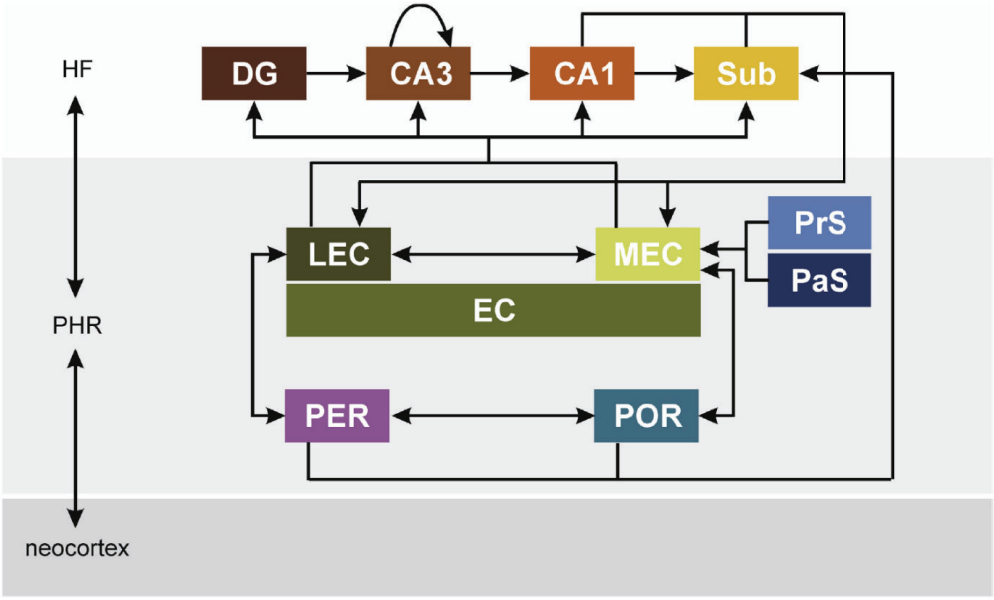

Figure 6. The standard representation of parahippocampal–hippocampal circuitry. Neocortical projections reach the parahippocampal region (PHR), which in turn provides the main input to the hippocampal formation (HF). In PHR, two parallel projection streams are discerned: the perirhinal cortex (PER) projects to the lateral entorhinal cortex (LEC), and the postrhinal cortex (POR) projects to the medial entorhinal cortex (MEC). The entorhinal cortex (EC) reciprocates the connections from PER and POR. Additionally, MEC receives input from the presubiculum (PrS) and the parasubiculum (PaS). The EC is the origin of the so called perforant pathway that projects to all HF subregions. An extended version of thetraditional trisynaptic pathway is a unidirectional route that connects all subregions of the HF sequentially. Output from the HF arises in CA1 and Sub and is directed to the PHR, in particular to the deep layers of the EC. With permission from Cappaert et al., 2015 [14].

1.2. The prevailing model of parallel spatial and non-spatial parahippocampal streams

Anatomical and functional observations have been combined into a coherent framework to propose the current prevailing model which assumes that two functionally different pathways enter MTL as parallel spatial POR-MEC ('where') and non-spatial PER-LEC ('what') streams which eventually converge within the hippocampus symbolized by the firing of 'place cells' as the pinnacle of a complete memory experience [42-46].

This model stemmed from early evidence that bilateral lesions within the PHR-HF system have been associated with the inability to form new episodic memories and cause deficits in spatial navigational abilities in humans and other animals [1, 47]. Therefore, specific functional contributions of distinct PHR-HF subdivisions to mammalian episodic memory processes have greatly benefited of spatial cognition studies in animal models. Initial recordings of single neurons in HF, more precisely in CA1, revealed that a significant proportion of neurons fired action potentials when an animal was situated in a particular location in space [5] . These neurons were thus coined 'place cells' and led to the theory that HF contains a 'cognitive map' composed of overlapping fields of multiple place cells that could potentially cover the entire environment [6]. The largely unidirectional HF connectivity together with CA3 extensive intrahippocampal associative network seemed to indicate that hippocampal structures upstream, i.e. DG/CA3, likely provided CA1 'place cells' with this peculiar spatial information (**fig.6**). However, a key experiment turned out to demonstrate sharp and stable place fields in CA1 after selectively removing their CA3 inputs, thereby switching the focus to EC whose superficial layers project to all HF subfields [48, 49]. Since septal HF had a well-established spatial learning role and had the sharpest place signal [50-52], attention turned to its main entorhinal input located along a dorsolateral band below the rhinal fissure [48, 53, 54] whose medial portion was known to receives most of EC visuospatial inputs [35, 36, 55-63] (**fig.5-6**).

The first recordings were thus done in superficial layers of caudomediodorsal MEC and revealed that a large population of cells fired action potentials regularly in multiple positions along apexes of equilateral triangles tessellating the entire environment and were thus coined 'grid cells' [64, 65]. Several other spatially modulated cell types were subsequently discovered in MEC such as head-direction (HD), borders, aperiodic spatial and speed cells

providing MEC with all elements needed for path integration [66-72]. In contrast, no clear spatial correlates were found in LEC [73]. Instead, single LEC cell recordings revealed scattered neurons across all layers encoding objects and their past locations [74, 75], reminiscent of a subpopulation of lateral entorhinal primate neurons with distinct sustained activity after removal of visual object stimuli, i.e. endowing their network to hold object traces [76]. This apparent functional dissociation between MEC and LEC was reinforced by an extensive body of work which demonstrated their respective roles in spatial path integration versus operant conditioning and item recognition tasks [77-83]. Moreover, similar correlates were also reported in the hippocampus since proximal and distal CA1 place cells demonstrated respective spatial and object preferences [84, 85] presumed to reflect their corresponding inputs from medial and lateral entorhinal perforant paths [86]. Furthermore, hippocampal place cells' firing rates encoding information content and place fields encoding spatial precision and stability where shown to be altered in case of LEC and MEC lesions respectively [87-91]. At last, several seminal neuroanatomical studies have been taken into account to show that POR/PHC coding for visuospatial context and PER for object information were preferentially connected with MEC and LEC respectively (**fig.6**) [35-41].

1.3. Pivotal role of layer II entorhinal principal neurons

The most abundant and well characterized functional entorhinal cell type are the MEC grid cells whose discovery has provided scientists with the exceptional opportunity to study a strikingly well-defined and regular neural pattern universal to the mammalian brain in a high polysensory cortical area [64, 65, 70, 71, 92-95]. Since they are predominantly distributed in layer II [65, 66], a legitimate question was whether potential chemical markers, projection patterns, morphological features or biophysical properties could distinguish grid cells from other neurons. In the entorhinal cortex, the majority of layer II principal neurons can be actually divided according two main categories based on immunochemical identities and corresponding projection patterns. Reelin (Re) expressing cells project primarily to DG but also likely CA3 and CA2 whereas Calbindin (Cb) expressing ones contribute to more widespread ipsilateral, homotopic contralateral and ipsilateral intrinsic projections [96-101]. Besides, the former usually demonstrate a pyramidal morphology while the latter have a stellate morphology in MEC and fan or multiform morphology in LEC [27, 96-98, 102-106]. It was initially hypothesized that stellate cells were canonical grid cells since they have

unique biophysical properties such as a strong sag potential, hyperpolarization-activated (I_h) current and subthreshold membrane potential oscillations that are absent in pyramidal cells [107-109]. Moreover, optogenetic circuit dissections identified that a significant number of grid cells projected to HF [110]. Consequently, *in vivo* whole cell recordings were performed in MEC while mice ran in a virtual-reality environment allowing researchers to identify grid cells and subsequently filled them with biocytin in order to assess their morphology and immunochemical identity postmortem [111, 112]. The conclusion was that both stellate cells and pyramidal cells could be grid cells although stellate cells comprised the majority of them [111-116]. This suggests that grid cells firing pattern result from specific cellular interconnectivity schemes rather than from pure cellular biophysical properties. One influential class of computational models predicted that the grid cell's hexagonal firing patterns likely emerge from a competition between excitatory and inhibitory elements in the circuit, similar to models proposed by Turing in the 1950s [95]. In this model, MEC grid cell activity pattern is thought to arise through attractor dynamics [117-120] achieved by prevailing disynaptic inhibitory connectivity demonstrated in case of stellate cells and pyramidal cells [96, 99, 121-123], strongly contrasting with the higher probability of connectivity between principal cells in layer II of the neocortex [124-126]. Therefore, the lack of grid cells in LEC [73, 127] predicted the presence of layer II principal cell local network architecture governed by different principles. Nevertheless, principal neurons in layer II of LEC have recently been shown to have a comparable circuit structure among members of their own class dominated by disynaptic inhibition [128]. Finally, other main principal layer II cell types in both entorhinal subdivisions have been also shown to be embedded into an overall comparable local circuit architecture [22, 96, 98, 121, 122, 128] suggesting that the difference in MEC and LEC functional phenotype likely depends on distinct extrinsic rather than intrinsic connectivity of principal neurons in layer II. Thus, the present thesis aims to investigate extrinsic inputs to MEC and LEC principal neurons in layer II in order to explore features that could determine their functional difference.

2. Objectives

Article I | Neurons & Networks in the Entorhinal Cortex: A reappraisal of the lateral and medial entorhinal subdivisions mediating parallel cortical pathways.

In paper I, we aim to reassess the accuracy of the underlying fundamental claim that PER and POR (in rodents; PHC in primates) are selective inputs to LEC and MEC respectively, emphasize substantial integration across multiple PHR subdivisions and review rodent and primate *in vitro* and *in vivo* electrophysiological studies to propose an updated PHR connectivity scheme.

Article II | The lateral, but not medial entorhinal cortex is the main recipient of multisensory parahippocampal inputs.

In paper II, we provide a comprehensive and systematic description of POR projections to the whole EC and further assess their potential convergence with PER inputs with the help of *in vitro* electrophysiology. We subsequently reevaluate published tract tracing data in the primate brain [37] with our knowledge gained in the rodent mammalian one.

Article III | Convergence of cortical inputs to layer II neurons in lateral entorhinal cortex.

In paper III, we build upon paper II findings to explore whether single cells in LEC layer II receive convergent monosynaptic inputs from multiple functionally and anatomically defined cortical areas, i.e. PER, PIR, MEC and cLEC. With tract tracing, we first determine that these areas all project to a comparable portion of dorsolateral superficial LEC. With the help of *in vitro* electrophysiology, we further assess their convergence onto one of the two major chemically identified principal layer II cell type of the entorhinal cortex, i.e. hippocampal projecting reelin neurons, essentially composed of fan cells whose lack of basal dendrites endow them for selective integration of inputs targeting superficial layers of LEC. At last we

use retrograde tracing combined with immunochemistry in wild type and transgenic mice to identify putative excitatory and inhibitory long-range projections from neurons located in each of the four cortical areas.

Article IV | Entorhinal layer II calbindin-expressing neurons originate widespread telencephalic and intrinsic projections

In paper IV, we explore the connectivity of the other major chemically identified principal neurons in layer II of the entorhinal cortex, i.e. the calbindin neurons, whose projections is more enigmatic than their reelin counterparts. With the use of elaborate quantitative retrograde tracing supplemented by anterograde experiments and immunohistochemistry, we provide the first systematic hodological study of the calbindin-expressing principal neurons in layer II of the entorhinal cortex.

3. Methodological considerations

3.1. Neuroanatomical tracing

Our current understanding of the brain connectivity relies essentially on four generations of tract tracing techniques that exploit respectively degeneration, retrograde cellular transport, anterograde cellular transport and selective fluorescent protein expression [129, 130]. In the present papers, we use the last three generations that all relied upon microneurosurgical stereotactic tracer injections into the extracellular space of anatomically defined brain regions leading to neuronal uptake of the tracer substance and subsequent transport in either retrograde (i.e. from axon terminals to somata) or anterograde direction (i.e. from somata to axon terminals).

For retrograde cellular transport, we used Fluorogold (FG), Fast Blue (FB), Cholera toxin subunit B (CTB), Retrobeads and recombinant Adeno associated virus (rAAV) that were pressure injected resulting in uptake by axon terminals. The uptake is followed by transport back to the cell bodies of the neurons where accumulation or metabolic degradation occurs. The site of injection of the tracer is visible as well as the retrogradely labelled somata but the pathways taken by the fibers remain invisible [129, 130]. A caveat from pressure injection is that tracer uptake might occur in physically damaged passing fibers by the glass capillary and results therefore in false positive labelled somata [131, 132]. A second important consideration is that retrograde tracing is not well suited to described precise projection patterns nor the density of upstream axonal terminals to the injection site. Indeed, an upstream area could have myriad of labelled neurons with a single axon terminals at the injection site while another one could have only few labelled neurons despite potential extensive axonal collateralization at the same injection site. To avoid these common biases, this method was only used to corroborate projection patterns and characterize projecting neurons that had already been established by anterograde tracing.

For anterograde cellular transport, we use the preconjugated or biotinylated dextran amine (BDA) as well as Phaseolus Vulgaris Leucoagglutin (PHA-L) that were iontophoretically injected resulting in uptake by dendrites and neuronal cell bodies within the injection sites

and filling homogeneously the entire axonal processes [133]. Since subtle projection pattern differences have been reported suggestive of different mechanisms of uptake and transport, we use both tracers at comparable sites but did not notice any marked projection pattern differences within PHR [134]. Even though both tracers are considered as gold standards for anterograde tracing [130], one should be aware about minor occurrence of retrograde transport, particularly for BDA. We employed therefore only the 10kDa isoform of BDA which, unlike the 3kDa isoform, has only limited potential for retrograde transport. Moreover, we systematically discarded tissue from the final analysis when we observed axonal labelling from putative retrogradely labelled somata as indicated by their granular appearance.

At last, we also use selective fluorescent protein expression in papers II, III and IV which is a fairly recent tracing method issue from the interaction of molecular biology and genetic engineering [130].
In paper IV, we used a specific approach with double rAAV injections approach to complement results obtained by traditional tracing. First, we pressure injected a retrograde-infecting AAV expressing Cre recombinase (AAV6-Cre) resulting in uptake by axon terminals at the injection site and subsequent retrogradely transport to distant somata. Second, we proceeded with a pressure injection of a cre-dependent reporter AAV expressing eYFP after recombination (AAV1/2-EF1α-DIO-EYFP) allowing us to selectively infect previously retrogradely labeled somata and visualize of their axonal distribution pattern.
In paper III, we used a SST-IRES-cre x c57 mice to label MEC SST+ long range GABAergic axonal terminals in LEC by pressure injection of a recombinant Adeno associated virus (rAAV). A potential weakness of this method is that the floxed gene expression is strictly cre-dependent and thus determined by the selectivity of the transgenic animal line. To circumvent this problem, we used beforehand classical anterograde and retrograde methods together with subsequent immunohistochemistry in wild type animals to support our findings. Finally, the overall viability of viral tracers has also been questioned since it has revealed several anatomical pathways which had not been consistently reported in experiments using second and third generations tracing methods [135, 136]. Therefore, we established projection patterns with multiple classical anterograde cellular tracer in papers II and III before rAAV with selective fluorescent protein expression that resulted in a clearly comparable projection pattern. Besides, the ultimate goal in these experiments was not tracing per se but rather endowing projecting neurons from different

areas with the ability to express ChR2 allowing *in vitro* electrophysiological investigation of their postsynaptic targets by photostimulation of their axonal terminal fibers with concomitant LEC layer II neuron patch-clamping.

3.2. *In vitro* slice physiology

In order to assess potential synaptic connectivity in papers II and III, we performed *in vitro* whole-cell current clamp recordings of LEC layer II neurons in combination with electrical activation of PER and optogenetic activation of virally transfected fibers originating from either POR, MEC, PIR or contralateral LEC. We injected an AAV to drive expression of channelrhodopsin under control of the human Synapsin promoter (AAV1.hSyn.ChR2(H134R)-eYFP.WPRE.hGH) to transfect neurons in these aforementioned areas leading to channelrhodopsin expression in their axons projecting to LEC [137, 138]. After a survival time of 2 to 3 weeks, we prepared acute semicoronal slices cut with an angle of approximately 20° with respect to the coronal plane in order to preserve the integrity of PER neuronal cell bodies and their axonal projections into LEC [139].

In the case of extracellular PER electrical stimulation, we used the absolute postsynaptic response onset latency and fluctuations in onset time (temporal jitter, defined as the standard deviation of the onset latency) in order to assess if the recorded postsynaptic responses were of monosynaptic or polysynaptic origins [140, 141]. We classified postsynaptic potentials exhibiting response jitters less than < 700 μs as presumed monosynaptic. This jitter criterion is consistent with similar experiments exploring inputs to MEC principal cells from presubiculum and parasubiculum [142]. Data obtained with this method should be interpreted with caution due to the possibility of activating passing fibers from other brain areas which also distribute axonal terminals within LEC, as well as possibility for antidromic activation of axons that originate from the recorded area. Therefore, we performed control using flash photolysis of caged glutamate. Caged compounds are inert precursors of active substances, such as neurotransmitters, which are converted to their active form upon exposure to certain light wavelength. This photochemical conversion is fast and leads to the release of active neurotransmitter at the stimulation site exclusively. This implies that the active neurotransmitter ligands released as a result of photolysis will interact with their corresponding receptors around the site of stimulation locally. Neuronal excitation mediated

by photolysis of caged glutamate can thus be limited to dendrites and somata confined to locations covered by the light stimulation [143, 144] preventing undesirable activation of passing axons or antidromic signal propagation.

In the case of optogenetic stimulation of the axonal terminal fields, we isolated recorded synaptic potentials evoked by monosynaptic pathways using a pharmacological test incorporating the voltage-gated sodium blocker tetrodotoxin (TTX), and 4-aminopyridine (4-AP), a blocker of voltage-gated potassium channels. In control conditions, the success of optogenetic circuit mapping relies on the ability to evoke action potentials in channelrhodopsin-expressing cells. Cation influx through channelrhodopsin channels must give rise to a suprathreshold depolarization such that the cell fires action potentials, which is normally required for triggering the release of neurotransmitter in such experiments. The observed complete block of postsynaptic responses following bath application of TTX confirms that electrotonic spread of potential is insufficient to trigger neurotransmitter release at axon terminals. However, such graded electrotonic potentials are adequate to induce neurotransmitter release if axon terminal excitability is restored, for example by the actions of 4-AP. Hence, the rationale behind a combined addition of TTX and 4-AP is to prevent action potential generation by the actions of TTX while at the same time increasing cell excitability by a 4-AP mediated decrease in potassium conductance. This means that under such conditions (+TTX/+4-AP) channelrhodopsin-mediated depolarizations are unable to drive network activity, i.e., polysynaptic transmission, because active signal propagation by way of actions potentials is repressed. However, cell excitability is recovered due to a lowered potassium conductance, which means that electrotonic potentials resulting from channelrhodopsin-mediated cation influx in or near axon terminals are sufficient to induce neurotransmitter release. Thus, synaptic responses recorded under these conditions (+TTX/+ 4-AP) resulting from selective optical stimulation of axon terminals presynaptic to the recorded cell can be considered monosynaptic [138, 145]. This pharmacological test is unfortunately not compatible with distant extracellular electrical stimulation of PER networks because mainly cell bodies and dendrites, and not axon terminals, are affected by this stimulation approach.

4. Synopsis of results

Article I | Neurons & Networks in the Entorhinal Cortex: A reappraisal of the lateral and medial entorhinal subdivisions mediating parallel cortical pathways.

In paper I, we review the main anatomical, cytoarchitectural, chemoarchitectural and hodological features of the medial and lateral entorhinal cortices. We further describe their respective cell types that have emerged as functional elements to read out their respective codes. In MEC, we argue that grid , spatially modulated non-grid, head-direction, speed, border and object-vector cells [64-66, 71, 72, 94, 146-148] indicate that MEC network is best considered as capable of computing path integration, an idiothetic navigation strategy in which the animal uses self-motion cues to track its current position relative to an arbitrary reference location [7, 149]. In LEC, we argue that the network is essentially involved in olfactory processing [98, 150-160] and multimodal object representation [161-168]. We further described entorhinal neurons and networks focusing on layers II, III and V in each entorhinal subdivision. In layer II, we emphasize that principal neurons identified by chemical and morphological features have limited monosynaptic connectivity among members of their own class, showing a preferred disynaptic connectivity mediated by interneurons [121, 122, 128] contrasting with a significant higher connection probability in layer III principal neurons [169-172]. Moreover, we review data showing that layer V can be subdivided between superficial Va and deep Vb which are interconnected to superficial layers locally and constitute the main entorhinal output and hippocampal input layers respectively [21, 22, 24]. We conclude that MEC and LEC neuron types, local circuit motifs, and the laminar origin and termination of inputs and outputs are strikingly similar and that they communicate with HF using the same network-dependent language. At last, we reassess the concept of parallel PHR pathways to HF mediated by suggested PER-LEC and PHC/POR-MEC streams. We argue that POR/PHC contributes in fact to both pathways [36, 173] providing both MEC and PER/LEC with what we propose to be a continuously stable representation of context, i.e. object-place associations [174-180]. We further point out to the highly polysensory character of the PER/LEC interface [15, 26, 173, 181-196] which seems

to provide the optimal substrate to detect changes in that context as reflected by its highly integrated, multidimensional representation of sensory information, including changes over time [197-202]. We conclude that the difference in extrinsic inputs, but not a difference in internal circuit organization is key to the functional differences between MEC and LEC.

Article II | The lateral, but not medial entorhinal cortex is the main recipient of multisensory parahippocampal inputs.

In paper II, we investigated the underlying claim that PHR is organized as two parallel pathways mediated by POR-MEC and PER-LEC. First, we performed anterograde tracer injections and reanalyzed previous material from our lab [35, 38] obtaining a comprehensive multiplane library of anterograde injections of BDA, conjugated DA and PHA-L in POR and PER (n=87). Although we confirmed that PER projects mostly to superficial dorsolateral LEC, we observed that POR projects to superficial layers of the entire rostrocaudal extend of dorsolateral LEC (areas DIE and DLE) as well as ventral MEC (area ME) but not dorsal MEC (area CE) [11] as previously assumed [35, 36]. However, we noticed a moderate projection originating from caudomedial postrhinal neurons to dorsal MEC (area CE) layer Va, suggesting that caudomedial POR rather modulates MEC output to the rest of the brain than influence neurons located in superficial layers where most of grid cells are found [21, 65, 66]. We also demonstrated with anterograde and retrograde tracing combined with triple immunohistochemical stainings (Cb, PV, NeuN) that the previously assumed POR projections to superficial layers of dorsal MEC (area CE) originated in fact from a dorsolateral PaS extension, notorious for its highly variable neuroanatomical borders [10, 13, 24, 69] that indeed projects to MEC layer II [55]. Furthermore, we placed retrograde tracer injections with regular (n=5) and lateral burrholes (n=4) in superficial layers of dorsolateral LEC demonstrating that neurons in ventral POR LII/III, including about 25% of calbindin positive cells, originate most of the projections to LEC.

In a second serie of experiments, we aimed to assess POR and PER convergence on principal cells in LEC LIIa and LIIb defined by their location within reelin or calbindin sublayers respectively. Therefore, we injected a viral vector carrying channelrhodopsin (AAV1.hSyn.ChR2(H134R)-eYFP.WPRE.hGH) in POR allowing expression of a photosensitive opsin in their axons present in LEC and subsequent *in vitro* current clamp

recordings of layer principal neurons in LEC II in combination with photostimulation of POR axons together with electrical stimulation of PER. We found that POR send synaptic excitatory projections onto all morphologically defined principal cell types, i.e., fan, multiform and pyramidal-like cells. We confirm the monosynaptic character of these inputs using bath application of TTX/4-AP in pyramidal-like cells and fan cells. In a like manner, postsynaptic potentials were recorded in all cell classes upon extracellular activation of PER. The majority of the potentials recorded in these principal cells as well as a small group of putative interneurons (n=4) were classified as presumed monosynaptic Thus we could demonstrate that cells both in layer IIa and IIb receive convergent cortical inputs originating from POR and PER.

Since our results seemed conflicting with the seminal study of Burwell and Amaral, we reanalyzed available anterograde flatmaps that had been into account to support the previously assumed parahippocampal streams concept [36] and demonstrated in fact that their results fully supported our findings. At last, we indicate similarities between our rodent POR projection to EC with available tract tracing data which described the non-human primate PHC projection to EC [37]. Taken together, our results and analysis challenge the currently accepted parallel pathway model of the PHR and point to LEC as the main recipient of polysensory inputs and integrating unit of the PHR.

Article III | Convergence of cortical inputs to layer II neurons in lateral entorhinal cortex.

In paper III, we first demonstrated with iontophoretic anterograde tracer injections of BDA and PHA-L that MEC, PER, PIR and commissural LEC send axonal terminals converging into a comparable portion of superficial dorsolateral LEC directly ventral to the rhinal fissure. MEC fibers had a bilaminar distribution pattern with a very dense labelling in superficial portion of LEC layer LI and deep layer II - superficial layer III. PER fibers were distributed rather homogeneously LEC layers I to III whereas PIR and cLEC projected essentially in the outermost and innermost portions of LEC layer I respectively. In a second series of experiments, we injected a viral vector carrying channelrhodopsin (AAV1.hSyn.ChR2(H134R)-eYFP.WPRE.hGH) into each of the aformentioned areas confirming their respective labelling observed in LEC. Then, we performed whole-cell

current clamp recordings of superficially located layer II cells, and verified by subsequent reelin counterstaining that the majority of them project to HF [96-99]. Most recorded principal cells had either a fan or multiform morphology but a few were classified as pyramidal or oblique pyramidal cells (Canto Witter 2012).

Photostimulation of PIR virally infected axons demonstrated prevalent monosynaptic, excitatory inputs to fan and multiform cells. Likewise, excitatory postsynaptic potentials were also detected in similar cell types following the photoactivation of contralateral LEC axons. In contrast, optogenetic stimulation of MEC virally transfected fibers demonstrated a combination of direct inhibitory and excitatory influence on recorded cells in LEC layer II, confirmed by consecutive application of TTX and TTX/4-AP to verify that responses reflected monosynaptic couplings. Regarding PER inputs, we used electrode electrical stimulation which was subsequently controlled by a series of glutamate uncaging experiments to minimize a potential antidromic stimulation component. The majority of principal cells i.e. fan cells, multiform cells and pyramidal-like cells displayed subthreshold postsynaptic potentials that were mainly excitatory, although sometimes followed by an inhibitory component. Based on the jitter synaptic latencies criteria used in paper II, we concluded that the majority of postsynaptic potentials recorded in LEC layer II likely reflected monosynaptic connections. We noticed that all recorded principal neurons in LEC layer II responded to conjunctive electrical stimulation of PER in combination with photostimulation of either PIR, MEC or contralateral LEC labelled fibers, thereby demonstrating that the convergence of these inputs arise at the level of single cells.

At last, we injected the retrograde tracer FG or rAAV2-tdtomato in dorsal LEC of GAD67 GFP x c57 mice to characterize putative long-range GABAergic neurons confirming their presence in PER and MEC but not in PIR nor cLEC .Since GABAergic projections from PER to LEC had been already been reported [203, 204], we further characterized MEC long-range GABAergic neurons and found that the majority of these expressed SST.To confirm that these cells could potentially form monosynaptic contact with LEC layer II cells, we injected AAV2/1-hSyn-Flex-TVA-mCherry-G in MEC of SST-IRES-cre x c57 mice (n=6) and observed in all cases that MEC SST+ GABAergic neurons displayed axonal terminals selectively distributed in LEC layer I.

Article IV | Entorhinal layer II calbindin-expressing neurons originate widespread telencephalic and intrinsic projections

First, we examined the distribution of reelin and calbindin neurons in layer II of the entorhinal cortex in rats and mice and confirm that they form two sublayers with subtle distribution differences in MEC and LEC [27, 97-99, 103, 104, 106, 203, 205]. Then, we essentially proceeded with a series of retrograde tracer injections (FB, FG, CTB555 or Retrobeads) combined with immunochemical counterstaining against Calbindin to quantify the respective contribution of MEC and LEC layer II Cb cells to different pathways.

We started by placing retrograde injections in different portions of dorsal HF (n=7) whose labelling resulted only in moderate colocalization with MEC and LEC layer II Cb cells irrespectively of the CA1 proximodistal injection position. In order to verify the previous claim that Cb cells in MEC and LEC are a major source of homotopic contralateral projections [98, 99] and investigate potential ipsilateral entorhinal intrinsic ones, we analyzed the distribution of retrogradely labeled neurons following injections in layers I and II of MEC (n=3) and LEC (n=3) in addition to injections at MEC-LEC border region (n=8). We noticed a relatively high percentages of double labelling (i.e. double-labeled neurons among the retrograde labelled cells) in ipsi- and contralateral of LEC and MEC, although the percentage was significantly higher in ipsilateral MEC than in LEC. In contrast, the reverse percentage (i.e. double-labeled neurons among the Cb cells) was significantly higher in ipsi- than in contralateral EC.

Although most entorhinal projections to telencephalic areas originate from layer Va [11, 21, 22], superficial layers II and III have been reported to project to parahippocampal and extra-parahippocampal areas [11, 14, 98, 206]. Thus, we wanted to assess potential contributions of EC principal layer II Cb cell projections to several telencephalic areas. Therefore, we placed RG injections in prelimbic (n=2), prefrontal (n=2), ventral medial prefrontal (n=2), ventral orbitofrontal (n=3), anterior piriform (n=2), posterior piriform (n=2), anterior insular (n=2), perirhinal (n=2), postrhinal (n=2) and retrosplenial (n=3) cortices as well as nucleus accumbens (n=2) and amygdaloid complex (n = 2). Although retrogradely labelled somata were primarily found in LVa, we did observe clear topographical patterns of double

colocalization in LII Cb cells in certain areas, e.g. a very restricted dorsal LEC portion in case of PER retrograde injections.
Besides, we also wanted to assess whether LEC layer II Cb neurons collateralize as previously reported in case of olfactory and contralateral projections [98]. However, a pilot experiment with double retrograde injections in vmPFC and ipsilateral EC resulted only in a low number of double labeled cells. Therefore, we opted for an alternative method using a double AAV infection approach, i.e. injecting in rostral LEC a retrograde-infecting AAV expressing Cre recombinase (AAV6-Cre) and subsequently injecting a cre-dependent reporter AAV expressing eYFP after recombination (AAV1/2-EF1α-DIO-EYFP) at the LEC/MEC border (n=2), resulting in massive fiber plexus labelling in ipsilateral LEC (LI–III) and MEC (LI) but also in olfactory areas, amygdala, perirhinal and ventromedial prefrontal cortices. Furthermore, we also injected retrograde tracer in the medial complex of rat since a recent mouse study reported that layer II MEC Cb neurons project to medial septum [96] but found only sparse labelling in ventral EC with very few double label colocalization. Retrograde tracer was also placed into nucleus reuniens of the thalamus (n = 3) but retrogradely labeled somata was neither observed in LEC nor MEC.

Finally, since Cb entorhinal cells comprise both GABAergic and glutamatergic neurons, we injected a retrograde tracer into dorsal CA1 and contralateral MEC of a GAD67 transgenic mouse line expressing GFP (n=2) resulting in similar EC layer II labelling than the one obtained in our previous experiments in rat. We did not find any potential inhibitory neurons in contralateral MEC nor ipsi- or contralateral LEC but only very few triple-labeled neurons in ipsilateral MEC suggesting that inhibitory Cb EC neurons contribute primarily to the short-range local projection.

In conclusion, we provide the first systematic and quantitative study of layer II Cb entorhinal neurons demonstrating that their largest percentage contribute to local intrinsic projections whose long-range component is mostly excitatory and tend to collateralize with distinct projection patterns depending on their origins across the caudomedio-rostrolateral extend of the entorhinal cortex.

5. General discussion

5.1. The entorhinal cortex is a functional continuum

5.1.1. Lack of anatomical and functional validity of the prevailing model

The prevailing model of the organization of the MTL memory system assumes that two functionally different parallel 'where' and 'what' pathways mediated by POR/PHC-MEC and PER-LEC respectively converge within HF to form a complete memory representation [42-46].

This model relies on several seminal neuroanatomical [35-41], behavioral and electrophysiological [65, 66, 71, 74, 75, 78, 93, 94, 146-148, 198, 199, 201, 202, 207-209] studies in rodents and primates. In paper I, we review existing data emphasizing the high level of anatomical cross-integration between these two suggested streams and scrutinize MEC and LEC micronetworks. We conclude that MEC and LEC implement similar internal computations delivering an output using the same network-dependent language to communicate with HF. We also question the validity of the prevailing functional spatial/non-spatial dichotomy in view of the consistent spatial correlates in LEC [75, 209-211] and non-spatial correlates in POR/PHC and MEC [148, 176-180, 211-214]. In fact, population analyses have recently revealed that MEC neurons (including "classical" spatially modulated grid, border and head direction cells) surprisingly encoded object information as strongly as PER and LEC neurons [211]. Since LEC lesions have been shown to alter HF place cells rate, i.e. non-spatial, remapping [87], the prevailing model implied that MEC should enable HF place cells to generate global, i.e. spatial, remapping. However, a recent report demonstrated that HF place cell global remapping can occur independently of MEC inputs [215] suggesting than other inputs to HF, such as LEC, are sufficient for stabilization of HF place cell spatial maps. The observations that MEC and LEC are not confined to spatial- and non-spatial computations respectively suggest that the segregated what/where pathway model is incomplete and needs revisions. In paper II, we demonstrate the inaccuracy of the anatomical core principle underlying the prevailing model by pointing to LEC as the major site of PER

and POR/PHC convergence while emphasizing the paucity of such extrinsic inputs to the canonical spatially modulated MEC i.e. area CE [11, 216, 217].

5.1.2. The entorhinal intrinsic organization precludes any sharp functional border

In rodents, significant biophysical cellular differences between LEC and MEC principal neurons have been limited to neurons in LII [109, 218]. Despite the fact that these are embedded into an overall comparable local circuit architecture [22, 96, 98, 121, 122, 128], only MEC layer II neurons display a grid functional phenotype during spatial navigation tasks [65, 66, 73]. Grid cell properties as well as their changes in firing scales have been attributed to a number of features including properties such as membrane oscillations and changes in their frequency [95, 111]. However, previous work from our lab demonstrated large differences between frequencies of membrane oscillations as high as 3.2Hz during simultaneous *in vitro* patch-clamping of up to four principal neurons spread across the whole mediolateral axis of MEC [109]. This prompted Canto and Witter to systematically analyzed changes in LII neurons' biophysical properties (frequency of membrane potential oscillations, resonance frequency, sag ratio, rebound amplitude, time constant, input resistance, depolarizing afterpotential amplitude after the first action potential) along the mediolateral axis of MEC and LEC revealing a gradient spanning across medial to lateral MEC and continuing into LEC such that LEC medially positioned neurons share properties with adjacent MEC cells (**fig.7**) [109]. Comparable observations were made when comparing stellate cells in LII of MEC along the dorsoventral axis [219, 220]. Furthermore, the existence of a functional gradient across the anatomical border between LEC and MEC is supported by the observation that principal neurons in LII in each entorhinal subdivisions have axons and dendrites crossing that border [109] strikingly contrasting with the PER one where layer II entorhinal fan cells even display a distorted morphology as their dendritic trees clearly bend away from the PER/EC border [221]. Thus, EC intrinsic organization precludes any sharp functional border and suggest instead that EC biophysical cellular properties evolve across a continuum.

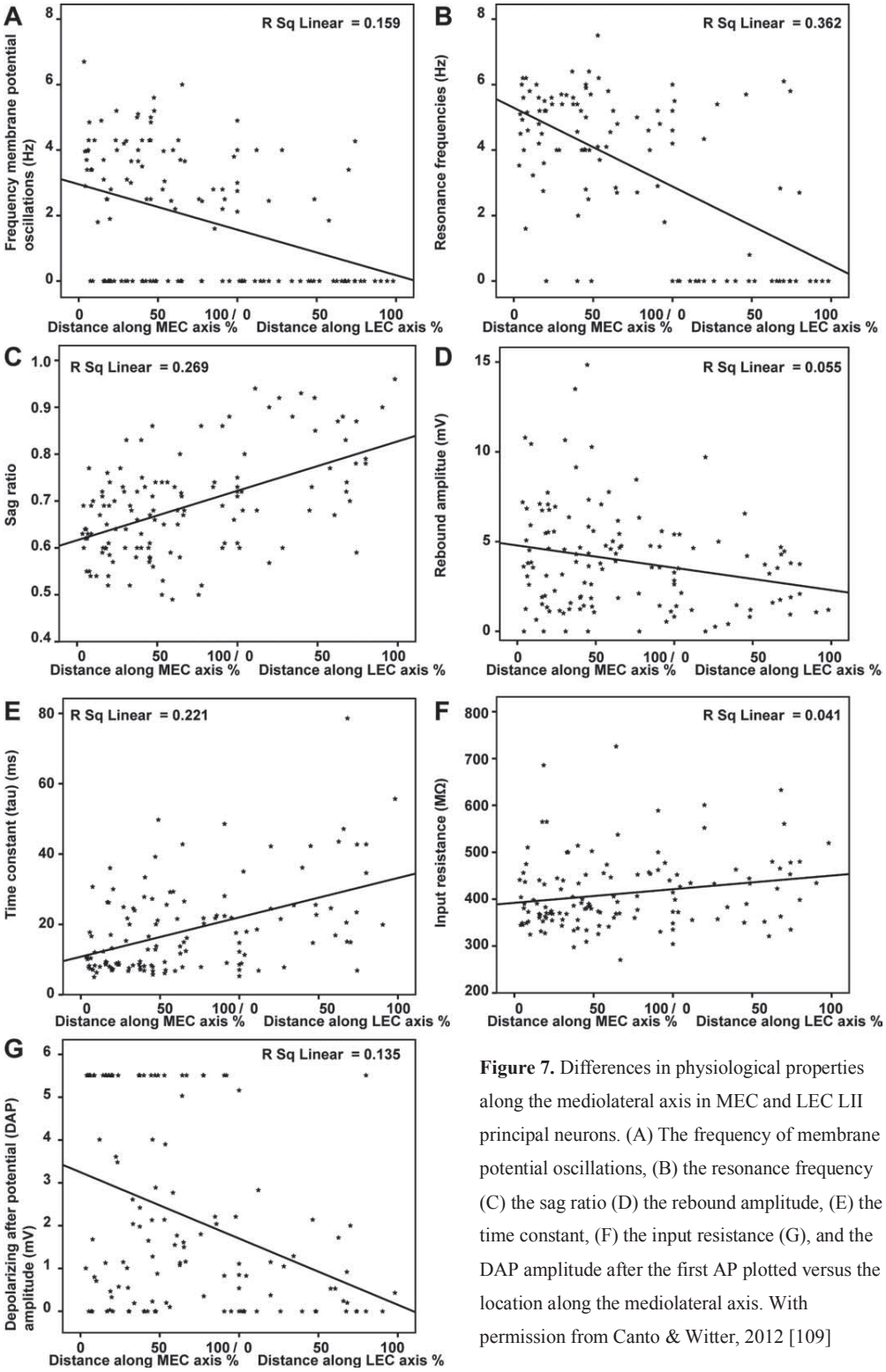

Figure 7. Differences in physiological properties along the mediolateral axis in MEC and LEC LII principal neurons. (A) The frequency of membrane potential oscillations, (B) the resonance frequency (C) the sag ratio (D) the rebound amplitude, (E) the time constant, (F) the input resistance (G), and the DAP amplitude after the first AP plotted versus the location along the mediolateral axis. With permission from Canto & Witter, 2012 [109]

Recently, caudomedial entorhinal cell ensembles recordings during navigation and sleep demonstrated that spatial phase offsets of grid cells were found to predict arousal-state-independent spike rate correlations. Similarly, state-invariant correlations between conjunctive grid–head direction and pure head direction cells were predicted by their head direction tuning offsets during awake behavior [222]. Thus, the entorhinal network appears to exhibit a comparable activity correlation structure that transcends behavioral states [222, 223], i.e. independent of extrinsic inputs [222-224]. A prediction to the existence of a structural entorhinal functional continuum, as I propose here, would suggest that activity correlation structure of the overall entorhinal network should transcend behavioral states as well.

5.1.3. The entorhinal cortex has features of a generalist circuit

In an elegant review by Hardcastle and colleagues about the search for cell types in MEC, the concept of generalist versus specialists networks are well explained [225]. Here, I aim to build on that by summarizing the main defining features of such circuit types. I will further add some details and apply the emerging principles to an analysis of what is known about MEC and LEC.

A generalist circuit is highly adaptive and the distribution of its physiological responses recorded in any experiments will depend strongly on the task used to probe its function. This is the case in higher order cortical regions in which input statistics can change rapidly to support flexible coding and operate as general-purpose (i.e. generalist) learning circuits such as the hippocampus, prefrontal cortex [226], motor cortex [227-229] and posterior parietal cortex [230] where emergent neural population dynamics, analyzed with the use of dimensionality-reduction methods, can reveal highly organized informative neural state space dynamics [231]. This was recently demonstrated in the case of LEC as well [201, 202].
In contrast, a specialist circuit performs invariant statistical transformation in which physiological function can be ascribed to individual cells in a manner that is correlated with each cell's genetic identity, connectivity pattern and morphology. For instance, the retina serves as an ideal example of a specialist circuit as it must transform spatiotemporal light patterns from a large number of photoreceptors into a limited number of retinal ganglion cell nerve fibers' firing patterns in the most efficient way given the bottleneck presented by the optic nerve [225].

The study of the PHR-HF system through the spectrum of spatial navigation has been successful in finding meaningful, recurring patterns such as the notion of a cell type [65-67, 71, 74, 75, 94, 146-148, 209]. However, this approach has labelled early on MEC as a specialist circuit for spatial navigation whereas it left LEC with the vague function of representing "non-spatial" information [73, 225]. This raised the question about the nature (i.e. right axis) of the coding dimension by which we should probe the function of LEC [74, 75, 209, 232]. It was not until overall cellular population state analyses revealed its potential role as encoding temporal information ([201]. Although appealing, the search for cell types must solve an essential statistical problem i.e. demonstrate the existence of distinct subpopulations, such that neurons within a subpopulation are significantly more similar that neurons across populations. While this approach is well suited for specialist circuits where each cell types form tight clusters along genetic, anatomical and/or physiological axes, cells in generalist circuits might spread out along a continuum. Furthermore, a serious pitfall of this approach is to fail choosing the right axes for defining the coding dimension leaving large populations of cells to lie at the origin of the feature space, essentially invisible to any cell type analysis. In this approach, neurons are classified according to "score" (e.g. grid score) which quantifies specific features of a neuron's tuning curve (e.g. 60° symmetry) which is then compared to that expected by chance determined from a null distribution of scores generated from shuffled data polled across the entire population or same cell [233-235]. Although exceptionally productive, this classification method has several limitations such as the dependency on the experimenter-defined shapes rather than the true heterogeneity of neuronal tuning, necessary score threshold leaving potential continuous representation of navigational variables aside and bold assumption of a static relationship between an external sensory stimulus and the neural response which will overall miss behavior- or state-dependent coding properties [225].

The functionally defined cell types in MEC remain difficult to classify by other features such as biophysical properties, morphology or immunochemical identity [109, 111-116] as it should be the case in a specialist circuit. By moving to tasks with more complex behavioral demands than open field foraging, MEC cells were shown to encode time elapsed, distance traveled or navigation into a unidimensional auditory space [213, 214] supporting flexible coding in navigational and non-navigational tasks [201, 211, 213, 214, 233, 236] (for review, see [237]). In fact, recent works employing statistical models have revealed an extremely high degrees of heterogeneity and multiplexing in MEC neurons including grid, border, HD,

speed, conjunctive and even unclassifiable ones by traditional spatial navigation tasks [211, 233, 238]. These are all features of a generalist circuit and such findings are similar to what has recently been described in LEC.

In conclusion, I propose that the functional entorhinal continuum is a generalist circuit which implements canonical computations that are largely uniform across its overall network, producing behavioral-state dependent physiological responses that are primarily dependent on the nature of its extrinsic inputs.

5.2. The concept of functionally distinct MEC and LEC depends on the PrS input selectivity

5.2.1. The historical role of the PrS-MEC-HF axis in MTL spatial representation system

The study of memory processes in the PHR-HF system examined through the spectrum of spatial cognition takes its roots in the first recordings of hippocampal place cell [5] contributing together with Tolman's work in the late 1940' [239] to the theory that HF contains a cognitive map of the external world [6]. Successive historical milestones were the discovery of head-direction cells in dorsal PrS [240-242] that are organized in a single functional coherent network [243-246] followed by the discovery of caudodorsal MEC grid cells [64, 247] structured as dorsoventral modules that are also organized as coherent functional networks [217, 222, 223, 248]. Subsequent discoveries of conjunctive grid-HD, border, speed, aperiodic spatial and object-vector cells [66, 72, 146-148] provided MEC with all parameters necessary for path integration resulting in a detailed mechanistic understanding of spatial mapping computation as one of the first cognitive functions [7]. Thus, it is interesting to notice that the three main functional cornerstones that support the concept of spatial cognition in the PHR-HF system, i.e. septal HF place cells, caudodorsal MEC grid cells and dorsal PrS head-direction cells, articulate around three of the strongest and most specific synaptically connected areas of the mammalian MTL memory system [17, 55, 56, 60]. Historically, this is also relevant since the discovery of MEC grid cells allowed to bind presubicular head-direction signal to the hippocampal place one into a coherent functional system potentially underlying spatial cognition [7]. Besides, these three specific subregions are also the ones enclosing each of their respective functional cell types in their most pristine

form i.e. sharpest head-direction tuning, finest grid scale and best defined place fields in dorsal PrS, MEC and HF respectively [50, 241, 242, 249-252]. In fact, no one has reported the presence of head-direction cells nor grid cells in ventral PrS and MEC (i.e. area ME) respectively [251-253].
Finally, PrS also contains border cells, conjunctive HD-grid, as well as pure grid cells whose modules continue into the neighboring MEC [69, 217, 254, 255] sharing comparable continuous attractor network properties [222-224, 256]. This indicates that PrS is more than a mere input to MEC but rather part of a complex system that support the very fundamentals of spatial cognition [118].

5.2.2. "Head direction" input signal is fundamental for EC grid formation

There is increasing evidence that single modules of grid cells can be modelled by low dimensional continuous-attractor networks [222-224, 248, 257] where activity is translated with a displacement and direction in the network that is proportional to the animal's movements in the spatial environment [95]. This translation process requires continuous access to two types of information: a sense of direction and a sense of speed that are represented by head-direction [66, 240-242] and speed cells [72] respectively. Interestingly, head-direction and speed cells maintain their relative tuning across environments [72, 241, 242, 258] supporting the observation that grid maps can and do form instantaneously in new environments [95, 118, 259-261]

On one hand, the speed signal can be derived from optic flow or self-locomotion information which seems ubiquitous in the PHR-HF system. In MEC for instance, a speed signal is known to originate partly from the medial septum and diagonal band of Broca (MS/DBB) which relay self-locomotion information from mesencephalic pedunculopontine nucleus [262, 263]. Besides, MS/DBB also projects to LEC [264] which in addition receives direct optic flow information from POR [265] as described in paper II [216]. Although this has not been reported experimentally yet, one might certainly expect to find speed correlations coded by subpopulations of LEC cells.

The direction signal originating in the vestibular cranial nerve which allows the estimation of linear and angular head displacement even in the absence of visual cues follows a selective anatomical pathway [266-270]. In vestibular nuclei, 'vestibular only' and 'vestibulo-ocular

reflex' neurons integrate multimodal information originating from a number of different sources including head, body and eye (i.e. gaze) motor commands, neck proprioceptive information and visual inputs [271, 272] and primates [273, 274]. Vestibulo-ocular reflex neurons project in turn to the nucleus prepositus also known as the oculomotor integrator due to its central role in shaping eye movements [275]. This points to nucleus prepositus as a crucial anatomical correlate explaining the universality of the entorhinal grid signal across mammals, since rodent and monkey grid cells have been demonstrated during spatial navigation tasks reflecting full body physical and eye saccades exploration respectively [64, 65, 71, 93, 94, 276-278]. In fact, although the head direction system is generally assumed to generate a fixed representation of perceived directional heading, its output contains a highly multimodal signal enclosing information about direction, proprioception and motor efference copy (including gaze related information) that are necessary for grid cell formation [279, 280]. The nucleus prepositus further projects to dorsal tegmental nucleus which project together with the lateral mammillary nucleus to the anterodorsal thalamic nucleus (ATN) [281-284]. From ATN, the head-direction signal is then projected to PrS that projects strongly and selectively to superficial MEC stopping sharply at the LEC border in the case of rodents [55, 56] and caudomedial entorhinal half in case of primates (Witter and Amaral, unpublished observations). Anatomical and electrophysiological experiments demonstrated that PrS projections monosynaptically contact principal cells in all layers of MEC, which also receive convergent inputs from PaS [142, 285, 286], potentially explaining that grid cells can be found across all layers of MEC [66, 67]. Furthermore, grid cells individual firing fields have multiple and different preferred directions [287] and certain manipulations such as temporary inactivation of the hippocampus can even unmask the inherent head-direction signal in EC grid cell [288]. This direction signal is not only inherent but also necessary since its disruption has been shown to break down grid cells regular hexagonal firing pattern [280, 289].

At last, our lab recently showed with the use of anatomical tracing, voltage-sensitive dye imaging and *in vitro* single cell patch recordings that anatomical connections from PrS and PaS to superficial EC emerge between postnatal day (P)4-6 and form monosynaptic connections measurable from P9-10). Maturations in the efficacy of PrS/PaS inputs are paralleled by maturation of cellular morphological properties, changes in EC intrinsic principal neurons characteristics as well as alteration of grid cells GABAergic networks in MEC between P9-21 [290]. Interestingly, *in vivo* electrophysiological recordings have

demonstrated that PrS/PaS head direction signal is present within a coherent network before P11, i.e. 3-4 days before pups' eyelids unseal. This indicates that directional tuning constitutes a hardwired network which develops even before the emergence of the immature EC grid signal at P16 that gradually refines as network synchrony among stellate cells increases [234, 291, 292]. This provides pups with an internal functional map of external space at the time they leave the nest for the first time around p16-18 [292, 293].

In conclusion, anatomical studies as well as *in vitro* and *in vivo* electrophysiological experiments strongly suggest that the direction signal from PrS, potentially in combination with PaS, is the crucial extrinsic input allowing the entorhinal continuum to compute its grid functional phenotype [55, 56, 64, 71, 142, 234, 280, 289-293] (Witter & Amaral, unpublished observations).

5.2.3. Phylogenetic considerations

The rodent LEC receives extensive inputs from almost all cortical areas including orbitofrontal, prefrontal, cingulate, somatosensory, insular and temporal cortices [14, 216, 294]. During evolution and along the phylogenetic tree all these cortical input areas considerably size up (**fig.2, fig.8**). In paper II, we demonstrate that the majority of POR inputs to superficial EC in close relation to the rhinal fissure are almost exclusively distributed in LEC, akin to PER inputs. We further argue that the homologous rodent POR and primate PHC structures share comparable projection patterns on the overall EC, although PHC fibers notably stretch across most of the rostrocaudal extend of superficial EC in close relation to RF [28]. Whereas monkey EC receives approximately 60% of its inputs from PHC and PER [295], unfolded maps of these regions have also revealed that the combined area of rodent PER/POR is about the same size as the EC while the primate PER/PHC area is about four times bigger (**fig.8**) [10, 296]. Albeit they account for roughly similar percentages (about 5%) of the entire neocortical surface area in the brain of each species [10]. At last, object trace cells were found across most of EC rostrocaudal extent in close relation to the rhinal fissure in primate [297] and LEC in rodent [75].
Taken together, these studies strongly suggest that LEC physically increases on the evolutionary tree at the expense of MEC (**fig.8**), a prediction in line with our conclusion in paper I that the former represents an evolutionary new and more complex sensory area than the latter.

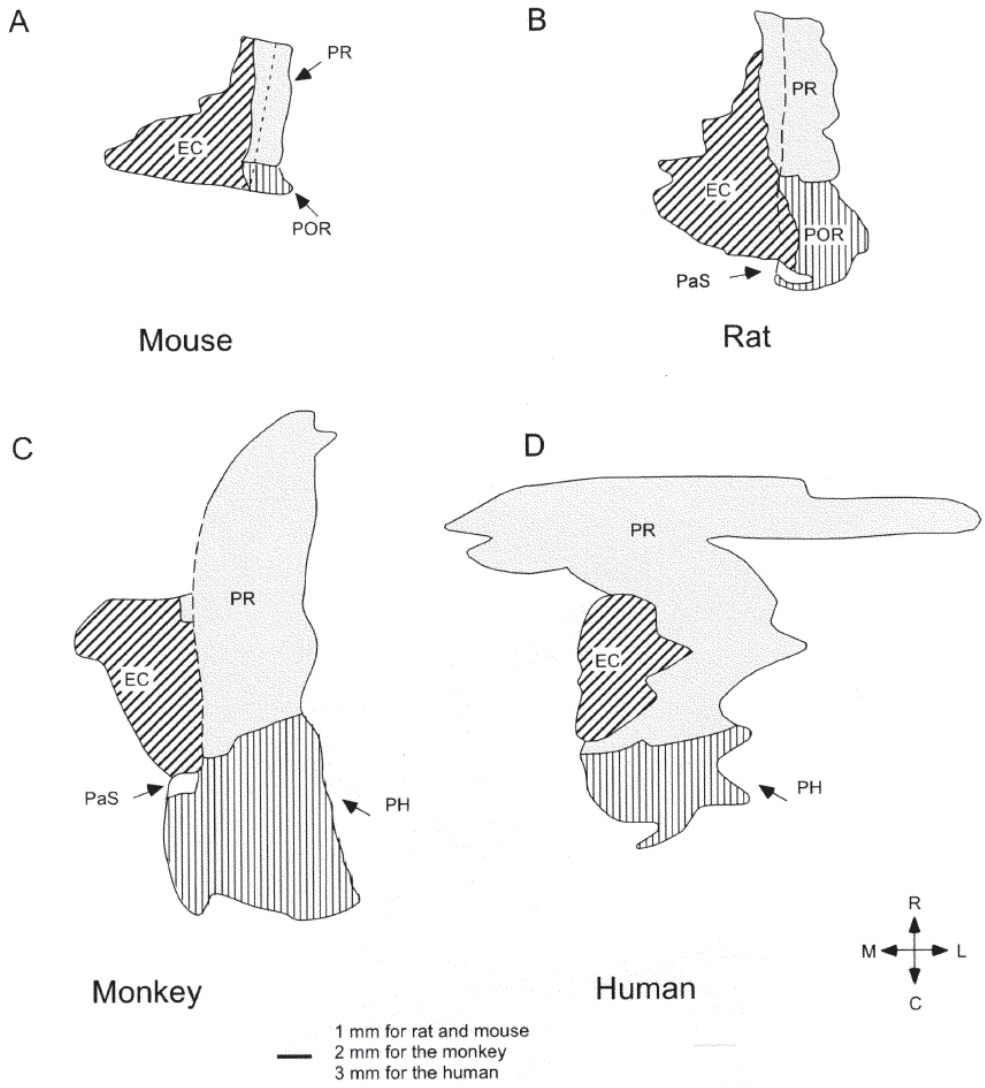

Figure 8. Representative unfolded two-dimensional maps informative about the parahippocampal region phylogeny. Perirhinal cortex areas 35 and 36 (PR) are shown in gray, parahippocampal (PH) and postrhinal (POR) cortices in vertical stripes, and the entorhinal cortex (EC) in diagonal stripes. The dorsolateral parasubiculum extension (PaS) discussed in paper II is indicated [216]. With permission from Burwell, 2000 [296].

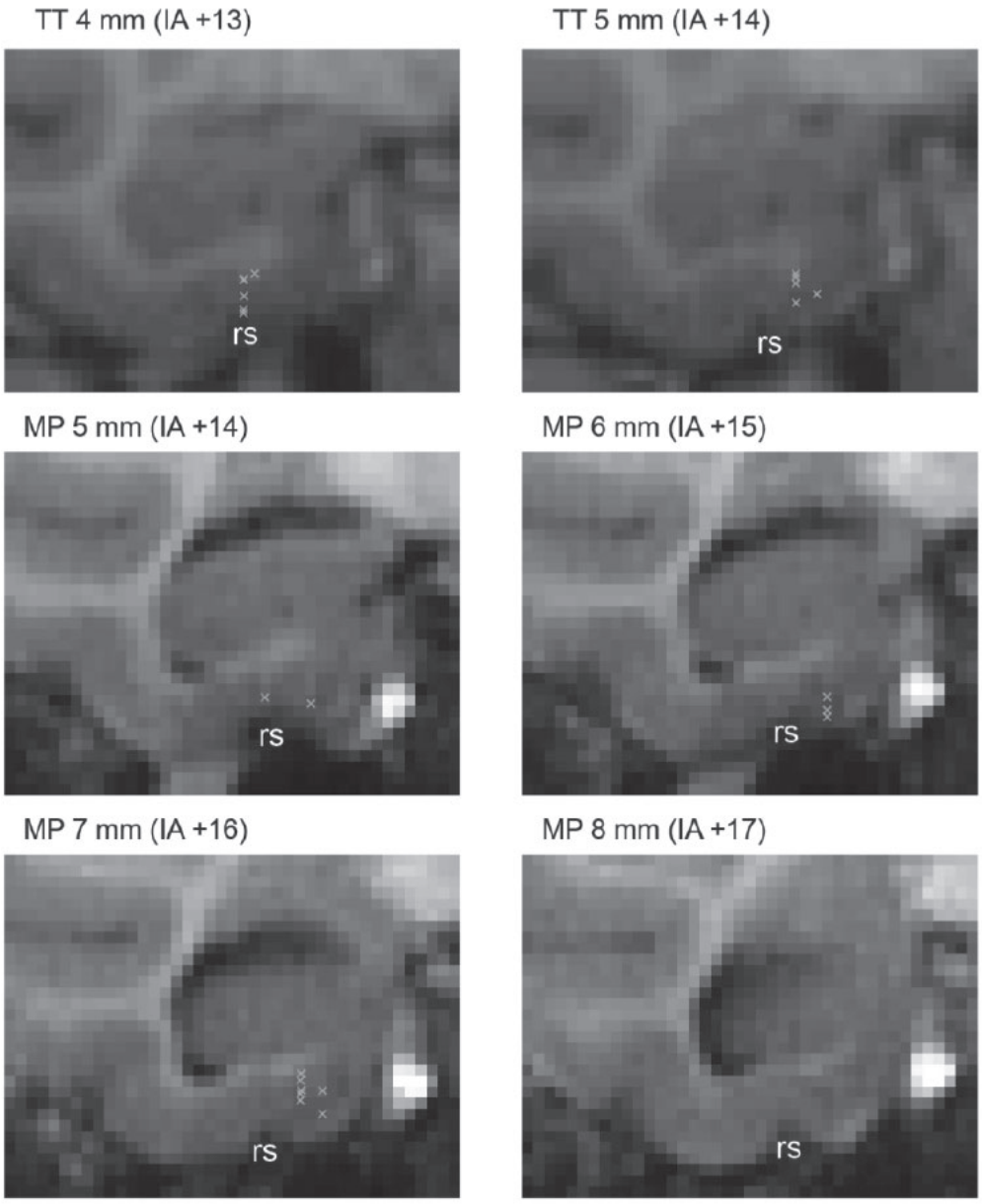

Figure 9. Locations of entorhinal grid cells in monkeys. Green markers label the locations of all 23 grid cells found in two monkeys (MP and TT). The monkey name, location anterior to the posterior border of the entorhinal cortex, and interaural location are given above each panel. rs: rhinal sulcus. 7 mm corresponded roughly to the midway point between the anterior and posterior borders of the EC. No grid cells were found anterior to this location. With permission from Killian et al., 2012 [71].

In the primate, PrS inputs project to the caudomedial entorhinal half, i.e. midway between the rostral and caudal borders of the EC, tapering off within area E*i* [16](Witter & Amaral, unpublished information) and thus partially impinging on what would qualify as "LEC" on the condition that our prediction that LEC is expanding is correct (**fig.8**). Experimental data in monkeys have demonstrated that grid cells, the defining "MEC" functional phenotype, have been found in the caudal EC half (**fig.9**) [71]. This is particularly interesting for two reasons. First, there is no cyto- nor chemoarchitectural border between medial and caudal EC in the primate at this level [16] emphasizing the discrepancy between the structural (i.e. based on neuronal chemo-architecture) and functional (i.e. behavioral-state dependent cellular physiological response) concepts of "MEC". Second, it would imply that the caudal part of the primate "LEC" could express a grid functional phenotype, i.e. a proof of concept that LEC and MEC implement uniform computations producing identical functional phenotype(s) dependent on the nature of their extrinsic inputs.

5.3. Remarkable features of the entorhinal network

5.3.1. Extrinsic input heterogeneity and entorhinal continuum

Prior to discovery of grid cells, it was generally assumed that EC was a high-order cortex buried too far away in the hierarchical organization of senses to reveal any readable spatial signal (**fig.10**) [298-300] and several *in vivo* electrophysiological recordings failed in fact to capture the grid one until electrodes were specifically placed in superficial layers of caudodorsal EC [64, 65]. Unlike the remaining EC, this caudodorsal portion in the rodent is in fact devoid of olfactory [14, 173, 181, 301, 302], prefrontal [173, 181, 183, 303-306], orbitofrontal [184, 307], insular [186], amygdaloid [308], POR and PER [36, 216] inputs while it receives only minor projections from somatosensory [173, 181] and posterior parietal [309] cortices. Olsen and colleagues analyzed in fact several injections of a genetically modified rabies virus distributed in caudomedial EC and found only substantial labelling in dorsal PrS and caudal PaS as well as POR and RSC [309], likely resulting from uptake in deep layers of area CE [183, 216, 310, 311]. In paper II, we conclude that substantial extrinsic inputs to superficial layers of caudomediodorsal EC originate exclusively from PrS and PaS, with both sharing the presence of strong direction signals [216, 281].

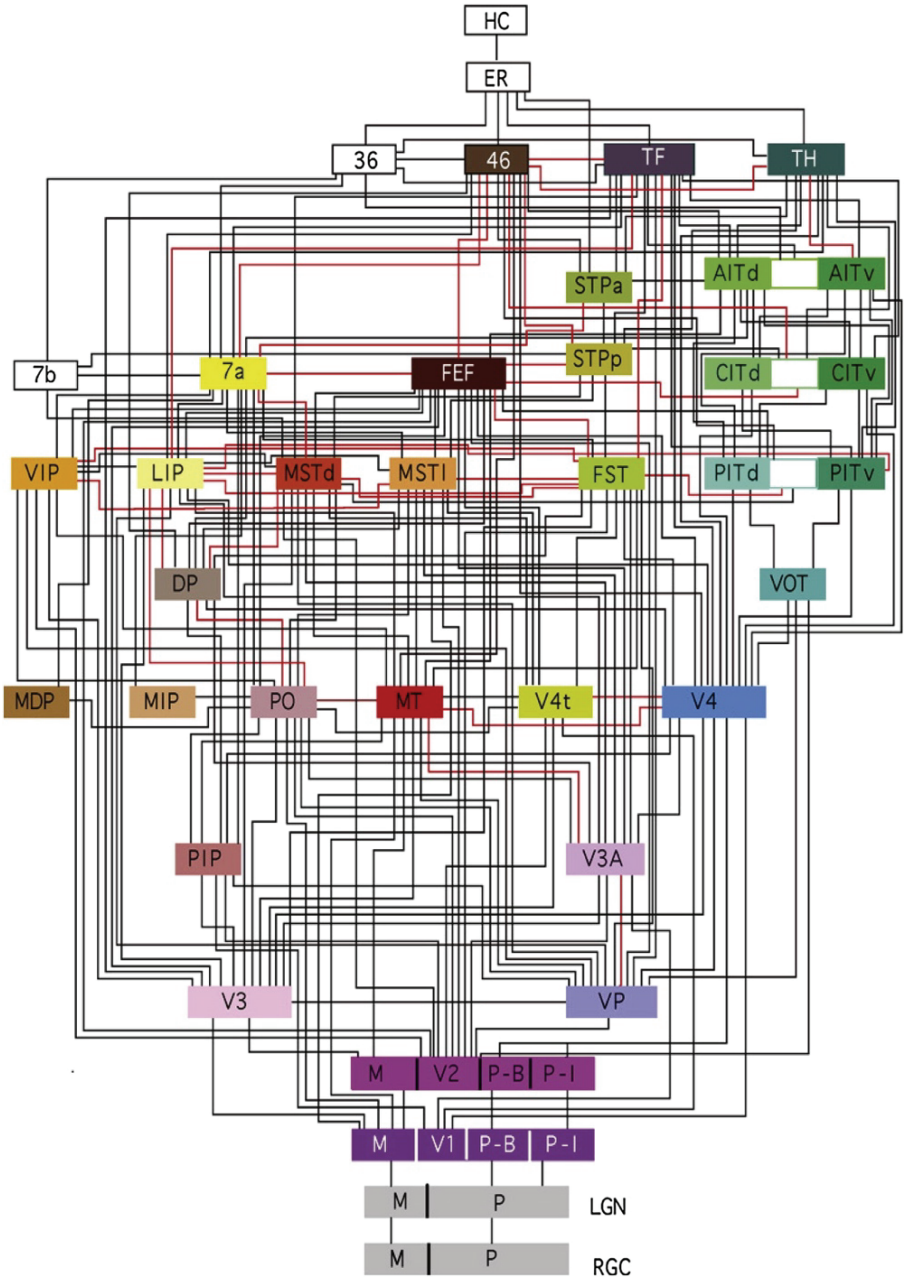

Figure 10. Hierarchy of visual areas. This hierarchy shows 32 visual cortical areas, starting at the retina ganglion cell (RGC) layer and projecting to the lateral geniculate nucleus (LGN) of the thalamus and further polysynaptically to perirhinal (Area 36, 36) and parahippocampal (TF/TH) cortices, which both project to entorhinal cortex (entorhinal region, ER) which further project to the hippocampal formation (hippocampus complex, HC). These areas are connected by 187 linkages, most of which have been demonstrated to be reciprocal pathways. Adapted with permission from Felleman & Van Essen, 1991 [312]

At the other entorhinal pole, rostrolateral EC contrasts with a surprising richness of input modalities such as the ones from the olfactory, prefrontal, orbitofrontal, insular, posterior parietal, postrhinal, perirhinal, ventral temporal association, dorsal anterior cingulate and somatosensory areas [14, 216, 294, 313]. In addition, it receives projections from the horizontal limb of the medial septal nuclei diagonal band, most of the amygdaloid nuclei, claustrum, several thalamic nuclei and ventral tegmental areas [14]. In fact, a recent network analysis performed on over 16.000 reports of histologically defined axonal connections between cortical regions in rat pointed to rostrolateral EC as comprising the richest set of association connections of any cerebral cortical region [314] in line with a previous large-scale anatomical study that reconstructed 240 intracortical connections manually within a common neuroanatomic framework [315]. In paper I, we argue that extrinsic inputs are primarily what shape the entorhinal functional output signal, which is in line with the critical function of this network to form high-order associations representing the external world [78, 198, 199, 201, 202, 208, 232, 316, 317] modulated by internal emotional states of the animal [186, 308, 318] producing an overall population signal which is unique for any point in time i.e. the temporal flow and content of the ongoing experience [201, 202, 232, 313].

However, it should be noted that between these two poles of the entorhinal continuum where extrinsic inputs are highly heterogeneous, certain set of extrinsic inputs usually considered to specifically impinge onto one or the other antipodal extreme converge. For instance, olfactory inputs strongly project onto EC but peculiarly avoid its caudomedial extreme [14, 173, 181, 301, 302]. In contrast, PrS and PaS inputs, which underpin the grid functional phenotype, strongly project onto EC but peculiarly avoid its rostrolateral extreme [55, 56](Witter Amaral, unpublished observations). Given that the entorhinal continuum process extrinsic inputs according to similar intrinsic network principles [22, 96, 98, 121, 122, 128, 313], it becomes intriguing to ponder how middle portions of the entorhinal continuum containing grid cells could process olfactory inputs.

Neuronal activity in rostrolateral portions of EC have been demonstrated to be clearly modulated by olfactory inputs [80, 98, 150]. In fact, *in vivo* two-photon calcium imaging of odor-evoked responses anesthetized mice demonstrated that over 90% of superficially located layer II Re neurons (i.e. putative fan cells) responded to olfactory stimulation either by a significant increase or decrease in overall activity [98]. These neurons showed a higher single

cell selectivity to specific odors and better population odor discrimination encoding than neighboring GABAergic layer II neurons by which they are interconnected [98, 313]. A possible explanation is that very sparse local excitatory connectivity between fan cells combined with surrounding stimulus-unselective inhibition may be what produce their restricted response spectra to olfactory stimuli [319]. If we now turn to fan cells counterpart at the caudomedial entorhinal pole, i.e. stellate cells, many qualify as grid cells with a clearly higher spatial selectivity than their neighboring fast spiking PV interneurons by which they are also interconnected [114, 115, 121-123, 128, 320]. Interestingly, fast spiking PV interneurons have been shown to be crucial for establishing the spatial periodicity characteristics of grid cells, as evident from observations that selective silencing of the former considerably reduces the spatial tuning of the latter [147]. Thus, it would be relevant to verify whether silencing GABAergic layer II entorhinal cells in different adjacent middle portions of the entorhinal continuum would similarly lead to a decrease stimulus selectivity in neighboring principal neurons to odor tuning. Favorable to this prediction, this mechanism has been reported in the neighboring piriform cortex [204, 321].

In conclusion, the concept of entorhinal continuum might allow us to interpret local changes in adjacent portions with identical structural network and functional phenotype while dissecting the effect of selected extrinsic inputs *in vivo*, *in vitro* and *in silico*. This approach will help us to relate the rodent entorhinal functional organization to the primate one where middle portions of the continuum likely expand as we suggested earlier [216, 313].

5.3.2. Functional intrinsic connectivity

Extensive AG and RG tracing experiments in the rat, cat and monkey have demonstrated that a dense network of intrinsic projections exists within the entire EC [36, 53, 100, 294, 322-325]. These projections have a comparable columnar radial, i.e. intra- and interlaminar local organization, distribution across the entire entorhinal continuum allowing intrinsic integration of extrinsic inputs locally as briefly touched upon in the introduction of the thesis [22, 96, 98, 121, 122, 128]. More relevant to the present discussion, neurons in deep and superficial layers also have extensive caudorostral intrinsic axonal projections, particularly the ones in close relation to RF [326], which distribute strongly to layers I-III [53, 294, 323, 325, 327]. By far, the most extensive fibers are the ones distributing in layer I which harbor multiple varicosities indicative of synaptic connectivity. Some fibers can also be found in deeper

layers, but they are generally thicker and smoother and appear mostly to represent passing fibers on their way to the angular bundle [53]. Thus, EC intrinsic connectivity suggests a strong functional integration across rostrocaudal bands parallel to RF where neurons with superficial dendritic trees appear to be the major postsynaptic targets, i.e. primarily located in layers II-III but also LV whose neurons have particularly developed apical dendritic tufts [109, 218, 328, 329]. Therefore, a better understanding of the rostrocaudal entorhinal intrinsic connectivity is instrumental to better understand its overall function.

Previous studies in the rodents and primates have demonstrated that intrinsic projections of the caudomedial entorhinal part are more pronounced than their rostrolateral counterparts [53, 325]. In paper IV, one of the key finding is that the projections of Cb cells in layer II of EC form a major excitatory drive within areas in the same caudomedio-rostrolateral bands [97, 99, 205, 330]. In paper III, we noticed that optogenetic fiber stimulation from distant caudodorsal entorhinal somata triggered both EPSPs and IPSPs in rostrolateral entorhinal layer II principal cells. We further postulated that the inhibitory component primarily arise from caudomedial entorhinal long range SOM GABAergic neurons which emit specific projections that runs intrinsically rostrolaterally within layer I [294]. As suggested by earlier work [96, 98, 205, 331], we report in paper IV that the vast majority of entorhinal layer II Cb neurons are excitatory and also project specifically and extensively within layer I [100, 294]. Interestingly, caudomedial entorhinal LII Cb neurons, i.e. pyramidal cells, have been reported to be able to harbor a grid functional phenotype [111, 112] contrasting with their local SOM GABAergic neighbors which are part of a distinct functional subcircuit that seems in fact to be more influential on non-spatial information processing [147, 332]. Together, this opens the interesting possibility that two distinctive cell types in caudomedial entorhinal cortex which contain different functional information potentially contact distant rostrolateral neurons with dendritic trees in layer I, e.g. layer II principal cells, with antagonistic effects [100, 294].

In paper II, we provide new data emphasizing that the rostrolateral entorhinal portion in close relation with RF constitutes the major polysensory gateway [11, 216] for uni- and polysensory inputs to enter EC [53, 325] which strikingly contrast with the paucity of inputs to superficial caudomediodorsal EC that enclose grid cells. This is of particular interest since grid cells have been shown to provide more than a fixed metric for space as their regular firing pattern can anchor to local cues such as the location of the walls of the recording arena [65], rotate in relation to cues on the walls [65], expand or contract when one of the walls is

moved to make the box longer or shorter respectively [217, 333], progressively merge into a single pattern when two environments with distinct grid patterns fuse [334] or exhibit stereotypical spatial distortions that depends on the environment geometry [335-338]. A recent pair of studies revealed in fact that grid cells can even be modulated by pure cognitive factors [339, 340] and encode navigational variables beyond euclidean space such as within an auditory space [214] or other abstract mental ones [341, 342]. Thus, grid cells have been recently proposed to map cognitive spaces spanned by relevant feature dimensions [237]. Anatomically, highly multimodal information contained within rostrolateral EC portions seems to be the most logical candidate to provide caudomedial portions with the relevant variable of the feature dimension(s). In paper IV, we demonstrate that rostrolateral entorhinal layer II Cb neurons distribute specifically and strongly to layer I of the caudomedial entorhinal portions [100]. In fact, retrograde monosynaptic tracing with a modified rabies virus have revealed that caudomedial stellate cells, i.e. putative grid cells, receive direct inputs from rostrolateral entorhinal layer II neurons [135]. Using a similar method, caudomedial fast spiking PV interneurons necessary for grid formation [121, 122, 147] have been demonstrated to receive their rostrolateral entorhinal input almost exclusively from LIIa neurons projecting to DG, i.e. Re cells [343]. In contrast, caudomedial SOM interneurons that are part of a distinct functional subcircuit [147] also receive monosynaptic inputs from rostrolateral EC albeit significantly less and essentially from non-hippocampal projecting neurons scattered across all layers [343]. Taken together, this suggests that rostrolateral entorhinal neurons in layer IIa (i.e. Re) could inhibit distant caudomedial superficial entorhinal ones indirectly by way of local caudomedial PV fast spiking INs [121, 122] while the ones located in layer IIb (i.e. Cb) could potentially excite distant caudomedial superficial entorhinal neurons directly.

In conclusion, deciphering the rostrocaudal connectivity of the intrinsic entorhinal cortex will indeed require further experimental investigations in order to assess their implication on the overall entorhinal continuum functions. It seems however that rostrolateral entorhinal cortex could potentially provide the relevant feature dimension in which caudomedial grid cells fire decipherable regular patterns[214, 237, 341, 342], which in return could provide to the rostrolateral entorhinal network with spatial information by way of an complex dominant input going into the opposite direction [100, 111, 112, 294].

5.3.3. The perirhinal-entorhinal interface

In rodents and primates, PER has been shown to integrate uni- and polysensory inputs into complex perceptual object representations as reflected by its ability to discriminate novelty from familiarity [161, 162, 164-168, 344]. As we saw in papers II and III, the whole PER rostrocaudal extend projects heavily to superficial layers of rostrolateral EC [35, 36, 173, 181, 216, 345, 346] where it targets both principal neurons but also local PV and SOM interneurons [139, 216, 294, 347, 348]. Although this projection is largely constituted by excitatory neurons [139], we noticed that over 10% originates in fact from long range GABAergic cells [294], which is in line with previous reports in the guinea pig [321]. Results from *in vivo* and *in vitro* electrophysiological recordings have demonstrated in fact that the PER-EC interface is endowed with a powerful intrinsic inhibitory system [321] that requires the convergence of at least two coincident inputs in time and space e.g. from the amygdala, perirhinal, temporal association, insular and medial prefrontal cortices [326, 349-355] to be overcome. This "wall of inhibition" actively gates signal traffic from the neocortex whose topographically segregated rostrocaudal projections contrasts with the extensive PER associative properties [36, 324, 345, 356-358]. Interestingly, PER is also extensively connected with POR [36], and we demonstrate in paper II that the latter also projects to EC in a strikingly similar manner than the former [216]. Although POR projections to EC seem essentially excitatory in nature, they form both monosynaptic contact with entorhinal principal neurons and interneurons [216]. Since it is believed that the mechanisms require amplification and selection of activity patterns along rhinal associative connections likely in relation with extrinsic inputs coincidence detection [349], POR might also be a player of substance in gating impulses through this "wall of inhibition". In paper III, we demonstrated that intrinsic projections from caudomedial entorhinal portions also emit long range GABAergic projections contacting principal rostrolateral entorhinal hippocampal projecting cells [294]. In paper IV, we demonstrate that principal layer II entorhinal Cb neurons located at the PER-EC interface strongly project to PER [100]. Thus, all these inputs certainly influence directly and indirectly the perirhinal-entorhinal-hippocampal interface in an elaborate manner which awaits further investigation to dissect relevant key mechanisms.
A noteworthy feature of the perirhinal-entorhinal interface relies on the simple observation that PER axons have an orthogonal distribution in relation to the remaining extrinsic inputs impinging on superficial rostrolateral EC [36, 37, 53, 57, 100, 184, 216, 294, 325, 327]. This is of particular interest in light of the peculiar morphology of hippocampal-projecting fan

cells with their unique large circular dendritic trees spanning 900 μm [218]. Thus, it might represent a fundamental physical organization principle for restricted parts of PER to select relevant entorhinal fan cells in light of their preferred disynaptic inhibitory connectivity [128] i.e. synonym of 'lateral inhibition' which increases contrast perception. they further shape the overall EC-HF signal according to selected sensory domains.

In paper I, the suggestion is brought up that extensive inputs to PER and EC such as the ones from insular cortex and amygdala might endow the PER/EC interface with the ability to evaluate sensory cues of a particular episodic memory together with the emotional value of individual elements of the context or the context as a whole [313]. In that regard, another relevant input originates from midbrain dopamine neurons [359], i.e. ventral tegmental area [57, 303, 360-362] and to a lesser degree substantia nigra [360, 363, 364], which project densely to rostrolateral portions of the entorhinal cortex where they form synaptic contact with principal neurons in layer II [361]. Dopamine is typically involve in maintaining memory processes by facilitating synaptic transmission [365], spontaneous activity, and firing rates of neurons [366-368]. In fact, rostrolateral entorhinal fan cells have been recently shown to display selective facilitation of excitatory postsynaptic potentials following exposure to low physiological dose of dopamine [369]. Thus, while amygdala and insular inputs might provide the entorhinal network with an emotional tag, dopamine modulation likely endows rostrolateral entorhinal high-order associations of the external world with a reward value.

6. Conclusion

In conclusion, a reappraisal of the prevailing model of the medial temporal lobe memory system is due and necessary. In this thesis, I aimed to demonstrate the historical conflict that gradually emerged between the concepts of structurally defined and functionally distinct medial and lateral entorhinal cortices. In order to reconciliate this discrepancy, I suggest that the entorhinal cortex might be best considered as a generalist circuit structurally organized as a functional continuum whose differences in probed phenotype reflect primarily local extrinsic inputs. In this continuum, caudomedial portions seemingly provide a positional code in space whereas rostrolateral ones encode the ongoing content of the external world experience. Of course, and logically, these portions interact and both signals seem present across the entire continuum likely supported by the extremely dense entorhinal intrinsic associational connectivity. This concept might help us to relate the functional organization of rodent and primate entorhinal cortices and thus provide ground for further translation into the human one.

7. References

1. Scoville, W.B. and B. Milner, *Loss of recent memory after bilateral hippocampal lesions.* J Neurol Neurosurg Psychiatry, 1957. 20(1): p. 11-21.
2. Annese, J., et al., *Postmortem examination of patient H.M.'s brain based on histological sectioning and digital 3D reconstruction.* Nat Commun, 2014. 5: p. 3122.
3. Augustinack, J.C., et al., *H.M.'s contributions to neuroscience: a review and autopsy studies.* Hippocampus, 2014. 24(11): p. 1267-86.
4. Bliss, T.V. and T. Lomo, *Plasticity in a monosynaptic cortical pathway.* J Physiol, 1970. 207(2): p. 61P.
5. O'Keefe, J. and J. Dostrovsky, *The hippocampus as a spatial map. Preliminary evidence from unit activity in the freely-moving rat.* Brain Res, 1971. 34(1): p. 171-5.
6. O'Keefe, J. and L. Nadel, *The Hippocampus as a cognitive map*. 1978, Oxford: Clarendon Press.
7. Moser, E.I., M.B. Moser, and B.L. McNaughton, *Spatial representation in the hippocampal formation: a history.* Nat Neurosci, 2017. 20(11): p. 1448-1464.
8. Manns, J.R. and H. Eichenbaum, *Evolution of declarative memory.* Hippocampus, 2006. 16(9): p. 795-808.
9. Strange, B.A., et al., *Functional organization of the hippocampal longitudinal axis.* Nat Rev Neurosci, 2014. 15(10): p. 655-69.
10. Burwell, R.D., M.P. Witter, and D.G. Amaral, *Perirhinal and postrhinal cortices of the rat: a review of the neuroanatomical literature and comparison with findings from the monkey brain.* Hippocampus, 1995. 5(5): p. 390-408.
11. Insausti, R., M.T. Herrero, and M.P. Witter, *Entorhinal cortex of the rat: cytoarchitectonic subdivisions and the origin and distribution of cortical efferents.* Hippocampus, 1997. 7(2): p. 146-83.
12. Burwell, R.D., *Borders and cytoarchitecture of the perirhinal and postrhinal cortices in the rat.* J Comp Neurol, 2001. 437(1): p. 17-41.
13. Boccara, C.N., et al., *A three-plane architectonic atlas of the rat hippocampal region.* Hippocampus, 2015. 25(7): p. 838-57.
14. Cappaert, N.L.M., N.M. Van Strien, and M.P. Witter, *Hippocampal Formation.* The Rat Nervous System, Paxinos G., 2015. 4th(20): p. 511-573.
15. Insausti, R., D.G. Amaral, and W.M. Cowan, *The entorhinal cortex of the monkey: II. Cortical afferents.* J Comp Neurol, 1987. 264(3): p. 356-95.
16. Amaral, D.G., R. Insausti, and W.M. Cowan, *The entorhinal cortex of the monkey: I. Cytoarchitectonic organization.* J Comp Neurol, 1987. 264(3): p. 326-55.
17. Witter, M.P., et al., *Functional organization of the extrinsic and intrinisic circuitry of the Parahippocampal region.* Prog Neurobiol, 1989. 33: p. 161-253.
18. van Strien, N.M., N.L. Cappaert, and M.P. Witter, *The anatomy of memory: an interactive overview of the parahippocampal-hippocampal network.* Nat Rev Neurosci, 2009. 10(4): p. 272-82.
19. Kjonigsen, L.J., et al., *Waxholm Space atlas of the rat brain hippocampal region: three-dimensional delineations based on magnetic resonance and diffusion tensor imaging.* Neuroimage, 2015. 108: p. 441-9.
20. Papp, E.A., et al., *Waxholm Space atlas of the Sprague Dawley rat brain.* Neuroimage, 2014. 97: p. 374-86.

21. Surmeli, G., et al., *Molecularly Defined Circuitry Reveals Input-Output Segregation in Deep Layers of the Medial Entorhinal Cortex.* Neuron, 2015. 88(5): p. 1040-1053.
22. Ohara, S., et al., *Intrinsic Projections of Layer Vb Neurons to Layers Va, III, and II in the Lateral and Medial Entorhinal Cortex of the Rat.* Cell Rep, 2018. 24(1): p. 107-116.
23. Kosel, K.C., G.W. Van Hoesen, and D.L. Rosene, *Non-hippocampal cortical projections from the entorhinal cortex in the rat and rhesus monkey.* Brain research, 1982. 244(2): p. 201-13.
24. Ramsden, H.L., et al., *Laminar and dorsoventral molecular organization of the medial entorhinal cortex revealed by large-scale anatomical analysis of gene expression.* PLoS Comput Biol, 2015. 11(1): p. e1004032.
25. Swanson, L.W. and C. Kohler, *Anatomical evidence for direct projections from the entorhinal area to the entire cortical mantle in the rat.* J Neurosci, 1986. 6(10): p. 3010-23.
26. van Hoesen, G.W., *The parahippocampal gyrus: New observations regarding its cortical connections in the monkey.* Trends Neurosci, 1982. 5 p. 345-350.
27. Witter, M.P., et al., *Architecture of the Entorhinal Cortex A Review of Entorhinal Anatomy in Rodents with Some Comparative Notes.* Front Syst Neurosci, 2017. 11: p. 46.
28. Kobro-Flatmoen, A. and M.P. Witter, *Neuronal chemo-architecture of the entorhinal cortex: A comparative review.* Eur J Neurosci, 2019.
29. Steward, O., *Topographic organization of the projections from the entorhinal area to the hippocampal formation of the rat.* J Comp Neurol, 1976. 167(3): p. 285-314.
30. Steward, O. and S.A. Scoville, *Cells of origin of entorhinal cortical afferents to the hippocampus and fascia dentata of the rat.* J Comp Neurol, 1976. 169(3): p. 347-70.
31. Witter, M.P. and D.G. Amaral, *Entorhinal cortex of the monkey: V. Projections to the dentate gyrus, hippocampus, and subicular complex.* J Comp Neurol, 1991. 307(3): p. 437-59.
32. Shipley, M.T., *The topographical and laminar organization of the presubiculum's projection to the ipsi- and contralateral entorhinal cortex in the guinea pig.* Journal of comparative neurology, 1975. 160(1): p. 127-45.
33. Kohler, C., *Morphological details of the projection from the presubiculum to the entorhinal area as shown with the novel PHA-L immunohistochemical tracing method in the rat.* Neuroscience Letters, 1984. 45(3): p. 285-290.
34. Room, P. and H.J. Groenewegen, *Connections of the parahippocampal cortex. I. Cortical afferents.* Journal of comparative neurology, 1986. 251(4): p. 415-450.
35. Naber, P.A., et al., *Parallel input to the hippocampal memory system through peri- and postrhinal cortices.* Neuroreport, 1997. 8(11): p. 2617-21.
36. Burwell, R.D. and D.G. Amaral, *Perirhinal and postrhinal cortices of the rat: interconnectivity and connections with the entorhinal cortex.* J Comp Neurol, 1998. 391(3): p. 293-321.
37. Suzuki, W.A. and D.G. Amaral, *Topographic Organization of the Reciprocal Connections between the Monkey Entorhinal Cortex and the Perirhinal and Parahippocampal Cortices.* Journal of Neuroscience, 1994. 14(3): p. 1856-1877.
38. Koganezawa, N., et al., *Excitatory Postrhinal Projections to Principal Cells in the Medial Entorhinal Cortex.* J Neurosci, 2015. 35(48): p. 15860-74.
39. Schultz, H., T. Sommer, and J. Peters, *Direct evidence for domain-sensitive functional subregions in human entorhinal cortex.* J Neurosci, 2012. 32(14): p. 4716-23.
40. Maass, A., et al., *Functional subregions of the human entorhinal cortex.* Elife, 2015. 4: p. e06426.

41. Navarro Schroder, T., et al., *Functional topography of the human entorhinal cortex.* Elife, 2015. 4: p. e06738.
42. Eichenbaum, H., A.P. Yonelinas, and C. Ranganath, *The medial temporal lobe and recognition memory.* Annu Rev Neurosci, 2007. 30: p. 123-52.
43. Eichenbaum, H., et al., *Towards a functional organization of episodic memory in the medial temporal lobe.* Neuroscience and Biobehavioral Reviews, 2012. 36(7): p. 1597-608.
44. Ritchey, M., L.A. Libby, and C. Ranganath, *Cortico-hippocampal systems involved in memory and cognition: the PMAT framework.* Prog Brain Res, 2015. 219: p. 45-64.
45. Ranganath, C. and M. Ritchey, *Two cortical systems for memory-guided behaviour.* Nat Rev Neurosci, 2012. 13(10): p. 713-26.
46. Knierim, J.J., I. Lee, and E.L. Hargreaves, *Hippocampal place cells: parallel input streams, subregional processing, and implications for episodic memory.* Hippocampus, 2006. 16(9): p. 755-64.
47. Jarrard, L.E., *Selective hippocampal lesions: differential effects on performance by rats of a spatial task with preoperative versus postoperative training.* Journal of Comparative and Physiological Psychology, 1978. 92(6): p. 1119-27.
48. Witter, M.P., et al., *Functional organization of the extrinsic and intrinsic circuitry of the parahippocampal region.* Prog Neurobiol, 1989. 33(3): p. 161-253.
49. Brun, V.H., et al., *Place cells and place recognition maintained by direct entorhinal-hippocampal circuitry.* Science, 2002. 296(5576): p. 2243-6.
50. Jung, M.W., S.I. Wiener, and B.L. McNaughton, *Comparison of spatial firing characteristics of units in dorsal and ventral hippocampus of the rat.* Journal of neuroscience, 1994. 14(12): p. 7347-7356.
51. Moser, E., M.B. Moser, and P. Andersen, *Spatial learning impairment parallels the magnitude of dorsal hippocampal lesions, but is hardly present following ventral lesions.* Journal of Neuroscience, 1993. 13(9): p. 3916-25.
52. Moser, M.B. and E.I. Moser, *Functional differentiation in the hippocampus.* Hippocampus, 1998. 8(6): p. 608-19.
53. Dolorfo, C.L. and D.G. Amaral, *Entorhinal cortex of the rat: organization of intrinsic connections.* J Comp Neurol, 1998. 398(1): p. 49-82.
54. Dolorfo, C.L. and D.G. Amaral, *Entorhinal cortex of the rat: topographic organization of the cells of origin of the perforant path projection to the dentate gyrus.* J Comp Neurol, 1998. 398(1): p. 25-48.
55. Caballero-Bleda, M. and M.P. Witter, *Regional and laminar organization of projections from the presubiculum and parasubiculum to the entorhinal cortex: an anterograde tracing study in the rat.* J Comp Neurol, 1993. 328(1): p. 115-29.
56. Honda, Y. and N. Ishizuka, *Organization of connectivity of the rat presubiculum: I. Efferent projections to the medial entorhinal cortex.* J Comp Neurol, 2004. 473(4): p. 463-84.
57. Beckstead, R.M., *Afferent conenctions of the entorhinal area in the rats as demonstrated by retrograde cell-labeling with horseradish peroxidase.* Brain Res, 1978.
58. Vogt, B.A. and M.W. Miller, *Cortical connections between rat cingulate cortex and visual, motor, and postsubicular cortices.* J Comp Neurol, 1983. 216(2): p. 192-210.
59. van Groen, T. and J.M. Wyss, *Connections of the retrosplenial granular a cortex in the rat.* J Comp Neurol, 1990. 300(4): p. 593-606.
60. van Groen, T. and J.M. Wyss, *The connections of presubiculum and parasubiculum in the rat.* Brain Res, 1990. 518(1-2): p. 227-43.

61. Van Groen, T. and J.M. Wyss, *Connections of the retrosplenial granular b cortex in the rat.* J Comp Neurol, 2003. 463(3): p. 249-63.
62. Wyss, J.M. and T. Vangroen, *Connections between the Retrosplenial Cortex and the Hippocampal-Formation in the Rat - a Review.* Hippocampus, 1992. 2(1): p. 1-12.
63. Shibata, H., *Terminal distribution of projections from the retrosplenial area to the retrohippocampal region in the rat, as studied by anterograde transport of biotinylated dextran amine.* Neurosci Res, 1994. 20(4): p. 331-6.
64. Fyhn, M., et al., *Spatial representation in the entorhinal cortex.* Science, 2004. 305(5688): p. 1258-64.
65. Hafting, T., et al., *Microstructure of a spatial map in the entorhinal cortex.* Nature, 2005. 436(7052): p. 801-6.
66. Sargolini, F., et al., *Conjunctive representation of position, direction, and velocity in entorhinal cortex.* Science, 2006. 312(5774): p. 758-62.
67. Boccara, C.N., et al., *Grid cells in pre- and parasubiculum.* Nat Neurosci, 2010. 13(8): p. 987-94.
68. Brandon, M.P., et al., *Reduction of theta rhythm dissociates grid cell spatial periodicity from directional tuning.* Science, 2011. 332(6029): p. 595-9.
69. Burgalossi, A., et al., *Microcircuits of functionally identified neurons in the rat medial entorhinal cortex.* Neuron, 2011. 70(4): p. 773-86.
70. Yartsev, M.M., M.P. Witter, and N. Ulanovsky, *Grid cells without theta oscillations in the entorhinal cortex of bats.* Nature, 2011. 479(7371): p. 103-7.
71. Killian, N.J., M.J. Jutras, and E.A. Buffalo, *A map of visual space in the primate entorhinal cortex.* Nature, 2012. 491(7426): p. 761-4.
72. Kropff, E., et al., *Speed cells in the medial entorhinal cortex.* Nature, 2015. 523(7561): p. 419-24.
73. Hargreaves, E.L., et al., *Major dissociation between medial and lateral entorhinal input to dorsal hippocampus.* Science, 2005. 308(5729): p. 1792-4.
74. Deshmukh, S.S. and J.J. Knierim, *Representation of non-spatial and spatial information in the lateral entorhinal cortex.* Front Behav Neurosci, 2011. 5: p. 69.
75. Tsao, A., M.B. Moser, and E.I. Moser, *Traces of experience in the lateral entorhinal cortex.* Curr Biol, 2013. 23(5): p. 399-405.
76. Suzuki, W.A., E.K. Miller, and R. Desimone, *Object and place memory in the macaque entorhinal cortex.* J Neurophysiol, 1997. 78(2): p. 1062-81.
77. Gauthier, M. and B. Soumireu-Mourat, *6-Hydroxydopamine and radiofrequency lesions of the lateral entorhinal cortex facilitate an operant appetitive conditioning task in mice.* Neurosci Lett, 1981. 24(2): p. 193-7.
78. Van Cauter, T., et al., *Distinct roles of medial and lateral entorhinal cortex in spatial cognition.* Cereb Cortex, 2013. 23(2): p. 451-9.
79. Zhu, X.O., M.W. Brown, and J.P. Aggleton, *Neuronal signalling of information important to visual recognition memory in rat rhinal and neighbouring cortices.* European Journal of Neuroscience, 1995. 7(4): p. 753-65.
80. Young, B.J., et al., *Memory representation within the parahippocampal region.* Journal of Neuroscience, 1997. 17(13): p. 5183-5195.
81. McNaughton, B.L., et al., *Path integration and the neural basis of the 'cognitive map'.* Nature reviews. Neuroscience, 2006. 7(8): p. 663-678.
82. Yoganarasimha, D., G. Rao, and J.J. Knierim, *Lateral entorhinal neurons are not spatially selective in cue-rich environments.* Hippocampus, 2010.
83. Ferbinteanu, J., R.M.D. Holsinger, and R.J. McDonald, *Lesions of the medial or lateral perforant path have different effects on hippocampal contributions to place*

learning and on fear conditioning to context. Behavioural Brain Research, 1999. 101(1): p. 65-84.
84. Henriksen, E.J., et al., *Spatial representation along the proximodistal axis of CA1.* Neuron, 2010. 68(1): p. 127-37.
85. Burke, S.N., et al., *The influence of objects on place field expression and size in distal hippocampal CA1.* Hippocampus, 2011. 21(7): p. 783-801.
86. Witter, M.P., et al., *Anatomical organization of the parahippocampal-hippocampal network.* Ann N Y Acad Sci, 2000. 911: p. 1-24.
87. Lu, L., et al., *Impaired hippocampal rate coding after lesions of the lateral entorhinal cortex.* Nat Neurosci, 2013. 16(8): p. 1085-93.
88. Hales, J.B., et al., *Medial entorhinal cortex lesions only partially disrupt hippocampal place cells and hippocampus-dependent place memory.* Cell Rep, 2014. 9(3): p. 893-901.
89. Brun, V.H., et al., *Impaired spatial representation in CA1 after lesion of direct input from entorhinal cortex.* Neuron, 2008. 57(2): p. 290-302.
90. Van Cauter, T., B. Poucet, and E. Save, *Unstable CA1 place cell representation in rats with entorhinal cortex lesions.* The European journal of neuroscience, 2008. 27(8): p. 1933-46.
91. Schlesiger, M.I., et al., *The medial entorhinal cortex is necessary for temporal organization of hippocampal neuronal activity.* Nature Neuroscience, 2015. 18(8): p. 1123-1132.
92. Fyhn, M., et al., *Grid cells in mice.* Hippocampus, 2008. 18(12): p. 1230-8.
93. Doeller, C.F., C. Barry, and N. Burgess, *Evidence for grid cells in a human memory network.* Nature, 2010. 463(7281): p. 657-61.
94. Jacobs, J., et al., *Direct recordings of grid-like neuronal activity in human spatial navigation.* Nat Neurosci, 2013. 16(9): p. 1188-90.
95. Rowland, D.C., et al., *Ten Years of Grid Cells.* Annu Rev Neurosci, 2016. 39: p. 19-40.
96. Fuchs, E.C., et al., *Local and Distant Input Controlling Excitation in Layer II of the Medial Entorhinal Cortex.* Neuron, 2016. 89(1): p. 194-208.
97. Kitamura, T., et al., *Island cells control temporal association memory.* Science, 2014. 343(6173): p. 896-901.
98. Leitner, F.C., et al., *Spatially segregated feedforward and feedback neurons support differential odor processing in the lateral entorhinal cortex.* Nat Neurosci, 2016. 19(7): p. 935-44.
99. Varga, C., S.Y. Lee, and I. Soltesz, *Target-selective GABAergic control of entorhinal cortex output.* Nat Neurosci, 2010. 13(7): p. 822-4.
100. Ohara, S., et al., *Entorhinal layer II calbindin-expressing neurons originate widespread telencephalic and intrinsic projections.* Front Syst Neurosci, 2019. 13:54.
101. Zutshi, I., et al., *Recurrent circuits within medial entorhinal cortex superficial layers support grid cell firing.* Nat Commun, 2018. 9(1): p. 3701.
102. Germroth, P., W.K. Schwerdtfeger, and E.H. Buhl, *Morphology of identified entorhinal neurons projecting to the hippocampus. A light microscopical study combining retrograde tracing and intracellular injection.* Neuroscience, 1989. 30(3): p. 683-91.
103. Tunon, T., et al., *Parvalbumin and calbindin D-28K in the human entorhinal cortex. An immunohistochemical study.* Brain Research, 1992. 589(1): p. 24-32.
104. Fujimaru, Y. and T. Kosaka, *The distribution of two calcium binding proteins, calbindin D-28K and parvalbumin, in the entorhinal cortex of the adult mouse.* Neurosci Res, 1996. 24(4): p. 329-43.

105. Wouterlood, F.G., *Spotlight on the neurones (I): cell types, local connectivity, microcircuits and distribution of markers*, in *The Parahippocampal Region. Organization and Role in Cognitive Function.*, M.P. Witter and F.G. Wouterlood, Editors. 2002, Oxford University Press: Oxford. p. 61-88.
106. Ramos-Moreno, T., et al., *Extracellular matrix molecules and synaptic plasticity: immunomapping of intracellular and secreted Reelin in the adult rat brain.* Eur J Neurosci, 2006. 23(2): p. 401-22.
107. Klink, R. and A. Alonso, *Ionic mechanisms of muscarinic depolarization in entorhinal cortex layer II neurons.* Journal of Neurophysiology, 1997. 77(4): p. 1829-43.
108. Alonso, A. and R.R. Llinas, *Subthreshold Na+-dependent theta-like rhythmicity in stellate cells of entorhinal cortex layer II.* Nature, 1989. 342(6246): p. 175-177.
109. Canto, C.B. and M.P. Witter, *Cellular properties of principal neurons in the rat entorhinal cortex. II. The medial entorhinal cortex.* Hippocampus, 2012. 22(6): p. 1277-99.
110. Zhang, S.J., et al., *Optogenetic dissection of entorhinal-hippocampal functional connectivity.* Science, 2013. 340(6128): p. 1232627.
111. Domnisoru, C., A.A. Kinkhabwala, and D.W. Tank, *Membrane potential dynamics of grid cells.* Nature, 2013. 495(7440): p. 199-204.
112. Schmidt-Hieber, C. and M. Hausser, *Cellular mechanisms of spatial navigation in the medial entorhinal cortex.* Nat Neurosci, 2013. 16(3): p. 325-31.
113. Sun, C., et al., *Distinct speed dependence of entorhinal island and ocean cells, including respective grid cells.* Proc Natl Acad Sci U S A, 2015. 112(30): p. 9466-71.
114. Rowland, D.C., et al., *Functional properties of stellate cells in medial entorhinal cortex layer II.* Elife, 2018. 7.
115. Tang, Q., et al., *Pyramidal and stellate cell specificity of grid and border representations in layer 2 of medial entorhinal cortex.* Neuron, 2014. 84(6): p. 1191-7.
116. Latuske, P., O. Toader, and K. Allen, *Interspike Intervals Reveal Functionally Distinct Cell Populations in the Medial Entorhinal Cortex.* J Neurosci, 2015. 35(31): p. 10963-76.
117. Fuhs, M.C. and D.S. Touretzky, *A spin glass model of path integration in rat medial entorhinal cortex.* Journal of neuroscience, 2006. 26(16): p. 4266-4276.
118. McNaughton, B.L., et al., *Path integration and the neural basis of the 'cognitive map'.* Nat Rev Neurosci, 2006. 7(8): p. 663-78.
119. Guanella, A., D. Kiper, and P. Verschure, *A model of grid cells based on a twisted torus topology.* International Journal of Neural Systems, 2007. 17(4): p. 231-240.
120. Burak, Y. and I.R. Fiete, *Accurate path integration in continuous attractor network models of grid cells.* PLoS Comput Biol, 2009. 5(2): p. e1000291.
121. Couey, J.J., et al., *Recurrent inhibitory circuitry as a mechanism for grid formation.* Nat Neurosci, 2013. 16(3): p. 318-24.
122. Pastoll, H., et al., *Feedback inhibition enables theta-nested gamma oscillations and grid firing fields.* Neuron, 2013. 77(1): p. 141-54.
123. Buetfering, C., K. Allen, and H. Monyer, *Parvalbumin interneurons provide grid cell-driven recurrent inhibition in the medial entorhinal cortex.* Nat Neurosci, 2014. 17(5): p. 710-8.
124. Lefort, S., et al., *The excitatory neuronal network of the C2 barrel column in mouse primary somatosensory cortex.* Neuron, 2009. 61(2): p. 301-16.
125. Seeman, S.C., et al., *Sparse recurrent excitatory connectivity in the microcircuit of the adult mouse and human cortex.* Elife, 2018. 7.

126. Jouhanneau, J.S., et al., *In Vivo Monosynaptic Excitatory Transmission between Layer 2 Cortical Pyramidal Neurons.* Cell Rep, 2015. 13(10): p. 2098-106.
127. Yoganarasimha, D., G. Rao, and J.J. Knierim, *Lateral entorhinal neurons are not spatially selective in cue-rich environments.* Hippocampus, 2011. 21(12): p. 1363-74.
128. Nilssen, E.S., et al., *Inhibitory Connectivity Dominates the Fan Cell Network in Layer II of Lateral Entorhinal Cortex.* J Neurosci, 2018. 38(45): p. 9712-9727.
129. Lanciego, J.L. and F.G. Wouterlood, *A half century of experimental neuroanatomical tracing.* J Chem Neuroanat, 2011. 42(3): p. 157-83.
130. Wouterlood, F.G., et al., *A fourth generation of neuroanatomical tracing techniques: exploiting the offspring of genetic engineering.* J Neurosci Methods, 2014. 235: p. 331-48.
131. Chen, S. and G. Aston-Jones, *Axonal collateral-collateral transport of tract tracers in brain neurons: false anterograde labelling and useful tool.* Neuroscience, 1998. 82(4): p. 1151-63.
132. Reiner, A., et al., *Pathway tracing using biotinylated dextran amines.* J Neurosci Methods, 2000. 103(1): p. 23-37.
133. Veenman, C.L., A. Reiner, and M.G. Honig, *Biotinylated dextran amine as an anterograde tracer for single- and double-labeling studies.* J Neurosci Methods, 1992. 41(3): p. 239-54.
134. Dolleman-Van der Weel, M.J., F.G. Wouterlood, and M.P. Witter, *Multiple anterograde tracing, combining Phaseolus vulgaris Leucoagglutinin with rhodamine- and biotin-conjugated dextranamine.* J Neurosci Methods, 1994. 51(1): p. 9-21.
135. Rowland, D.C., et al., *Transgenically targeted rabies virus demonstrates a major monosynaptic projection from hippocampal area CA2 to medial entorhinal layer II neurons.* J Neurosci, 2013. 33(37): p. 14889-98.
136. Rajasethupathy, P., et al., *Projections from neocortex mediate top-down control of memory retrieval.* Nature, 2015. 526(7575): p. 653-9.
137. Petreanu, L., et al., *Channelrhodopsin-2-assisted circuit mapping of long-range callosal projections.* Nature Neuroscience, 2007. 10(5): p. 663-8.
138. Cruikshank, S.J., et al., *Pathway-specific feedforward circuits between thalamus and neocortex revealed by selective optical stimulation of axons.* Neuron, 2010. 65(2): p. 230-45.
139. de Villers-Sidani, E., B. Tahvildari, and A. Alonso, *Synaptic activation patterns of the perirhinal-entorhinal inter-connections.* Neuroscience, 2004. 129(1): p. 255-65.
140. Debanne, D., et al., *Paired-recordings from synaptically coupled cortical and hippocampal neurons in acute and cultured brain slices.* Nature protocols, 2008. 3(10): p. 1559-68.
141. Doyle, M.W. and M.C. Andresen, *Reliability of monosynaptic sensory transmission in brain stem neurons in vitro.* J Neurophysiol, 2001. 85(5): p. 2213-23.
142. Canto, C.B., et al., *All layers of medial entorhinal cortex receive presubicular and parasubicular inputs.* J Neurosci, 2012. 32(49): p. 17620-31.
143. Callaway, E.M. and L.C. Katz, *Photostimulation using caged glutamate reveals functional circuitry in living brain slices.* Proc Natl Acad Sci U S A, 1993. 90(16): p. 7661-5.
144. Katz, L.C. and M.B. Dalva, *Scanning laser photostimulation: a new approach for analyzing brain circuits.* J Neurosci Methods, 1994. 54(2): p. 205-18.
145. Petreanu, L., et al., *The subcellular organization of neocortical excitatory connections.* Nature, 2009. 457(7233): p. 1142-5.
146. Solstad, T., et al., *Representation of geometric borders in the entorhinal cortex.* Science, 2008. 322(5909): p. 1865-8.

147. Miao, C., et al., *Parvalbumin and Somatostatin Interneurons Control Different Space-Coding Networks in the Medial Entorhinal Cortex.* Cell, 2017. 171(3): p. 507-521 e17.
148. Hoydal, O.A., et al., *Object-vector coding in the medial entorhinal cortex.* Nature, 2019. 568(7752): p. 400-404.
149. Buzsaki, G. and E.I. Moser, *Memory, navigation and theta rhythm in the hippocampal-entorhinal system.* Nat Neurosci, 2013. 16(2): p. 130-8.
150. Xu, W. and D.A. Wilson, *Odor-evoked activity in the mouse lateral entorhinal cortex.* Neuroscience, 2012. 223: p. 12-20.
151. Young, B.J., et al., *Memory representation within the parahippocampal region.* J Neurosci, 1997. 17(13): p. 5183-95.
152. Biella, G. and M. de Curtis, *Olfactory inputs activate the medial entorhinal cortex via the hippocampus.* J Neurophysiol, 2000. 83(4): p. 1924-31.
153. Boeijinga, P.H. and T. van Groen, *Inputs from the olfactory bulb and olfactory cortex to the entorhinal cortex in the cat. II. Physiological studies.* Experimental Brain Research, 1984. 57(1): p. 40-48.
154. Habets, A.M., F.H. Lopes da Silva, and W.J. Mollevanger, *An olfactory input to the hippocampus of the cat: field potential analysis.* Brain Research, 1980. 182(1): p. 47-64.
155. Schwerdtfeger, W.K., E.H. Buhl, and P. Germroth, *Disynaptic olfactory input to the hippocampus mediated by stellate cells in the entorhinal cortex.* J Comp Neurol, 1990. 292(2): p. 163-77.
156. Van Groen, T., F.H. Lopes da Silva, and W.J. Wadman, *Synaptic organization of olfactory inputs and local circuits in the entorhinal cortex: a current source density analysis in the cat.* Exp Brain Res, 1987. 67(3): p. 615-22.
157. Wilson, R.C. and O. Steward, *Polysynaptic activation of the dentate gyrus of the hippocampal formation: an olfactory input via the lateral entorhinal cortex.* Exp Brain Res, 1978. 33: p. 523-34.
158. Staubli, U., et al., *Studies on retrograde and anterograde amnesia of olfactory memory after denervation of the hippocampus by entorhinal cortex lesions.* Behavioral and Neural Biology, 1986. 46(3): p. 432-44.
159. Otto, T., et al., *Hippocampus and olfactory discrimination learning: effects of entorhinal cortex lesions on olfactory learning and memory in a successive-cue, go-no-go task.* Behav Neurosci, 1991. 105(1): p. 111-9.
160. Wirth, S., B. Ferry, and G. Di Scala, *Facilitation of olfactory recognition by lateral entorhinal cortex lesion in rats.* Behav Brain Res, 1998. 91(1-2): p. 49-59.
161. Brown, M.W., *Hippocampal and perirhinal functions in recognition memory.* Nature reviews. Neuroscience, 2008. 9(5): p. 405; author reply 405.
162. Buckley, M.J. and D. Gaffan, *Perirhinal cortical contributions to object perception.* Trends Cogn Sci, 2006. 10(3): p. 100-7.
163. Bussey, T.J. and L.M. Saksida, *Object memory and perception in the medial temporal lobe: an alternative approach.* Current Opinion in Neurobiology, 2005. 15(6): p. 730-737.
164. Bussey, T.J. and L.M. Saksida, *Memory, perception, and the ventral visual-perirhinal-hippocampal stream: thinking outside of the boxes.* Hippocampus, 2007. 17(9): p. 898-908.
165. Bussey, T.J., L.M. Saksida, and E.A. Murray, *Perirhinal cortex and feature-ambiguous discriminations.* Learning and Memory, 2006. 13(2): p. 103-105.
166. Kealy, J. and S. Commins, *The rat perirhinal cortex: A review of anatomy, physiology, plasticity, and function.* Prog Neurobiol, 2011. 93(4): p. 522-48.

167. Naya, Y., *Declarative association in the perirhinal cortex.* Neurosci Res, 2016. 113: p. 12-18.
168. Taylor, K.I., et al., *Binding crossmodal object features in perirhinal cortex.* Proc Natl Acad Sci U S A, 2006. 103(21): p. 8239-44.
169. Dhillon, A. and R.S. Jones, *Laminar differences in recurrent excitatory transmission in the rat entorhinal cortex in vitro.* Neuroscience, 2000. 99(3): p. 413-422.
170. Kloosterman, F., et al., *Electrophysiological characterization of interlaminar entorhinal connections: an essential link for re-entrance in the hippocampal-entorhinal system.* Eur J Neurosci, 2003. 18(11): p. 3037-52.
171. Tang, Q., et al., *Anatomical Organization and Spatiotemporal Firing Patterns of Layer 3 Neurons in the Rat Medial Entorhinal Cortex.* J Neurosci, 2015. 35(36): p. 12346-54.
172. van der Linden, S. and F.H. Lopes da Silva, *Comparison of the electrophysiology and morphology of layers III and II neurons of the rat medial entorhinal cortex in vitro.* Eur J Neurosci, 1998. 10(4): p. 1479-89.
173. Kerr, K.M., et al., *Functional neuroanatomy of the parahippocampal region: the lateral and medial entorhinal areas.* Hippocampus, 2007. 17(9): p. 697-708.
174. Gaffan, E.A., A.N. Healey, and M.J. Eacott, *Objects and positions in visual scenes: effects of perirhinal and postrhinal cortex lesions in the rat.* Behav Neurosci, 2004. 118(5): p. 992-1010.
175. Norman, G. and M.J. Eacott, *Dissociable effects of lesions to the perirhinal cortex and the postrhinal cortex on memory for context and objects in rats.* Behav Neurosci, 2005. 119(2): p. 557-66.
176. Furtak, S.C., O.J. Ahmed, and R.D. Burwell, *Single neuron activity and theta modulation in postrhinal cortex during visual object discrimination.* Neuron, 2012. 76(5): p. 976-88.
177. Aminoff, E., N. Gronau, and M. Bar, *The parahippocampal cortex mediates spatial and nonspatial associations.* Cereb Cortex, 2007. 17(7): p. 1493-503.
178. Bohbot, V.D., et al., *Spatial memory deficits in patients with lesions to the right hippocampus and to the right parahippocampal cortex.* Neuropsychologia, 1998. 36(11): p. 1217-38.
179. Hayes, S.M., L. Nadel, and L. Ryan, *The effect of scene context on episodic object recognition: parahippocampal cortex mediates memory encoding and retrieval success.* Hippocampus, 2007. 17(9): p. 873-89.
180. Maguire, E.A., et al., *Knowing where things are parahippocampal involvement in encoding object locations in virtual large-scale space.* J Cogn Neurosci, 1998. 10(1): p. 61-76.
181. Burwell, R.D. and D.G. Amaral, *Cortical afferents of the perirhinal, postrhinal, and entorhinal cortices of the rat.* J Comp Neurol, 1998. 398(2): p. 179-205.
182. Insausti, R., D.G. Amaral, and W.M. Cowan, *The entorhinal cortex of the monkey: III. Subcortical afferents.* J Comp Neurol, 1987. 264(3): p. 396-408.
183. Jones, B.F. and M.P. Witter, *Cingulate cortex projections to the parahippocampal region and hippocampal formation in the rat.* Hippocampus, 2007. 17(10): p. 957-76.
184. Kondo, H. and M.P. Witter, *Topographic organization of orbitofrontal projections to the parahippocampal region in rats.* J Comp Neurol, 2014. 522(4): p. 772-93.
185. Krettek, J.E. and J.L. Price, *Projections from the amygdaloid complex and adjacent olfactory structures to the entorhinal cortex and to the subiculum in the rat and cat.* The Journal of comparative neurology, 1977. 172(4): p. 723-52.
186. Mathiasen, M.L., L. Hansen, and M.P. Witter, *Insular projections to the parahippocampal region in the rat.* J Comp Neurol, 2015. 523(9): p. 1379-98.

187. Mohedano-Moriano, A., et al., *Topographical and laminar distribution of cortical input to the monkey entorhinal cortex.* J Anat, 2007. 211(2): p. 250-60.
188. Pitkanen, A., J.L. Kelly, and D.G. Amaral, *Projections from the lateral, basal, and accessory basal nuclei of the amygdala to the entorhinal cortex in the macaque monkey.* Hippocampus, 2002. 12(2): p. 186-205.
189. Room, P. and H.J. Groenewegen, *Connections of the parahippocampal cortex in the cat. II. Subcortical afferents.* Journal of comparative neurology, 1986. 251(4): p. 451-73.
190. Stefanacci, L. and D.G. Amaral, *Topographic organization of cortical inputs to the lateral nucleus of the macaque monkey amygdala: a retrograde tracing study.* J Comp Neurol, 2000. 421(1): p. 52-79.
191. Suzuki, W.A. and D.G. Amaral, *Perirhinal and parahippocampal cortices of the macaque monkey: cortical afferents.* J Comp Neurol, 1994. 350(4): p. 497-533.
192. Van Hoesen, G. and D.N. Pandya, *Some connections of the entorhinal (area 28) and perirhinal (area 35) cortices of the rhesus monkey. I. Temporal lobe afferents.* Brain Res, 1975. 95(1): p. 1-24.
193. Van Hoesen, G., D.N. Pandya, and N. Butters, *Some connections of the entorhinal (area 28) and perirhinal (area 35) cortices of the rhesus monkey. II. Frontal lobe afferents.* Brain Res, 1975. 95(1): p. 25-38.
194. Van Hoesen, G.W., D.N. Pandya, and N. Butters, *Cortical afferents to the entorhinal cortex of the Rhesus monkey.* Science, 1972. 175(4029): p. 1471-3.
195. Vaudano, E., C.R. Legg, and M. Glickstein, *Afferent and Efferent Connections of Temporal Association Cortex in the Rat: A Horseradish Peroxidase Study.* Eur J Neurosci, 1991. 3(4): p. 317-330.
196. Vertes, R.P., *Differential projections of the infralimbic and prelimbic cortex in the rat.* Synapse, 2004. 51(1): p. 32-58.
197. Scaplen, K.M., et al., *Inactivation of the Lateral Entorhinal Area Increases the Influence of Visual Cues on Hippocampal Place Cell Activity.* Front Syst Neurosci, 2017. 11: p. 40.
198. Wilson, D.I., et al., *Lateral entorhinal cortex is critical for novel object-context recognition.* Hippocampus, 2013. 23(5): p. 352-66.
199. Wilson, D.I., et al., *Lateral entorhinal cortex is necessary for associative but not nonassociative recognition memory.* Hippocampus, 2013. 23(12): p. 1280-90.
200. Pilkiw, M., et al., *Phasic and tonic neuron ensemble codes for stimulus-environment conjunctions in the lateral entorhinal cortex.* Elife, 2017. 6.
201. Tsao, A., et al., *Integrating time from experience in the lateral entorhinal cortex.* Nature, 2018. 561(7721): p. 57-62.
202. Montchal, M.E., Z.M. Reagh, and M.A. Yassa, *Precise temporal memories are supported by the lateral entorhinal cortex in humans.* Nat Neurosci, 2019. 22(2): p. 284-288.
203. Tang, Q., et al., *Functional Architecture of the Rat Parasubiculum.* J Neurosci, 2016. 36(7): p. 2289-301.
204. Apergis-Schoute, J., A. Pinto, and D. Pare, *Muscarinic control of long-range GABAergic inhibition within the rhinal cortices.* J Neurosci, 2007. 27(15): p. 4061-71.
205. Ray, S., et al., *Grid-layout and theta-modulation of layer 2 pyramidal neurons in medial entorhinal cortex.* Science, 2014. 343(6173): p. 891-6.
206. Shipley, M.T. and G.D. Adamek, *The connections of the mouse olfactory bulb: a study using orthograde and retrograde transport of wheat germ agglutinin conjugated to horseradish peroxidase.* Brain Research Bulletin, 1984. 12(6): p. 669-88.

207. Reagh, Z.M. and M.A. Yassa, *Object and spatial mnemonic interference differentially engage lateral and medial entorhinal cortex in humans.* Proc Natl Acad Sci U S A, 2014. 111(40): p. E4264-73.
208. Rodo, C., F. Sargolini, and E. Save, *Processing of spatial and non-spatial information in rats with lesions of the medial and lateral entorhinal cortex: Environmental complexity matters.* Behav Brain Res, 2017. 320: p. 200-209.
209. Wang, C., et al., *Egocentric coding of external items in the lateral entorhinal cortex.* Science, 2018. 362(6417): p. 945-949.
210. Igarashi, K.M., et al., *Coordination of entorhinal-hippocampal ensemble activity during associative learning.* Nature, 2014. 510(7503): p. 143-7.
211. Keene, C.S., et al., *Complementary Functional Organization of Neuronal Activity Patterns in the Perirhinal, Lateral Entorhinal, and Medial Entorhinal Cortices.* J Neurosci, 2016. 36(13): p. 3660-75.
212. Epstein, R.A., W.E. Parker, and A.M. Feiler, *Where am I now? Distinct roles for parahippocampal and retrosplenial cortices in place recognition.* J Neurosci, 2007. 27(23): p. 6141-9.
213. Kraus, B.J., et al., *During Running in Place, Grid Cells Integrate Elapsed Time and Distance Run.* Neuron, 2015. 88(3): p. 578-89.
214. Aronov, D., R. Nevers, and D.W. Tank, *Mapping of a non-spatial dimension by the hippocampal-entorhinal circuit.* Nature, 2017. 543(7647): p. 719-722.
215. Schlesiger, M.I., et al., *Hippocampal Global Remapping Can Occur without Input from the Medial Entorhinal Cortex.* Cell Rep, 2018. 22(12): p. 3152-3159.
216. Doan, T.P., et al., *Convergent projections from perirhinal and postrhinal cortices suggest a multisensory nature of lateral but not medial entorhinal cortex.* Cell Rep, 2019. 29(3):617-627.e7
217. Stensola, H., et al., *The entorhinal grid map is discretized.* Nature, 2012. 492(7427): p. 72-8.
218. Canto, C.B. and M.P. Witter, *Cellular properties of principal neurons in the rat entorhinal cortex. I. The lateral entorhinal cortex.* Hippocampus, 2012. 22(6): p. 1256-76.
219. Giocomo, L.M., et al., *Temporal frequency of subthreshold oscillations scales with entorhinal grid cell field spacing.* Science, 2007. 315(5819): p. 1719-1722.
220. Garden, D.L., et al., *Tuning of synaptic integration in the medial entorhinal cortex to the organization of grid cell firing fields.* Neuron, 2008. 60(5): p. 875-89.
221. Fjeld, G., E.S. Nilssen, and M.P. Witter, *Immunohistochemical and electrophysiological characterization of principal cells in layer II of the lateral entorhinal cortex.* Master thesis, 2015.
222. Gardner, R.J., et al., *Correlation structure of grid cells is preserved during sleep.* Nat Neurosci, 2019. 22(4): p. 598-608.
223. Trettel, S.G., et al., *Grid cell co-activity patterns during sleep reflect spatial overlap of grid fields during active behaviors.* Nat Neurosci, 2019. 22(4): p. 609-617.
224. Almog, N., et al., *During hippocampal inactivation, grid cells maintain their synchrony, even when the grid pattern is lost.* BioRxiv, 2019.
225. Hardcastle, K., S. Ganguli, and L.M. Giocomo, *Cell types for our sense of location: where we are and where we are going.* Nat Neurosci, 2017. 20(11): p. 1474-1482.
226. Mante, V., et al., *Context-dependent computation by recurrent dynamics in prefrontal cortex.* Nature, 2013. 503(7474): p. 78-84.
227. Kaufman, M.T., et al., *Cortical activity in the null space: permitting preparation without movement.* Nat Neurosci, 2014. 17(3): p. 440-8.

228. Churchland, M.M., A. Afshar, and K.V. Shenoy, *A central source of movement variability.* Neuron, 2006. 52(6): p. 1085-96.
229. Shenoy, K.V., M. Sahani, and M.M. Churchland, *Cortical control of arm movements: a dynamical systems perspective.* Annu Rev Neurosci, 2013. 36: p. 337-59.
230. Raposo, D., M.T. Kaufman, and A.K. Churchland, *A category-free neural population supports evolving demands during decision-making.* Nat Neurosci, 2014. 17(12): p. 1784-1792.
231. Cunningham, J.P. and B.M. Yu, *Dimensionality reduction for large-scale neural recordings.* Nat Neurosci, 2014. 17(11): p. 1500-9.
232. Tsao, A., *Revising the Parallel-Pathways Hypothesis with Time.* Front Syst Neurosci, 2017. 11: p. 59.
233. Diehl, G.W., et al., *Grid and Nongrid Cells in Medial Entorhinal Cortex Represent Spatial Location and Environmental Features with Complementary Coding Schemes.* Neuron, 2017. 94(1): p. 83-92.e6.
234. Langston, R.F., et al., *Development of the spatial representation system in the rat.* Science, 2010. 328(5985): p. 1576-80.
235. Wills, T.J., C. Barry, and F. Cacucci, *The abrupt development of adult-like grid cell firing in the medial entorhinal cortex.* Front Neural Circuits, 2012. 6: p. 21.
236. Krupic, J., N. Burgess, and J. O'Keefe, *Neural representations of location composed of spatially periodic bands.* Science, 2012. 337(6096): p. 853-7.
237. Bellmund, J.L.S., et al., *Navigating cognition: Spatial codes for human thinking.* Science, 2018. 362(6415).
238. Hardcastle, K., et al., *A Multiplexed, Heterogeneous, and Adaptive Code for Navigation in Medial Entorhinal Cortex.* Neuron, 2017. 94(2): p. 375-387 e7.
239. Tolman, E.C., *Cognitive maps in rats and men.* Psychol Rev, 1948. 55(4): p. 189-208.
240. Ranck, J.B., *Head direction cells in the deep cell layer of dorsal presubiculum in freely moving rats.*, in *Electrical Activity of the Archicortex*, G. Buzsaki and C.H. Vanderwolf, Editors. 1985, Akademiai Kiado: Budapest. p. 217-220.
241. Taube, J.S., R.U. Muller, and J.B. Ranck, Jr., *Head-direction cells recorded from the postsubiculum in freely moving rats. I. Description and quantitative analysis.* J Neurosci, 1990. 10(2): p. 420-35.
242. Taube, J.S., R.U. Muller, and J.B. Ranck, Jr., *Head-direction cells recorded from the postsubiculum in freely moving rats. II. Effects of environmental manipulations.* J Neurosci, 1990. 10(2): p. 436-47.
243. Skaggs, W.E., et al., *A model of the neural basis of the rat's sense of direction.* Advances in Neural Information Processing Systems, 1995. 7: p. 173-180.
244. Knierim, J.J., H.S. Kudrimoti, and B.L. McNaughton, *Place cells, head direction cells, and the learning of landmark stability.* Journal of neuroscience, 1995. 15(3 Pt 1): p. 1648-1659.
245. Zhang, K., *Representation of spatial orientation by the intrinsic dynamics of the head-direction cell ensemble: a theory.* Journal of Neuroscience, 1996. 16(6): p. 2112-26.
246. Touretzky, D.S. and A.D. Redish, *Theory of rodent navigation based on interacting representations of space.* Hippocampus, 1996. 6(3): p. 247-70.
247. Hafting, T., et al., *Microstructure of a spatial map in the entorhinal cortex.* Nature, 2005. 436(7052): p. 801-806.
248. Fyhn, M., et al., *Hippocampal remapping and grid realignment in entorhinal cortex.* Nature, 2007. 446(7132): p. 190-4.
249. Kjelstrup, K.B., et al., *Finite scale of spatial representation in the hippocampus.* Science (New York, N.Y.), 2008. 321(5885): p. 140-3.

250. Giocomo, L.M., et al., *Topography of head direction cells in medial entorhinal cortex.* Curr Biol, 2014. 24(3): p. 252-62.
251. Brun, V.H., et al., *Progressive increase in grid scale from dorsal to ventral medial entorhinal cortex.* Hippocampus, 2008. 18(12): p. 1200-12.
252. Stensola, H., et al., *The entorhinal grid map is discretized.* Nature, 2012. 492(7427): p. 72-78.
253. Taube, J.S., *The head direction signal: origins and sensory-motor integration.* Annual Review of Neuroscience, 2007. 30: p. 181-207.
254. Boccara, C.N., et al., *Grid cells in pre- and parasubiculum.* Nature Neuroscience, 2010. (8):987-94.
255. Ray, S., et al., *Complementary Modular Microcircuits of the Rat Medial Entorhinal Cortex.* Front Syst Neurosci, 2017. 11: p. 20.
256. Peyrache, A., et al., *Internally organized mechanisms of the head direction sense.* Nat Neurosci, 2015. 18(4): p. 569-75.
257. Yoon, K., et al., *Specific evidence of low-dimensional continuous attractor dynamics in grid cells.* Nat Neurosci, 2013. 16(8): p. 1077-84.
258. Yoganarasimha, D., X. Yu, and J.J. Knierim, *Head direction cell representations maintain internal coherence during conflicting proximal and distal cue rotations: comparison with hippocampal place cells.* J Neurosci, 2006. 26(2): p. 622-31.
259. Moser, E.I., E. Kropff, and M.B. Moser, *Place cells, grid cells, and the brain's spatial representation system.* Annu Rev Neurosci, 2008. 31: p. 69-89.
260. Hasselmo, M.E., L.M. Giocomo, and E.A. Zilli, *Grid cell firing may arise from interference of theta frequency membrane potential oscillations in single neurons.* Hippocampus, 2007. 17(12): p. 1252-71.
261. Burgess, N., C. Barry, and J. O'Keefe, *An oscillatory interference model of grid cell firing.* Hippocampus, 2007. 17(9): p. 801-12.
262. Carvalho, M., et al., *A circuit for neuronal coding of locomotion speed: from the pedunculopontine tegmental nucleus to the medial entorhinal cortex.* SfN asbtract, 2016.
263. Justus, D., et al., *Glutamatergic synaptic integration of locomotion speed via septoentorhinal projections.* Nat Neurosci, 2017. 20(1): p. 16-19.
264. Gaykema, R.P., et al., *Cortical projection patterns of the medial septum-diagonal band complex.* J Comp Neurol, 1990. 293(1): p. 103-24.
265. Beltramo, R. and M. Scanziani, *A collicular visual cortex: Neocortical space for an ancient midbrain visual structure.* Science, 2018. 363(6422): p. 64-69.
266. Berthoz, A., et al., *Spatial memory of body linear displacement: what is being stored?* Science, 1995. 269(5220): p. 95-8.
267. Glasauer, S., et al., *Goal-directed linear locomotion in normal and labyrinthine-defective subjects.* Exp Brain Res, 1994. 98(2): p. 323-35.
268. Grasso, R., Y. Ivanenko, and F. Lacquaniti, *Time course of gaze influences on postural responses to neck proprioceptive and galvanic vestibular stimulation in humans.* Neurosci Lett, 1999. 273(2): p. 121-4.
269. Israel, I., et al., *Spatial memory and path integration studied by self-driven passive linear displacement. I. Basic properties.* J Neurophysiol, 1997. 77(6): p. 3180-92.
270. Ivanenko, Y.P. and R. Grasso, *Integration of somatosensory and vestibular inputs in perceiving the direction of passive whole-body motion.* Brain Res Cogn Brain Res, 1997. 5(4): p. 323-7.
271. Beraneck, M. and K.E. Cullen, *Activity of vestibular nuclei neurons during vestibular and optokinetic stimulation in the alert mouse.* J Neurophysiol, 2007. 98(3): p. 1549-65.

272. Medrea, I. and K.E. Cullen, *Multisensory integration in early vestibular processing in mice: the encoding of passive vs. active motion.* J Neurophysiol, 2013. 110(12): p. 2704-17.
273. Cullen, K.E., *The neural encoding of self-motion.* Curr Opin Neurobiol, 2011. 21(4): p. 587-95.
274. Cullen, K.E., *The vestibular system: multimodal integration and encoding of self-motion for motor control.* Trends Neurosci, 2012. 35(3): p. 185-96.
275. McCrea, R.A. and A.K. Horn, *Nucleus prepositus.* Prog Brain Res, 2006. 151: p. 205-30.
276. Dale, A. and K.E. Cullen, *The nucleus prepositus predominantly outputs eye movement-related information during passive and active self-motion.* J Neurophysiol, 2013. 109(7): p. 1900-11.
277. Dale, A. and K.E. Cullen, *Local population synchrony and the encoding of eye position in the primate neural integrator.* J Neurosci, 2015. 35(10): p. 4287-95.
278. McFarland, J.L. and A.F. Fuchs, *Discharge patterns in nucleus prepositus hypoglossi and adjacent medial vestibular nucleus during horizontal eye movement in behaving macaques.* J Neurophysiol, 1992. 68(1): p. 319-32.
279. Cullen, K.E. and J.S. Taube, *Our sense of direction: progress, controversies and challenges.* Nat Neurosci, 2017. 20(11): p. 1465-1473.
280. Winter, S.S., et al., *Passive Transport Disrupts Grid Signals in the Parahippocampal Cortex.* Curr Biol, 2015. 25(19): p. 2493-502.
281. Taube, J.S., *The head direction signal: origins and sensory-motor integration.* Annu Rev Neurosci, 2007. 30: p. 181-207.
282. Bassett, J.P. and J.S. Taube, *Neural correlates for angular head velocity in the rat dorsal tegmental nucleus.* J Neurosci, 2001. 21(15): p. 5740-51.
283. Sharp, P.E., A. Tinkelman, and J. Cho, *Angular velocity and head direction signals recorded from the dorsal tegmental nucleus of gudden in the rat: implications for path integration in the head direction cell circuit.* Behav Neurosci, 2001. 115(3): p. 571-88.
284. Biazoli, C.E., Jr., et al., *The supragenual nucleus: a putative relay station for ascending vestibular signs to head direction cells.* Brain Res, 2006. 1094(1): p. 138-48.
285. van Haeften, T., et al., *GABAergic presubicular projections to the medial entorhinal cortex of the rat.* J Neurosci, 1997. 17(2): p. 862-74.
286. Wouterlood, F.G., et al., *Input from the presubiculum to dendrites of layer-V neurons of the medial entorhinal cortex of the rat.* Brain Research, 2004. 1013(1): p. 1-12.
287. Gerlei, K., et al., *Grid cells implement a location-dependent directional code.* BioRxiv, 2019.
288. Bonnevie, T., et al., *Grid cells require excitatory drive from the hippocampus.* Nat Neurosci, 2013. 16(3): p. 309-17.
289. Winter, S.S., B.J. Clark, and J.S. Taube, *Spatial navigation. Disruption of the head direction cell network impairs the parahippocampal grid cell signal.* Science, 2015. 347(6224): p. 870-874.
290. Canto, C.B., et al., *Postnatal development of functional projections from para- and presubiculum to medial entorhinal cortex in the rat.* The Journal of Neuroscience, 2019: p. 1623-19.
291. Wills, T.J., et al., *Development of the hippocampal cognitive map in preweanling rats.* Science, 2010. 328(5985): p. 1573-6.
292. Bjerknes, T.L., et al., *Coherence among head direction cells before eye opening in rat pups.* Curr Biol, 2015. 25(1): p. 103-8.

293. Bjerknes, T.L., E.I. Moser, and M.B. Moser, *Representation of geometric borders in the developing rat.* Neuron, 2014. 82(1): p. 71-8.
294. Nilssen, E.S., T.P. Doan, and M.P. Witter, *Convergence of cortical inputs onto hippocampal-projecting cells in layer II of the lateral entorhinal cortex.* Manuscript, 2019.
295. Insausti, R. and D.G. Amaral, *Entorhinal cortex of the monkey: IV. Topographical and laminar organization of cortical afferents.* J Comp Neurol, 2008. 509(6): p. 608-41.
296. Burwell, R.D., *The parahippocampal region: corticocortical connectivity.* Ann N Y Acad Sci, 2000. 911: p. 25-42.
297. Suzuki, W.A., E.K. Miller, and R. Desimone, *Object and place memory in the macaque entorhinal cortex.* Journal of Neurophysiology, 1997. 78(2): p. 1062-81.
298. Barnes, C.A., et al., *Comparison of spatial and temporal characteristics of neuronal activity in sequential stages of hippocampal processing.* Progress in Brain Research, 1990: p. 83:287-300.
299. Quirk, G.J., et al., *The positional firing properties of medial entorhinal neurons: description and comparison with hippocampal place cells.* Journal of Neuroscience, 1992. 12(5): p. 1945-63.
300. Frank, L.M., E.N. Brown, and M. Wilson, *Trajectory encoding in the hippocampus and entorhinal cortex.* Neuron, 2000. 27(1): p. 169-78.
301. Kosel, K.C., G.W. Van Hoesen, and J.R. West, *Olfactory bulb projections to the parahippocampal area of the rat.* The Journal of comparative neurology, 1981. 198(3): p. 467-82.
302. Haberly, L.B. and J.L. Price, *Association and commissural fiber systems of the olfactory cortex of the rat.* The Journal of comparative neurology, 1978. 178(4): p. 711-40.
303. Beckstead, R.M., *An autoradiographic examination of corticocortical and subcortical projections of the mediodorsal-projection (prefrontal) cortex in the rat.* The Journal of comparative neurology, 1979. 184(1): p. 43-62.
304. Sesack, S.R., et al., *Topographical organization of the efferent projections of the medial prefrontal cortex in the rat: an anterograde tract-tracing study with Phaseolus vulgaris leucoagglutinin.* J Comp Neurol, 1989. 290(2): p. 213-42.
305. White, T.D., A.M. Tan, and D.M. Finch, *Functional reciprocal connections of the rat entorhinal cortex and subicular complex with the medial frontal cortex: an in vivo intracellular study.* Brain Res, 1990. 533(1): p. 95-106.
306. Takagishi, M. and T. Chiba, *Efferent projections of the infralimbic (area 25) region of the medial prefrontal cortex in the rat: an anterograde tracer PHA-L study.* Brain Res, 1991. 566(1-2): p. 26-39.
307. Hoover, W.B. and R.P. Vertes, *Projections of the medial orbital and ventral orbital cortex in the rat.* J Comp Neurol, 2011. 519(18): p. 3766-801.
308. Pitkanen, A., et al., *Reciprocal connections between the amygdala and the hippocampal formation, perirhinal cortex, and postrhinal cortex in rat. A review.* Ann.N.Y.Acad.Sci., 2000. 911: p. 369-391.
309. Olsen, G.M., et al., *Parahippocampal and retrosplenial connections of rat posterior parietal cortex.* Hippocampus, 2017. 27(4): p. 335-358.
310. Czajkowski, R., et al., *Superficially projecting principal neurons in layer V of medial entorhinal cortex in the rat receive excitatory retrosplenial input.* Journal of Neuroscience, 2013. 33(40): p. 15779-92.
311. Sugar, J. and M.P. Witter, *Postnatal development of retrosplenial projections to the parahippocampal region of the rat.* Elife, 2016. 5.

312. Felleman, D.J. and D.C. Van Essen, *Distributed hierarchical processing in the primate cerebral cortex.* Cereb Cortex, 1991. 1(1): p. 1-47.
313. Nilssen, E.S., et al., *Neurons and networks in the entorhinal cortex: A reappraisal of the lateral and medial entorhinal subdivisions mediating parallel cortical pathways.* Hippocampus, 2019. in press.
314. Bota, M., O. Sporns, and L.W. Swanson, *Architecture of the cerebral cortical association connectome underlying cognition.* Proc Natl Acad Sci U S A, 2015. 112(16): p. E2093-101.
315. Zingg, B., et al., *Neural networks of the mouse neocortex.* Cell, 2014. 156(5): p. 1096-111.
316. Esclassan, F., et al., *A cholinergic-dependent role for the entorhinal cortex in trace fear conditioning.* J Neurosci, 2009. 29(25): p. 8087-93.
317. Morrissey, M.D., et al., *Functional dissociation within the entorhinal cortex for memory retrieval of an association between temporally discontiguous stimuli.* J Neurosci, 2012. 32(16): p. 5356-61.
318. Glovaci, I., *Dopaminergic Facilitation of Synaptic Transmission in Layer II of the Lateral Entorhinal Cortex.* PhD thesis, 2018.
319. Nilssen, E.S., *Synaptic connectivity of principal cells in layer II of the lateral entorhinal cortex.* PhD thesis, 2019.
320. Gu, Y., et al., *A Map-like Micro-Organization of Grid Cells in the Medial Entorhinal Cortex.* Cell, 2018. 175(3): p. 736-750.e30.
321. Pinto, A., C. Fuentes, and D. Pare, *Feedforward inhibition regulates perirhinal transmission of neocortical inputs to the entorhinal cortex: ultrastructural study in guinea pigs.* J Comp Neurol, 2006. 495(6): p. 722-34.
322. Kohler, C., *Intrinsic connections of the retrohippocampal region in the rat brain. II. The medial entorhinal area.* Journal of comparative neurology, 1986. 246(2): p. 149-69.
323. Kohler, C., *Intrinsic connections of the retrohippocampal region in the rat brain: III. The lateral entorhinal area.* J Comp Neurol, 1988. 271(2): p. 208-28.
324. Witter, M.P., et al., *Connections of the parahippocampal cortex in the cat. V. Intrinsic connections; comments on input/output connections with the hippocampus.* J Comp Neurol, 1986. 252(1): p. 78-94.
325. Chrobak, J.J. and D.G. Amaral, *Entorhinal cortex of the monkey: VII. intrinsic connections.* J Comp Neurol, 2007. 500(4): p. 612-33.
326. de Curtis, M. and G. Biella, *Communication between subregions of the parahippocampal region*, in *The Parahippocampal Region: Organization and Role in Cognitive Functions* 2002, Oxford University Press: USA. p. 107-126.
327. Köhler, C., *Intrinsic connections of the retrohippocampal region in the rat brain. II. The medial entorhinal area.* J Comp Neurol, 1986. 246(2): p. 149-69.
328. Hamam, B.N., D.G. Amaral, and A.A. Alonso, *Morphological and electrophysiological characteristics of layer V neurons of the rat lateral entorhinal cortex.* J Comp Neurol, 2002. 451(1): p. 45-61.
329. Hamam, B.N., et al., *Morphological and electrophysiological characteristics of layer V neurons of the rat medial entorhinal cortex.* J Comp Neurol, 2000. 418(4): p. 457-72.
330. Winterer, J., et al., *Excitatory Microcircuits within Superficial Layers of the Medial Entorhinal Cortex.* Cell Rep, 2017. 19(6): p. 1110-1116.
331. Kohler, C., *Intrinsic connections of the retrohippocampal region in the rat brain. II. The medial entorhinal area.* J Comp Neurol, 1986. 246(2): p. 149-69.

332. Varga, C., et al., *Network effects of dendritic inhibition in the medial entorhinal cortex.* SfN asbtract, 2018. 445.
333. Barry, C., et al., *Experience-dependent rescaling of entorhinal grids.* Nature Neuroscience, 2007. 10(6): p. 682-684.
334. Wernle, T., et al., *Integration of grid maps in merged environments.* Nat Neurosci, 2018. 21(1): p. 92-101.
335. Derdikman, D., et al., *Fragmentation of grid cell maps in a multicompartment environment.* Nat Neurosci, 2009. 12(10): p. 1325-32.
336. Krupic, J., et al., *Grid cell symmetry is shaped by environmental geometry.* Nature, 2015. 518(7538): p. 232-235.
337. Stensola, T., et al., *Shearing-induced asymmetry in entorhinal grid cells.* Nature, 2015. 518(7538): p. 207-12.
338. Hagglund, M., et al., *Grid-Cell Distortion along Geometric Borders.* Curr Biol, 2019. 29(6): p. 1047-1054.e3.
339. Boccara, C.N., et al., *The entorhinal cognitive map is attracted to goals.* Science, 2019. 363(6434): p. 1443-1447.
340. Butler, W.N., K. Hardcastle, and L.M. Giocomo, *Remembered reward locations restructure entorhinal spatial maps.* Science, 2019. 363(6434): p. 1447-1452.
341. Constantinescu, A.O., J.X. O'Reilly, and T.E.J. Behrens, *Organizing conceptual knowledge in humans with a gridlike code.* Science, 2016. 352(6292): p. 1464-1468.
342. Wilming, N., et al., *Entorhinal cortex receptive fields are modulated by spatial attention, even without movement.* Elife, 2018. 7.
343. Jacobsen, B., et al., *Local and long-range monosynaptic inputs to parvalbumin and somatostatin interneurons in the medial entorhinal cortex of mice.* in prep, 2019.
344. Bussey, T.J., L.M. Saksida, and E.A. Murray, *The perceptual-mnemonic/feature conjunction model of perirhinal cortex function.* Quarterly Journal of Experimental Psychology.B, Comparative and Physiological Psychology, 2005. 58(3-4): p. 269-282.
345. Deacon, T.W., et al., *Afferent connections of the perirhinal cortex in the rat.* J Comp Neurol, 1983. 220(2): p. 168-90.
346. Furtak, S.C., et al., *Functional neuroanatomy of the parahippocampal region in the rat: the perirhinal and postrhinal cortices.* Hippocampus, 2007. 17(9): p. 709-22.
347. Wouterlood, F., J. Lanciego, and E. Mengual, *Ultrastructure and postsynaptic targets of terminals of perirhinal fibers in the entorhinal cortex of the rat.* Abstr Soc Neurosci 1418, 1998. 24
348. Jacobsen, B., R.R. Nair, and M.P. Witter, *Local and long-range monosynaptic inputs to parvalbumin and somatostatin interneurons in the lateral entorhinal cortex of mice.* in prep, 2019.
349. de Curtis, M. and D. Pare, *The rhinal cortices: a wall of inhibition between the neocortex and the hippocampus.* Prog Neurobiol, 2004. 74(2): p. 101-10.
350. Kajiwara, R., et al., *Amygdala input promotes spread of excitatory neural activity from perirhinal cortex to the entorhinal-hippocampal circuit.* J Neurophysiol, 2003. 89(4): p. 2176-84.
351. Paz, R., et al., *Emotional enhancement of memory via amygdala-driven facilitation of rhinal interactions.* Nature Neuroscience, 2006. 9(10): p. 1321-1329.
352. Paz, R., E.P. Bauer, and D. Pare, *Learning-related facilitation of rhinal interactions by medial prefrontal inputs.* Journal of neuroscience, 2007. 27(24): p. 6542-6551.
353. Pelletier, J.G., J. Apergis, and D. Pare, *Low-probability transmission of neocortical and entorhinal impulses through the perirhinal cortex.* Journal of Neurophysiology, 2004. 91(5): p. 2079-89.

354. Koganezawa, N., et al., *Significance of the deep layers of entorhinal cortex for transfer of both perirhinal and amygdala inputs to the hippocampus.* Neurosci Res, 2008. 61(2): p. 172-81.
355. Willems, J.G., W.J. Wadman, and N.L. Cappaert, *Distinct Spatiotemporal Activation Patterns of the Perirhinal-Entorhinal Network in Response to Cortical and Amygdala Input.* Front Neural Circuits, 2016. 10: p. 44.
356. Suzuki, W.A. and D.G. Amaral, *Topographic organization of the reciprocal connections between the monkey entorhinal cortex and the perirhinal and parahippocampal cortices.* J Neurosci, 1994. 14(3 Pt 2): p. 1856-77.
357. Lavenex, P., W.A. Suzuki, and D.G. Amaral, *Perirhinal and parahippocampal cortices of the macaque monkey: Intrinsic projections and interconnections.* J Comp Neurol, 2004. 472(3): p. 371-94.
358. Unal, G., J. Apergis-Schoute, and D. Pare, *Associative properties of the perirhinal network.* Cereb Cortex, 2012. 22(6): p. 1318-32.
359. Descarries, L., et al., *Regional and laminar density of the dopamine innervation in adult rat cerebral cortex.* Neuroscience, 1987. 21(3): p. 807-24.
360. Oades, R.D. and G.M. Halliday, *Ventral tegmental (A10) system: neurobiology. 1. Anatomy and connectivity.* Brain Res, 1987. 434(2): p. 117-65.
361. Collier, T.J. and A. Routtenberg, *Entorhinal cortex: catecholamine fluorescence and Nissl staining of identical Vibratome sections.* Brain Res, 1977. 128(2): p. 354-60.
362. Fallon, J.H., D.A. Koziell, and R.Y. Moore, *Catecholamine innervation of the basal forebrain. II. Amygdala, suprarhinal cortex and entorhinal cortex.* J Comp Neurol, 1978. 180(3): p. 509-32.
363. Haglund, L., et al., *Forebrain projections of the ventral tegmentum as studied by axonal transport of [3H]dopamine in the rat.* Neurosci Lett, 1979. 12(2-3): p. 301-6.
364. Akil, M. and D.A. Lewis, *The dopaminergic innervation of monkey entorhinal cortex.* Cereb Cortex, 1993. 3(6): p. 533-50.
365. Sawaguchi, T. and P.S. Goldman-Rakic, *D1 dopamine receptors in prefrontal cortex: involvement in working memory.* Science, 1991. 251(4996): p. 947-50.
366. Sawaguchi, T., M. Matsumura, and K. Kubota, *Catecholaminergic effects on neuronal activity related to a delayed response task in monkey prefrontal cortex.* J Neurophysiol, 1990. 63(6): p. 1385-400.
367. Collins, P., et al., *Perseveration and strategy in a novel spatial self-ordered sequencing task for nonhuman primates: effects of excitotoxic lesions and dopamine depletions of the prefrontal cortex.* J Cogn Neurosci, 1998. 10(3): p. 332-54.
368. Seamans, J.K., S.B. Floresco, and A.G. Phillips, *D1 receptor modulation of hippocampal-prefrontal cortical circuits integrating spatial memory with executive functions in the rat.* J Neurosci, 1998. 18(4): p. 1613-21.
369. Glovaci, I. and C.A. Chapman, *Dopamine induces release of calcium from internal stores in layer II lateral entorhinal cortex fan cells.* Cell Calcium, 2019. 80: p. 103-111.

8. Contributions (Article I - IV)

Received: 23 January 2019 | Revised: 29 June 2019 | Accepted: 11 July 2019

DOI: 10.1002/hipo.23145

COMMENTARY

WILEY

Neurons and networks in the entorhinal cortex: A reappraisal of the lateral and medial entorhinal subdivisions mediating parallel cortical pathways

Eirik S. Nilssen[1] | Thanh P. Doan[1] | Maximiliano J. Nigro[1] | Shinya Ohara[1,2] | Menno P. Witter[1]

[1]Kavli Institute for Systems Neuroscience, Centre for Neural Computation, Egil and Pauline Braathen and Fred Kavli Centre for Cortical Microcircuits, NTNU Norwegian University of Science and Technology, Trondheim, Norway

[2]Laboratory of Systems Neuroscience, Tohoku University Graduate School of Life Sciences, Sendai, Japan

Correspondence
Menno P. Witter, Kavli Institute for Systems Neuroscience, MTFS, The Faculty of Medicine and Health Sciences, NTNU, PO Box 8905, 7491 Trondheim, Norway.
Email: menno.witter@ntnu.no

Funding information
Kavli Foundation; Norges Forskningsråd, Grant/Award Numbers: 197467, 223262, 227769

Abstract

In this review, we aim to reappraise the organization of intrinsic and extrinsic networks of the entorhinal cortex with a focus on the concept of parallel cortical connectivity streams. The concept of two entorhinal areas, the lateral and medial entorhinal cortex, belonging to two parallel input–output streams mediating the encoding and storage of respectively what and where information hinges on the claim that a major component of their cortical connections is with the perirhinal cortex and postrhinal or parahippocampal cortex in, respectively, rodents or primates. In this scenario, the lateral entorhinal cortex and the perirhinal cortex are connectionally associated and likewise the postrhinal/parahippocampal cortex and the medial entorhinal cortex are partners. In contrast, here we argue that the connectivity matrix emphasizes the potential of substantial integration of cortical information through interactions between the two entorhinal subdivisions and between the perirhinal and postrhinal/parahippocampal cortices, but most importantly through a new observation that the postrhinal/parahippocampal cortex projects to both lateral and medial entorhinal cortex. We suggest that entorhinal inputs provide the hippocampus with high-order complex representations of the external environment, its stability, as well as apparent changes either as an inherent feature of a biological environment or as the result of navigating the environment. This thus indicates that the current connectional model of the parahippocampal region as part of the medial temporal lobe memory system needs to be revised.

KEYWORDS
anatomy, episodic memory, hippocampus, neural network, parahippocampal gyrus

1 | INTRODUCTION

Memory is an important capacity of the brain and has intrigued scientists ever since they started to study the brain. The ability to store and recall information comes of use in a variety of daily behaviors, and the likely most important role is for us to make predictions based on previous experiences. Previous experiences with a high similarity become eventually stored as generalized concepts or schemes, which are being updated with new experiences. The efficacy of our memory system to make accurate predictions about future events depends on the relative robustness of our stored memories. This same robustness, however, provides a potential threat in that memories might become

harder to change and thus our behavior may become guided by concepts that are no longer an adequate representation of the current situation. Research on memory suffers from a comparable threat in that well-established theories might become difficult to adjust to encompass new insights.

The focus on the medial temporal lobe as being critically involved in episodic memory was essentially initiated by the influential paper on patient HM, reporting the devastating anterograde amnesia as the result of bilateral resections of the antero-medial portions of the temporal lobe. The lesions included a substantial part of the hippocampal formation (HF), the amygdala and the parahippocampal region (PHR), in particular the entorhinal cortex (EC) and perirhinal cortex (PER) (Annese et al., 2014; Augustinack et al., 2014; Scoville & Milner, 1957). Irrespective of the fact that the lesions included several different brain structures aside HF bilaterally, the field quickly zoomed in on HF as the likely most critical structure underlying episodic memory (Milner, Squire, & Kandel, 1998). This emphasis on HF was strengthened by a large body of existing data reporting the beautiful morphological simplicity of HF and its intrinsic organization (Blackstad, 1956, 1958; Haug, 1976; Hjorth-Simonsen, 1971; Hjorth-Simonsen & Jeune, 1972; Lorente de Nó, 1934; Ramón y Cajal, 1893), the first description of the spatially modulated "place cell" (O'Keefe, 1976; O'Keefe & Dostrovsky, 1971), the phenomenon of long-term potentiation (Bliss & Lømo, 1973), all culminating in the very influential book in which O'Keefe and Nadel proposed the theory of the hippocampus as a cognitive map (O'Keefe & Nadel, 1978). These authors managed to integrate all these seemingly disparate observations into a coherent theoretical framework organized around the concept of place cells as the cellular basis for representation of space as well as events and experiences associated with space. Although clearly unintended by these two authors at that time, the appealing experimental simplicity of the navigational focus set the scene for a hippocampal-centric hierarchical view of the medial temporal lobe memory system. The latter includes the amygdala and the PHR. Although the amygdala does affect memory functions through influencing consolidation of emotional stimuli (Adolphs, Cahill, Schul, & Babinsky, 1997; Sutherland & McDonald, 1990; Zola-Morgan, Squire, Alvarez-Royo, & Clower, 1991), restricted lesions to the amygdala do not produce appreciable memory impairments (Mishkin, 1978; Sutherland & McDonald, 1990; Zola-Morgan, Squire, & Amaral, 1989). In contrast, PHR with the entorhinal cortex (EC) as a nodal point, eventually became recognized as a player of substance. The latter structure was positioned to mediate the overall reciprocal connections of HF with the cortex (Buzsaki, 1996; Eichenbaum, 2000; Kosel, Van Hoesen, & Rosene, 1982; Squire, Stark, & Clark, 2004).

Ramon y Cajal drew attention to EC or the "sphenoidal cortex"/"angular ganglion" as he initially referred to it (Ramón y Cajal, 1902), describing the massive bundle of entorhinal fibers, perforating the subiculum on its way to HF. This led him to suggest that the functional significance of EC had to be related to that of HF. Subsequent anatomical studies showed that EC provides a main input to HF (Witter, Groenewegen, Lopes da Silva, & Lohman, 1989). A second seminal observation was that in the monkey, HF distributes a main output to deep layers of EC, which in turn originates major projections to adjacent parts of PHR as well as to frontal cortical domains (Kosel et al., 1982; Van Hoesen & Pandya, 1975a; G. Van Hoesen, Pandya, & Butters, 1975; Van Hoesen & Pandya, 1975b). This was later corroborated and further detailed in the monkey (Munoz & Insausti, 2005) and in a number of other species, including rodents (Witter, et al., 1989). Although in subsequent years anatomical studies detailed the connectional organization of PHR, and EC in particular, the role of EC was not really appreciated; the functional attributes of EC remained in the shadow, only to achieve recognition more recently, resulting in a still ongoing explosion of rich and surprising new details. One initial finding contributing to this recognition was that damage to EC results in strong functional impairments in episodic memory (Buckmaster, Eichenbaum, Amaral, Suzuki, & Rapp, 2004; Leonard, Amaral, Squire, & Zola-Morgan, 1995; Meunier, Bachevalier, Mishkin, & Murray, 1993). In addition, the discovery of place fields in area CA1 of HF initiated a discussion on whether these functional properties were the result of internal HF computations or depended on inputs from outside HF. A recent comprehensive review (Moser, Moser, & McNaughton, 2017) summarized this debate in detail and introduced the subsequent discovery of spatially modulated grid cells in the most dorsal part of the medial entorhinal cortex (MEC) in rodents. This and subsequent reports on many functional cell types, all relevant to path-integration-based representation of self-location in MEC, contributed to the current strong interest in the functional attributes of MEC. The discovery of the grid cell further led to a substantial number of studies aiming to describe or model the neuronal networks underlying their specific firing properties (Moser et al., 2017).

The focus on MEC as the location of the myriad of functional cell types relevant for spatial navigation and spatial memory has enhanced our understanding of the entorhinal-hippocampal interplay and led to an interaction between computational and experimental neuroscience, aiming to identify and study generic circuit motifs underlying spatial perception and navigation. Although very productive, this focus distracted from the fact that there is a nonspatial side to episodic memory. For example, although partial or even complete lesions of MEC do impact the precision and long-term stability of place cells in HF (Brun et al., 2008; Hales et al., 2018), they do not abolish them. Such lesions do impair performance in the water maze of rats, similar to HF-lesions, but do not affect other HF-dependent tasks such as memory for object-location and context (Hales et al., 2018). For an episodic memory, one needs not only to store where the event took place and the position of the observer/participant in an allocentric parametric space, but also what happened and when it happened. This final convergence likely takes place in HF (Eichenbaum, 2017). Anatomical and functional data in rodents, monkeys, and humans suggest that the "What" is represented in the lateral entorhinal cortex (LEC) (Ritchey, Libby, & Ranganath, 2015; M. P. Witter et al., 2000), whereas time was suggested to be mediated through MEC (Eichenbaum, 2017) though more recent data indicated a role for LEC as well (Montchal, Reagh, & Yassa, 2019; Tsao et al., 2018).

It was particularly the knowledge about cortical connectivity that led to the notion of two functionally different portions in EC. The concept of LEC and MEC as entorhinal areas belonging to two parallel

input–output streams mediating the encoding and storage of respectively what and where information is currently well accepted (Eichenbaum, Yonelinas, & Ranganath, 2007; Ritchey et al., 2015). An important component of this concept hinges on the claim that a major component of their cortical connections is with the PER cortex and postrhinal (POR) in rodents, or parahippocampal cortex (PHC) in primates. In this scenario, LEC and PER are connectionally associated and POR and MEC are likewise partners. However, already in the early anatomical studies, there are indications that this connectional dissociation is not as evident as generally portrayed (Burwell & Amaral, 1998a, 1998b; Insausti & Amaral, 2008; Suzuki & Amaral, 1994b). Moreover, several authors emphasized that both PER and POR as well as LEC and MEC are interconnected (Burwell & Amaral, 1998b; Dolorfo & Amaral, 1998; Köhler, 1986, 1988; Lavenex, Suzuki, & Amaral, 2004). Although these interconnections have been included by some authors (Burke et al., 2018; Knierim, Neunuebel, & Deshmukh, 2014; Lisman, 2007; Ranganath & Ritchey, 2012), they have not really surfaced as relevant components in the appraisal of the potential functional roles of LEC and MEC and likewise PER and POR/PHC (cf. Furtak, Ahmed, & Burwell, 2012). So, a reappraisal of the parallel model is considered relevant (Figure 1) to prevent the field from consolidating on an incomplete model of the functional relevance of PHR.

We further need to consider that although the multitude of functionally specialized cell types in MEC is remarkable, many of them express more than one type of information. Such conjunctive neurons are particularly abundant in deeper Layers III and V of MEC, whereas pure grid cells are predominant in Layer II. In the deeper layers of MEC, a majority of the not so numerous grid cells fire conjunctively for position and head direction or speed, and many border cells are direction-selective (Hardcastle, Maheswaranathan, Ganguli, & Giocomo, 2017; Kropff, Carmichael, Moser, & Moser, 2015; Sargolini et al., 2006; Solstad, Boccara, Kropff, Moser, & Moser, 2008). Until recently, very little was known about the local intra—and interlaminar networks in MEC, except for the local network in Layer II, associated with the grid cell phenotype, briefly mentioned earlier. The emergent functional properties of the deeper cells are thus still poorly understood in terms of local architecture and its interactions with input/output connectivity. Even less is known about LEC. Based on the striking difference in functional cell types in LEC and MEC (Deshmukh & Knierim, 2011; Hargreaves, Rao, Lee, & Knierim, 2005; Neunuebel, Yoganarasimha, Rao, & Knierim, 2013; Tsao et al., 2018; Tsao, Moser, & Moser, 2013; Wang et al., 2018) expectations were that local circuits might differ between the two EC subdivisions. This has only recently been studied in detail, and these recent results indicate that the local circuits in LEC and MEC might not be all that

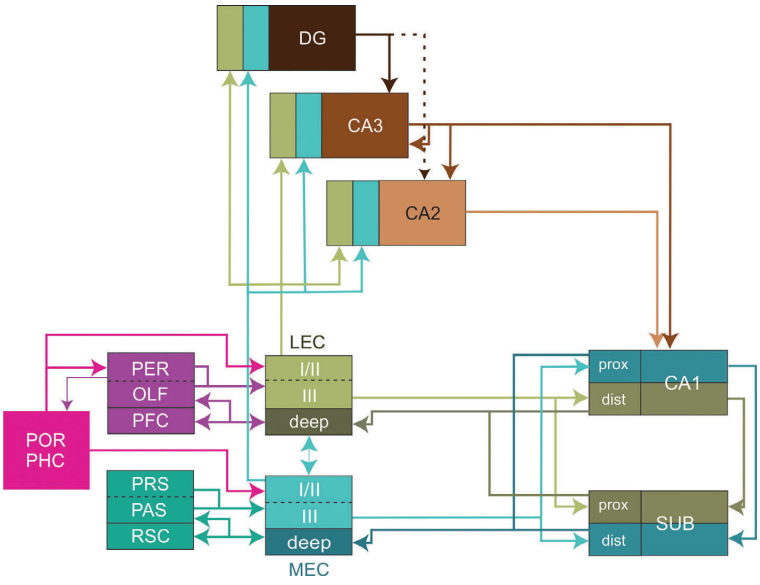

FIGURE 1 Schematic representation of the proposed updated version of the wiring scheme of the parahippocampal-hippocampal system. The lateral and medial entorhinal cortex mediate parallel input streams, conveying integrated representations of two complementary sets of cortical inputs to the hippocampus. The lateral entorhinal cortex (LEC) receives strong inputs from perirhinal (PER), orbitofrontal, medial prefrontal and insular cortices (PFC), and olfactory structures (OLF) including the olfactory bulb and the olfactory or piriform cortex. In contrast, MEC receives main inputs from presubiculum (PRS), parasubiculum (PAS), and retrosplenial cortex (RSC). The postrhinal/parahippocampal cortex (POR/PHC) provides inputs to both MEC and LEC as well as to PER. Dashed dividers in boxes imply that incoming projections distribute to both components of the box. CA3, CA2, CA1, subfields of the hippocampus proper; DG, dentate gyrus; dist, distal part; prox, proximal part [Color figure can be viewed at wileyonlinelibrary.com]

different (Fuchs et al., 2016; Leitner et al., 2016; Nilssen et al., 2018; Ohara et al., 2018).

In this review, we aim to relate the organization of local networks to what is known about cortical inputs and their postsynaptic targets, with a focus on the concept of parallel cortical connectivity streams. Although this review is dominated by rodent data, we aim to integrate relevant primate data. We will argue that EC, changed from being insignificant into possibly one of the most important characters in the tale of the medial temporal lobe. Moreover, instead of considering LEC and MEC as mediating segregated parallel input pathways to HF, the network structure emphasizes the potential of substantial integration of cortical information through interactions between LEC and MEC. Integration is likely reflected in the complex conjunctive properties of neurons seen throughout EC, and more in particular in LEC (Deshmukh & Knierim, 2011; Naya & Suzuki, 2011; Suzuki, Miller, & Desimone, 1997; Tsao et al., 2013; Wang et al., 2018). We therefore feel the need to revise the current parallel model where the medial and lateral entorhinal cortex provide parallel input streams to HF into one where EC is considered as an area allowing for integration of two or even more parallel cortical streams (Yoo & Lee, 2017), providing HF with high-order complex representations of the external environment, its stability, as well as apparent changes either as an inherent feature of a biological environment or as the result of navigating the environment.

1.1 | The entorhinal cortex comprises two subdivisions

EC can be best defined based on its projections to the hippocampus, which target neurons in all main hippocampal subdivisions. Although EC projections to some of the HF fields, particularly those to CA1 and subiculum are paralleled by projections from PER and POR, the EC projections to DG are currently considered a unique projection, identifying EC (Cappaert, Van Strien, & Witter, 2014; Witter, Doan, Jacobsen, Nilssen, & Ohara, 2017). EC is associated with the rhinal sulcus and in many if not all mammalian species, EC is characterized by a regular six-layered structure with a neuron-sparse superficial Layer I and a similarly neuron-sparse Layer IV in the center, sandwiched between Layer III and Layer V. In the posteromedially positioned MEC, all layers are clearly demarcated and show a relatively homogeneous distribution of neurons. The opposite, anterolateral part, LEC, has a less stringent laminar structure, and the overall distribution of neurons is less homogeneous. Note that there is generally an area in between these extremes and in particular this intermediate area has been subdivided differently in various species. It is a common observation that the cytoarchitectonically based subdivision of this intermediate area is increasingly complex in primates (Amaral, Insausti, & Cowan, 1987; Insausti, Tunon, Sobreviela, Insausti, & Gonzalo, 1995; Krimer, Hyde, Herman, & Saunders, 1997). A detailed description and comparison of all subdivisional schemes that have been proposed is beyond the scope of the review but has been covered in several papers in detail (Insausti, Munoz-Lopez, Insausti, & Artacho-Perula, 2017; Witter, Groenewegen, et al., 1989). For this review we will use LEC and MEC as indications for two areas, irrespective of species, for which most functional data are available, including in humans (Maass, Berron, Libby, Ranganath, & Duzel, 2015; Montchal et al., 2019; Navarro Schroder, Haak, Zaragoza Jimenez, Beckmann, & Doeller, 2015). Moreover, in a recent comparative review on the distribution of chemically defined neurons and neuropil, we have argued that these are best described as a gradient related to the distance from the rhinal/collateral sulcus and not related to any of the traditional cytorarchitectural subdivisions (Kobro-Flatmoen & Witter, 2019).

In most if not all studied nonprimate species, the organization of the EC projection to DG, originating from reelin expressing neurons in Layer II of both LEC and MEC, supports the subdivision of EC into two subareas, whereby LEC targets dendritic compartments located distally to those targeted by MEC fibers (Hjorth-Simonsen, 1972; Hjorth-Simonsen & Jeune, 1972; Witter, 2007; Witter et al., 2017). Whereas axons from LEC terminate in the outer one-third of the DG molecular layer, those from MEC terminate in the middle one-third. This spatial segregation is less evident in the monkey (Witter & Amaral, 1991; Witter, Van Hoesen, & Amaral, 1989). Irrespective of these anatomical differences, it is likely that in all species the projections from all parts of EC, irrespective of the number of subdivisions recognized by various authors, converge onto single neurons in DG and likely this holds true for CA3 and CA2 as well. In rodents and monkeys, entorhinal Layer III projections to CA1 and subiculum show a strikingly different organization from those arising from Layer II in that axons from LEC target neuronal populations different from those targeted by projections from MEC (Naber, Lopes da Silva, & Witter, 2001; van Groen, Miettinen, & Kadish, 2003; Witter & Amaral, 1991). Fibers from LEC innervate a part of CA1 close to the subiculum and the directly adjacent portion of the subiculum, whereas fibers from MEC terminate in the CA1 part adjacent to CA2 and in the subicular part adjacent to the presubiculum. The return projections to Layer V of EC from CA1 and subiculum follow a similar topographical organization, thus creating segregated anatomical connectivity loops between LEC and MEC on the one hand and discrete portions of CA1 and subiculum on the other hand (Tamamaki & Nojyo, 1995; Witter, 1993).

Further data in support of a dissociation between the two EC subdivisions come from recent gene expression studies. Embryonic gene expression patterns in mice indicate that the two subdivisions of EC originate from two different pallial structures. Whereas MEC originates in close association with HF, LEC has its origin in a specific dorsoposterior part of the cortical anlage. Interestingly, these genetically defined subdivisions of EC were also recognized in birds and reptiles (Medina, Abellan, & Desfilis, 2017). In line with this is a report that LEC and MEC in adult mice show strikingly different enhancer-expression profiles (Blankvoort, Witter, Noonan, Cotney & Kentros, 2018).

1.2 | Emergent functional cell types

1.2.1 | MEC

In MEC, most if not all of the functionally defined neuron types seem to relate to coding aspects of space or navigation relevant to path-

integration-based representation of self-location. One finds at least two types of spatially modulated cells types, grid cells, which have multiple equidistant firing fields organized in a hexagonal pattern (Fyhn, Molden, Witter, Moser, & Moser, 2004; Hafting, Fyhn, Molden, Moser, & Moser, 2005), as well as spatially modulated nongrid cells (Miao, Cao, Moser, & Moser, 2017; Rowland et al., 2018). Grid cells have been reported in rats (Hafting et al., 2005), mice (Fyhn, Hafting, Witter, Moser, & Moser, 2008), bats (Yartsev, Witter, & Ulanovsky, 2011), and nonhuman primates (Killian, Jutras, & Buffalo, 2012). Periodic, grid-like signals have been identified also in the human EC (Doeller, Barry, & Burgess, 2010; J. Jacobs & Lee, 2016). Grid cells coexist in MEC with other functionally defined cell types that code for the heading of the animal (head-direction cells), for speed (speed cells), environmental borders (border cells), or the distance and angle to objects (object-vector cells) (Høydal, Skytøen, Moser, & Moser, 2018; Kropff et al., 2015; Sargolini et al., 2006; Solstad et al., 2008). MEC is thus best considered as a cortical structure capable of computations underpinning path integration, an idiothetic navigation strategy in which the animal uses self-motion cues to track its current position relative to an arbitrary reference location (Buzsaki & Moser, 2013; Moser et al., 2017).

The complement of cortical relationships of MEC seems to match this overall presence of functional neuron-types. Main inputs to MEC originate from presubiculum and parasubiculum (Caballero-Bleda & Witter, 1993; Köhler, 1985; Room & Groenewegen, 1986; Shipley, 1975; van Groen & Wyss, 1990a, 1990b). Likewise, in rodents, cats, and monkeys, the retrosplenial cortex projects densely to MEC (Burwell & Amaral, 1998a; Jones & Witter, 2007; Kobayashi & Amaral, 2007; Room & Groenewegen, 1986). Additional inputs to MEC originate in visual association areas of the occipital cortex in the rat (Burwell & Amaral, 1998a; Kerr, Agster, Furtak, & Burwell, 2007), whereas these areas in monkeys primarily target PHC (Van Hoesen, 1982; Van Hoesen, Pandya, & Butters, 1972), and might thus influence MEC activity only indirectly. Projections from parietal cortex to MEC are weak to absent in all species studied; likely parietal cortex projects to PER and POR/PHC instead (Burwell & Amaral, 1998a; Kerr et al., 2007; Olsen, Ohara, Iijima, & Witter, 2017).

A final input that was historically specifically associated with MEC, a notion refuted in this paper, originates in POR in rodents and the cat or PHC as the likely homologous area in the monkey is referred to (Burwell, Witter, & Amaral, 1995). This notion of POR/PHC preferred connectivity with MEC seems in line with recent resting state connectional studies in humans (Maass et al., 2015; Navarro Schroder et al., 2015). However, a reanalysis of the available data has made us to reconsider this notion (Doan, Donate Lagartos, Nilssen, & Witter, 2018). As it turns out, in the monkey, the largest subdivision of PHC (area TF) sends projections that cover almost the entire AP axis of EC, showing an oblique distribution from caudomedial to rostrolateral, thus interacting with neurons in both MEC and LEC. Interestingly, the TF projections show an increasing density more rostrally in close association with the collateral sulcus (Insausti & Amaral, 2008; Suzuki & Amaral, 1994b). A reanalysis of the three main rodent studies (Burwell & Amaral, 1998a, 1998b; Naber, Caballero-Bleda, Jorritsma-Byham, & Witter, 1997) and analysis of own additional anterograde tracing material in mice and rats led to a comparable conclusion that POR in the rat projects to both LEC and MEC. These analyses indicate that, in rodents at least, these projections do not differ much in anatomical strength, in line with quantitative retrograde data indicating that POR provide 7% of cortical input to MEC and 5% to LEC (Burwell & Amaral, 1998a). Like in the monkey, the projections from POR in the rat preferentially target more lateral and central parts of EC (Doan et al., 2018).

1.2.2 | Lateral entorhinal cortex

Functional descriptions of neurons in LEC are unfortunately less detailed and less numerous. It is clear that space does not represent a main correlate. In the rodent, grid cells have not been recorded in LEC and spatially modulated cells are scarce (Hargreaves et al., 2005; Yoganarasimha, Rao, & Knierim, 2011). Across cortical layers, LEC contains a low number of neurons that show emerging spatially confined firing fields, resembling hippocampal place fields, following the exposure to objects. These neurons signal either the current or previous locations of the introduced objects, that is, some represent a memory for object location or show spatial firing not associated to current or past object presence, but these cells seem to require objects present in the environment (Deshmukh & Knierim, 2011; Tsao et al., 2013). Similar physiological responses have been reported in upstream connected areas, including PER (Burke et al., 2012; Deshmukh, Johnson, & Knierim, 2012). Likewise, in the monkey EC, cells that responded specifically to the visual presentation of objects or their spatial location have been reported. Furthermore, a number of cells displayed sustained activity after the removal of the visual stimulus, indicating that object features, or locations were maintained in memory (Suzuki et al., 1997), thus strongly resembling neurons in LEC in the rat (Tsao et al., 2013). Whereas such object-in-place neurons are found preferentially in the anterior parts of EC, likely thus in LEC, place-selective neurons were more equally distributed along the anteroposterior extent of EC, thus likely such cells are common to both LEC and MEC (Suzuki et al., 1997).

Neurons in LEC are also involved in olfactory processing, as witnessed by the modulation of LEC neuronal activity by olfactory stimuli in rats (Leitner et al., 2016; Xu & Wilson, 2012; Young, Otto, Fox, & Eichenbaum, 1997). Such a role of LEC is in line with data from studies in rats, guinea pigs, and cats demonstrating that olfactory information to HF is mediated by way of LEC (Biella & de Curtis, 2000; Boeijinga & van Groen, 1984; Habets, Lopes da Silva, & Mollevanger, 1980; Schwerdtfeger, Buhl, & Germroth, 1990; Van Groen, Lopes da Silva, & Wadman, 1987; R. C. Wilson & Steward, 1978). The importance of the LEC in olfactory memory processes is indicated by observations of altered behavior in olfactory-dependent tasks following electrolytic damage of the LEC. Such interventions in rats have been shown to result in olfactory anterograde amnesia (Staubli, Fraser, Kessler, & Lynch, 1986; Staubli, Ivy, & Lynch, 1984), but also facilitation of olfactory recognition abilities (Otto, Schottler, Staubli, Eichenbaum, & Lynch, 1991; Wirth, Ferry, & Di Scala, 1998).

These effects are in line with the important role of LEC in olfactory associate learning (Ferry, Ferreira, Traissard, & Majchrzak, 2006; Igarashi, Lu, Colgin, Moser, & Moser, 2014). For example, coherence in the slow gamma range (20–40 Hz) between LEC and distal CA1 has been demonstrated during successful odor–place associations in an associative learning task. This coherence suggests a state of synchronized activity likely mediating information transfer between LEC and the HF during odor learning or facilitating the use of retrieved olfactory memory from HF to fine-tune olfactory discrimination (Colgin, 2016). Interestingly, for similar trials, such coherence was not observed between MEC and CA1 (Igarashi et al., 2014). Note that during spatial navigation MEC and CA1 showed coherence in the high gamma range (Colgin & Moser, 2010).

Like for MEC, also for LEC the accompaniment of cortical relationships seems to match this overall presence of functional neuron-types. Evoked odor responses in LEC are in agreement with extensive axonal projections to LEC from the piriform cortex and the olfactory bulb, reported in several species including mice, rat, cat, and monkey (Boeijinga & van Groen, 1984; Burwell & Amaral, 1998a; Haberly & Price, 1977; Insausti, Amaral, & Cowan, 1987; Kerr et al., 2007; Kosel, Van Hoesen, & West, 1981; Room, Groenewegen, & Lohman, 1984; Shipley & Adamek, 1984; G. W. Van Hoesen et al., 1972; Wouterlood, Mugnaini, & Nederlof, 1985; Wouterlood & Nederlof, 1983). Note that the projection from the olfactory bulb in monkeys is restricted to more rostral areas of LEC (Insausti et al., 1987).

Representation of objects likely reflect LEC's prominent input from PER, which only provide weak input to MEC (Burwell & Amaral, 1998b; Suzuki & Amaral, 1994b). PER is involved in discrimination between novel and familiar objects both in rodents and primates, and its activity reflects the integration of multimodal sensory aspects of objects, items, or events (Brown, 2008; Buckley & Gaffan, 2006; Bussey & Saksida, 2005, 2007; Bussey, Saksida, & Murray, 2006; Kealy & Commins, 2011; Naya, 2016; Taylor, Moss, Stamatakis, & Tyler, 2006).

1.3 | Neurons and networks in MEC and LEC are remarkably similar

The EC comprises six cortical layers, four of which contain the main populations of neurons, Layers II, III, V, and VI. The molecular Layer I contains only a low number of interneurons, and Layer IV or the lamina dissecans as it is often referred to, also contains very low numbers of neurons. Here we focus on the networks of Layers II, III, and V, because for the remaining layers, detailed connectional data for both entorhinal subdivisions are lacking.

1.3.1 | Layer II

Principal cells in Layer II of LEC and MEC come in at least two chemical types, calbindin- and reelin-expressing cells. In MEC, stellate cells make up most of the principal neurons and they are typically reelin-positive and calbindin-negative. The main counterparts in Layer II of MEC are the calbindin-positive pyramidal neurons. In LEC, a comparable subdivision has been reported with fan and multipolar neurons forming a substantial part of the reelin-positive principal cells and pyramidal neurons corresponding largely to calbindin-positive neurons (for review see Kobro-Flatmoen & Witter, 2019; Witter et al., 2017). In MEC, these two main principal cell types can also be distinguished based on their electrophysiological profiles. Stellate cells have a prominent sag potential, resonance, and membrane oscillations, whereas in the pyramidal neurons these properties are absent (Canto & Witter, 2012b; Fuchs et al., 2016). Note that the typical stellate properties are most pronounced in medially located neurons and become less apparent in more laterally positioned neurons. This gradient continues into LEC, such that in LEC medially positioned stellate/multipolar neurons share some of these properties with adjacent MEC stellate cells (Canto & Witter, 2012b). In lateral LEC, more subtle electrophysiological differences between the two chemically and morphologically defined neuron classes have been reported (Leitner et al., 2016; Tahvildari & Alonso, 2005) though this is not supported by others (Canto & Witter, 2012a; Desikan, Koser, Neitz, & Monyer, 2018).

Reelin-positive neurons in Layer II of both LEC and MEC give rise to the projections to DG, and likely also to CA3 and CA2. Likewise, calbindin-positive neurons show connectional motifs in both LEC and MEC that are very similar, in that they contribute to a wide range of extrinsic projections including hippocampal field CA1, many if not all of EC extrahippocampal target areas as well as commissural projections (Fuchs et al., 2016; Kitamura et al., 2014; Leitner et al., 2016; Varga, Lee, & Soltesz, 2010). Interestingly, recent data in rodents show that almost 50% of Layer II calbindin-positive neurons originate local excitatory projections, with MEC neurons projecting within MEC and sending projections to LEC, whereas the local LEC calbindin-positive projections predominantly distribute within LEC (Ohara et al., 2016; Figure 2).

The local circuits of principal cells in Layer II of MEC have been probed extensively and all data indicate that individual stellate reelin-positive cells lack monosynaptic connections with other principal cells, and the same is the common connectivity pattern between pyramidal calbindin-positive neurons. However, pyramidal neurons do have a relatively strong connection with stellate neurons (Fuchs et al., 2016; Winterer et al., 2017). Communication among neurons of the same class occurs through an intermediate inhibitory interneuron, in a mechanism by which activation of one or more principal neurons evokes disynaptic inhibitory currents in neighboring principal neurons (Couey et al., 2013; Fuchs et al., 2016; Pastoll, Solanka, van Rossum, & Nolan, 2013). The functional disynaptic link that illustrates the core principle of the stellate reelin-positive microcircuit is mediated by a single type of inhibitory neuron, the PV positive fast spiking cell (Armstrong, Szabadics, Tamas, & Soltesz, 2011; Fuchs et al., 2016; Varga et al., 2010) and in case of grid cells in Layer II the same has been reported (Buetfering, Allen, & Monyer, 2014). In case of calbindin-positive pyramidal cells, the interneuron in between belongs to the heterogeneous $5HT_{3A}$ expressing population of interneurons (Fuchs et al., 2016). In a recent study, the Layer II network in LEC was analyzed, showing that very similar connectivity motifs are present.

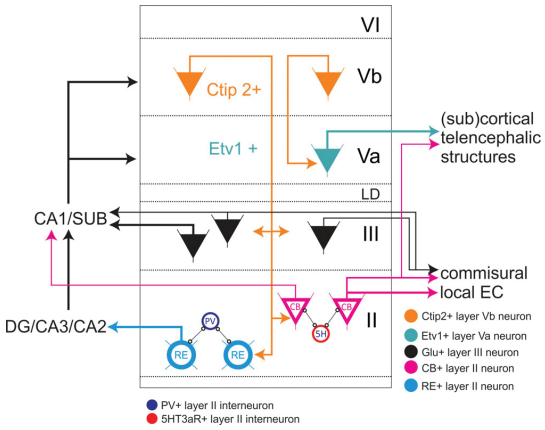

FIGURE 2 Summary of shared neuron types and local circuit motifs of the lateral and medial entorhinal cortex. Because very little to nothing is known concerning Layer VI, no neurons and circuits are indicated. In Layer II, we show the two types of principal neurons, reelin (RE) and calbindin (CB) positive, and their specific local connectivity to parvalbumin (PV) and 5HT3a-receptor (5H) expressing interneurons, respectively. Also shown are the main projections to hippocampal fields and intrinsic and commissural projections. Not included is the observation that these two populations of principal cells do communicate through a separate class of pyramidal neurons. In Layer III, about 40% of the neurons projecting to CA1 and subiculum do give rise to commissural collaterals. Pyramidal cells in Layer III show a relatively strong developed local excitatory network (not indicated). In Layer V, we indicate that VB neurons project to Va as well as to Layers II and III. Note that although data indicate that the superficially projecting Layer Vb neurons also project to Laver Va, conclusive evidence for that is still lacking, so we have depicted as if these respective projections originate from different principal neurons. Inputs to layers and identified neurons therein are not indicated since they differ between LEC and MEC. CA3, CA2, CA1 subfields of the hippocampus proper; CB, calbindin-positive neuron; DG, dentate gyrus; EC, entorhinal cortex; LD, lamina dissecans; RE, reelin-positive neuron [Color figure can be viewed at wileyonlinelibrary.com]

Like in MEC, principal neurons in LEC lack monosynaptic connectivity among members of their own class, showing a preferred disynaptic connectivity mediated by interneurons (Nilssen et al., 2018). Note that the prevalent types of interneurons mediating disynaptic inhibitory connectivity between principal neurons in LEC are partially different from those in MEC. A detailed analysis of the diverse population of interneurons in EC is not yet available and the relevance of these interneuronal differences is not yet fully understood.

1.3.2 | Layer III

Layer III in both LEC and MEC comprises a homogenous population of spiny excitatory pyramidal neurons, multipolar neurons, and interneurons (Germroth, Schwerdtfeger, & Buhl, 1989; Gloveli, Schmitz, Empson, Dugladze, & Heinemann, 1997; Köhler & Chan-Palay, 1983; Wouterlood & Pothuizen, 2000; Wouterlood, van Denderen, van Haeften, & Witter, 2000). The pyramidal and multipolar neurons are the source of the projections to CA1 and subiculum (Canto & Witter, 2012a, 2012b; Germroth et al., 1989; Tahvildari & Alonso, 2005; Tang et al., 2015). Layer III neurons also project contralaterally to the hippocampus and EC (Steward & Scoville, 1976), with about 40% of the Layer III hippocampal projecting cells in MEC sending collaterals to the contralateral MEC (Tang et al., 2015).

The microcircuits of Layer III seem markedly different from those seen in Layer II, showing higher connection probability between principal neurons (Dhillon & Jones, 2000; Kloosterman, Van Haeften, Witter, & Lopes Da Silva, 2003; Tang et al., 2015; van der Linden & Lopes da Silva, 1998). Neurons in Layer III, like those in Layer II, are main recipients of the local deep-to-superficial projections, which predominantly originate from neurons in Layer V (Kloosterman et al., 2003; Ohara et al., 2018; van Haeften, Baks-Te Bulte, Goede, Wouterlood, & Witter, 2003). Currently, no correlations have been reported between morphology, connectional profile, and electrophysiological in vitro and in vivo properties (Canto & Witter, 2012a, 2012b; Tang et al., 2015) (Figure 2).

1.3.3 | Layer V

Layer V is commonly subdivided into a Layer Va and Vb (Amaral et al., 1987; Boccara et al., 2015; Canto & Witter, 2012a, 2012b; Hamam, Amaral, & Alonso, 2002; Hamam, Kennedy, Alonso, & Amaral, 2000). In mice and rats, the expression pattern of the transcription factors Etv1 and Ctip2 provides for the differentiation between the two sublayers Va and Vb, respectively. This organization prevails across the whole mediolateral and dorsoventral extent of EC. In both MEC and LEC, Layer Va cells are the major output neurons projecting to diverse cortical and subcortical structures (Kosel et al., 1982; Ohara et al., 2018; Ramsden, Surmeli, McDonagh, & Nolan, 2015; Surmeli et al., 2015; Swanson & Köhler, 1986; G. W. van Hoesen, 1982). Surprisingly, Layer Vb cells are selectively targeted by the outputs from the hippocampus, originating in CA1 and subiculum (Surmeli et al., 2015), though this is apparently only true for projections originating from dorsal levels of subiculum and CA1; increasingly more ventral levels apparently innervate neurons in both Layer Va and Vb (Egorov, Lorenz, Rozov, & Draguhn, 2017; Ohara and Witter, unpublished data). Layer Vb neurons in both LEC and MEC innervate Layer Va as well as Layers II and III (Ohara et al., 2018), corroborating older data that neurons in Layer Vb issue superficially directed axon collaterals (Canto & Witter, 2012a, 2012b; Hamam et al., 2000; Hamam et al., 2002). Preliminary in vitro single cell recordings indicate that the effective connectivity to Layer III neurons is higher than the connectivity to Layer II (Ohara and Witter, unpublished data). Layer Vb neurons, but not Layer Va neurons, are also targeted by projections originating from reelin neurons in Layer II of MEC (Surmeli et al., 2015). Layer V is also innervated by cortical projections from frontal and cingular domains, including the anterior cingular cortex (Area 24) in case of LEC and retrosplenial cortex (Area 29 and 30) in case of

MEC. Projections from the retrosplenial cortex target, among others, spiny pyramidal neurons that issue axons to superficial layers (Czajkowski et al., 2013).

In conclusion, neuron types, local circuit motifs, and the laminar origin and termination of outputs and inputs respectively, in MEC and LEC are strikingly similar (Figure 2). This seems somewhat counterintuitive to the striking functional differences described earlier, and reports that LEC and MEC develop from different parts of the pallium (Medina et al., 2017). As concisely and eloquently reviewed by Desfilis and colleagues (Desfilis, Abellan, Sentandreu, & Medina, 2018), MEC shares its embryological pallial origin with HF, whereas LEC shares its origin with PER, orbitofrontal, and insular domains of the cortex. The latter are cortical structures with which LEC selectively is connected and that are also strongly interconnected as argued earlier. Data on the origin of POR are currently lacking. Both LEC and MEC share an input from the olfactory or piriform cortex, but the connections with the olfactory bulb are almost exclusive with LEC. Comparable patterns can be found in case of the presumed homologous regions in lizards and chicken (Desfilis et al., 2018). Interestingly, LEC and MEC also differ with respect to the sequential developmental origin of the different layers, in that LEC follows the "neocortical" inside-out pattern, whereas in MEC, like in HF, the developmental gradient is such that outside layers, that is, Layer II in case of MEC, develop first. This latter observation is supported by developmental data recently reported in the mouse (Donato, Jacobsen, Moser, & Moser, 2017). The latter authors not only reported that neurons in MEC Layer II are the first to mature, but that interfering with the maturation of these early developing Layer II MEC neurons postpones the subsequent maturation of all neurons in LEC. This suggests that MEC layer II neurons already in early stages of development directly influence the development of LEC.

One way for such a developmental influence to take place is through the presence of projections from MEC to LEC. Though long-ranging intrinsic connections may already be partially present in the postnatally developing brain (O'Reilly et al., 2015), they are quite extensive in adults; note that in the monkey the long-range extent does not cover the total AP axis of EC but seems to indicate that the connectional hub is formed by the central portion of EC (Chrobak & Amaral, 2007; Dolorfo & Amaral, 1998; Köhler, 1986, 1988; Witter, Room, Groenewegen, & Lohman, 1986). It would be of interest to know whether similar connections exist in the reptilian brain. Comparable long-range projections exist between PER and POR in rats (Burwell & Amaral, 1998b) and PER and PHC in monkeys (Lavenex et al., 2004). Similar to what was noted above for intrinsic EC connections in the monkey, the caudal part of PER, located centrally along the AP axis of PER/PHC is the main hub for these long-range connections. The overall patterns of origin and terminal distributions of these projections supports the conjecture that POR/PHC projections to PER are of the feedforward type whereas the reverse projections fit more the patterns of feedback projections (Barbas & Rempel-Clower, 1997).

These observations, taken together with the data described above that the projections of POR/PHC are not restricted to MEC but also target LEC, makes it relevant to ask the question what these posterior parts of PHR contribute functionally to PHR and thus to HF. To address this question, it is worthwhile to summarize the cortical input patterns described earlier by emphasizing that the widespread projections from POR/PHC to both MEC and LEC is the exception to the rule because most cortical afferents to LEC and MEC, like those to PER and POR/PHC, are selective for one or the other.

1.4 | Connectional and functional position of POR/PHC

Inputs from POR/PHC and PER in monkeys give rise to 60% of the cortical input to the EC (Insausti et al., 1987; Insausti & Amaral, 2008). This percentage includes the temporal polar cortex, which is considered part of the perirhinal cortex, likely specific for primates (Insausti et al., 1987). Within the primate PHC, there are two main subdivisions, TH and TF, where TF is further subdivided into lateral and medial components. Whereas area TH receives mainly auditory input from the superior temporal gyrus but weak or no direct visual input, both subdivisions of area TF receives strong visual inputs from areas TEO and V4, as well as from the retrosplenial cortex and the dorsal bank of the superior temporal sulcus. The lateral part of TF receives additional inputs from posterior parietal areas (Suzuki & Amaral, 1994a). In the rat, approximately 13% of the total cortical inputs to EC originate in PER and POR (Kerr et al., 2007). In case of POR, 40% of its cortical inputs originate in visual areas, 7% in posterior parietal cortex, and 16% in temporal association cortex; inputs from auditory, somatosensory, olfactory as well as frontal areas including insular, orbitofrontal, and medial prefrontal areas are negligible (Burwell & Amaral, 1998a; Furtak, Wei, Agster, & Burwell, 2007). Note that these input patterns are very different from those reported for PER (see later). In line with these prominent cortical inputs, which are largely reciprocated, POR is typically portrayed as providing visuospatial information to EC. This is supported by reports in humans that the PHC supports spatial perception in real time (Epstein, Parker, & Feiler, 2007), though there are also strong data both in rats and primates that POR/PHC is particularly relevant in relation to processing contextual associations (Aminoff, Gronau, & Bar, 2007; Furtak et al., 2012). In many instances the data relate to object-in-space/location or object-in-context associations (Bohbot et al., 1998; Hayes, Nadel, & Ryan, 2007; Maguire, Frith, Burgess, Donnett, & O'Keefe, 1998). Data in rats are sparser, but single cells responses of neurons in POR indicate that around 30% of POR cells showed object-location conjunctive encoding (Furtak et al., 2012). The latter authors suggested that POR combines object and pattern information from PER with incoming contextual and spatial information from retrosplenial and posterior parietal cortices to represent specific environmental contexts. This is in line with results of lesion studies in rats, showing that POR processes information about objects in relation to place or context (Gaffan, Healey, & Eacott, 2004; Norman & Eacott, 2005). Furtak and colleagues (Furtak et al., 2012) further reported that neuronal responses in POR show evidence of reflecting changes in context, or responses that relate to egocentric coding, which they relate to inputs

from parietal cortex, as well as. The latter is reminiscent of recent reports of egocentric coding in LEC (Wang et al., 2018; see also below) whereas the former is suggested to be associated with the strong connectivity from PER to POR. Based on these additional neuronal properties, they suggest that POR monitors the context for changes and updates the representation of the context accordingly. This updated representation would be a subsequent input to downstream areas, such as PER, EC, and HF. This suggestion seems to conflict somewhat with data indicating that PHC in humans is more active in response to stationary, spatially defining objects than to spatially ambiguous objects (Mullally & Maguire, 2011).

An alternative proposal, which we prefer to entertain, might be that changes in object/contextual or spatial relationships are perceived in downstream areas, such as PER, and fed back to the POR network to allow for an update of the contextual representation as to secure stability. This fits with the laminar pattern of projections between PER and POR/PHC (Lavenex et al., 2004). Interestingly, the proposition that POR plays a critical role in providing a stable representation of object-place associations is in line with very recent data showing that POR receives information from the superior colliculus, via its connections to LP (Beltramo & Scanziani, 2019; Bennett et al., 2019), which might provide an unconscious representation of self-movement related changes in the perceived position of objects. It further fits with the recent suggestion that both LEC and MEC may process visual context information, likely thus derived from POR, but that both use this information in a completely different functional way, related to the appropriate motor output (Yoo & Lee, 2017). Based on this notion one could predict that silencing of visual inputs to POR or silencing POR itself might change the representation of the context and thus will induce place cell remapping the hippocampus.

1.5 | Connectional and functional position of the PER/LEC interface

Neurons in LEC are responsive to objects-in-position associations, likely without discriminating between the nature of the object (Deshmukh & Knierim, 2011; Tsao et al., 2013). However, neurons and networks in LEC code beyond this by incorporating representations of context, because LEC is critically involved in complex object-context associations binding together information relating to objects, places, and contexts (Scaplen, Ramesh, Nadvar, Ahmed, & Burwell, 2017; Wilson et al., 2013; Wilson, Watanabe, Milner, & Ainge, 2013). Recent electrophysiological studies provide data suggesting that distinct contextual features of experiences are represented in LEC both at the single-cell and population level (Pilkiw et al., 2017; Tsao et al., 2018). Further analysis of LEC ensemble activity indicated a shift of population states according to the temporal progression of the experimental event. These data suggest that the activity of LEC populations carries a representation of time, brought about by the encoding of sequences of ongoing events. Although comparable data have been obtained in the anterolateral parts of the monkey and human EC (Montchal et al., 2019; Naya & Suzuki, 2011), the representation of incremental timing information, based on the sequence of ongoing events is weaker in EC compared to that in PER and HF (Naya & Suzuki, 2011). Likewise, although LEC neurons can integrate item and time information (Naya & Suzuki, 2011) conjunctive item neurons seem to be a more prevalent type in monkey LEC (Naya, Chen, Yang, & Suzuki, 2017).

Neurons and networks in the lateral part of LEC may embed other features to these already complex representations, including olfactory and salience percepts. The proposition that LEC neurons code for high order associations is in line with recent observations, indicating that individual principal cells in Layer II of LEC receive convergent inputs from PER, POR, MEC, olfactory piriform cortex, and from contralateral LEC Doan, Nilssen, & Witter, 2016). It is worth reiterating that the connectivity motif in Layer II in LEC is comparable to that of Layer II in MEC (Nilssen et al., 2018). We thus proposed that neurons in Layer II of LEC may show hexagonal, or at least regularly repeating, firing patterns along dimensions defined by their inputs (Nilssen et al., 2018). In contrast to the pure spatial representation observed in MEC, periodic patterns might arise in LEC to represent complex features of the context as part of a particular episode (Bellmund, Gardenfors, Moser, & Doeller, 2018; Constantinescu, O'Reilly, & Behrens, 2016). In this view, the inputs from POR and MEC provide LEC with relevant information to act as an integrative hub between what has been referred to as an egocentric representation of a context with the allocentric representation of self-position in that context (Wang et al., 2018; Yoo & Lee, 2017).

Here we emphasize the relevance of the PER/LEC interface. As argued earlier, multimodal representations of objects depend on perirhinal networks and PER also plays a relevant role in novelty-familiarity discriminations. Such functions likely reflect the variety of inputs targeting PER. Interestingly, PER shares most of these inputs with the strongly reciprocally connected directly adjacent lateral parts of LEC. These inputs include dense inputs from insular, orbitofrontal cortex, anterior cingulate cortex, temporal association cortex, as well as from the lateral and basal amygdala. In rats, additional inputs originate from the medial prefrontal prelimbic and infralimbic cortex, although these projections do target MEC and POR as well, be it with a lesser density of termination (Burwell & Amaral, 1998a; Insausti et al., 1987; Jones & Witter, 2007; Kerr et al., 2007; Kondo & Witter, 2014; Krettek & Price, 1977; Mathiasen, Hansen, & Witter, 2015; Mohedano-Moriano et al., 2007; Pitkanen, Kelly, & Amaral, 2002; Room & Groenewegen, 1986; Stefanacci & Amaral, 2000; Suzuki & Amaral, 1994a; Van Hoesen & Pandya, 1975a; Van Hoesen et al., 1975; Van Hoesen, 1982; Van Hoesen et al., 1972; Vaudano, Legg, & Glickstein, 1991; Vertes, 2004). Many of these forebrain areas play a role in coding of information concerning the salience or the reinforcing value of a particular context or elements in that context (Dixon, Thiruchselvam, Todd, & Christoff, 2017; Ritchey, Wang, Yonelinas, & Ranganath, 2018; Wallis, 2007). This would enable the PER/LEC interface to evaluate sensory cues not only as part of a particular context or episode but add information about the current emotional value of individual elements of the context or the context as a whole. Note that the frontal cortical inputs mainly, though not exclusively, target deeper layers of the PER/LEC interface and thus are in a

potential position to influence the main cortical output stream, mediated by the deep EC layers. Irrespective, we argued that deep entorhinal circuits also influence superficial circuits, so likely these frontal inputs have a role to play in modifying sensory representations in the superficial input network of PER/LEC as well. Of course, the lateral amygdala input might be the most relevant, because it terminates densely in superficial layers and it shares this superficial termination with olfactory inputs and those from higher order temporal sensory association cortex (Pitkanen et al., 2002; Pitkanen, Pikkarainen, Nurminen, & Ylinen, 2000).

In line with this shared input, we propose that it is the PER/LEC interface that provides the optimal substrate to detect changes in the context. This proposition is strengthened by an additional unique transmission property in this network. Connectivity from PER to adjacent LEC is governed by a striking inhibitory gating (de Curtis & Pare, 2004). This "wall of inhibition" is overcome by the convergence in time and space of at least two coincident inputs (Samarth, Ball, Unal, Pare, & Nair, 2017). These could be coincident inputs from temporal cortex or PER with lateral amygdala (Kajiwara, Takashima, Mimura, Witter, & Iijima, 2003; R. Paz, Pelletier, Bauer, & Pare, 2006; Pelletier, Apergis-Schoute, & Pare, 2005), mPFC and PER (Rony Paz, Bauer, & Pare, 2007), or insular cortex and amygdala (Willems, Wadman, & Cappaert, 2016). Coincident changes in sensory and saliency inputs would thus allow activation of LEC where neurons are capable of coding such changes over time. As already proposed, POR/PHC inputs would provide a stable representation of the current context, allowing the PER/LEC interface to detect relevant changes in the context over time, in line with the aforedescribed sequence coding that apparently occurs in the network. Subsequent transmission of salient changes in these contextual features would then result in updating HF representations of an episode. At the same time PER projections to POR and LEC projections to MEC would provide feedback information allowing these networks to incorporate these changes into their updated stable representations.

1.6 | Conclusions and future perspectives

We started this review with the concept of parallel pathways connecting HF with the cortical mantle and that there might be subdivisions of EC mediating such parallel pathways, because EC forms a major cortical input and output hub for HF. A key element in the development of this notion was the conceived preferred connectivity of PER with LEC and PHC/POR with MEC. Of likely similar influence was the notion of a hierarchical organization of the parallel streams culminating in the final convergence at the level of the networks in HF. We have argued that this conceived preferred connectivity in case of POR/PHC is incorrect. POR/PHC contributes to both pathways, providing both MEC and PER/LEC with what we propose is a continuously stable representation of context.

We support earlier suggestions that convergence takes place at multiple levels in the EC-HF memory system and provide new evidence, integrated in already existing data that this happens predominantly in LEC. In addition, we conclude that the connectional differences between LEC and MEC strongly support the concept of functional differences. Whereas the PER/LEC interface provides the hippocampus with a highly integrated, multidimensional representation of sensory information, including changes over time, constituting the content of an episodic memory, MEC provides the position of the subject, coded in an allocentric space (Eichenbaum et al., 2007; Lisman, 2007).

Contrary to previous expectations, all data concerning the intrinsic network motifs of LEC and MEC point to a striking overall similarity, notwithstanding that subtle differences in interneuron contributions may exist. The delicate role, undoubtedly played by interneurons, will be important to refine our understanding of information coding in the two subdivisions of EC. Our current knowledge leads to the intriguing conclusion that two embryologically different parts of the cortex, that even follow different developmental schemes, inside-out, versus outside-in, eventually result in two similar and strongly interconnected areas, which independently cannot fully support hippocampal functions. The shared network motifs of LEC and MEC suggest that HF requires an input that uses a particular "language" that originates from these network motifs. The developmental dependence of LEC on MEC input (Donato et al., 2017) supports the notion that the hippocampal anlage shapes its LEC input system to represent evolutionary new, more complex sensory and higher order stimuli, and communicates with HF using the same network dependent language to communicate with HF as the developmentally HF-associated-MEC system. It would be of interest to study this conjecture experimentally. One approach might be to use the reptilian brain as a simple model comparing olfactory and spatial representations in the likely homologues of LEC and MEC, which, like in the mammalian brain, project to all subdivisions of HF (Desfilis et al., 2018). Understanding this coding principle might be relevant, because olfaction has been proposed as a universal system among the sensory systems to mediate navigation and memory formation (L. F. Jacobs, Arter, Cook, & Sulloway, 2015). A second, very relevant and promising approach would be to pursue computational modeling of the output of such a network motif and study how HF responses depend on this input by systematically perturbing the input language. A similar argument can be made for the functional relevance of the hippocampal output network mediated by EC deep layers, which is still grossly understudied.

ACKNOWLEDGEMENTS

This study has been supported by grant number 227769 of the Research Council of Norway, the Centre of Excellence scheme of the Research Council of Norway—Centre for Neural Computation, grant number 223262, the National Infrastructure scheme of the Research Council of Norway—NORBRAIN, grant number 197467, and the Kavli Foundation. We thank Bente Jacobsen for stimulating discussions and comments on the semi-final version of the manuscript.

CONFLICT OF INTERESTS

The authors declare no potential conflict of interest.

ORCID

Menno P. Witter https://orcid.org/0000-0003-0285-1637

REFERENCES

Adolphs, R., Cahill, L., Schul, R., & Babinsky, R. (1997). Impaired declarative memory for emotional material following bilateral amygdala damage in humans. *Learning and Memory*, *4*(3), 291–300.

Amaral, D. G., Insausti, R., & Cowan, W. M. (1987). The entorhinal cortex of the monkey: I. Cytoarchitectonic organization. *Journal of Comparative Neurology*, *264*(3), 326–355. https://doi.org/10.1002/cne.902640305

Aminoff, E., Gronau, N., & Bar, M. (2007). The parahippocampal cortex mediates spatial and nonspatial associations. *Cerebral Cortex*, *17*(7), 1493–1503. https://doi.org/10.1093/cercor/bhl078

Annese, J., Schenker-Ahmed, N. M., Bartsch, H., Maechler, P., Sheh, C., Thomas, N., … Corkin, S. (2014). Postmortem examination of patient H.M.'s brain based on histological sectioning and digital 3D reconstruction. *Nature Communications*, *5*, 3122. https://doi.org/10.1038/ncomms4122

Armstrong, C., Szabadics, J., Tamas, G., & Soltesz, I. (2011). Neurogliaform cells in the molecular layer of the dentate gyrus as feed-forward gamma-aminobutyric acidergic modulators of entorhinal-hippocampal interplay. *Journal of Comparative Neurology*, *519*(8), 1476–1491. https://doi.org/10.1002/cne.22577

Augustinack, J. C., van der Kouwe, A. J., Salat, D. H., Benner, T., Stevens, A. A., Annese, J., … Corkin, S. (2014). H.M.'s contributions to neuroscience: A review and autopsy studies. *Hippocampus*, *24*(11), 1267–1286. https://doi.org/10.1002/hipo.22354

Barbas, H., & Rempel-Clower, N. (1997). Cortical structure predicts the pattern of corticocortical connections. *Cerebral Cortex*, *7*(7), 635–646.

Bellmund, J. L. S., Gardenfors, P., Moser, E. I., & Doeller, C. F. (2018). Navigating cognition: Spatial codes for human thinking. *Science*, *362*(6415), eaat6766. https://doi.org/10.1126/science.aat6766

Beltramo, R., & Scanziani, M. (2019). A collicular visual cortex: Neocortical space for an ancient midbrain visual structure. *Science*, *363*(6422), 64–69. https://doi.org/10.1126/science.aau7052

Bennett, C., Gale, S. D., Garrett, M. E., Newton, M. L., Callaway, E. M., Murphy, G. J., & Olsen, S. R. (2019). Higher-order thalamic circuits channel parallel streams of visual information in mice. *Neuron*, *102*(2), 477–492.e475. https://doi.org/10.1016/j.neuron.2019.02.010

Biella, G., & de Curtis, M. (2000). Olfactory inputs activate the medial entorhinal cortex via the hippocampus. *Journal of Neurophysiology*, *83*(4), 1924–1931.

Blackstad, T. W. (1956). Commissural connections of the hippocampal region in the rat, with special reference to their mode of termination. *Journal of Comparative Neurology*, *105*(3), 417–537.

Blackstad, T. W. (1958). On the termination of some afferents to the hippocampus and fascia dentata. An experimental study in the rat. *Acta Anatomica*, *35*, 202–214.

Blankvoort, S., Witter, M. P., Noonan, J., Cotney, J., & Kentros, C. (2018). Marked diversity of unique cortical enhancers enables neuron-specific tools by enhancer-driven gene expression. *Current Biology*, *28*(13), 2103–2114 e2105. https://doi.org/10.1016/j.cub.2018.05.015

Bliss, T. V., & Lømo, T. (1973). Long-lasting potentiation of synaptic transmission in the dentate area of the anaesthetized rabbit following stimulation of the perforant path. *The Journal of Physiology*, 232(2):331–56.

Boccara, C. N., Kjonigsen, L. J., Hammer, I. M., Bjaalie, J. G., Leergaard, T. B., & Witter, M. P. (2015). A three-plane architectonic atlas of the rat hippocampal region. *Hippocampus*, *25*(7), 838–857. https://doi.org/10.1002/hipo.22407

Boeijinga, P. H., & van Groen, T. (1984). Inputs from the olfactory bulb and olfactory cortex to the entorhinal cortex in the cat. II. Physiological studies. *Experimental Brain Research*, *57*(1), 40–48.

Bohbot, V. D., Kalina, M., Stepankova, K., Spackova, N., Petrides, M., & Nadel, L. (1998). Spatial memory deficits in patients with lesions to the right hippocampus and to the right parahippocampal cortex. *Neuropsychologia*, *36*(11), 1217–1238.

Brown, M. W. (2008). Hippocampal and perirhinal functions in recognition memory. *Nature Reviews. Neuroscience*, *9*(5), 405. doi:nrn2154-c1 [pii]. https://doi.org/10.1038/nrn2154-c1

Brun, V. H., Leutgeb, S., Wu, H. Q., Schwarcz, R., Witter, M. P., Moser, E. I., & Moser, M. B. (2008). Impaired spatial representation in CA1 after lesion of direct input from entorhinal cortex. *Neuron*, *57*(2), 290–302.

Buckley, M. J., & Gaffan, D. (2006). Perirhinal cortical contributions to object perception. *Trends in Cognitive Sciences*, *10*(3), 100–107.

Buckmaster, C. A., Eichenbaum, H., Amaral, D. G., Suzuki, W. A., & Rapp, P. R. (2004). Entorhinal cortex lesions disrupt the relational organization of memory in monkeys. *Journal of Neuroscience*, *24*(44), 9811–9825.

Buetfering, C., Allen, K., & Monyer, H. (2014). Parvalbumin interneurons provide grid cell-driven recurrent inhibition in the medial entorhinal cortex. *Nature Neuroscience*, *17*(5), 710–718. https://doi.org/10.1038/nn.3696

Burke, S. N., Gaynor, L. S., Barnes, C. A., Bauer, R. M., Bizon, J. L., Roberson, E. D., & Ryan, L. (2018). Shared functions of perirhinal and parahippocampal cortices: Implications for cognitive aging. *Trends in Neurosciences*, *41*, 349–359. https://doi.org/10.1016/j.tins.2018.03.001

Burke, S. N., Maurer, A. P., Hartzell, A. L., Nematollahi, S., Uprety, A., Wallace, J. L., & Barnes, C. A. (2012). Representation of three-dimensional objects by the rat perirhinal cortex. *Hippocampus*, *22*(10), 2032–2044. https://doi.org/10.1002/hipo.22060

Burwell, R. D., & Amaral, D. G. (1998a). Cortical afferents of the perirhinal, postrhinal, and entorhinal cortices of the rat. *Journal of Comparative Neurology*, *398*(2), 179–205.

Burwell, R. D., & Amaral, D. G. (1998b). Perirhinal and postrhinal cortices of the rat: Interconnectivity and connections with the entorhinal cortex. *Journal of Comparative Neurology*, *391*(3), 293–321.

Burwell, R. D., Witter, M. P., & Amaral, D. G. (1995). Perirhinal and postrhinal cortices of the rat: A review of the neuroanatomical literature and comparison with findings from the monkey brain. *Hippocampus*, *5*(5), 390–408. https://doi.org/10.1002/hipo.450050503

Bussey, T. J., & Saksida, L. M. (2005). Object memory and perception in the medial temporal lobe: An alternative approach. *Current Opinion in Neurobiology*, *15*(6), 730–737.

Bussey, T. J., & Saksida, L. M. (2007). Memory, perception, and the ventral visual-perirhinal-hippocampal stream: Thinking outside of the boxes. *Hippocampus*, *17*(9), 898–908.

Bussey, T. J., Saksida, L. M., & Murray, E. A. (2006). Perirhinal cortex and feature-ambiguous discriminations. *Learning and Memory*, *13*(2), 103–105.

Buzsaki, G. (1996). The hippocampo-neocortical dialogue. *Cerebral Cortex*, *6*(2), 81–92. https://doi.org/10.1093/cercor/6.2.81

Buzsaki, G., & Moser, E. I. (2013). Memory, navigation and theta rhythm in the hippocampal-entorhinal system. *Nature Neuroscience*, *16*(2), 130–138. https://doi.org/10.1038/nn.3304 nn.3304 [pii].

Caballero-Bleda, M., & Witter, M. P. (1993). Regional and laminar organization of projections from the presubiculum and parasubiculum to the entorhinal cortex: An anterograde tracing study in the rat. *Journal of Comparative Neurology*, *328*(1), 115–129. https://doi.org/10.1002/cne.903280109

Canto, C. B., & Witter, M. P. (2012a). Cellular properties of principal neurons in the rat entorhinal cortex. I. The lateral entorhinal cortex. *Hippocampus*, *22*(6), 1256–1276. https://doi.org/10.1002/hipo.20997

Canto, C. B., & Witter, M. P. (2012b). Cellular properties of principal neurons in the rat entorhinal cortex. II. The medial entorhinal cortex. *Hippocampus*, *22*(6), 1277–1299. https://doi.org/10.1002/hipo.20993

Cappaert, N. L. M., Van Strien, N. M., & Witter, M. P. (2014). Hippocampal formation. In G. Paxinos (Ed.), *The rat nervous system* (4th ed.). San Diego: Academic Press.

Chrobak, J. J., & Amaral, D. G. (2007). Entorhinal cortex of the monkey: VII. Intrinsic connections. *Journal of Comparative Neurology*, *500*(4), 612–633. https://doi.org/10.1002/cne.21200

Colgin, L. L. (2016). Rhythms of the hippocampal network. *Nature Reviews. Neuroscience*, *17*(4), 239–249. https://doi.org/10.1038/nrn.2016.21

Colgin, L. L., & Moser, E. I. (2010). Gamma oscillations in the hippocampus. *Physiology (Bethesda)*, *25*(5), 319–329. doi:25/5/319 [pii]. https://doi.org/10.1152/physiol.00021.2010

Constantinescu, A. O., O'Reilly, J. X., & Behrens, T. E. J. (2016). Organizing conceptual knowledge in humans with a gridlike code. *Science*, *352* (6292), 1464–1468. https://doi.org/10.1126/science.aaf0941

Couey, J. J., Witoelar, A., Zhang, S. J., Zheng, K., Ye, J., Dunn, B., … Witter, M. P. (2013). Recurrent inhibitory circuitry as a mechanism for grid formation. *Nature Neuroscience*, *16*(3), 318–324. https://doi.org/10.1038/nn.3310 nn.3310 [pii].

Czajkowski, R., Sugar, J., Zhang, S. J., Couey, J. J., Ye, J., & Witter, M. P. (2013). Superficially projecting principal neurons in layer V of medial entorhinal cortex in the rat receive excitatory retrosplenial input. *Journal of Neuroscience*, *33*(40), 15779–15792. https://doi.org/10.1523/JNEUROSCI.2646-13.2013

de Curtis, M., & Pare, D. (2004). The rhinal cortices: A wall of inhibition between the neocortex and the hippocampus. *Progress in Neurobiology*, *74*(2), 101–110.

Desfilis, E., Abellan, A., Sentandreu, V., & Medina, L. (2018). Expression of regulatory genes in the embryonic brain of a lizard and implications for understanding pallial organization and evolution. *Journal of Comparative Neurology*, *526*(1), 166–202. https://doi.org/10.1002/cne.24329

Deshmukh, S. S., Johnson, J. L., & Knierim, J. J. (2012). Perirhinal cortex represents nonspatial, but not spatial, information in rats foraging in the presence of objects: Comparison with lateral entorhinal cortex. *Hippocampus*, *22*(10), 2045–2058. https://doi.org/10.1002/hipo.22046

Deshmukh, S. S., & Knierim, J. J. (2011). Representation of non-spatial and spatial information in the lateral entorhinal cortex. *Frontiers in Behavioral Neuroscience*, *5*, *69*. https://doi.org/10.3389/fnbeh.2011.00069

Desikan, S., Koser, D. E., Neitz, A., & Monyer, H. (2018). Target selectivity of septal cholinergic neurons in the medial and lateral entorhinal cortex. *Proceedings of the National Academy of Sciences of the United States of America*, *115*(11), E2644–E2652. https://doi.org/10.1073/pnas.1716531115

Dhillon, A., & Jones, R. S. (2000). Laminar differences in recurrent excitatory transmission in the rat entorhinal cortex in vitro. *Neuroscience*, *99*(3), 413–422.

Dixon, M. L., Thiruchselvam, R., Todd, R., & Christoff, K. (2017). Emotion and the prefrontal cortex: An integrative review. *Psychological Bulletin*, *143*(10), 1033–1081. https://doi.org/10.1037/bul0000096

Doan, T. P., Donate Lagartos, M. J., Nilssen, E. S., & Witter, M. P. (2018). Challenging the concept of parellel parahippocampal input streams to the hippocampus. *FENS Abstract*, *F18*, 2143.

Doan, T. P., Nilssen, E. S., & Witter, M. P. (2016). Postsynaptic targets of inputs to the lateral entorhinal cortex. *SFN Abstracts*, *16*(16), 183.

Doeller, C. F., Barry, C., & Burgess, N. (2010). Evidence for grid cells in a human memory network. *Nature*, *463*(7281), 657–661. https://doi.org/10.1038/nature08704

Dolorfo, C. L., & Amaral, D. G. (1998). Entorhinal cortex of the rat: Organization of intrinsic connections. *Journal of Comparative Neurology*, *398* (1), 49–82.

Donato, F., Jacobsen, R. I., Moser, M. B., & Moser, E. I. (2017). Stellate cells drive maturation of the entorhinal-hippocampal circuit. *Science*, *355* (6330), eaai8178. https://doi.org/10.1126/science.aai8178

Egorov, A. V., Lorenz, F. S., Rozov, A., & Draguhn, A. (2017). Local circuitry in the medial entorhinal cortex layer V. *SFN Abstracts*, *474*, 09.

Eichenbaum, H. (2000). A cortical-hippocampal system for declarative memory. *Nature Reviews Neuroscience*, *1*(1), 41–50. https://doi.org/10.1038/35036213

Eichenbaum, H. (2017). On the integration of space, time, and memory. *Neuron*, *95*(5), 1007–1018. https://doi.org/10.1016/j.neuron.2017.06.036

Eichenbaum, H., Yonelinas, A. P., & Ranganath, C. (2007). The medial temporal lobe and recognition memory. *Annual Review of Neuroscience*, *30*, 123–152. https://doi.org/10.1146/annurev.neuro.30.051606.094328

Epstein, R. A., Parker, W. E., & Feiler, A. M. (2007). Where am I now? Distinct roles for parahippocampal and retrosplenial cortices in place recognition. *Journal of Neuroscience*, *27*(23), 6141–6149.

Ferry, B., Ferreira, G., Traissard, N., & Majchrzak, M. (2006). Selective involvement of the lateral entorhinal cortex in the control of the olfactory memory trace during conditioned odor aversion in the rat. *Behavioral Neuroscience*, *120*(5), 1180–1186.

Fuchs, E. C., Neitz, A., Pinna, R., Melzer, S., Caputi, A., & Monyer, H. (2016). Local and distant input controlling excitation in layer II of the medial entorhinal cortex. *Neuron*, *89*(1), 194–208. https://doi.org/10.1016/j.neuron.2015.11.029

Furtak, S. C., Ahmed, O. J., & Burwell, R. D. (2012). Single neuron activity and theta modulation in postrhinal cortex during visual object discrimination. *Neuron*, *76*(5), 976–988. https://doi.org/10.1016/j.neuron.2012.10.039

Furtak, S. C., Wei, S. M., Agster, K. L., & Burwell, R. D. (2007). Functional neuroanatomy of the parahippocampal region in the rat: The perirhinal and postrhinal cortices. *Hippocampus*, *17*(9), 709–722. https://doi.org/10.1002/hipo.20314

Fyhn, M., Hafting, T., Witter, M. P., Moser, E. I., & Moser, M. B. (2008). Grid cells in mice. *Hippocampus*, *18*(12), 1230–1238. https://doi.org/10.1002/hipo.20472

Fyhn, M., Molden, S., Witter, M. P., Moser, E. I., & Moser, M. B. (2004). Spatial representation in the entorhinal cortex. *Science*, *305*(5688), 1258–1264. https://doi.org/10.1126/science.1099901

Gaffan, E. A., Healey, A. N., & Eacott, M. J. (2004). Objects and positions in visual scenes: Effects of perirhinal and postrhinal cortex lesions in the rat. *Behavioral Neuroscience*, *118*(5), 992–1010.

Germroth, P., Schwerdtfeger, W. K., & Buhl, E. H. (1989). Morphology of identified entorhinal neurons projecting to the hippocampus. A light microscopical study combining retrograde tracing and intracellular injection. *Neuroscience*, *30*(3), 683–691.

Gloveli, T., Schmitz, D., Empson, R. M., Dugladze, T., & Heinemann, U. (1997). Morphological and electrophysiological characterization of layer III cells of the medial entorhinal cortex of the rat. *Neuroscience*, *77*(3), 629–648.

Haberly, L. B., & Price, J. L. (1977). The axonal projection patterns of the mitral and tufted cells of the olfactory bulb in the rat. *Brain Research*, *129*(1), 152–157 doi:0006-8993(77)90978-7 [pii].

Habets, A. M., Lopes da Silva, F. H., & Mollevanger, W. J. (1980). An olfactory input to the hippocampus of the cat: Field potential analysis. *Brain Research*, *182*(1), 47–64.

Hafting, T., Fyhn, M., Molden, S., Moser, M. B., & Moser, E. I. (2005). Microstructure of a spatial map in the entorhinal cortex. *Nature*, *436* (7052), 801–806.

Hales, J. B., Vincze, J. L., Reitz, N. T., Ocampo, A. C., Leutgeb, S., & Clark, R. E. (2018). Recent and remote retrograde memory deficit in rats with medial entorhinal cortex lesions. *Neurobiology of Learning and Memory*, *155*, 157–163. https://doi.org/10.1016/j.nlm.2018.07.013

Hamam, B. N., Amaral, D. G., & Alonso, A. A. (2002). Morphological and electrophysiological characteristics of layer V neurons of the rat lateral

entorhinal cortex. *Journal of Comparative Neurology*, *451*(1), 45–61. https://doi.org/10.1002/cne.10335

Hamam, B. N., Kennedy, T. E., Alonso, A., & Amaral, D. G. (2000). Morphological and electrophysiological characteristics of layer V neurons of the rat medial entorhinal cortex. *Journal of Comparative Neurology*, *418* (4), 457–472.

Hardcastle, K., Maheswaranathan, N., Ganguli, S., & Giocomo, L. M. (2017). A multiplexed, heterogeneous, and adaptive code for navigation in medial entorhinal cortex. *Neuron*, *94*(2), 375–387 e377. https://doi.org/10.1016/j.neuron.2017.03.025

Hargreaves, E. L., Rao, G., Lee, I., & Knierim, J. J. (2005). Major dissociation between medial and lateral entorhinal input to dorsal hippocampus. *Science*, *308*(5729), 1792–1794.

Haug, F. M. (1976). Sulphide silver pattern and cytoarchitectonics of parahippocampal areas in the rat. Special reference to the subdivision of area entorhinalis (area 28) and its demarcation from the pyriform cortex. *Advances in Anatomy, Embryology and Cell Biology*, *52*(4), 3–73.

Hayes, S. M., Nadel, L., & Ryan, L. (2007). The effect of scene context on episodic object recognition: Parahippocampal cortex mediates memory encoding and retrieval success. *Hippocampus*, *17*(9), 873–889.

Hjorth-Simonsen, A. (1971). Hippocampal efferents to the ipsilateral entorhinal area: An experimental study in the rat. *Journal of Comparative Neurology*, *142*(4), 417–437. https://doi.org/10.1002/cne.901420403

Hjorth-Simonsen, A. (1972). Projection of the lateral part of the entorhinal area to the hippocampus and fascia dentata. *Journal of Comparative Neurology*, *146*(2), 219–232. https://doi.org/10.1002/cne.901460206

Hjorth-Simonsen, A., & Jeune, B. (1972). Origin and termination of the hippocampal perforant path in the rat studied by silver impregnation. *Journal of Comparative Neurology*, *144*(2), 215–232. https://doi.org/10.1002/cne.901440206

Høydal, O. A., Skytøen, E. R., Moser, M.-B., & Moser, E. I. (2018). Object-vector coding in the medial entorhinal cotex. *bioRxiv*. *568*(7752):400–404. https://doi.org/10.1038/s41586-019-1077-7.

Igarashi, K. M., Lu, L., Colgin, L. L., Moser, M. B., & Moser, E. I. (2014). Coordination of entorhinal-hippocampal ensemble activity during associative learning. *Nature*, *510*(7503), 143–147. https://doi.org/10.1038/nature13162

Insausti, R., & Amaral, D. G. (2008). Entorhinal cortex of the monkey: IV. Topographical and laminar organization of cortical afferents. *Journal of Comparative Neurology*, *509*(6), 608–641. https://doi.org/10.1002/cne.21753

Insausti, R., Amaral, D. G., & Cowan, W. M. (1987). The entorhinal cortex of the monkey: II. Cortical afferents. *Journal of Comparative Neurology*, *264*(3), 356–395. https://doi.org/10.1002/cne.902640306

Insausti, R., Munoz-Lopez, M., Insausti, A. M., & Artacho-Perula, E. (2017). The human periallocortex: Layer pattern in presubiculum, parasubiculum and entorhinal cortex. A review. *Frontiers in Neuroanatomy*, *11*, 84. https://doi.org/10.3389/fnana.2017.00084

Insausti, R., Tunon, T., Sobreviela, T., Insausti, A. M., & Gonzalo, L. M. (1995). The human entorhinal cortex: A cytoarchitectonic analysis. *Journal of Comparative Neurology*, *355*(2), 171–198. https://doi.org/10.1002/cne.903550203

Jacobs, J., & Lee, S. A. (2016). Spatial cognition: Grid cells support imagined navigation. *Current Biology*, *26*(7), R277–R279. https://doi.org/10.1016/j.cub.2016.02.032

Jacobs, L. F., Arter, J., Cook, A., & Sulloway, F. J. (2015). Olfactory orientation and navigation in humans. *PLoS One*, *10*(6), e0129387. https://doi.org/10.1371/journal.pone.0129387

Jones, B. F., & Witter, M. P. (2007). Cingulate cortex projections to the parahippocampal region and hippocampal formation in the rat. *Hippocampus*, *17*(10), 957–976. https://doi.org/10.1002/hipo.20330

Kajiwara, R., Takashima, I., Mimura, Y., Witter, M. P., & Iijima, T. (2003). Amygdala input promotes spread of excitatory neural activity from perirhinal cortex to the entorhinal-hippocampal circuit. *Journal of Neurophysiology*, *89*(4), 2176–2184. https://doi.org/10.1152/jn.01033.2002

Kealy, J., & Commins, S. (2011). The rat perirhinal cortex: A review of anatomy, physiology, plasticity, and function. *Progress in Neurobiology*, *93* (4), 522–548. https://doi.org/10.1016/j.pneurobio.2011.03.002

Kerr, K. M., Agster, K. L., Furtak, S. C., & Burwell, R. D. (2007). Functional neuroanatomy of the parahippocampal region: The lateral and medial entorhinal areas. *Hippocampus*, *17*(9), 697–708. https://doi.org/10.1002/hipo.20315

Killian, N. J., Jutras, M. J., & Buffalo, E. A. (2012). A map of visual space in the primate entorhinal cortex. *Nature*, *491*(7426), 761–764. https://doi.org/10.1038/nature11587

Kitamura, T., Pignatelli, M., Suh, J., Kohara, K., Yoshiki, A., Abe, K., & Tonegawa, S. (2014). Island cells control temporal association memory. *Science*, *343*(6173), 896–901. https://doi.org/10.1126/science.1244634

Kloosterman, F., Van Haeften, T., Witter, M. P., & Lopes Da Silva, F. H. (2003). Electrophysiological characterization of interlaminar entorhinal connections: An essential link for re-entrance in the hippocampal-entorhinal system. *European Journal of Neuroscience*, *18*(11), 3037–3052.

Knierim, J. J., Neunuebel, J. P., & Deshmukh, S. S. (2014). Functional correlates of the lateral and medial entorhinal cortex: Objects, path integration and local-global reference frames. *Philosophical Transactions of the Royal Society of London. Series B: Biological Sciences*, *369*(1635), 20130369. https://doi.org/10.1098/rstb.2013.0369

Kobayashi, Y., & Amaral, D. G. (2007). Macaque monkey retrosplenial cortex: III. Cortical efferents. *Journal of Comparative Neurology*, *502*(5), 810–833. https://doi.org/10.1002/cne.21346

Kobro-Flatmoen, A., & Witter, M. P. (2019). Neuronal chemo-architecture of the entorhinal cortex: A comparative review. *European Journal of Neuroscience* in press. https://doi.org/10.1111/ejn.14511

Köhler, C. (1985). Intrinsic projections of the retrohippocampal region in the rat brain. I. The subicular complex. *Journal of Comparative Neurology*, *236*(4), 504–522.

Köhler, C. (1986). Intrinsic connections of the retrohippocampal region in the rat brain. II. The medial entorhinal area. *Journal of Comparative Neurology*, *246*(2), 149–169.

Köhler, C. (1988). Intrinsic connections of the retrohippocampal region in the rat brain: III. The lateral entorhinal area. *Journal of Comparative Neurology*, *271*(2), 208–228. https://doi.org/10.1002/cne.902710204

Köhler, C., & Chan-Palay, V. (1983). Gamma-aminobutyric acid interneurons in the rat hippocampal region studied by retrograde transport of glutamic acid decarboxylase antibody after in vivo injections. *Anatomy and Embryology*, *166*(1), 53–66.

Kondo, H., & Witter, M. P. (2014). Topographic organization of orbitofrontal projections to the parahippocampal region in rats. *Journal of Comparative Neurology*, *522*(4), 772–793. https://doi.org/10.1002/cne.23442

Kosel, K. C., Van Hoesen, G. W., & Rosene, D. L. (1982). Non-hippocampal cortical projections from the entorhinal cortex in the rat and rhesus monkey. *Brain Research*, *244*(2), 201–213.

Kosel, K. C., Van Hoesen, G. W., & West, J. R. (1981). Olfactory bulb projections to the parahippocampal area of the rat. *The Journal of Comparative Neurology*, *198*(3), 467–482.

Krettek, J. E., & Price, J. L. (1977). Projections from the amygdaloid complex and adjacent olfactory structures to the entorhinal cortex and to the subiculum in the rat and cat. *The Journal of Comparative Neurology*, *172*(4), 723–752.

Krimer, L. S., Hyde, T. M., Herman, M. M., & Saunders, R. C. (1997). The entorhinal cortex: An examination of cyto- and myeloarchitectonic organization in humans. *Cerebral Cortex*, *7*(8), 722–731.

Kropff, E., Carmichael, J. E., Moser, M. B., & Moser, E. I. (2015). Speed cells in the medial entorhinal cortex. *Nature*, *523*(7561), 419–424. https://doi.org/10.1038/nature14622

Lavenex, P., Suzuki, W. A., & Amaral, D. G. (2004). Perirhinal and parahippocampal cortices of the macaque monkey: Intrinsic projections

and interconnections. *Journal of Comparative Neurology*, *472*(3), 371–394. https://doi.org/10.1002/cne.20079

Leitner, F. C., Melzer, S., Lutcke, H., Pinna, R., Seeburg, P. H., Helmchen, F., & Monyer, H. (2016). Spatially segregated feedforward and feedback neurons support differential odor processing in the lateral entorhinal cortex. *Nature Neuroscience*, *19*(7), 935–944. https://doi.org/10.1038/nn.4303

Leonard, B. W., Amaral, D. G., Squire, L. R., & Zola-Morgan, S. M. (1995). Transient memory impairment in monkeys with bilateral lesions of the entorhinal cortex. *Journal of Neuroscience*, *15*(8), 5637–5659.

Lisman, J. E. (2007). Role of the dual entorhinal inputs to hippocampus: A hypothesis based on cue/action (non-self/self) couplets. *Progress in Brain Research*, *163*, 615–818.

Lorente de Nó, R. (1934). Studies on the structure of the cerebral cortex. II. Continuation of the study of the ammonic system. *Journal für Psychologie Und Neurologie*, *46*, 113–177.

Maass, A., Berron, D., Libby, L. A., Ranganath, C., & Duzel, E. (2015). Functional subregions of the human entorhinal cortex. *eLife*, *4*. https://doi.org/10.7554/eLife.06426

Maguire, E. A., Frith, C. D., Burgess, N., Donnett, J. G., & O'Keefe, J. (1998). Knowing where things are parahippocampal involvement in encoding object locations in virtual large-scale space. *Journal of Cognitive Neuroscience*, *10*(1), 61–76.

Mathiasen, M. L., Hansen, L., & Witter, M. P. (2015). Insular projections to the parahippocampal region in the rat. *Journal of Comparative Neurology*, *523*(9), 1379–1398. https://doi.org/10.1002/cne.23742

Medina, L., Abellan, A., & Desfilis, E. (2017). Contribution of genoarchitecture to understanding hippocampal evolution and development. *Brain, Behavior and Evolution*, *90*(1), 25–40. https://doi.org/10.1159/000477558

Meunier, M., Bachevalier, J., Mishkin, M., & Murray, E. A. (1993). Effects on visual recognition of combined and separate ablations of the entorhinal and perirhinal cortex in rhesus monkeys. *Journal of Neuroscience*, *13*(12), 5418–5432.

Miao, C., Cao, Q., Moser, M. B., & Moser, E. I. (2017). Parvalbumin and somatostatin interneurons control different space-coding networks in the medial entorhinal cortex. *Cell*, *171*(3), 507–521.e517. https://doi.org/10.1016/j.cell.2017.08.050

Milner, B., Squire, L. R., & Kandel, E. R. (1998). Cognitive neuroscience and the study of memory. *Neuron*, *20*(3), 445–468.

Mishkin, M. (1978). Memory in monkeys severely impaired by combined but not by separate removal of amygdala and hippocampus. *Nature*, *273*(5660), 297–298.

Mohedano-Moriano, A., Pro-Sistiaga, P., Arroyo-Jimenez, M. M., Artacho-Perula, E., Insausti, A. M., Marcos, P., … Insausti, R. (2007). Topographical and laminar distribution of cortical input to the monkey entorhinal cortex. *Journal of Anatomy*, *211*(2), 250–260. https://doi.org/10.1111/j.1469-7580.2007.00764.x

Montchal, M. E., Reagh, Z. M., & Yassa, M. A. (2019). Precise temporal memories are supported by the lateral entorhinal cortex in humans. *Nature Neuroscience*., *22*, 284–288. https://doi.org/10.1038/s41593-018-0303-1

Moser, E. I., Moser, M. B., & McNaughton, B. L. (2017). Spatial representation in the hippocampal formation: A history. *Nature Neuroscience*, *20*(11), 1448–1464. https://doi.org/10.1038/nn.4653

Mullally, S. L., & Maguire, E. A. (2011). A new role for the parahippocampal cortex in representing space. *Journal of Neuroscience*, *31*(20), 7441–7449. https://doi.org/10.1523/jneurosci.0267-11.2011

Munoz, M., & Insausti, R. (2005). Cortical efferents of the entorhinal cortex and the adjacent parahippocampal region in the monkey (*Macaca fascicularis*). *European Journal of Neuroscience*, *22*(6), 1368–1388. https://doi.org/10.1111/j.1460-9568.2005.04299.x

Naber, P. A., Caballero-Bleda, M., Jorritsma-Byham, B., & Witter, M. P. (1997). Parallel input to the hippocampal memory system through peri- and postrhinal cortices. *Neuroreport*, *8*(11), 2617–2621.

Naber, P. A., Lopes da Silva, F. H., & Witter, M. P. (2001). Reciprocal connections between the entorhinal cortex and hippocampal fields CA1 and the subiculum are in register with the projections from CA1 to the subiculum. *Hippocampus*, *11*(2), 99–104.

Navarro Schroder, T., Haak, K. V., Zaragoza Jimenez, N. I., Beckmann, C. F., & Doeller, C. F. (2015). Functional topography of the human entorhinal cortex. *eLife*, *4*. https://doi.org/10.7554/eLife.06738

Naya, Y. (2016). Declarative association in the perirhinal cortex. *Neuroscience Research*, *113*, 12–18. https://doi.org/10.1016/j.neures.2016.07.001

Naya, Y., Chen, H., Yang, C., & Suzuki, W. A. (2017). Contributions of primate prefrontal cortex and medial temporal lobe to temporal-order memory. *Proceedings of the National Academy of Sciences of the United States of America*, *114*(51), 13555–13560. https://doi.org/10.1073/pnas.1712711114

Naya, Y., & Suzuki, W. A. (2011). Integrating what and when across the primate medial temporal lobe. *Science*, *333*(6043), 773–776. https://doi.org/10.1126/science.1206773

Neunuebel, J. P., Yoganarasimha, D., Rao, G., & Knierim, J. J. (2013). Conflicts between local and global spatial frameworks dissociate neural representations of the lateral and medial entorhinal cortex. *Journal of Neuroscience*, *33*(22), 9246–9258. https://doi.org/10.1523/JNEUROSCI.0946-13.2013

Nilssen, E. S., Jacobsen, B., Fjeld, G., Nair, R. R., Blankvoort, S., Kentros, C., & Witter, M. P. (2018). Inhibitory connectivity dominates the fan cell network in layer II of lateral entorhinal cortex. *Journal of Neuroscience*, *38*(45), 9712–9727. https://doi.org/10.1523/JNEUROSCI.1290-18.2018

Norman, G., & Eacott, M. J. (2005). Dissociable effects of lesions to the perirhinal cortex and the postrhinal cortex on memory for context and objects in rats. *Behavioral Neuroscience*, *119*(2), 557–566. doi: 2005-03585-020 [pii]. https://doi.org/10.1037/0735-7044.119.2.557

Ohara, S., Itou, K., Shiraishi, M., Gianatti, M., Sota, Y., Kabashima S., … Iijima T (2016) Efferent projections of the calbindin-positiveentorhinal neurons in the rat: Connectional differences between the medial and lateral entorhinal cortex. SFN Abstr 84.13.96.

Ohara, S., Onodera, M., Simonsen, O. W., Yoshino, R., Hioki, H., Iijima, T., … Witter, M. P. (2018). Intrinsic projections of layer Vb neurons to layers Va, III, and II in the lateral and medial entorhinal cortex of the rat. *Cell Reports*, *24*(1), 107–116. https://doi.org/10.1016/j.celrep.2018.06.014

O'Keefe, J. (1976). Place units in the hippocampus of the freely moving rat. *Experimental Neurology*, *51*(1), 78–109.

O'Keefe, J., & Dostrovsky, J. (1971). The hippocampus as a spatial map. Preliminary evidence from unit activity in the freely-moving rat. *Brain Research*, *34*(1), 171–175.

O'Keefe, J., & Nadel, L. (1978). *The hippocampus as a cognitive map*. Oxford: Clarendon Press.

Olsen, G. M., Ohara, S., Iijima, T., & Witter, M. P. (2017). Parahippocampal and retrosplenial connections of rat posterior parietal cortex. *Hippocampus*, *27*(4), 335–358. https://doi.org/10.1002/hipo.22701

O'Reilly, K. C., Flatberg, A., Islam, S., Olsen, L. C., Kruge, I. U., & Witter, M. P. (2015). Identification of dorsal-ventral hippocampal differentiation in neonatal rats. *Brain Structure & Function*, *220*(5), 2873–2893. https://doi.org/10.1007/s00429-014-0831-8

Otto, T., Schottler, F., Staubli, U., Eichenbaum, H., & Lynch, G. (1991). Hippocampus and olfactory discrimination learning: Effects of entorhinal cortex lesions on olfactory learning and memory in a successive-cue, go-no-go task. *Behavioral Neuroscience*, *105*(1), 111–119.

Pastoll, H., Solanka, L., van Rossum, M. C., & Nolan, M. F. (2013). Feedback inhibition enables theta-nested gamma oscillations and grid firing fields. *Neuron*, *77*(1), 141–154. https://doi.org/10.1016/j.neuron.2012.11.032 S0896-6273(12)01119-1 [pii].

Paz, R., Bauer, E. P., & Pare, D. (2007). Learning-related facilitation of rhinal interactions by medial prefrontal inputs. *Journal of Neuroscience*, *27* (24), 6542–6551.

Paz, R., Pelletier, J. G., Bauer, E. P., & Pare, D. (2006). Emotional enhancement of memory via amygdala-driven facilitation of rhinal interactions. *Nature Neuroscience*, *9*(10), 1321–1329.

Pelletier, J. G., Apergis-Schoute, J., & Pare, D. (2005). Interaction between amygdala and neocortical inputs in the perirhinal cortex. *Journal of Neurophysiology*, *94*(3), 1837–1848.

Pilkiw, M., Insel, N., Cui, Y., Finney, C., Morrissey, M. D., & Takehara-Nishiuchi, K. (2017). Phasic and tonic neuron ensemble codes for stimulus-environment conjunctions in the lateral entorhinal cortex. *eLife*, *6*. https://doi.org/10.7554/eLife.28611

Pitkanen, A., Kelly, J. L., & Amaral, D. G. (2002). Projections from the lateral, basal, and accessory basal nuclei of the amygdala to the entorhinal cortex in the macaque monkey. *Hippocampus*, *12*(2), 186–205. https://doi.org/10.1002/hipo.1099

Pitkanen, A., Pikkarainen, M., Nurminen, N., & Ylinen, A. (2000). Reciprocal connections between the amygdala and the hippocampal formation, perirhinal cortex, and postrhinal cortex in rat. A review. *Ann.N.Y.Acad. Sci*, *911*, 369–391.

Ramón y Cajal, S. (1893). Estructura del asta de Ammon y fascia dentata. *Ann Soc Esp his Nat*, *22*, 53–114.

Ramón y Cajal, S. (1902). Sobre un ganglio especial de la corteza esfenooccipital. *Trabajos del Laboratorio de Investigaciones Biologicas de la Universidad de Madrid*, *1*, 189–206.

Ramsden, H. L., Surmeli, G., McDonagh, S. G., & Nolan, M. F. (2015). Laminar and dorsoventral molecular organization of the medial entorhinal cortex revealed by large-scale anatomical analysis of gene expression. *PLoS Computational Biology*, *11*(1), e1004032. https://doi.org/10.1371/journal.pcbi.1004032

Ranganath, C., & Ritchey, M. (2012). Two cortical systems for memory-guided behaviour. *Nature Reviews Neuroscience*, *13*(10), 713–726. https://doi.org/10.1038/nrn3338 nrn3338 [pii].

Ritchey, M., Libby, L. A., & Ranganath, C. (2015). Cortico-hippocampal systems involved in memory and cognition: The PMAT framework. *Progress in Brain Research*, *219*, 45–64. https://doi.org/10.1016/bs.pbr.2015.04.001

Ritchey, M., Wang, S. F., Yonelinas, A. P., & Ranganath, C. (2018). Dissociable medial temporal pathways for encoding emotional item and context information. *Neuropsychologia*, *124*, 66–78. https://doi.org/10.1016/j.neuropsychologia.2018.12.015

Room, P., & Groenewegen, H. J. (1986). Connections of the parahippocampal cortex. I. Cortical afferents. *Journal of Comparative Neurology*, *251*(4), 415–450.

Room, P., Groenewegen, H. J., & Lohman, A. H. (1984). Inputs from the olfactory bulb and olfactory cortex to the entorhinal cortex in the cat. I. Anatomical observations. *Experimental Brain Research*, *56*(3), 488–496.

Rowland, D. C., Obenhaus, H. A., Skytoen, E. R., Zhang, Q., Kentros, C. G., Moser, E. I., & Moser, M. B. (2018). Functional properties of stellate cells in medial entorhinal cortex layer II. *eLife*, *7*. https://doi.org/10.7554/eLife.36664

Samarth, P., Ball, J. M., Unal, G., Pare, D., & Nair, S. S. (2017). Mechanisms of memory storage in a model perirhinal network. *Brain Structure & Function*, *222*(1), 183–200. https://doi.org/10.1007/s00429-016-1210-4

Sargolini, F., Fyhn, M., Hafting, T., McNaughton, B. L., Witter, M. P., Moser, M. B., & Moser, E. I. (2006). Conjunctive representation of position, direction, and velocity in entorhinal cortex. *Science*, *312* (5774), 758–762. https://doi.org/10.1126/science.1125572

Scaplen, K. M., Ramesh, R. N., Nadvar, N., Ahmed, O. J., & Burwell, R. D. (2017). Inactivation of the lateral entorhinal area increases the influence of visual cues on hippocampal place cell activity. *Frontiers in Systems Neuroscience*, *11*, 40. https://doi.org/10.3389/fnsys.2017.00040

Schwerdtfeger, W. K., Buhl, E. H., & Germroth, P. (1990). Disynaptic olfactory input to the hippocampus mediated by stellate cells in the entorhinal cortex. *Journal of Comparative Neurology*, *292*(2), 163–177.

Scoville, W. B., & Milner, B. (1957). Loss of recent memory after bilateral hippocampal lesions. *Journal of Neurology, Neurosurgery and Psychiatry*, *20*(1), 11–21.

Shipley, M. T. (1975). The topographical and laminar organization of the presubiculum's projection to the ipsi- and contralateral entorhinal cortex in the guinea pig. *Journal of Comparative Neurology*, *160*(1), 127–145.

Shipley, M. T., & Adamek, G. D. (1984). The connections of the mouse olfactory bulb: A study using orthograde and retrograde transport of wheat germ agglutinin conjugated to horseradish peroxidase. *Brain Research Bulletin*, *12*(6), 669–688.

Solstad, T., Boccara, C. N., Kropff, E., Moser, M. B., & Moser, E. I. (2008). Representation of geometric borders in the entorhinal cortex. *Science*, *322*(5909), 1865–1868. doi:322/5909/1865 [pii]. https://doi.org/10.1126/science.1166466

Squire, L. R., Stark, C. E., & Clark, R. E. (2004). The medial temporal lobe. *Annual Review of Neuroscience*, *27*, 279–306. https://doi.org/10.1146/annurev.neuro.27.070203.144130

Staubli, U., Fraser, D., Kessler, M., & Lynch, G. (1986). Studies on retrograde and anterograde amnesia of olfactory memory after denervation of the hippocampus by entorhinal cortex lesions. *Behavioral and Neural Biology*, *46*(3), 432–444.

Staubli, U., Ivy, G., & Lynch, G. (1984). Hippocampal denervation causes rapid forgetting of olfactory information in rats. *Proceedings of the National Academy of Sciences of the United States of America*, *81*(18), 5885–5887.

Stefanacci, L., & Amaral, D. G. (2000). Topographic organization of cortical inputs to the lateral nucleus of the macaque monkey amygdala: A retrograde tracing study. *Journal of Comparative Neurology*, *421*(1), 52–79.

Steward, O., & Scoville, S. A. (1976). Cells of origin of entorhinal cortical afferents to the hippocampus and fascia dentata of the rat. *Journal of Comparative Neurology*, *169*(3), 347–370. https://doi.org/10.1002/cne.901690306

Surmeli, G., Marcu, D. C., McClure, C., Garden, D. L., Pastoll, H., & Nolan, M. F. (2015). Molecularly defined circuitry reveals input-output segregation in deep layers of the medial entorhinal cortex. *Neuron*, *88* (5), 1040–1053. https://doi.org/10.1016/j.neuron.2015.10.041

Sutherland, R. J., & McDonald, R. J. (1990). Hippocampus, amygdala, and memory deficits in rats. *Behavioural Brain Research*, *37*(1), 57–79.

Suzuki, W. A., & Amaral, D. G. (1994a). Perirhinal and parahippocampal cortices of the macaque monkey: Cortical afferents. *Journal of Comparative Neurology*, *350*(4), 497–533. https://doi.org/10.1002/cne.903500402

Suzuki, W. A., & Amaral, D. G. (1994b). Topographic organization of the reciprocal connections between the monkey entorhinal cortex and the perirhinal and parahippocampal cortices. *Journal of Neuroscience*, *14*(3 Pt 2), 1856–1877.

Suzuki, W. A., Miller, E. K., & Desimone, R. (1997). Object and place memory in the macaque entorhinal cortex. *Journal of Neurophysiology*, *78* (2), 1062–1081.

Swanson, L. W., & Köhler, C. (1986). Anatomical evidence for direct projections from the entorhinal area to the entire cortical mantle in the rat. *Journal of Neuroscience*, *6*(10), 3010–3023.

Tahvildari, B., & Alonso, A. (2005). Morphological and electrophysiological properties of lateral entorhinal cortex layers II and III principal neurons. *Journal of Comparative Neurology*, *491*(2), 123–140. https://doi.org/10.1002/cne.20706

Tamamaki, N., & Nojyo, Y. (1995). Preservation of topography in the connections between the subiculum, field CA1, and the entorhinal cortex in rats. *Journal of Comparative Neurology*, *353*(3), 379–390. https://doi.org/10.1002/cne.903530306

Tang, Q., Ebbesen, C. L., Sanguinetti-Scheck, J. I., Preston-Ferrer, P., Gundlfinger, A., Winterer, J., … Burgalossi, A. (2015). Anatomical organization and spatiotemporal firing patterns of layer 3 neurons in the rat medial entorhinal cortex. *Journal of Neuroscience*, *35*(36), 12346–12354. https://doi.org/10.1523/JNEUROSCI.0696-15.2015

Taylor, K. I., Moss, H. E., Stamatakis, E. A., & Tyler, L. K. (2006). Binding crossmodal object features in perirhinal cortex. *Proceedings of the National Academy of Sciences of the United States of America*, *103*(21), 8239–8244. https://doi.org/10.1073/pnas.0509704103

Tsao, A., Moser, M. B., & Moser, E. I. (2013). Traces of experience in the lateral entorhinal cortex. *Current Biology*, *23*(5), 399–405. https://doi.org/10.1016/j.cub.2013.01.036

Tsao, A., Sugar, J., Lu, L., Wang, C., Knierim, J. J., Moser, M. B., & Moser, E. I. (2018). Integrating time from experience in the lateral entorhinal cortex. *Nature*, *561*, 57–62. https://doi.org/10.1038/s41586-018-0459-6

van der Linden, S., & Lopes da Silva, F. H. (1998). Comparison of the electrophysiology and morphology of layers III and II neurons of the rat medial entorhinal cortex in vitro. *European Journal of Neuroscience*, *10*(4), 1479–1489.

Van Groen, T., Lopes da Silva, F. H., & Wadman, W. J. (1987). Synaptic organization of olfactory inputs and local circuits in the entorhinal cortex: A current source density analysis in the cat. *Experimental Brain Research*, *67*(3), 615–622.

van Groen, T., Miettinen, P., & Kadish, I. (2003). The entorhinal cortex of the mouse: Organization of the projection to the hippocampal formation. *Hippocampus*, *13*(1), 133–149.

van Groen, T., & Wyss, J. M. (1990a). The connections of presubiculum and parasubiculum in the rat. *Brain Research*, *518*(1–2), 227–243.

van Groen, T., & Wyss, J. M. (1990b). The postsubicular cortex in the rat: Characterization of the fourth region of the subicular cortex and its connections. *Brain Research*, *529*(1–2), 165–177.

van Haeften, T., Baks-Te Bulte, L. T., Goede, P. H., Wouterlood, F. G., & Witter, M. P. (2003). Morphological and numerical analysis of synaptic interactions between neurons in deep and superficial layers of the entorhinal cortex of the rat. *Hippocampus*, *13*(8), 943–952.

Van Hoesen, G., & Pandya, D. N. (1975a). Some connections of the entorhinal (area 28) and perirhinal (area 35) cortices of the rhesus monkey. I. Temporal lobe afferents. *Brain Research*, *95*(1), 1–24.

Van Hoesen, G., Pandya, D. N., & Butters, N. (1975). Some connections of the entorhinal (area 28) and perirhinal (area 35) cortices of the rhesus monkey. II. Frontal lobe afferents. *Brain Research*, *95*(1), 25–38.

van Hoesen, G. W. (1982). The parahippocampal gyrus: New observations regarding its cortical connections in the monkey. *Trends in Neurosciences*, *5*, 345–350.

Van Hoesen, G. W., & Pandya, D. N. (1975b). Some connections of the entorhinal (area 28) and perirhinal (area 35) cortices of the rhesus monkey. III. Efferent connections. *Brain Research*, *95*(1), 39–59.

Van Hoesen, G. W., Pandya, D. N., & Butters, N. (1972). Cortical afferents to the entorhinal cortex of the rhesus monkey. *Science*, *175*(4029), 1471–1473.

Varga, C., Lee, S. Y., & Soltesz, I. (2010). Target-selective GABAergic control of entorhinal cortex output. *Nature Neuroscience*, *13*(7), 822–824. https://doi.org/10.1038/nn.2570

Vaudano, E., Legg, C. R., & Glickstein, M. (1991). Afferent and efferent connections of temporal association cortex in the rat: A horseradish peroxidase study. *European Journal of Neuroscience*, *3*(4), 317–330.

Vertes, R. P. (2004). Differential projections of the infralimbic and prelimbic cortex in the rat. *Synapse*, *51*(1), 32–58.

Wallis, J. D. (2007). Orbitofrontal cortex and its contribution to decision-making. *Annual Review of Neuroscience*, *30*, 31–56. https://doi.org/10.1146/annurev.neuro.30.051606.094334

Wang, C., Chen, X., Lee, H., Deshmukh, S. S., Yoganarasimha, D., Savelli, F., & Knierim, J. J. (2018). Egocentric coding of external items in the lateral entorhinal cortex. *Science*, *362*(6417), 945–949. https://doi.org/10.1126/science.aau4940

Willems, J. G., Wadman, W. J., & Cappaert, N. L. (2016). Distinct spatiotemporal activation patterns of the perirhinal-entorhinal network in response to cortical and amygdala input. *Front Neural Circuits*, *10*, 44. https://doi.org/10.3389/fncir.2016.00044

Wilson, D. I., Langston, R. F., Schlesiger, M. I., Wagner, M., Watanabe, S., & Ainge, J. A. (2013). Lateral entorhinal cortex is critical for novel object-context recognition. *Hippocampus*, *23*(5), 352–366. https://doi.org/10.1002/hipo.22095

Wilson, D. I., Watanabe, S., Milner, H., & Ainge, J. A. (2013). Lateral entorhinal cortex is necessary for associative but not nonassociative recognition memory. *Hippocampus*, *23*(12), 1280–1290. https://doi.org/10.1002/hipo.22165

Wilson, R. C., & Steward, O. (1978). Polysynaptic activation of the dentate gyrus of the hippocampal formation: An olfactory input via the lateral entorhinal cortex. *Experimental Brain Research*, *33*, 523–534.

Winterer, J., Maier, N., Wozny, C., Beed, P., Breustedt, J., Evangelista, R., … Schmitz, D. (2017). Excitatory microcircuits within superficial layers of the medial entorhinal cortex. *Cell Reports*, *19*(6), 1110–1116. https://doi.org/10.1016/j.celrep.2017.04.041

Wirth, S., Ferry, B., & Di Scala, G. (1998). Facilitation of olfactory recognition by lateral entorhinal cortex lesion in rats. *Behavioural Brain Research*, *91*(1–2), 49–59.

Witter, M. P. (1993). Organization of the entorhinal hippocampal system - a review of current anatomical data. *Hippocampus*, *3*, 33–44.

Witter, M. P. (2007). The perforant path: Projections from the entorhinal cortex to the dentate gyrus. *Dentate Gyrus: A Comprehensive Guide to Structure, Function, and Clinical Implications*, *163*, 43–61. https://doi.org/10.1016/s0079-6123(07)63003-9

Witter, M. P., & Amaral, D. G. (1991). Entorhinal cortex of the monkey: V. Projections to the dentate gyrus, hippocampus, and subicular complex. *Journal of Comparative Neurology*, *307*(3), 437–459. https://doi.org/10.1002/cne.903070308

Witter, M. P., Doan, T. P., Jacobsen, B., Nilssen, E. S., & Ohara, S. (2017). Architecture of the entorhinal cortex: A review of entorhinal anatomy in rodents with some comparative notes. *Frontiers in Systems Neuroscience*, *11*, 46. https://doi.org/10.3389/fnsys.2017.00046

Witter, M. P., Groenewegen, H. J., Lopes da Silva, F. H., & Lohman, A. H. (1989). Functional organization of the extrinsic and intrinsic circuitry of the parahippocampal region. *Progress in Neurobiology*, *33*(3), 161–253.

Witter, M. P., Naber, P. A., van Haeften, T., Machielsen, W. C., Rombouts, S. A., Barkhof, F., … Lopes da Silva, F. H. (2000). Cortico-hippocampal communication by way of parallel parahippocampal-subicular pathways. *Hippocampus*, *10*(4), 398–410. https://doi.org/10.1002/1098-1063(2000)10:4<398::AID-HIPO6>3.0.CO;2-K

Witter, M. P., Room, P., Groenewegen, H. J., & Lohman, A. H. (1986). Connections of the parahippocampal cortex in the cat. V. Intrinsic connections; comments on input/output connections with the hippocampus. *Journal of Comparative Neurology*, *252*(1), 78–94.

Witter, M. P., Van Hoesen, G. W., & Amaral, D. G. (1989). Topographical organization of the entorhinal projection to the dentate gyrus of the monkey. *Journal of Neuroscience*, *9*(1), 216–228.

Wouterlood, F. G., Mugnaini, E., & Nederlof, J. (1985). Projection of olfactory bulb efferents to layer I GABAergic neurons in the entorhinal area. Combination of anterograde degeneration and immunoelectron microscopy in rat. *Brain Research*, *343*(2), 283–296.

Wouterlood, F. G., & Nederlof, J. (1983). Terminations of olfactory afferents on layer II and III neurons in the entorhinal area: Degeneration-Golgi-electron microscopic study in the rat. *Neuroscience Letters*, *36*(2), 105–110.

Wouterlood, F. G., & Pothuizen, H. (2000). Sparse colocalization of somatostatin- and GABA-immunoreactivity in the entorhinal cortex of the rat. *Hippocampus*, *10*(1), 77–86. https://doi.org/10.1002/(SICI)1098-1063(2000)10:1<77::AID-HIPO8>3.0.CO;2-P

Wouterlood, F. G., van Denderen, J. C., van Haeften, T., & Witter, M. P. (2000). Calretinin in the entorhinal cortex of the rat: Distribution, morphology, ultrastructure of neurons, and co-localization with gamma-aminobutyric acid and parvalbumin. *Journal of Comparative Neurology*, *425*(2), 177–192.

Xu, W., & Wilson, D. A. (2012). Odor-evoked activity in the mouse lateral entorhinal cortex. *Neuroscience*, *223*, 12–20. https://doi.org/10.1016/j.neuroscience.2012.07.067

Yartsev, M. M., Witter, M. P., & Ulanovsky, N. (2011). Grid cells without theta oscillations in the entorhinal cortex of bats. *Nature*, *479*(7371), 103–107. https://doi.org/10.1038/nature10583

Yoganarasimha, D., Rao, G., & Knierim, J. J. (2011). Lateral entorhinal neurons are not spatially selective in cue-rich environments. *Hippocampus*, *21*(12), 1363–1374. https://doi.org/10.1002/hipo.20839

Yoo, S. W., & Lee, I. (2017). Functional double dissociation within the entorhinal cortex for visual scene-dependent choice behavior. *eLife*, *6*. https://doi.org/10.7554/eLife.21543

Young, B. J., Otto, T., Fox, G. D., & Eichenbaum, H. (1997). Memory representation within the parahippocampal region. *Journal of Neuroscience*, *17*(13), 5183–5195.

Zola-Morgan, S. M., Squire, L. R., Alvarez-Royo, P., & Clower, R. P. (1991). Independence of memory functions and emotional behavior: Separate contributions of the hippocampal formation and the amygdala. *Hippocampus*, *1*(2), 207–220.

Zola-Morgan, S. M., Squire, L. R., & Amaral, D. G. (1989). Lesions of the amygdala that spare adjacent cortical regions do not impair memory or exacerbate the impairment following lesions of the hippocampal formation. *Journal of Neuroscience*, *9*(6), 1922–1936.

How to cite this article: Nilssen ES, Doan TP, Nigro MJ, Ohara S, Witter MP. Neurons and networks in the entorhinal cortex: A reappraisal of the lateral and medial entorhinal subdivisions mediating parallel cortical pathways. *Hippocampus*. 2019;1–17. https://doi.org/10.1002/hipo.23145

Article

Cell Reports

Convergent Projections from Perirhinal and Postrhinal Cortices Suggest a Multisensory Nature of Lateral, but Not Medial, Entorhinal Cortex

Graphical Abstract

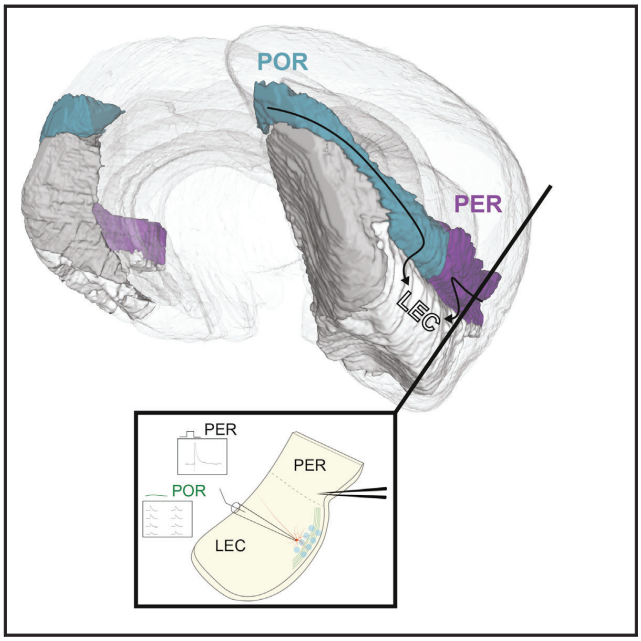

Authors

Thanh P. Doan, Maria J. Lagartos-Donate, Eirik S. Nilssen, Shinya Ohara, Menno P. Witter

Correspondence

menno.witter@ntnu.no

In Brief

Doan et al. demonstrate with the use of tract tracing and *in vitro* electrophysiological recordings that the rat lateral entorhinal cortex receives convergent perirhinal and postrhinal inputs. They further argue that a comparable input organization scheme also exists in the primate, challenging the prevailing concept of parallel parahippocampal pathways to the hippocampus.

Highlights

- Postrhinal cortex preferably targets lateral instead of medial entorhinal cortex
- Postrhinal and perirhinal projections converge on lateral entorhinal layer 2 cells
- Lateral entorhinal cortex is the main parahippocampal multimodal integrative area
- A comparable input organization scheme likely exists in the primate

Doan et al., 2019, Cell Reports 29, 617–627
October 15, 2019
https://doi.org/10.1016/j.celrep.2019.09.005

CellPress

Cell Reports
Article

Convergent Projections from Perirhinal and Postrhinal Cortices Suggest a Multisensory Nature of Lateral, but Not Medial, Entorhinal Cortex

Thanh P. Doan,[1] Maria J. Lagartos-Donate,[1] Eirik S. Nilssen,[1] Shinya Ohara,[2] and Menno P. Witter[1,3,*]
[1]Kavli Institute for Systems Neuroscience, Centre for Computational Neuroscience, Egil and Pauline Braathen and Fred Kavli Centre for Cortical Microcircuits, NTNU Norwegian University of Science and Technology, Trondheim, Norway
[2]Laboratory of Systems Neuroscience, Tohoku University Graduate School of Life Science, Sendai, Japan
[3]Lead Contact
*Correspondence: menno.witter@ntnu.no
https://doi.org/10.1016/j.celrep.2019.09.005

SUMMARY

The current model of the organization of the medial temporal lobe (MTL) episodic memory system assumes that two functionally different "where" and "what" pathways enter MTL as parallel parahippocampal cortex (PHC)-medial entorhinal cortex (MEC) and perirhinal cortex (PER)-lateral entorhinal cortex (LEC) streams, respectively. With the use of tract tracing and *in vitro* electrophysiological recordings, we show that, in the rat LEC, all main principal neuron types in layer II receive convergent inputs from PER and postrhinal cortex (POR), homologous to PHC in primates. Projections to MEC from POR are much less prominent than previously assumed. These findings thus challenge the prevailing concept that LEC and MEC are defined by different inputs from the PER and PHC/POR, respectively. Our findings point to LEC as the main parahippocampal multimodal integrative structure whose unique set of external sensory-derived inputs allows its network to represent a continuously fluctuating extrinsic environment.

INTRODUCTION

The entorhinal cortex (EC) is the main hub connecting the cortex with the hippocampal formation (HF). Together, EC and HF form the core of the medial temporal lobe episodic memory system (Eichenbaum, 2017; Moser et al., 2017). The prevailing notion is that EC is composed of a medial (MEC) and a lateral (LEC) subdivision. Though both LEC and MEC project to the entire longitudinal extent of HF, there is a clear topology such that their more dorsal and lateral parts project predominantly to dorsal parts of HF (Witter et al., 1989). The current model of the organization of the parahippocampal region (PHR) assumes that two functionally different "where" and "what" pathways enter the medial temporal lobe as parallel streams, mediated by parahippocampal cortex (PHC)-MEC and perirhinal cortex (PER)-LEC connections, respectively. According to this model, the two streams eventually converge within HF, which combines the two information streams into a complete memory representation (Eichenbaum et al., 2007; Ranganath and Ritchey, 2012; Yonelinas and Ritchey, 2015). This model is based on several seminal neuroanatomical studies that have been taken to indicate that PHC (in primates, homologous to the postrhinal cortex [POR] in rodents) carrying visuospatial information and PER carrying object information are among the principal and categorical inputs to MEC and LEC, respectively (Suzuki and Amaral, 1994; Naber et al., 1997; Burwell and Amaral, 1998b; Schultz et al., 2012; Maass et al., 2015; Navarro Schröder et al., 2015).

The more dorsal parts of MEC contain a high percentage of spatially modulated neurons, such as grid, head direction, border, aperiodic spatial, and object-vector cells, i.e., parameters necessary for spatial navigation (Hafting et al., 2005; Sargolini et al., 2006; Solstad et al., 2008; Doeller et al., 2010; Killian et al., 2012; Jacobs et al., 2013; Miao et al., 2017; Høydal et al., 2019). In contrast, dorsolateral parts of LEC contain neurons and networks representing information about objects and their complexity, object traces over time, and sequences of an event, i.e., parameters relevant in the realm of representing the specific content and temporal order of an ongoing experience (Deshmukh and Knierim, 2011; Tsao et al., 2013, 2018; Van Cauter et al., 2013; Wilson et al., 2013a, 2013b; Reagh and Yassa, 2014; Rodo et al., 2017; Wang et al., 2018; Montchal et al., 2019). Notwithstanding these striking functional differences, the main hippocampal-projecting cell types in both entorhinal subdivisions are embedded into an overall comparable local circuit architecture (Couey et al., 2013; Pastoll et al., 2013; Fuchs et al., 2016; Leitner et al., 2016; Nilssen et al., 2018; Ohara et al., 2018). Therefore, it is likely that specific input sets to each EC subdivision contribute fundamentally to their functional differences (Nilssen et al., 2019).

In the present paper, we test whether the current model of MTL organization described above is correct. In contrast to that model, we demonstrate anatomically that, in the rat, the entorhinal projections originating in POR preferentially target LEC instead of MEC. *In vitro* electrophysiology corroborates the observation of strong POR inputs to LEC and further shows that these inputs converge with PER inputs onto all main principal cell types in layer II. Using available anatomical data in the non-human primate, we argue that a comparable input

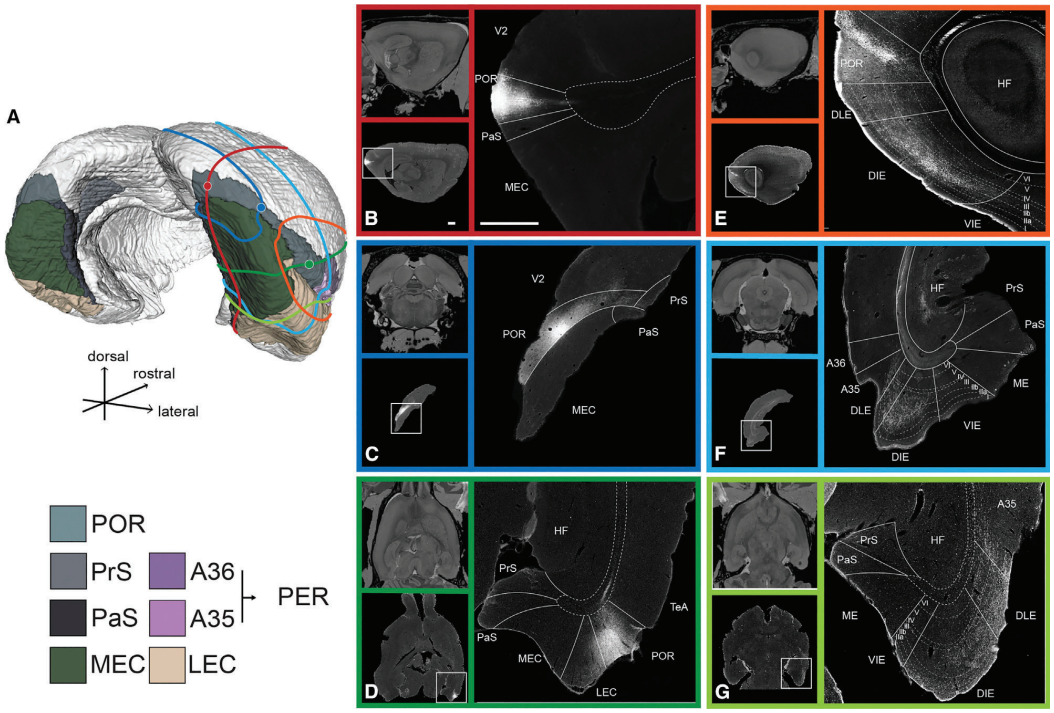

Figure 1. Distribution of POR Axon Terminals into LEC

(A) 3D Waxholm Space model (WHS) (based on *ex vivo* ultra-high-resolution MRI with PHR cytoarchitectural delineations corroborated in all main anatomical plans; Papp et al., 2014; Boccara et al., 2015) with 3 representative POR injections at different positions along its longitudinal extent.

(B) Sagittal section showing an injection in caudomedial POR.

(C) Coronal section showing an injection in mid-caudorostral POR.

(D) Horizontal section with an injection in rostrolateral POR.

(E) Sagittal section demonstrating anterogradely labeled projections of caudomedial POR in LEC.

(F) Coronal section demonstrating mid-caudorostral POR projections into LEC.

(G) Horizontal section demonstrating rostrolateral POR projections into LEC.

(B–G) MRI plane section from WHS (upper left panel), corresponding to the complete histological section (lower left panel) and high-power images taken from the area indicated by the white square in complete histological section (right panel). Scale bar in low- and high-power histological sections in (B) equals 1,000 μm and applies to all histological sections (B)–(G). See Figure S1 for definitions of subdivisions of EC and Videos S1 and S2, Tables S1 and S2, and Figure S2 for details on anterograde and retrograde cases.

organization scheme likely exists in the primate as well. Our findings thus challenge the concept that the two functionally different parallel HF input pathways mediated by MEC and LEC are defined by their respective inputs from the two adjacent parahippocampal POR/PHC and PER domains. Our data clearly indicate that LEC receives strong inputs from both domains and that projections of POR to MEC are less prominent. These data lead to an altered functional connectional model of PHR in which LEC represents a main integrative input structure for the hippocampus.

RESULTS

In the rodent, POR is one of the three main components of the six-layered rhinal cortex together with PER and EC (Figure 1). Out of these three, POR is the caudomedial-most area and it is composed of a ventral (PORv) and a dorsal (PORd) subdivision (Burwell, 2001). Likewise, the rostrolateral PER comprises a ventral (A35) and a dorsal (A36) subdivision (Burwell et al., 1995). Both POR and PER run almost parallel with the rhinal fissure, occupying the fundus and/or its dorsal and ventral banks. These two areas, in association with the rhinal fissure, mark the lateral and dorsal border of EC. In the current paper, we divide EC into MEC composed of caudal (CE) and medial (ME) subdivisions and LEC composed of dorsal lateral (DLE), dorsal intermediate (DIE), and ventral intermediate (VIE) subdivisions (Insausti et al., 1997; Figure S1).

POR is located caudal to PER and mostly dorsal to the rhinal fissure, where it rises steeply and wraps obliquely around the caudal pole of EC. POR cytoarchitecture features a homogeneous neuronal distribution across layers II–IV and a resulting

lack of a prominent laminar structure. Nonetheless, PORd cells in layer III appear more organized with a clear radial appearance that is absent in PORv (Burwell 2001). Similar to A35, PORv is completely devoid of parvalbumin (PV) positivity, and PORd stains stronger for PV similarly to A36. The distribution of calbindin (Cb) neuropil in PORv is also similar to that in areas 35 and 36, respectively. PORv is bordered ventrally by EC for the most part, which is, however, replaced caudomedially by a highly variable dorsolateral extension of the parasubiculum (PaS), which can easily be mistaken for MEC (Burgalossi et al., 2011; Boccara et al., 2015; Ramsden et al., 2015; Tang et al., 2016). A striking feature of PaS is its lack of a clear differentiation between superficial layers II and III, seen in dorsal CE, whereas its neuron diameters are substantially larger than the one seen in POR. In addition, PaS markedly lacks reactivity for Cb in its superficial layers, which contrasts with the moderate to strong reactivity for that protein of the superficial layers of EC and POR. PV staining also makes these borders stand out because MEC and PaS superficial layers stain strongly for PV, contrary to PORv. The anterior border of POR is with PER, slightly rostral to the ventrally adjacent border between DLE and CE. The rostral border of PER is with the insular cortex, and this border in coronal sections coincides with the emergence of the claustrum deep to the insular cortex (Burwell, 2001). The border between LEC and A35 is indicated by the loss of the typical lamina dissecans in LEC. The superficial layers of A35 are homogeneously packed with small neurons, whereas DLE demonstrates a clear lamination in its superficial layers, with layer II cells being larger and more darkly stained than layer III cells. Besides, superficial layers of DLE stain heavily for PV, although such staining is essentially absent in A35. Vice versa, in material stained for Cb, a marked increase of staining in area 35 is noticeable. At last, each EC subdivision is differentiated based on subtle cytoarchitectonic differences and mainly serve detailed anatomical comparisons, but a general pattern is that deep layers (V and VI) are clearly distinguishable from superficial layers (II and III), as the thin acellular layer IV, i.e., lamina dissecans, separates them, and this is particularly well developed in MEC. In the present paper, a border of interest is between the two MEC subdivisions, i.e., areas CE and ME. The most striking change that defines this border is an overall less conspicuous lamination in ME than in CE. The superficial layers of ME are less homogeneous than their CE counterparts: ME layer II breaks up into two or three clusters of cells, which makes it less sharply delineated from both layers I and III and ME layer III tends to split into sublayers. Differences exist also in the superficial portion of their deep layers (layer Va, in opposition to layer Vb), as CE layer Va is sparsely populated by large pyramidal cells and ME is characterized by a more regularly structured layer Va with a higher number of large pyramidals positioned at regular intervals. Finally, the superficial layers of ventral CE exhibit moderate homogeneous reactivity for parvalbumin, unlike ME, where the staining is less strong to absent (Figure S1).

POR Projections to LEC Are Extensive and Comparable to Their PER Counterparts

Analysis of all POR anterograde injections (n = 64) in our multiplane library (Video S1; Table S1) revealed that the entire POR projects strongly to the full rostrocaudal extent of LEC. Anterogradely labeled terminal axons were densest in LEC superficial layers and restricted to its more dorsal and lateral parts, including DLE and DIE, whereas the ventral-intermediate part of LEC (VIE) was virtually devoid of POR fibers (Figure 1). Branching axons with synapse-like varicosities were seen in deep layer (L)I and LIIa, showing an increased density in LIIb and throughout LIII. Labeling in deeper layers was weak or absent, except in DLE, where a moderate density of axonal terminal labeling could be observed. The POR projections to LEC showed a topographical organization such that caudal and medial parts of POR projected densest to DIE, and projections that originated in increasingly more lateral and rostral parts of POR progressively shifted toward the rhinal fissure into DLE (Figures 1E–1G, right panels). All anterograde injections involving superficial layers of PORv resulted in very dense labeling in superficial LEC, and the ones confined to PORd resulted in comparably distributed but weaker labeling. In contrast, injections confined to deep layers of POR labeled only minor projections to deep layers of DLE.

To further characterize POR projecting neurons, we injected the retrograde tracers cholera toxin subunit B (CTB) (n = 3) or Fluorogold (FG) (n = 2) in the dorsolateral LEC of adult rats (Figures S2A and S2B; Video S2; Table S2). In POR, the majority of retrogradely labeled cells were located in LII/III (78.4% or n = 3,044/3,885 cells; σ = 9.4; n = 5; Figure S2B). These injections were made through vertically oriented glass pipettes, which thus enter LEC through PER. This may have caused some tracer leakage into PER, explaining the more or less equal distribution of retrogradely labeled neurons in PORv and PORd, which did not seem in line with our anterograde tracing data. To control for possible leakage along the needle track, we assessed additional retrograde FG injections (n = 4), deposited directly into superficial layers of dorsolateral LEC through laterally drilled burr holes (Figures S2A–S2C; Video S2; Table S2). In all latter cases, retrogradely labeled neurons were present almost exclusively in a clear band spreading across PORv LII/III, confirming our anterograde observations that superficial layers of PORv originate most of the projection to superficial layers of LEC (Figure S2C). Because LII/III of POR/PHC contain a significant number of Calbindin (Cb)-positive cells in mammals (Suzuki and Porteros, 2002; Uva et al., 2004; Boccara et al., 2015), we assessed whether LEC-projecting POR neurons included Cb-positive cells. Immunostaining against Cb showed that over a quarter of superficial POR cells projecting to LEC expressed Cb (27.2% or n = 828/3,044 cells; σ = 1.1; n = 5; Figures S2D and S2E).

Next, we confirmed in our dataset of anterograde tracer injections in PER (n = 23) that PER projected mainly to LEC II and III (Burwell and Amaral, 1998a). In line with previous reports (Burwell and Amaral, 1998b), our data show that these projections mainly target DIE and DLE, with a clear preference for DLE in case of rostral PER injections (Figures S2F–S2H). Additionally, A35 (ventral PER) sends stronger projections to LEC than A36 (dorsal PER; Burwell and Amaral, 1998b). We thus conclude that dorsolateral parts of LEC receive inputs from both POR and PER and that both these projections show very similar topological features, indicative of a potential for convergent innervation of neurons in dorsolateral LEC.

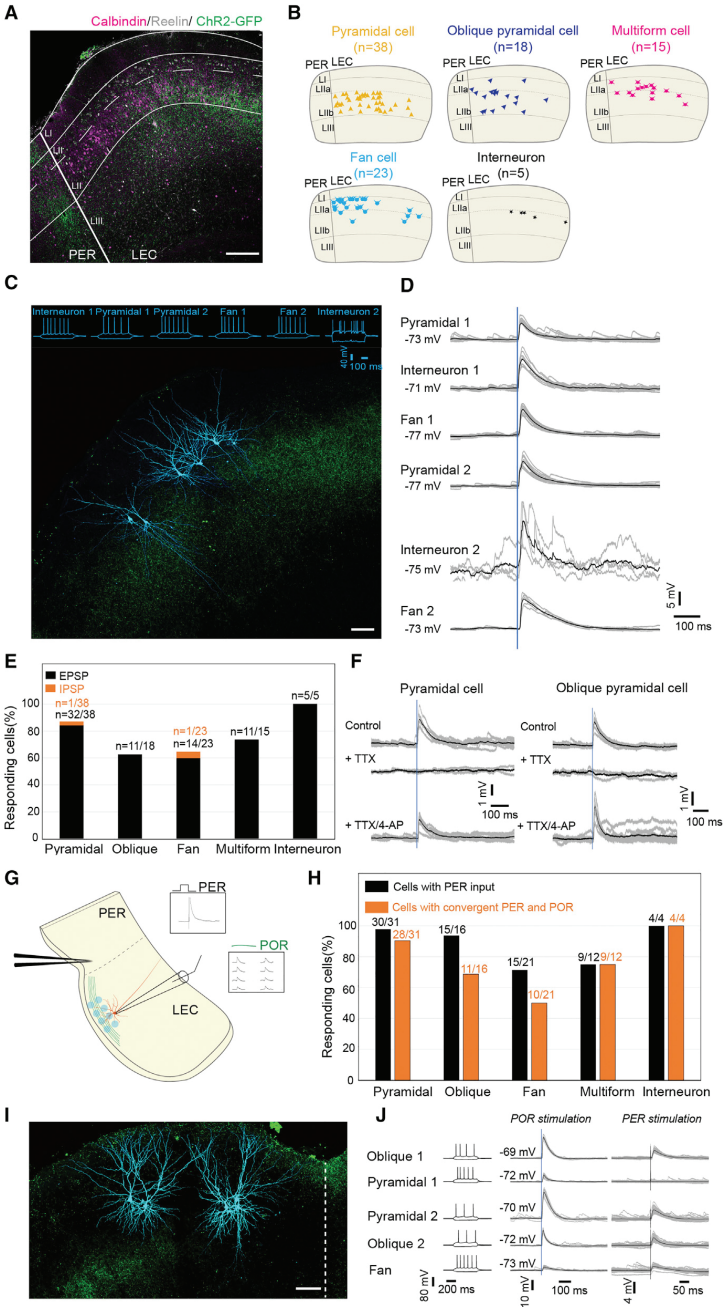

(legend on next page)

Single LEC II Cells Receive Convergent PER and POR Monosynaptic Inputs

We next assessed whether the anatomically established POR to LEC projections form functional inputs to LEC and aimed to determine the postsynaptic targets in LEC. We carried out *in vitro* current clamp recordings of single LEC LII neurons in slices prepared from animals, in which the POR axonal projections were expressing the light-sensitive cation channel channelrhodopsin2 (ChR2). Injection of an adeno-associated virus (AAV) (AAV1.hSyn.ChR2(H134R)-eYFP.WPRE.hGH) into POR in female and male rats (n = 13) resulted in a clearly identifiable plexus of yellow fluorescent protein (YFP)-positive axons in layers II and III of LEC, allowing us to photostimulate the labeled axons and presynaptic terminals. It is well established that layer II in LEC comprises two main types of principal cells, which are characterized by the selective expression of the molecular markers reelin and calbindin (Figure 2A). Reelin-positive neurons are the ones that project to the dentate gyrus, and all fan cells belong to this chemically defined cell group. In contrast, calbindin-positive neurons do not contribute to this projection and send their axons to a number of extrahippocampal targets as well as contribute to inter- and intra-entorhinal excitatory projections (Leitner et al., 2016; S. Ohara et al., 2016, Soc. Neurosci., abstract; Witter et al., 2017). We therefore used post hoc immunohistochemistry to differentiate between reelin- and calbindin-positive neurons that are mainly confined, respectively, to superficial or deep layer II (layer IIa and IIb, respectively; Figure 2A). We recorded from principal cells (n = 94) located in layer IIa (n = 28) and IIb (n = 66). We classified principal cells based on post hoc characterization of somato-dendritic morphology, in accordance with established morphological descriptions and reports that electrophysiological properties are not or only weakly correlated with neuronal morphology (Canto and Witter, 2012; Leitner et al., 2016; Desikan et al., 2018; Nilssen et al., 2018). We found that most recorded cells displaying a pyramidal-like (pyramidal and oblique pyramidal) morphology were located in layer IIb (n = 53/56), whereas most recorded cells displaying a fan cell morphology were located in layer IIa (n = 17/23; Figure 2B; Tahvildari and Alonso, 2005; Canto and Witter, 2012; Leitner et al., 2016; Nilssen et al., 2018). Optogenetic stimulation of ChR2-labeled POR fibers elicited responses across all main classes of layer II principal cells in LEC (74% or n = 70/94 cells), in addition to a small number of recorded putative inhibitory interneurons (n = 5; Figures 2C–2E). Recorded potentials were in most cases excitatory (97% or n = 68/70 cells), though inhibitory postsynaptic potentials were detected in one fan and one pyramidal cell. In a subset of recorded cells (n = 4 cells from 3 rats), we demonstrated through bath application of tetrodotoxin (TTX) (1 μM) and 4-aminopyridine (4-AP) (100 μM) that these excitatory postsynaptic potentials reflected monosynaptic inputs from POR axons (Figure 2F; Petreanu et al., 2009).

To test whether cells postsynaptic to POR inputs were also recipients of PER synaptic inputs, we also applied electrical stimulation of PER by way of a bipolar extracellular electrode in the superficial layers of PER (de Villers-Sidani et al., 2004; T.P. Doan et al., 2016, Soc. Neurosci., conference), immediately adjacent to the LEC border (Figure 2G). We have previously shown that activation of neurons in PER by way of photostimulation of caged glutamate elicits excitatory postsynaptic potentials in simultaneously recorded LEC layer II principal cells. Neurons providing synaptic inputs to LEC were found within a ventral portion of PER adjacent to LEC, and electrical stimulation in that ventral area consistently resulted in postsynaptic potentials in recorded LEC layer II cells (T.P. Doan et al., 2016, Soc. Neurosci., conference). Hence, we reasoned in the present study that extracellular electrical stimulation of this same ventral portion of PER is suitable to activate the pathway connecting PER to LEC. Similar to POR inputs, excitatory postsynaptic potentials evoked by activation of PER were detected in all

Figure 2. PER and POR Inputs Converge on Single LEC II Cells

(A) Axonal projections (green) from postrhinal cortex (POR) mainly target LIIb and LIII of the lateral entorhinal cortex (LEC). Reelin (white) and calbindin immunoreactivity (magenta) delineate superficial LIIa, deep LIIb, and LIII. Scale bar: 200 μm.

(B) Distribution of recorded cells according to morphological type in LII of LEC.

(C) Six current clamp recorded LEC LII cells (two interneurons, two pyramidal cells, and two fan cells; cyan) in the same slice together with POR afferent fibers (green). For each recorded cell, electrophysiological responses to weak depolarizing and hyperpolarizing current step injections are shown (top of panel). Scale bar: 100 μm.

(D) Excitatory postsynaptic potentials recorded from the cells in (C) during a single laser stimulation pulse of ChR2-expressing axons originating in POR. The average resting potential at which connectivity was tested is indicated for each cell.

(E) Distribution of recorded cells in LEC layer II receiving synaptic inputs in response to optogenetic activation of POR axons. Cells are grouped according to morphological type.

(F) Monosynaptic POR inputs to LEC LII neurons. Shown are traces from a pyramidal and an oblique pyramidal cell (top row) demonstrating that synaptic responses are action potential dependent (+TTX, middle row) and can be partially recovered by the addition of 4-AP (+TTX/4-AP, bottom row).

(G) Schematic of the experiment to demonstrate convergence of synaptic inputs from PER and POR onto LEC LII cells. Current clamp recordings of cells in LII of LEC during optogenetic stimulation (blue circles) of ChR2-labeled axonal fibers (green) following AAV injection in POR. Electrical stimulation with a bipolar electrode in PER is used to demonstrate PER input onto LEC LII cells. Insets: example synaptic responses following a single stimulation pulse of PER (left) and synaptic responses following grid patterned laser-scanning photostimulation of POR fibers (right) are shown.

(H) Distribution of recorded LEC LII cells receiving PER inputs (black) and convergent PER and POR inputs (orange).

(I) Five current clamp recorded LEC LII cells (two oblique pyramidal cells, two pyramidal cells, and one fan cell; cyan) together with afferent Chr2-labeled POR fibers (green). Dotted line indicates the border with PER. Scale bar: 100 μm.

(J) Electrophysiological responses to weak depolarizing and hyperpolarizing current step injections (left) for each of the recorded cells in (I). Middle and right panels show recorded synaptic responses for the five cells to POR and PER stimulation, respectively. Time of stimulation is indicated by the blue and black vertical lines, respectively. The average resting potential at which connectivity was tested is indicated for each cell.

See also Figure S2I.

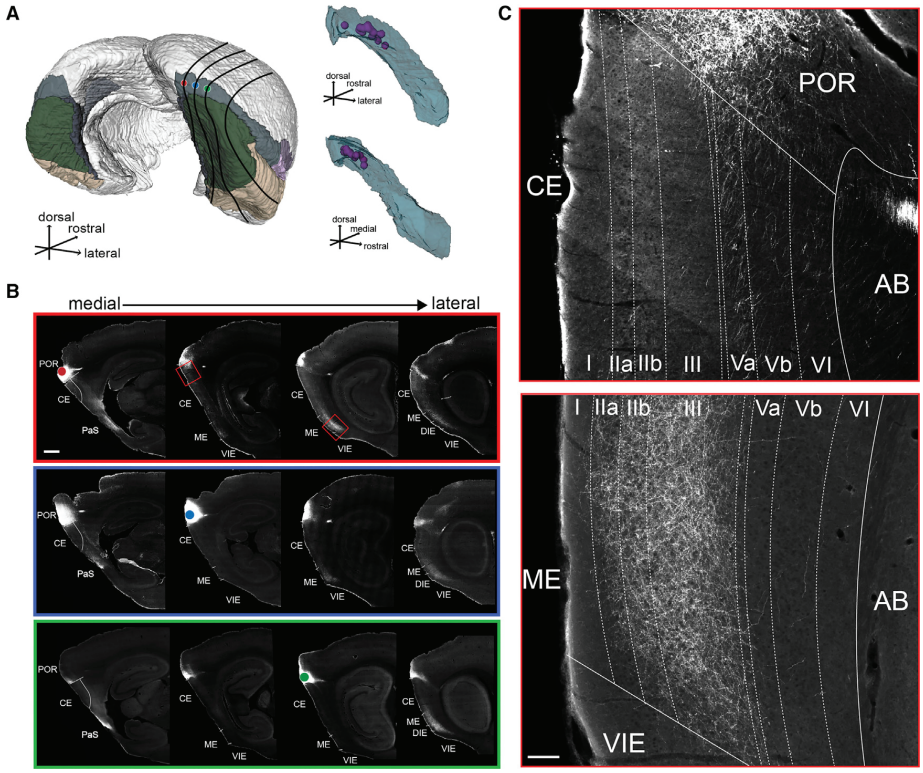

Figure 3. Distribution of POR Axon Terminals into MEC

(A) 3D WHS model with 3 representative injections distributed in caudomedial POR (left panel) and isolated POR 3D representation with center of mass of all pure anterograde injections (purple) that resulted in dense projections in MEC (caudal and lateral views in upper and lower right panels, respectively).

(B) POR projections from the 3 injections in (A), left panel, showing distributions in PHR at 4 sagittal levels corresponding to the black lines in (A). Colored dots indicate the center of mass of each injection site. Labeled axonal terminal plexus in MEC appears always laterally from the injection sites. Red square boxes in upper panels are insets displayed at higher magnification in (C), representing typical axonal labeling in dorsal MEC (area CE) and ventromedial MEC (area ME). Scale bar: 1,000 μm.

(C) Magnification of areas marked with an asterisk in red square boxes in upper (B). Panels demonstrating representative POR axonal distribution in dorsal MEC (area CE; upper panel) and ventromedial MEC (area ME; lower panel) are shown. Scale bar: 100 μm.

See Figure S1 for delineations of subdivisions of EC and Figure S3 for additional anterograde and retrograde material.

principal cells groups as well as a small group of putative inhibitory interneurons (Figure 2H). Most of the synaptic potentials recorded in principal cells and putative interneurons following stimulation of PER were presumed monosynaptic (74%; n = 54/73 cells), evident by minimal jitter (<700 μs) in the observed onset latencies. Recorded postsynaptic potentials following extracellular PER activation were abolished by bath application of TTX (1 μM; n = 8 from 3 rats), indicating that these were not evoked by direct volume conduction but instead required action-potential-induced release of neurotransmitter (Figure S2I). The majority of principal cells (73%; n = 58/80) that were tested for both inputs responded to POR optogenetic stimulation as well as extracellular electrical stimulation of PER (Figures 2H–2J). Taken together, our data show that projections from POR provide input to all main principal cell types in layer II of LEC and that these cells very likely also receive additional input from PER.

POR Projections to the Canonical Spatially Modulated MEC Are Relatively Sparse

Injections in both PORd and PORv resulted in terminal-like labeling as well as labeled passing fibers ventrally and laterally in deep layers of the caudodorsal part of MEC (area CE) with a notable preference for LVa. The labeled passing fibers continued ventrally reaching area ME, where they collateralized abundantly in superficial layers (Figures 3A–3C). This specific pattern, including the dense terminal labeling in superficial layers of ventral MEC, was only seen following injections in a restricted caudomedial portion of POR (Figure 3A, right panel; for lack of POR projections in area ME

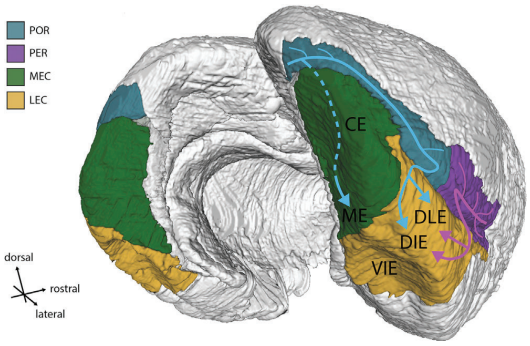

Figure 4. Schematic Summary of POR and PER Connectivity to EC
Summarized projections of POR and PER to superficial layers of EC showing a strong preference for lateral parts of LEC (DLE and DIE). For more details, see Figure S4.

following injections in lateral and rostral POR, see Figures 1A, 1F, and 1G).

Next, we searched our entire dataset for injections that resulted in dense projections to superficial layers of dorsal MEC (area CE), as reported in previous studies (Naber et al., 1997; Burwell and Amaral, 1998b; Koganezawa et al., 2015). This assessment showed that all injections resulting in the aforementioned pattern involved labeling of the ventrally positioned PaS or dorsal MEC (n = 12), meticulously delineated with a complementary triple immunostaining procedure of NeuN, Cb, and PV (Figures S3A and S3B; Boccara et al., 2015). None of the injections that were confined to PORv showed terminal labeling in superficial layers of the dorsal MEC subdivision CE (Figures 3C, upper panel, and S3D). The conclusion that superficial layers of dorsal MEC indeed receive only minimal POR input was corroborated by a series of retrograde tracer injections in superficial layers of CE (n = 4; Figure S3A). In all cases, we observed many retrogradely labeled cells in the thin dorsolateral extension of PaS intercalated between PORv and caudodorsal CE, whereas the immediate neighboring POR contained hardly any labeled somata (Figure S3C). The dorsolateral extension of PaS, notorious for its highly variable neuroanatomical boundaries (Burwell et al., 1995; Burgalossi et al., 2011; Boccara et al., 2015; Ramsden et al., 2015; Tang et al., 2016), projects indeed ventrally to layer II of dorsal MEC (Caballero-Bleda and Witter, 1993).

In conclusion, our anterograde and retrograde material indicate that superficial layers of the dorsal MEC area CE are largely devoid of POR inputs, which is in line with previously published data using retrograded rabies tracing of specific inputs to layer II of dorsal MEC (Rowland et al., 2013). In contrast, superficial layers of the more ventrally positioned area ME receive strong projections from the caudomedial portions of POR (Figures 3A, right panels; 3C, lower panel; 4; and S4). It is of particular interest that even the most ventral MEC recordings of spatially modulated cells were still confined within area CE (Brun et al., 2008; Stensola et al., 2012). Thus, area ME remains to this day a functionally unexplored area whose role seems in fact unrelated to spatial navigation memory, contrasting with the canonical spatially modulated area CE (Steffenach et al., 2005).

DISCUSSION

The present findings directly challenge the core anatomical principle of the current model on the organization of the medial temporal lobe episodic memory system and point to LEC as a unique site of convergence within PHR (Figures 4 and S4). Although our observations may seem in conflict with prior studies, a careful reanalysis of the projection patterns as described in the seminal work of Burwell and Amaral (1998b) actually supports our findings. Their data factually show that POR projections preferentially terminate dorsolaterally in LEC (64.5%; σ = 13.1; n = 3), along its rostrocaudal extent. In contrast, the projections to MEC are less strong (35.5%; σ = 13.1; n = 3) and largely restricted to ventral MEC, likely corresponding to area ME (Figures S5A–S5C). Furthermore, re-evaluation of available non-human primate tract tracing data on entorhinal projections from the PHC, the likely homolog of the rodent POR, reveals similarities with our current description in the rat. First, PHC projects obliquely from caudomedial to rostrolateral EC (Insausti et al., 1987; Suzuki and Amaral, 1994; Insausti and Amaral, 2008), similar to the oblique distribution of projections from POR that extend from medioventral (area ME) to rostrolateral EC (areas DIE and DLE; present study). Second, both caudal and rostral PHC emit projections spanning the rostrocaudal extent of LEC (Insausti et al., 1987; Suzuki and Amaral, 1994; Insausti and Amaral, 2008). Third, a restricted portion of caudal PHC seems to originate the main projections to caudomedial EC (Suzuki and Amaral, 1994; Insausti and Amaral, 2008), akin to the restricted portion of caudomedial POR projecting to medioventral area ME (current data). Fourth, PHC projections to LEC show a topographical organization similar to the rodent, such that caudal PHC projects densest to mediolateral levels of LEC and projections that originate in increasingly more rostral parts of PHC appear to progressively shift laterally toward the collateral sulcus (lateral rostral and lateral caudal entorhinal cortex subfields; areas ELr and ELc, respectively) EC (Insausti and Amaral, 2008). Therefore, PHC projects to an LEC area positioned close to the collateral sulcus, i.e., similar to the rodent dorsolateral LEC, which is close to the rhinal fissure (Kobro-Flatmoen and Witter, 2019). Finally, in this lateral area in the monkey, similar to what we showed in the present paper for POR and PER inputs, PHC and PER inputs seemingly converge in EC (Insausti et al., 1987; Suzuki and Amaral, 1994; Insausti and Amaral, 2008). Thus, we propose that LEC integrates POR/PHC and PER inputs as well as almost all other cortical inputs that distribute to EC (Insausti et al., 1987; Vaudano et al., 1991; Burwell and Amaral, 1998a; Jones and Witter, 2007; Kerr et al., 2007; Kondo and Witter, 2014; Mathiasen et al., 2015). Exceptions are inputs originating from the presubiculum (PrS) and the retrosplenial cortex (RSC), which are unique for MEC in all species studied so far (Amaral et al., 1984; Köhler, 1984; Saunders and Rosene, 1988; van Groen and Wyss, 1990; Wyss and Van Groen, 1992; Caballero-Bleda and Witter, 1993; Honda and Ishizuka, 2004; Jones and Witter, 2007; Kobayashi and Amaral, 2007). Neurons in LEC further receive inputs from MEC and PaS (Köhler, 1986; Caballero-Bleda and Witter, 1993; Dolorfo

and Amaral, 1998; Chrobak and Amaral, 2007). Recently, we have shown that neurons in LEC layer II integrate PER inputs with other main cortical inputs targeting superficial layers of LEC, i.e., inputs from piriform cortex, MEC, and contralateral LEC (T.P. Doan et al., 2016, Soc. Neurosci., conference). Together, the available data point to a unique multimodal nature of LEC, supported by a network analysis of over 16,000 articles of histologically defined axonal connections, revealing that LEC holds the richest set of association connections of any cerebral cortical region in the rat (Bota et al., 2015).

When focusing on cortical inputs to the superficial layers, the described input features of LEC in both rodents and non-human primates are thus strikingly different from those to superficial layers of MEC, which are restricted to PrS, PaS, and contralateral MEC (Cappaert et al., 2015). The PrS contains the highest proportion of sharply tuned head direction (HD) cells, inherited from a selective input from the anterior thalamic complex (Boccara et al., 2010; Cullen and Taube, 2017). In line with predictions from path-integration models (Burak and Fiete, 2006; McNaughton et al., 2006; Bush and Burgess, 2014), MEC grid cells intrinsically contain this HD signal (Bonnevie et al., 2013), which is fundamental, because disruption of the HD input leads to loss of their grid cell phenotype (Winter et al., 2015). The other exclusive MEC input structure, RSC that selectively targets layer V (Czajkowski et al., 2013), has also been portrayed as providing visuospatial information to the PHR-HF system (Julian et al., 2018), because it contains HD cells and is involved in their relationships to available landmarks in the environment, similar to what has been reported for PrS and PaS (Peck and Taube, 2017).

In contrast, the POR network encodes, monitors, and updates representations of the visuospatial context (Furtak et al., 2012), in line with its recently reported retinotopic representation, which is apparently unique to the parahippocampal region (Burgess et al., 2016) and specific potential to discriminate moving objects (Beltramo and Scanziani, 2019). In the present study, we demonstrate that POR projects strongly to superficial layers of dorsolateral LEC and not to MEC (area CE) as previously assumed. Interestingly, the integration of POR input with other externally driven sensory inputs in the LEC network fits with data indicating that neurons in LEC encode object complexity and object-place-context associations as well as egocentric bearing of the external world (Deshmukh and Knierim, 2011; Tsao et al., 2013; Van Cauter et al., 2013; Wilson et al., 2013a, 2013b; Rodo et al., 2017; Wang et al., 2018). At the population level, LEC cells have been found to code for episodic time, reflecting sequences of events within an episode (Tsao et al., 2018; Montchal et al., 2019). We thus propose that the convergence of a unique set of external sensory-derived inputs allows the LEC network to faithfully represent a continuously fluctuating extrinsic environment.

STAR★METHODS

Detailed methods are provided in the online version of this paper and include the following:

- KEY RESOURCES TABLE
- LEAD CONTACT AND MATERIALS AVAILABILITY
- EXPERIMENTAL MODEL AND SUBJECT DETAILS
- METHOD DETAILS
  - Surgeries
  - Histology and immunohistochemistry of neuroanatomical tracing slices
  - POR borders and delineations
  - PER borders and delineations
  - EC borders and delineations
  - PaS borders and delineations
  - Anatomical tracing studies analysis
  - Construction of two-dimensional unfolded flatmap
  - Electrophysiological slice preparation
  - *In vitro* electrophysiology protocol
  - Optogenetic stimulation of POR fibers
  - Extracellular stimulation of PER
  - Histology and immunohistochemistry of electrophysiological slices
  - Confocal microscopy and EC cell classification
- QUANTIFICATION AND STATISTICAL ANALYSIS
  - Quantification of POR axon terminals in MEC and LEC
  - Optogenetic stimulation of POR fibers
  - Extracellular stimulation of PER
- DATA AND CODE AVAILABILITY

SUPPLEMENTAL INFORMATION

Supplemental Information can be found online at https://doi.org/10.1016/j.celrep.2019.09.005.

ACKNOWLEDGMENTS

We thank Grethe Mari Olsen, Bruno Monterotti, Paulo Girão, and Hanne Tegnander Soligard for technical help; in particular, Paulo Girão helped with the cell colocalization counts that led to Figures S2A–S2E. We also thank Jørgen Sugar and Maximiliano Nigro for their comments on the manuscript. We further thank the staff in the animal facility at the Kavli Institute for Systems Neuroscience. This work was supported by Research Council of Norway grant 227769, the Kavli Foundation, United States, the Centre of Excellence scheme of the Research Council of Norway-Centre for Neural Computation grant 223262, and the National Infrastructure scheme of the Research Council of Norway-NORBRAIN grant 197467.

AUTHOR CONTRIBUTIONS

T.P.D. and M.P.W. conceived the study design. T.P.D., M.J.L.D., E.S.N., and S.O. collected the data. All anatomical quantifications were carried out by T.P.D. Data collection and quantification for Figure 2 was carried out by E.S.N. All authors contributed to the discussions that resulted in the current paper, which was written by T.P.D. and M.P.W. All authors approved the final version of the manuscript.

DECLARATION OF INTERESTS

The authors declare no competing interests.

Received: May 20, 2019
Revised: August 6, 2019
Accepted: August 30, 2019
Published: October 15, 2019

REFERENCES

Amaral, D.G., Insausti, R., and Cowan, W.M. (1984). The commissural connections of the monkey hippocampal formation. J. Comp. Neurol. *224*, 307–336.

Beltramo, R., and Scanziani, M. (2019). A collicular visual cortex: neocortical space for an ancient midbrain visual structure. Science *363*, 64–69.

Boccara, C.N., Sargolini, F., Thoresen, V.H., Solstad, T., Witter, M.P., Moser, E.I., and Moser, M.B. (2010). Grid cells in pre- and parasubiculum. Nat. Neurosci. *13*, 987–994.

Boccara, C.N., Kjonigsen, L.J., Hammer, I.M., Bjaalie, J.G., Leergaard, T.B., and Witter, M.P. (2015). A three-plane architectonic atlas of the rat hippocampal region. Hippocampus *25*, 838–857.

Bonnevie, T., Dunn, B., Fyhn, M., Hafting, T., Derdikman, D., Kubie, J.L., Roudi, Y., Moser, E.I., and Moser, M.B. (2013). Grid cells require excitatory drive from the hippocampus. Nat. Neurosci. *16*, 309–317.

Bota, M., Sporns, O., and Swanson, L.W. (2015). Architecture of the cerebral cortical association connectome underlying cognition. Proc. Natl. Acad. Sci. USA *112*, E2093–E2101.

Brun, V.H., Solstad, T., Kjelstrup, K.B., Fyhn, M., Witter, M.P., Moser, E.I., and Moser, M.B. (2008). Progressive increase in grid scale from dorsal to ventral medial entorhinal cortex. Hippocampus *18*, 1200–1212.

Burak, Y., and Fiete, I. (2006). Do we understand the emergent dynamics of grid cell activity? J. Neurosci. *26*, 9352–9354, discussion 9354.

Burgalossi, A., Herfst, L., von Heimendahl, M., Förste, H., Haskic, K., Schmidt, M., and Brecht, M. (2011). Microcircuits of functionally identified neurons in the rat medial entorhinal cortex. Neuron *70*, 773–786.

Burgess, C.R., Ramesh, R.N., Sugden, A.U., Levandowski, K.M., Minnig, M.A., Fenselau, H., Lowell, B.B., and Andermann, M.L. (2016). Hunger-dependent enhancement of food cue responses in mouse postrhinal cortex and lateral amygdala. Neuron *91*, 1154–1169.

Burwell, R.D. (2001). Borders and cytoarchitecture of the perirhinal and postrhinal cortices in the rat. J. Comp. Neurol. *437*, 17–41.

Burwell, R.D., and Amaral, D.G. (1998a). Cortical afferents of the perirhinal, postrhinal, and entorhinal cortices of the rat. J. Comp. Neurol. *398*, 179–205.

Burwell, R.D., and Amaral, D.G. (1998b). Perirhinal and postrhinal cortices of the rat: interconnectivity and connections with the entorhinal cortex. J. Comp. Neurol. *391*, 293–321.

Burwell, R.D., Witter, M.P., and Amaral, D.G. (1995). Perirhinal and postrhinal cortices of the rat: a review of the neuroanatomical literature and comparison with findings from the monkey brain. Hippocampus *5*, 390–408.

Bush, D., and Burgess, N. (2014). A hybrid oscillatory interference/continuous attractor network model of grid cell firing. J. Neurosci. *34*, 5065–5079.

Caballero-Bleda, M., and Witter, M.P. (1993). Regional and laminar organization of projections from the presubiculum and parasubiculum to the entorhinal cortex: an anterograde tracing study in the rat. J. Comp. Neurol. *328*, 115–129.

Canto, C.B., and Witter, M.P. (2012). Cellular properties of principal neurons in the rat entorhinal cortex. I. The lateral entorhinal cortex. Hippocampus *22*, 1256–1276.

Cappaert, N.L.M., Van Strien, N.M., and Witter, M.P. (2015). Hippocampal formation. In The Rat Nervous System, Fourth Edition, G. Paxinos, ed. (Academic), pp. 511–573.

Chrobak, J.J., and Amaral, D.G. (2007). Entorhinal cortex of the monkey: VII. intrinsic connections. J. Comp. Neurol. *500*, 612–633.

Couey, J.J., Witoelar, A., Zhang, S.J., Zheng, K., Ye, J., Dunn, B., Czajkowski, R., Moser, M.B., Moser, E.I., Roudi, Y., and Witter, M.P. (2013). Recurrent inhibitory circuitry as a mechanism for grid formation. Nat. Neurosci. *16*, 318–324.

Cullen, K.E., and Taube, J.S. (2017). Our sense of direction: progress, controversies and challenges. Nat. Neurosci. *20*, 1465–1473.

Czajkowski, R., Sugar, J., Zhang, S.J., Couey, J.J., Ye, J., and Witter, M.P. (2013). Superficially projecting principal neurons in layer V of medial entorhinal cortex in the rat receive excitatory retrosplenial input. J. Neurosci. *33*, 15779–15792.

de Villers-Sidani, E., Tahvildari, B., and Alonso, A. (2004). Synaptic activation patterns of the perirhinal-entorhinal inter-connections. Neuroscience *129*, 255–265.

Deshmukh, S.S., and Knierim, J.J. (2011). Representation of non-spatial and spatial information in the lateral entorhinal cortex. Front. Behav. Neurosci. *5*, 69.

Desikan, S., Koser, D.E., Neitz, A., and Monyer, H. (2018). Target selectivity of septal cholinergic neurons in the medial and lateral entorhinal cortex. Proc. Natl. Acad. Sci. USA *115*, E2644–E2652.

Doeller, C.F., Barry, C., and Burgess, N. (2010). Evidence for grid cells in a human memory network. Nature *463*, 657–661.

Dolorfo, C.L., and Amaral, D.G. (1998). Entorhinal cortex of the rat: organization of intrinsic connections. J. Comp. Neurol. *398*, 49–82.

Eichenbaum, H. (2017). On the integration of space, time, and memory. Neuron *95*, 1007–1018.

Eichenbaum, H., Yonelinas, A.P., and Ranganath, C. (2007). The medial temporal lobe and recognition memory. Annu. Rev. Neurosci. *30*, 123–152.

Fuchs, E.C., Neitz, A., Pinna, R., Melzer, S., Caputi, A., and Monyer, H. (2016). Local and distant input controlling excitation in layer II of the medial entorhinal cortex. Neuron *89*, 194–208.

Furtak, S.C., Ahmed, O.J., and Burwell, R.D. (2012). Single neuron activity and theta modulation in postrhinal cortex during visual object discrimination. Neuron *76*, 976–988.

Hafting, T., Fyhn, M., Molden, S., Moser, M.B., and Moser, E.I. (2005). Microstructure of a spatial map in the entorhinal cortex. Nature *436*, 801–806.

Honda, Y., and Ishizuka, N. (2004). Organization of connectivity of the rat presubiculum: I. Efferent projections to the medial entorhinal cortex. J. Comp. Neurol. *473*, 463–484.

Høydal, O.A., Skytøen, E.R., Andersson, S.O., Moser, M.B., and Moser, E.I. (2019). Object-vector coding in the medial entorhinal cortex. Nature *568*, 400–404.

Insausti, R., and Amaral, D.G. (2008). Entorhinal cortex of the monkey: IV. Topographical and laminar organization of cortical afferents. J. Comp. Neurol. *509*, 608–641.

Insausti, R., Amaral, D.G., and Cowan, W.M. (1987). The entorhinal cortex of the monkey: II. Cortical afferents. J. Comp. Neurol. *264*, 356–395.

Insausti, R., Herrero, M.T., and Witter, M.P. (1997). Entorhinal cortex of the rat: cytoarchitectonic subdivisions and the origin and distribution of cortical efferents. Hippocampus *7*, 146–183.

Jacobs, J., Weidemann, C.T., Miller, J.F., Solway, A., Burke, J.F., Wei, X.X., Suthana, N., Sperling, M.R., Sharan, A.D., Fried, I., and Kahana, M.J. (2013). Direct recordings of grid-like neuronal activity in human spatial navigation. Nat. Neurosci. *16*, 1188–1190.

Jones, B.F., and Witter, M.P. (2007). Cingulate cortex projections to the parahippocampal region and hippocampal formation in the rat. Hippocampus *17*, 957–976.

Julian, J.B., Keinath, A.T., Marchette, S.A., and Epstein, R.A. (2018). The neurocognitive basis of spatial reorientation. Curr. Biol. *28*, R1059–R1073.

Kerr, K.M., Agster, K.L., Furtak, S.C., and Burwell, R.D. (2007). Functional neuroanatomy of the parahippocampal region: the lateral and medial entorhinal areas. Hippocampus *17*, 697–708.

Killian, N.J., Jutras, M.J., and Buffalo, E.A. (2012). A map of visual space in the primate entorhinal cortex. Nature *491*, 761–764.

Kjonigsen, L.J., Lillehaug, S., Bjaalie, J.G., Witter, M.P., and Leergaard, T.B. (2015). Waxholm Space atlas of the rat brain hippocampal region: three-dimensional delineations based on magnetic resonance and diffusion tensor imaging. Neuroimage *108*, 441–449.

Kobayashi, Y., and Amaral, D.G. (2007). Macaque monkey retrosplenial cortex: III. Cortical efferents. J. Comp. Neurol. *502*, 810–833.

Kobro-Flatmoen, A., and Witter, M.P. (2019). Neuronal chemo-architecture of the entorhinal cortex: A comparative review. Eur. J. Neurosci. Published online July 10, 2019. https://doi.org/10.1111/ejn.14511.

Koganezawa, N., Gisetstad, R., Husby, E., Doan, T.P., and Witter, M.P. (2015). Excitatory postrhinal projections to principal cells in the medial entorhinal cortex. J. Neurosci. *35*, 15860–15874.

Köhler, C. (1984). Morphological details of the projection from the presubiculum to the entorhinal area as shown with the novel PHA-L immunohistochemical tracing method in the rat. Neurosci. Lett. *45*, 285–290.

Köhler, C. (1986). Intrinsic connections of the retrohippocampal region in the rat brain. II. The medial entorhinal area. J. Comp. Neurol. *246*, 149–169.

Kondo, H., and Witter, M.P. (2014). Topographic organization of orbitofrontal projections to the parahippocampal region in rats. J. Comp. Neurol. *522*, 772–793.

Leitner, F.C., Melzer, S., Lütcke, H., Pinna, R., Seeburg, P.H., Helmchen, F., and Monyer, H. (2016). Spatially segregated feedforward and feedback neurons support differential odor processing in the lateral entorhinal cortex. Nat. Neurosci. *19*, 935–944.

Maass, A., Berron, D., Libby, L.A., Ranganath, C., and Düzel, E. (2015). Functional subregions of the human entorhinal cortex. eLife *4*, e06426.

Mathiasen, M.L., Hansen, L., and Witter, M.P. (2015). Insular projections to the parahippocampal region in the rat. J. Comp. Neurol. *523*, 1379–1398.

McNaughton, B.L., Battaglia, F.P., Jensen, O., Moser, E.I., and Moser, M.B. (2006). Path integration and the neural basis of the 'cognitive map'. Nat. Rev. Neurosci. *7*, 663–678.

Miao, C., Cao, Q., Moser, M.B., and Moser, E.I. (2017). Parvalbumin and somatostatin interneurons control different space-coding networks in the medial entorhinal cortex. Cell *171*, 507–521.e17.

Montchal, M.E., Reagh, Z.M., and Yassa, M.A. (2019). Precise temporal memories are supported by the lateral entorhinal cortex in humans. Nat. Neurosci. *22*, 284–288.

Moser, E.I., Moser, M.B., and McNaughton, B.L. (2017). Spatial representation in the hippocampal formation: a history. Nat. Neurosci. *20*, 1448–1464.

Naber, P.A., Caballero-Bleda, M., Jorritsma-Byham, B., and Witter, M.P. (1997). Parallel input to the hippocampal memory system through peri- and postrhinal cortices. Neuroreport *8*, 2617–2621.

Navarro Schröder, T., Haak, K.V., Zaragoza Jimenez, N.I., Beckmann, C.F., and Doeller, C.F. (2015). Functional topography of the human entorhinal cortex. eLife *4*, e06738.

Nilssen, E.S., Jacobsen, B., Fjeld, G., Nair, R.R., Blankvoort, S., Kentros, C., and Witter, M.P. (2018). Inhibitory connectivity dominates the fan cell network in layer II of lateral entorhinal cortex. J. Neurosci. *38*, 9712–9727.

Nilssen, E.S., Doan, T.P., Nigro, M.J., Ohara, S., and Witter, M.P. (2019). Neurons and networks in the entorhinal cortex: A reappraisal of the lateral and medial entorhinal subdivisions mediating parallel cortical pathways. Hippocampus, Published August 13, 2019. https://doi.org/10.1002/hipo.23145.

Ohara, S., Onodera, M., Simonsen, O.W., Yoshino, R., Hioki, H., Iijima, T., Tsutsui, K.I., and Witter, M.P. (2018). Intrinsic projections of layer Vb neurons to layers Va, III, and II in the lateral and medial entorhinal cortex of the rat. Cell Rep. *24*, 107–116.

Papp, E.A., Leergaard, T.B., Calabrese, E., Johnson, G.A., and Bjaalie, J.G. (2014). Waxholm Space atlas of the Sprague Dawley rat brain. Neuroimage *97*, 374–386.

Pastoll, H., Solanka, L., van Rossum, M.C., and Nolan, M.F. (2013). Feedback inhibition enables θ-nested γ oscillations and grid firing fields. Neuron *77*, 141–154.

Paxinos, G., and Watson, C. (2007). The Rat Brain in Stereotaxic Coordinates (Academic).

Peck, J.R., and Taube, J.S. (2017). The postrhinal cortex is not necessary for landmark control in rat head direction cells. Hippocampus *27*, 156–168.

Petreanu, L., Mao, T., Sternson, S.M., and Svoboda, K. (2009). The subcellular organization of neocortical excitatory connections. Nature *457*, 1142–1145.

Ramsden, H.L., Sürmeli, G., McDonagh, S.G., and Nolan, M.F. (2015). Laminar and dorsoventral molecular organization of the medial entorhinal cortex revealed by large-scale anatomical analysis of gene expression. PLoS Comput. Biol. *11*, e1004032.

Ranganath, C., and Ritchey, M. (2012). Two cortical systems for memory-guided behaviour. Nat. Rev. Neurosci. *13*, 713–726.

Reagh, Z.M., and Yassa, M.A. (2014). Object and spatial mnemonic interference differentially engage lateral and medial entorhinal cortex in humans. Proc. Natl. Acad. Sci. USA *111*, E4264–E4273.

Rodo, C., Sargolini, F., and Save, E. (2017). Processing of spatial and non-spatial information in rats with lesions of the medial and lateral entorhinal cortex: Environmental complexity matters. Behav. Brain Res. *320*, 200–209.

Rowland, D.C., Weible, A.P., Wickersham, I.R., Wu, H., Mayford, M., Witter, M.P., and Kentros, C.G. (2013). Transgenically targeted rabies virus demonstrates a major monosynaptic projection from hippocampal area CA2 to medial entorhinal layer II neurons. J. Neurosci. *33*, 14889–14898.

Sargolini, F., Fyhn, M., Hafting, T., McNaughton, B.L., Witter, M.P., Moser, M.B., and Moser, E.I. (2006). Conjunctive representation of position, direction, and velocity in entorhinal cortex. Science *312*, 758–762.

Saunders, R.C., and Rosene, D.L. (1988). A comparison of the efferents of the amygdala and the hippocampal formation in the rhesus monkey: I. Convergence in the entorhinal, prorhinal, and perirhinal cortices. J. Comp. Neurol. *271*, 153–184.

Schultz, H., Sommer, T., and Peters, J. (2012). Direct evidence for domain-sensitive functional subregions in human entorhinal cortex. J. Neurosci. *32*, 4716–4723.

Solstad, T., Boccara, C.N., Kropff, E., Moser, M.B., and Moser, E.I. (2008). Representation of geometric borders in the entorhinal cortex. Science *322*, 1865–1868.

Steffenach, H.A., Witter, M., Moser, M.B., and Moser, E.I. (2005). Spatial memory in the rat requires the dorsolateral band of the entorhinal cortex. Neuron *45*, 301–313.

Stensola, H., Stensola, T., Solstad, T., Frøland, K., Moser, M.B., and Moser, E.I. (2012). The entorhinal grid map is discretized. Nature *492*, 72–78.

Suzuki, W.A., and Amaral, D.G. (1994). Topographic organization of the reciprocal connections between the monkey entorhinal cortex and the perirhinal and parahippocampal cortices. J. Neurosci. *14*, 1856–1877.

Suzuki, W.A., and Porteros, A. (2002). Distribution of calbindin D-28k in the entorhinal, perirhinal, and parahippocampal cortices of the macaque monkey. J. Comp. Neurol. *451*, 392–412.

Tahvildari, B., and Alonso, A. (2005). Morphological and electrophysiological properties of lateral entorhinal cortex layers II and III principal neurons. J. Comp. Neurol. *491*, 123–140.

Tang, Q., Burgalossi, A., Ebbesen, C.L., Sanguinetti-Scheck, J.I., Schmidt, H., Tukker, J.J., Naumann, R., Ray, S., Preston-Ferrer, P., Schmitz, D., and Brecht, M. (2016). Functional architecture of the rat parasubiculum. J. Neurosci. *36*, 2289–2301.

Tsao, A., Moser, M.B., and Moser, E.I. (2013). Traces of experience in the lateral entorhinal cortex. Curr. Biol. *23*, 399–405.

Tsao, A., Sugar, J., Lu, L., Wang, C., Knierim, J.J., Moser, M.B., and Moser, E.I. (2018). Integrating time from experience in the lateral entorhinal cortex. Nature *561*, 57–62.

Uva, L., Grüschke, S., Biella, G., De Curtis, M., and Witter, M.P. (2004). Cytoarchitectonic characterization of the parahippocampal region of the guinea pig. J. Comp. Neurol. *474*, 289–303.

Van Cauter, T., Camon, J., Alvernhe, A., Elduayen, C., Sargolini, F., and Save, E. (2013). Distinct roles of medial and lateral entorhinal cortex in spatial cognition. Cereb. Cortex *23*, 451–459.

van Groen, T., and Wyss, J.M. (1990). The postsubicular cortex in the rat: characterization of the fourth region of the subicular cortex and its connections. Brain Res. *529*, 165–177.

Vaudano, E., Legg, C.R., and Glickstein, M. (1991). Afferent and efferent connections of temporal association cortex in the rat: a horseradish peroxidase study. Eur. J. Neurosci. *3*, 317–330.

Wang, C., Chen, X., Lee, H., Deshmukh, S.S., Yoganarasimha, D., Savelli, F., and Knierim, J.J. (2018). Egocentric coding of external items in the lateral entorhinal cortex. Science *362*, 945–949.

Wilson, D.I., Langston, R.F., Schlesiger, M.I., Wagner, M., Watanabe, S., and Ainge, J.A. (2013a). Lateral entorhinal cortex is critical for novel object-context recognition. Hippocampus *23*, 352–366.

Wilson, D.I., Watanabe, S., Milner, H., and Ainge, J.A. (2013b). Lateral entorhinal cortex is necessary for associative but not nonassociative recognition memory. Hippocampus *23*, 1280–1290.

Winter, S.S., Clark, B.J., and Taube, J.S. (2015). Spatial navigation. Disruption of the head direction cell network impairs the parahippocampal grid cell signal. Science *347*, 870–874.

Witter, M.P., Groenewegen, H.J., Lopes da Silva, F.H., and Lohman, A.H.M. (1989). Functional organization of the extrinsic and intrinsic circuitry of the parahippocampal region. Prog. Neurobiol. *33*, 161–253.

Witter, M.P., Doan, T.P., Jacobsen, B., Nilssen, E.S., and Ohara, S. (2017). Architecture of the entorhinal cortex: a review of entorhinal anatomy in rodents with some comparative notes. Front. Syst. Neurosci. *11*, 46.

Wyss, J.M., and Van Groen, T. (1992). Connections between the retrosplenial cortex and the hippocampal formation in the rat: a review. Hippocampus *2*, 1–11.

Yonelinas, A.P., and Ritchey, M. (2015). The slow forgetting of emotional episodic memories: an emotional binding account. Trends Cogn. Sci. *19*, 259–267.

STAR★METHODS

KEY RESOURCES TABLE

REAGENT or RESOURCE	SOURCE	IDENTIFIER
Antibodies		
Goat anti-PHA-L	Vector Laboratories	#AS-2224
Donkey anti-goat (AF 405, 488, 546, 633)	Invitrogen	#ab175664, #A-11055, #A-11056, #A-21082
Rabbit anti-Cb	Swant	#CB38
Guinea pig anti-NeuN	Sigma Aldrich	#ABN90P
Mouse anti-PV	Sigma Aldrich	#P3088
Mouse anti-PV	Merck Millipore	# MAB1572
Donkey anti-rabbit (AF 488, 546, 633)	Invitrogen	#A-21206, #A10040, #A-21071
Donkey anti guinea pig (AF 488, 546, 633)	Invitrogen	#A-11073, #A-11074, #A-21105
Donkey anti mouse (AF 488, 546, 633)	Invitrogen	#A21202, #A10036, #A-21082
Chicken anti-GFP	Abcam	#ab13970
Mouse anti-Re	Merck Millipore	#MAB5364
Goat anti-mouse (AF 405)	Thermo Fisher Scientific	#A31553
Goat anti-chicken (AF 488)	Thermo Fisher Scientific	#A-11039
Goat anti-rabbit (AF 633)	Thermo Fisher Scientific	# 35562
Bacterial and Virus Strains		
AAV1.hSyn.ChR2(H134R)-eYFP.WPRE.hGH	UPenn Vector Core	#CS0581
Biological Samples		
Normal Goat Serum	Abcam	#AB7481
Chemicals, Peptides, and Recombinant Proteins		
Biotinylated dextran amine	Invitrogen	#D1956
Conjugated dextran amine (AF 488, 546)	Invitrogen	#D22910, #D22911
Phaseolus vulgaris leucoagglutinin	Vector Laboratories	#L-1110
Fast Blue	EMS Chemie	#9000002
Fluorogold	Fluorochrome	#fluoro-gold
Cholera toxin Subunit B 555	Invitrogen	# C22843
Tagged streptavidin (AF 405, 488, 546, 633)	Invitrogen	#S11225, # S21375, # S32354, # S32351
Biocytin	Iris Biotech	#B4261
Tetrodotoxin	Tocris Bioscience	#1078
Bicuculline	Sigma-Aldrich	#14343
Paraformaldehyde	Merck Chemicals	#16005
Dimethyl sulfoxide	VWR	#23486
Deposited Data		
Rat Hippocampus Atlas online dataset	http://cmbn-navigator.uio.no/rat_hippocampus_atlas	N/A
Waxholm SD rat atlas v2	https://www.nitrc.org/projects/whs-sd-atlas	N/A
Experimental Models: Organisms/Strains		
Rat Long Evans	Charles River	#006
Rat Wistar	Charles River	#003
Rat Sprague Dawley	Charles River	#400
Software and Algorithms		
Adobe Photoshop CS6	Adobe Systems	N/A
Adobe Illustrator CS6	Adobe Systems	N/A
Patchmaster	Heka Elektronik	N/A

(*Continued on next page*)

Continued

REAGENT or RESOURCE	SOURCE	IDENTIFIER
MATLAB	MathWorks	N/A
ITK snap	Upenn / UNC	N/A
Amira	Thermo Fisher Scientific	N/A
Material		
Stereotaxic frame	Kopf Instruments	N/A
Stereotaxic frame SR-5R	Narishige	N/A
Glass micropipette	Harvard Apparatus	N/A
PP-830 puller	Narishige	N/A
Digital Midgard Precision current source	Stoelting	N/A
Microinjection pump WPI Nanoliter 2010	Heco	N/A
Freezing microtome	Thermo Scientific	N/A
Menzel-glass slides	Thermo Scientific	N/A
Axio Imager M1/2	Zeiss	N/A
Axio Scan Z1	Zeiss	N/A
Leica VT1000S	Leica Biosystems	N/A
Borosilicate glass capillaries	Harvard Apparatus	N/A
Axio Examiner D1	Zeiss	N/A
EPC 10 Quadro USB amplifier	Heka Elektronik	N/A
UGA-42 GEO point scanning system	Rapp OptoElectronic	N/A
Flex isolation unit	AMPI	N/A
LSM 880 AxioImager Z2	Zeiss	N/A

LEAD CONTACT AND MATERIALS AVAILABILITY

Further information and requests for resources and reagents should be directed to and will be fulfilled by the Lead Contact, Menno P. Witter (menno.witter@ntnu.no). This study did not generate new unique reagents.

EXPERIMENTAL MODEL AND SUBJECT DETAILS

In total, 100 adult female and male Wistar (200-230 g), Sprague Dawley (200-260 g) and Long Evans (190-320 g) rats, including animals from previous projects from our lab (Naber et al., 1997; Koganezawa et al., 2015), were used for the neuroanatomical studies (Tables S1 and S2). Thirteen female and male Long Evans rats aged between P14 and P21 were used for the electrophysiological studies. We did not perform analysis of the influence of sex in the present study at these fundamental neuroanatomical pathways are certainly conserved across genders. Animals were group housed with food and water available *ad libitum*. After surgery, the animals were individually housed until euthanasia. All experiments using male Wistar rats (Table S2) were performed at Tohoku University and conducted according to the Guidelines of the National Institutes of Health and the Tohoku University Guidelines for Animal Care and Use. All remaining experiments were performed at the Kavli Institute for Systems Neuroscience/Centre for Neural Computation at the Norwegian University of Science and Technology (NTNU) where animals were housed and handled according to the Norwegian laws and regulations concerning animal welfare and animal research. Experimental protocols were approved by the Norwegian Animal Research Authority and were in accordance with the European Convention for the Protection of Vertebrate Animals used for Experimental and Other Scientific Purposes.

METHOD DETAILS

Surgeries

Methods for tracer injections have been described in detail previously (Koganezawa et al., 2015). Briefly, under deep isoflurane gas-induced anesthesia, rats were mounted in a stereotaxic frame (Kopf Instruments, Tujunga, CA) and were injected with anterograde or retrograde tracers or adeno-associated virus using coordinates derived from a stereotaxic brain atlas (Paxinos and Watson, 2007) adjusted according to the weight of adult rats or 0.2mm from Bregma, 4.0mm lateral to the sagittal sinus and 2.2mm deep from the brain surface for younger rats (P14-21). Regarding the retrograde tracer injections to LEC from the lateral side (Table S2), the rats were deeply anaesthetized with ketamine (80.0 mg/kg, i.p.) and xylazine (0.8 mg/kg, i.p.) and were mounted in a stereotaxic

frame (Narishige, SR-5R). The lateral skull was exposed, and a burrhole was drilled to visualize the caudal rhinal vein. The injection was conducted ventral to the caudal rhinal vein at a 30-45 degree angle in the coronal plan, with the glass micropipette pointing to the midline.

Anterograde tracers consisted of 10 kDa biotinylated dextran amine (BDA, Invitrogen, Molecular Probes, Eugene, OR; 5% solution in 0.125 M phosphate buffer, pH 7.4), 10kDa preconjugated dextran amines (Alexa 488 or −546 DA; Invitrogen, Molecular Probes, Eugene, OR; 5% solution in 0.125 M phosphate buffer, pH 7.4) and Phaseolus vulgaris leucoagglutinin (PHA-L, Vector Laboratories; 2.5% solution in 10 mM phosphate buffer, pH 7.4). Animals received between 1-4 iontophoretic anterograde tracer injections via a glass micropipette (20–25 μm tip diameter, 30–0044, Harvard Apparatus; pulled with a PP-830 puller) connected to a current source (alternating 6 s on/off current of 7 μA in case of PHA-L and 6 μA in case of BDA and DA for 5-15min, 51595; Stoelting Midgard current source) into various portions of POR and PER (Table S1; Video S1). As retrograde tracers, we used Fast Blue (FB; 1% in PBS, EMS Chemie), Fluorogold (FG; 2.5% in H2O, Fluorochrome) and Cholera toxin Subunit B 555 (CTB555; 4% in H2O, Invitrogen). Animals received between 1-2 retrograde tracer pressure injections via a glass micropipette (30-60 μm tip diameter, 30–0044, Harvard Apparatus, Holliston, MA; pulled with a PP-830 puller) connected to an automated microinjection pump (WPI Nanoliter 2010, Heco) into various portions of MEC and LEC (Table S2; Video S2). For electrophysiological studies, younger rats (age 14 – 21 days postnatally) received pressure injections of adeno-associated virus 1 mediated targeted expression of channelrhodopsin-2-eYFP (AAV1.hSyn.ChR2 H134R-eYFP.WPRE, Addgene) via a glass micropipette (30-40 μm tip diameter, 30–0044, Harvard Apparatus, Holliston, MA; pulled with a PP-830 puller) connected to an automated microinjection pump (WPI Nanoliter 2010, Heco) into various portions of caudal POR. All animals were given a dose of buprenorphine (temgesic, RB Pharmaceuticals, 0.05 mg/kg, subcutaneously) 30 min before the end of the surgery, to reduce postsurgical pain. Upon completion of injections, the wound was cleaned and sutured, and the animal was put back in its home cage.

Histology and immunohistochemistry of neuroanatomical tracing slices

After 7–14 d of survival, adult rats received an overdose of equithesin (a mixture of chloral hydrate, magnesium sulfate, and sodium-pentobarbital; 11 mg/kg body weight i.p.; Sanofi Sante). They were subsequently transcardially perfused with 200 mL of a fresh filtrated oxygenated Ringer's solution (0.85% NaCl, 0.025% KCl, 0.02% NaHCO3, 4°C, brought to pH 6.9 with CO2) followed by 200 mL 4% filtrated freshly depolymerized PFA (1.04005; Merck) in PBS at 4°C. Subsequently, the brain was removed from the skull and postfixed at 4°C in the same fixative for minimum of 2 hours and stored overnight in a mixture of 20% glycerol (VWR, no.24387.292) and 2% dimethyl sulfoxide (DMSO; VWR, no.23486.297). We cut 30-50μm thick brain sections with a freezing microtome (Thermo Scientific) and stored them in 4-6 equally spaced series in the DMSO solution (Table S1). In sections, we visualized BDA with fluorophore-tagged streptavidin (Invitrogen, Molecular Probes, Alexa Fluor 405, 488, 546 or 633), PHA-L with primary (goat anti-PHA-L, Vector Laboratories) and fluorophore-tagged secondary (donkey anti-goat, Invitrogen, Molecular Probes, Alexa Fluor 405, 488, 546 or 633) antibodies. In the case of animals in which both anterograde tracers were injected or had concomitant preconjugated dextran amines injections, we used fluorophores with different emission wave-lengths to discriminate between them and the respective anterograde labeling. For delineation purpose, adjacent series were immunostained for the neuronal stain NeuN and calcium-binding proteins parvalbumin (PV) and calbindin D-28 (Cb) with primary (rabbit anti-Cb, Swant; guinea pig anti-NeuN, Sigma Aldrich; mouse anti-PV, Sigma Aldrich Merck Millipore) and fluorophore-tagged secondary (donkey -anti-rabbit, -guinea pig or -mouse for Cb, NeuN and mouse immunostaining respectively, Invitrogen, Molecular Probes, Alexa Fluor 488, 546 or 633) antibodies. For all immunohistochemical staining, we used the same procedure. Sections were rinsed 3 × 10 minutes in 0.125 M phosphate buffer (PB; pH 7.4) followed by 60 min blocking and permeabilization in 0.125 M PBS-Tx (0.5% Triton X-100, 10% normal goat serum, pH 7.6). Sections were incubated with the primary antibody (1:1000 in PBS-Tx; 48h at 4°C), rinsed 3 × 10 minutes (PBS-Tx) and incubated with the secondary antibody and/or streptavidin (1:200, PBS-Tx, overnight at 4°C, pH 7.6). Finally, sections were rinsed 2 × 10 min in PB 0.125M and then 2 × 10min in a Tris buffer (0.606% Tris(hydroxymethyl)aminomethane, pH 7.6) before being mounted on Menzel-glass slides (Thermo Scientific) from a Tris-gelatin solution (0.2% gelatin in Tris-buffer, pH 7.6) and coverslipped with entelan in a toluene solution (Merck Chemicals, Darmstadt, Germany). When needed, we used the similar protocol on remaining series that were previously delineated using dark-field or cresyl violet from previous studies (Naber et al., 1997; Koganezawa et al., 2015; Table S1).

POR borders and delineations

POR is a six layered cortex located caudal to PER and mostly dorsal to the rhinal fissure where it rises steeply and wraps obliquely around the caudal pole of EC. POR is composed of a ventral (PORv) and a dorsal (PORd) subdivision (Burwell, 2001). POR cytoarchitecture features a homogeneous neuronal distribution across layers II–IV and a resulting lack of a prominent laminar structure. Nonetheless, PORd cells in layer III appear more organized with a clear radial appearance that is absent in PORv (Burwell, 2001). Similar to A35, PORv is completely devoid of parvalbumin (PV) positivity, while PORd stains stronger for PV similarly to A36. The distribution of Cb neuropil in PORv is also similar to that in area 35 and 36 respectively. PORv is bordered ventrally by EC for the most part, which is however replaced caudomedially by a highly variable dorsolateral PaS extension (Burgalossi et al., 2011; Boccara et al., 2015; Ramsden et al., 2015; Tang et al., 2016). PV staining makes these borders stand out since MEC and PaS superficial layers stain strongly for PV, contrary to PORv. In contrast, a marked Cb staining in POR is noticeable, which is absent from PaS or the directly adjacent layers III-VI of EC (Boccara et al., 2015).

PER borders and delineations

PER is a six layered cortex that runs almost parallel with the rhinal fissure, occupying the fundus and/or its dorsal and ventral banks and also comprises a ventral (A35) and a dorsal (A36) subdivision (Burwell et al., 1995). The posterior border of PER is with POR, and is positioned slightly rostral to the ventrally adjacent border between DLE and CE. The rostral border of PER is with the insular cortex and it is generally accepted that this border in coronal sections coincides with the emergence of the claustrum deep to the insular cortex (Burwell, 2001). The border between EC and A35 is indicated by the loss of the typical lamina dissecans in LEC. The superficial layers of A35 are homogeneously packed with small neurons whereas DLE demonstrates a a clear lamination in its superficial layers with layer II cells being larger and more darkly stained than layer III cells. Besides, superficial layers of DLE stain heavily for PV, while staining is essentially absent in A35. Vice versa, in material stained for Cb, a marked increase of staining in area 35 is noticeable.

EC borders and delineations

EC is a six layered cortex delineated by the rhinal fissure on its lateral and dorsal side. In the current paper, we divide EC into MEC composed of caudal (CE) and medial (ME) subdivisions, and LEC composed of dorsal lateral (DLE), dorsal intermediate (DIE) and ventral intermediate (VIE) subdivisions (Insausti et al., 1997). Each EC subdivision is differentiated based on subtle cytoarchitectonic differences and mainly serve detailed anatomical comparisons, but a general pattern is that deep layers (V–VI) are clearly distinguishable from superficial layers (II–III), as the thin acellular layer IV, i.e., lamina dissecans, separates them and this is particularly well developed in MEC. In the present paper, a border of interest is between the two MEC subdivisions, i.e., areas CE and ME. The most striking change that defines this border is an overall less conspicuous lamination in ME than in CE. The superficial layers of ME are less homogeneous than their CE counterparts, ME layer II breaks up into two or three clusters of cells, which makes it less sharply delineated from both layers I and III, and ME layer III tends to split into sublayers. Differences exist also in the superficial portion of their deep layers (layer Va, in opposition to layer Vb) as CE layer Va is sparsely populated by large pyramidal cells, and ME is characterized by a more regularly structured layer Va with a higher number of large pyramidals positioned at regular intervals. Finally, the superficial layers of ventral CE exhibit moderate homogeneous reactivity for parvalbumin, unlike ME where the staining is less strong to absent.

PaS borders and delineations

PaS is a six layered cortex wedged in between PrS and EC, whose most dorsal portion forms a dorsolateral extension which curves around the most caudodorsal part of MEC. This dorsolateral extension of PaS shows a very variable mediolateral extent, and the more laterally extending part can easily be mistaken for MEC (Burgalossi et al., 2011; Boccara et al., 2015; Ramsden et al., 2015; Tang et al., 2016). A striking feature of PaS is its lack of a clear differentiation between superficial layers II and III, seen in dorsal CE, whereas the neuron diameters are substantially larger than the ones seen in POR. In addition, PaS markedly lacks reactivity for calbindin in its superficial layers, which contrasts with the moderate to strong reactivity for that protein of the superficial layers of EC and POR.

Anatomical tracing studies analysis

Sections were inspected with fluorescence illumination at the appropriate excitation wavelengths (Zeiss Axio Imager M1/2), and digital images were obtained using an automated scanner (Zeiss Axio Scan Z1). We thus obtained a library of POR (n = 64) and PER (n = 23) anterograde injections in brains (n = 64) cut in coronal (n = 25), horizontal (n = 18) and sagittal (n = 21) planes (Table S1) as well as retrograde injections into superficial layers of dorsal MEC (ie. area CE; n = 4) and dorsolateral LEC (ie. areas DIE and DLE; n = 9; Table S2). Precise PHR delineations with the help of NeuN, Parvalbumin and Calbindin immunostaining (Boccara et al., 2015) allowed to plot the center of mass for each injections into the 3D Waxholm space atlas reference frame (Papp et al., 2014) which leveraged possibilities for comprehensive multiplanar comparative analysis corroborating anterograde and retrograde tracing datasets in all three main anatomical plans (Kjonigsen et al., 2015; Videos S1 and S2). All injections were made with distinct tracers in the right hemisphere except for 3 animals that had already received bilateral BDA injections as part of a previous study (Table S1). All images selected for illustration purposes were saved as gray-level images of which the contrast and brightness were equalized using Adobe Photoshop and Illustrator (CS6, Adobe Systems).

Construction of two-dimensional unfolded flatmap

We used the methods described in detail previously (Burwell and Amaral, 1998b). In brief, we used coronal sections from the available Rat Hippocampus Atlas online dataset (http://cmbn-navigator.uio.no/rat_hippocampus_atlas), which includes MEC and LEC subdivisions based on NeuN, Cb and PV stainings (Insausti et al., 1997; Boccara et al., 2015). A subset of the sections used to construct the map are visible with distance from Bregma visible above in mm. The fundus of the rhinal sulcus was marked for use as the alignment point. At more caudal levels, where the rhinal sulcus is little more than a shallow indentation, a point was marked at the center of the indentation. A spreadsheet program (Excel, Microsoft) and Adobe Photoshop and Illustrator (CS6, Adobe Systems) were used to create straight-line and colored EC subdivisions unfolded maps (Figure S5A).

Electrophysiological slice preparation

After 2-3 weeks survival time after AAV injection, acute semicoronal slices were prepared from Long Evans rats (P31-P45) following procedures described in detail previously (Nilssen et al., 2018). In short, the animals were anesthetized with isoflurane and killed by decapitation. The brain was quickly dissected out and placed in ice-cold artificial cerebrospinal fluid (ACSF) containing: 110 mM choline chloride, 2.5 mM KCl, 25 mM D-Glucose, 25 mM NaHCO3, 11.5 mM sodium ascorbate, 3 mM sodium pyruvate, 1.25 mM NaH2PO4, 100 mM D-Mannitol, 7 mM MgCl2 and 0.5 mM CaCl2. PH was adjusted to 7.4, and osmolality to 430 mOsm. 400 μm thick slices from the brain hemisphere ipsilateral to the POR injection site were acquired using a vibrating slicer (Leica VT1000S, Leica Biosystems). The slices were cut with an angle of approximately 20° with respect to the coronal plane to preserve the connection between PER and LEC (de Villers-Sidani et al., 2004). Slices were kept at 35° in ACSF containing 126 mM NaCl, 3 mM KCl, 1.2 mM Na2HPO4, 10 mM D-glucose, 26 mM NaHCO3, 3 mM MgCl2 and 0.5 mM CaCl2. The slices were then maintained at room temperature for at least 30 minutes before transferred one-by-one to the recording chamber.

In vitro electrophysiology protocol

Patch clamp recording pipettes (resistance:3-8 MΩ) were made from borosilicate glass capillaries (1.5 outer diameter x 0.86 inner diameter; Harvard Apparatus) and back-filled with internal solution of the following composition: 120 mM K-gluconate, 10 mM KCL, 10 mM Na2-phosphocreatine, 10 mM HEPES, 4 mM Mg-ATP, 0.3 mM Na-GTP, with pH adjusted to 7.3 and osmolality to 300-305 mOsm. Biocytin (5mg/mL; Iris Biotech) was added to the internal solution in order to recover cell morphology. Acute slices were moved to the recording setup and visualized using infrared differential interference contrast optics aided by a 20x/1.0 NA water immersion objective (Zeiss Axio Examiner D1, Carl Zeiss). Electrophysiological recordings were performed at 35°C and slices superfused with oxygenated recording ACSF containing 126 mM NaCl, 3 mM KCl, 1.2mM Na2HPO4, 10 mM D-Glucose, 26 mM NaHCO3 1.5 mM MgCl2 and 1.6 mM CaCl2. Layer IIa of LEC was identified by the presence of large cells aggregated in small clusters. Layer IIb of LEC was identified based on its smaller-sized cells, usually pyramidal-shaped, situated deep to the large cell islands of layer IIa. Up to three neighboring cells situated near virally transduced fibers were selected for simultaneous recordings. Gigaohm resistance seals were acquired for all cells before rupturing the membrane to enter whole-cell mode. Pipette capacitance compensation was performed prior to entering whole-cell configuration, and bridge balance adjustments were carried out at the start of current clamp recordings. Data acquisition was performed by Patchmaster (Heka Elektronik) controlling an EPC 10 Quadro USB amplifier (Heka Elektronik). Acquired data were low-pass filtered (Bessel filter, 4 kHz) and digitized (10 kHz). No correction was made for the liquid junction potential (13 mV as measured experimentally). Negative and positive current pulses (500 ms, −400 to +500 pA, 50 pA incremental steps, 3 s waiting time between stimuli) were injected into the cells to aid classification of recorded cells as principal cells or interneurons. In a subset of experiments, putative monosynaptic laser-evoked synaptic inputs were isolated by sequential application of tetrodotoxin (TTX, 1μM Tocris Bioscience) followed by combined 4-Aminopyridine (4-AP, 100 μM, Sigma-Aldrich) and TTX (Petreanu et al., 2009). Putative inhibitory potentials were confirmed by bath application of the GABAA-receptor antagonist bicuculline (10 μM, Sigma-Aldrich).

Optogenetic stimulation of POR fibers

Optogenetic stimulation was carried out using a patterned laser scanning device (UGA-42 GEO point scanning system, Rapp OptoElectronic) controlling a continuous diode laser (473 nm). The tissue was illuminated with laser pulses of 1 ms in duration and beam diameters between 20-35 μm. Laser stimuli were delivered at a rate of 1 Hz, irradiating the tissue in a 4x5 grid pattern. The grid stimulation protocol was repeated 5-15 times. Laser intensity (1.5-5.0 mW) was adjusted depending on the virus expression level in the slice for each simultaneously recorded cluster as to evoke sub-threshold membrane potential deflections.

Extracellular stimulation of PER

A tungsten bipolar electrode (tip separation: 150-300 μm) was placed in the superficial layers of PER, directly adjacent to the border to LEC, in agreement with a previous report describing that the main projection to dorsolateral LEC originates from layers II and III of PER (Burwell and Amaral, 1998b). A single pulse stimulation (100 μs, 0.3-3 mA) was generated by an Iso-Flex isolation unit (AMPI, Israel) controlled by Patchmaster. The stimulation protocol was repeated 20-50 times. Slices in which extracellular stimulation did not evoke responses in any of the recorded cells indicated unsuccessful preservation of PER to LEC connectivity and were consequently excluded from the dataset. The individual recorded voltage traces (n = 20-50) during electrical activation of PER were used to compute an average trace.

Histology and immunohistochemistry of electrophysiological slices

Immediately following patch clamp recordings, the slices were exposed to 4% paraformaldehyde (PFA, pH 7.4, Merck Chemicals) for 48 hours at 4°C. Slices from electrophysiological experiments were washed in phosphate buffer (PB, 2x15 min, room temperature) followed by membrane permeabilization in Tris buffered saline containing 0.5% Triton X-100 (TBS-Tx. 5x15 min, room temperature). Next, slices were pretreated for 90 minutes in TBS-Tx containing 10% Normal Goat Serum (NGS, Abcam: AB7481) at room temperature. Slices were incubated with primary antibodies rabbit anti-Cb (1:3000, Swant), chicken anti-GFP (1:500, Abcam) and mouse anti-Re (1:1000, Merck Millipore) for 72 hours at 4°C. Slices were incubated simultaneously with the three primary antibodies. After thorough washing in TBS-Tx (5x15 min), slices were incubated in all four secondary antibodies goat anti-mouse (1:400, AF405,

Thermo Fisher Scientific), goat anti-chicken (1:500, AF488, Thermo Fisher Scientific), fluorescent conjugated streptavidin (1:600, AF546, Thermo Fisher Scientific) and Goat anti-rabbit (1:400, AF633, Thermo Fisher Scientific) for 24 hours at 4°C. Slices were rinsed repeatedly in TBS-Tx (3x15 min) at room temperature and dehydrated by increasing ethanol concentrations (30%, 50%, 70%, 90%, 100%, 100%, 10 min each). They were treated to a 1:1 mixture of 100% ethanol and methyl salicylate for 10 minutes before clearing and storage in methyl salicylate.

Confocal microscopy and EC cell classification

Visualization of recorded cells using laser scanning confocal microscopy and subsequent classification of LEC layer II morphological cell types was described in detail previously (Nilssen et al., 2018). In brief, slices were mounted in methyl salicylate in custom made metal slides and imaged using a laser scanning confocal microscope (Zeiss LSM 880 AxioImager Z2). Single images and z stacks were acquired with low magnification (Plan-Apochromat 10x, NA 0.45 and Plan-Apochromat 20x, NA 0.8). These images were used to determine the morphology of the recorded cells, as well as confirm their position relative to the virally transfected fibers and within LEC molecularly defined (reelin versus calbindin) cell populations. All images were acquired with 8 bit depth. Classification of principal cell morphology was based on their somatodendritic morphology, in line with previously published criteria (Tahvildari and Alonso, 2005; Canto and Witter, 2012; Nilssen et al., 2018). Interneurons had small cell bodies, extensive local axonal ramifications and aspiny dendrites. Principal cells had large somata and dendrites covered with spines. These cells had a main axon that could be traced extending from the cell body toward the deep white matter. Fan cells had a round soma and multiple apical dendrites that ramified superficial to the cell body, creating a fan-like appearance. Few, if any, basal dendrites extending toward deeper layers were present. Pyramidal cells had an elongated, pyramid-shaped, cell body oriented perpendicular to the pia. Pyramidal cells had multiple dendrites extending from the base of the soma, and typically one long apical dendrite extending to the pial surface. Oblique pyramidal cells resembled pyramidal cells but were tilted approximately 45° with respect to the pia. These cells frequently had more than one main apical dendrite. Multiform cells were classified as all cells that did not fall into the other categories. Multiform cells usually had a multipolar morphology without polarization of the dendritic tree, exhibiting both well-developed basal and apical dendrites.

QUANTIFICATION AND STATISTICAL ANALYSIS

Characterization and quantification of POR cells projecting to dorsolateral LEC. Retrograde tracers Cholera toxin Subunit B (CTB; n = 3) or Fluorogold (FG; n = 2) were injected in the dorsolateral LEC of adult rats with regular burrholes (Figure S2B; Video S2; Table S2) in addition to retrograde FG injections (n = 4) deposited directly into superficial layers of dorsolateral LEC through laterally drilled burrholes (Figure S2C; Video S2; Table S2). Quantification of POR retrogradely labeled cells were made in a single serie for each animal using a laser scanning confocal microscope (Zeiss LSM 880 AxioImager Z2). Single images and z stacks were acquired with low magnification (Plan-Apochromat 10x, NA 0.45 and Plan-Apochromat 20x, NA 0.8) with 8 bit depth (Figure S2D). Images were transferred to a Neurolucida system (Neurolucida 360, MicroBrightField) in order to count the total number of retrogradely labeled cells that colocalized with NeuN and Cb at different Z-levels (Figure S2D). At last, we calculated the standard deviation (σ) of POR cells co-expressing Cb and NeuN in each animal groups (Figure S2E).

Quantification of POR axon terminals in MEC and LEC

Normalization of POR axonal terminal densities in MEC and LEC was obtained using the 3 available anterograde flatmaps (Figure S5B) from Burwell and Amaral (1998b). First, we reversed the five-level set of standards designated from none (0) to very light (1), light (2), moderate (3), heavy (4) and very heavy (5) into corresponding numerical values in each MEC and LEC bins. For single bins containing a neighboring region, their numerical value was divided by 2. The percentage of POR axonal terminal was then calculated by dividing the sum of each bin's numerical values by the total amount of bin by area. At last, we calculated the standard deviation (σ) of POR axonal terminals for each animal (Figure S5C).

Optogenetic stimulation of POR fibers

Acquired traces from each stimulation spot (5-15 sweeps) were averaged, producing an average response for each stimulation spot in the grid. Deflections in this overall average trace exceeding 10 standard deviations (±10 SD) of the baseline, defined as the average potential derived from the 50 ms interval prior to laser stimulation onset, were classified as true laser-evoked synaptic responses. The response amplitude of this voltage deflection was measured as the peak voltage minus the baseline potential. Potentials were identified as excitatory if they crossed the threshold to elicit action potential firing, or when depolarizing responses were observed at membrane potentials positive to the calculated chloride reversal potential (−69.2 mV, calculated using the Nernst equation). Inhibitory potentials were hyperpolarizing potentials and/or sensitive to application of bicuculline. Data analyses were conducted using customized scripts in MATLAB (MathWorks).

Extracellular stimulation of PER

Membrane potential deflections were considered stimulus-evoked according to the same criterion as for the optogenetic experiments. The individual voltage traces were used to measure the latency of the postsynaptic potentials, in order to compute the jitter

in the synaptic response. The synaptic jitter was defined as the standard deviation of the latency. Connections in which the synaptic jitter was < 700 μs were classified as presumed monosynaptic (Canto and Witter, 2012). In cases where synaptic latency could not be extracted from the individual traces, the connections were deemed unclassifiable with respect to being mono- or polysynaptic.

DATA AND CODE AVAILABILITY

Data and code to reproduce the analyses reported in the paper will be made available at request via the Witter Lab repository (https://www.ntnu.edu/kavli/research/witter).

Cell Reports, Volume *29*

Supplemental Information

Convergent Projections from Perirhinal and Postrhinal Cortices Suggest a Multisensory Nature of Lateral, but Not Medial, Entorhinal Cortex

Thanh P. Doan, Maria J. Lagartos-Donate, Eirik S. Nilssen, Shinya Ohara, and Menno P. Witter

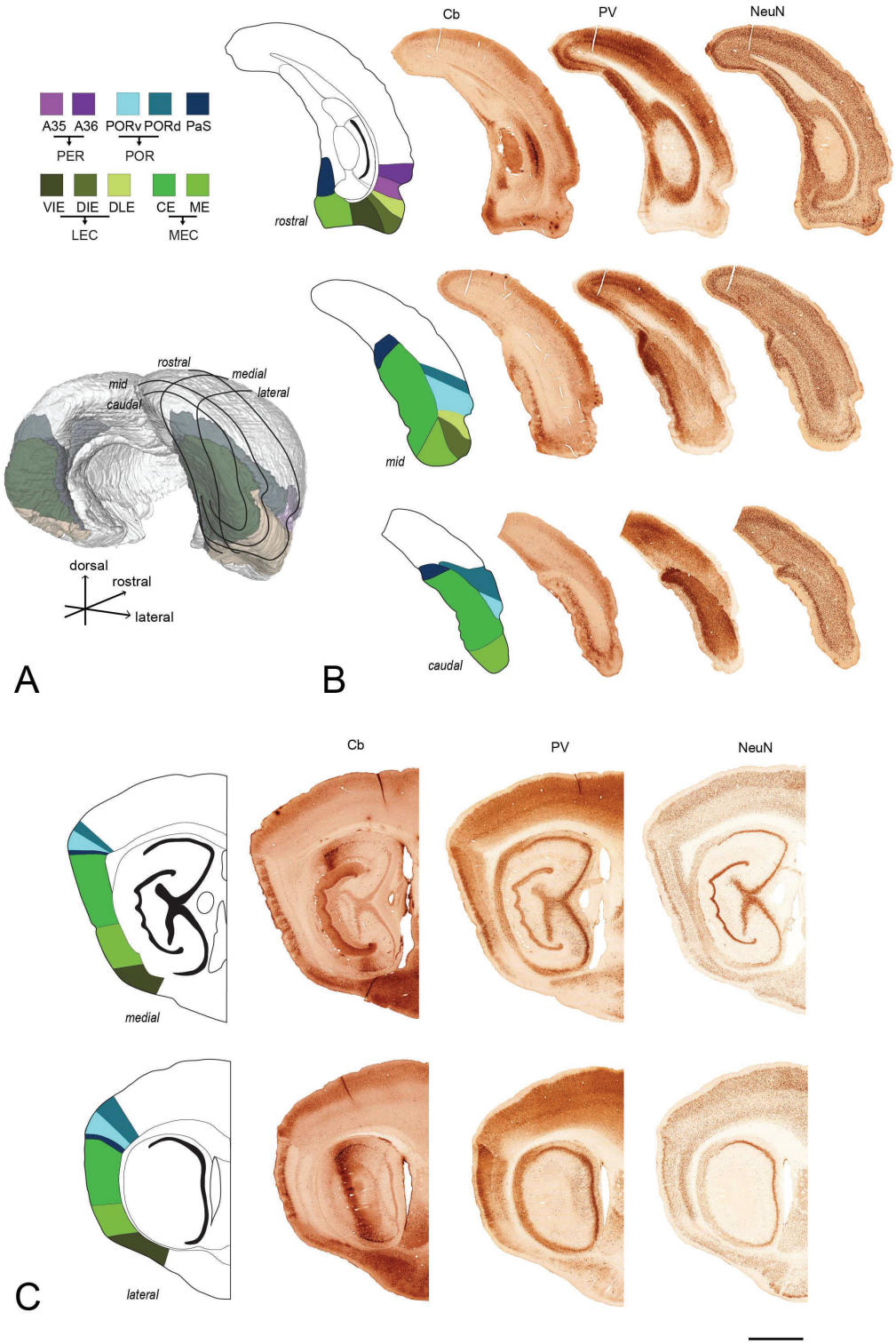

Supplementary figure 1. PHR borders and delineations (Relates to fig. 1)

A. WHS 3D model with black lines representing the different coronal and sagittal levels of sections in B and C respectively. B. Coronal sections from 3 different rostrocaudal levels as indicated in A (rostral, mid for mid-rostrocaudal and caudal). From left to right, delineated schematic, Calbindin (Cb), Parvalbumin (PV) and NeuN staining (Boccara, Kjonigsen et al. 2015). C. Sagittal sections from 2 different mediolateral levels as indicated in A (medial and lateral). From left to right, delineated schematic, Cb, PV and NeuN staining. Figure is a modification of figures 2-3 from Boccara, Kjonigsen et al. (2015) with permission. Scale bar 2mm.

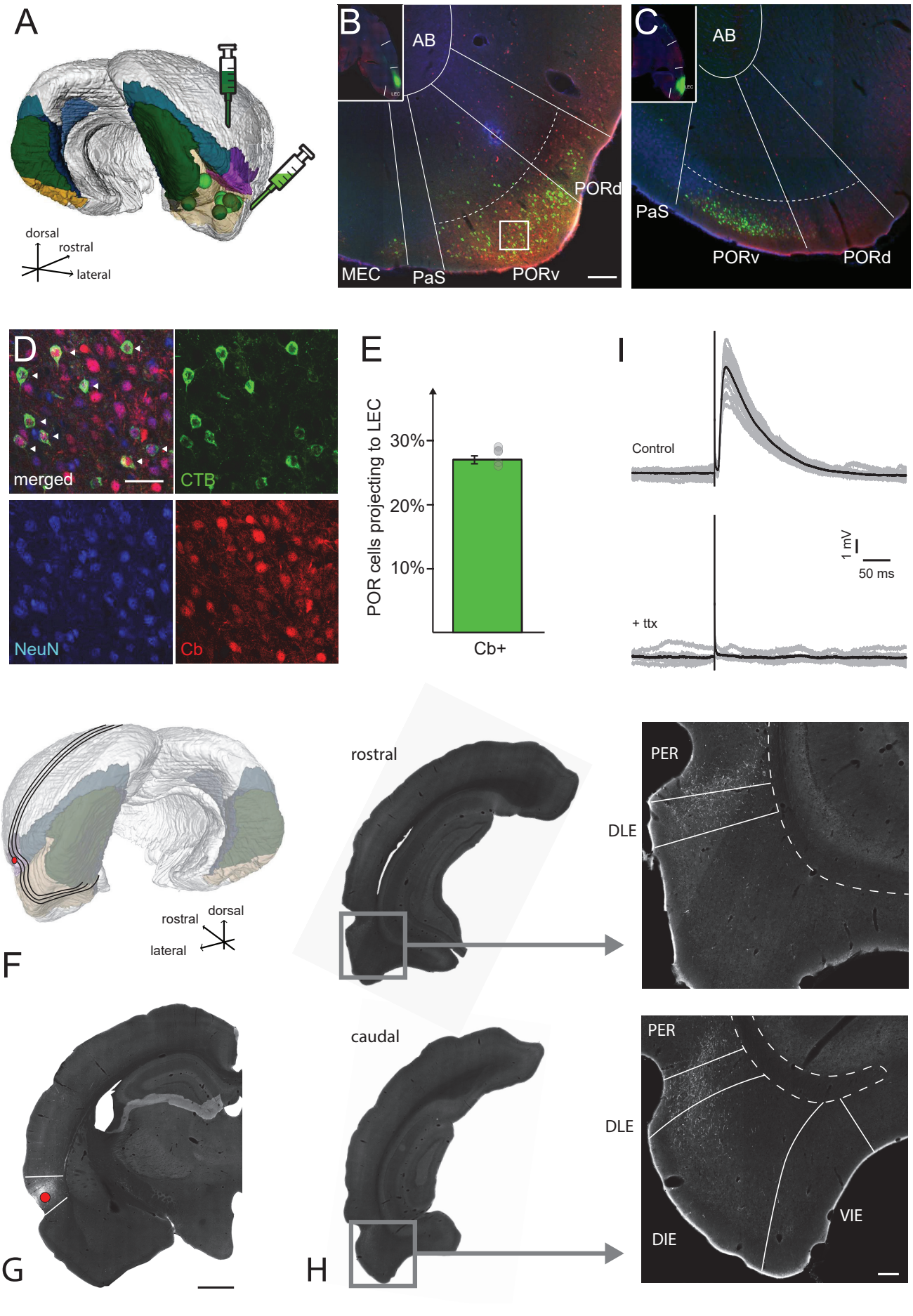
A
dorsal
rostral
lateral
B
AB
PORd
MEC
PaS
PORv
C
AB
PaS
PORv
PORd
D
merged
CTB
NeuN
Cb
E
POR cells projecting to LEC
30%
20%
10%
Cb+
I
Control
1 mV
50 ms
+ ttx
F
rostral
dorsal
lateral
rostral
PER
DLE
G
caudal
H
PER
DLE
VIE
DIE

Supplementary figure 2. POR and PER projections to LEC (Relates to fig. 1)

A. Characterization of POR cells projecting to dorsolateral LEC demonstrated by a WHS 3D model with all RG injections in LEC. Dark green injections were made through vertically oriented glass pipettes. Light green injections were deposited directly into superficial layers of dorsolateral LEC through laterally drilled burr-holes (see method section for details). B. Representative labelling of retrogradely labelled POR somata following injections in LEC through vertically oriented glass pipettes showing distribution in superficial layers of PORv and PORd. Dashed line represents border between POR LII/III from deep layers. Injection site visible in upper left panel. White square box inset represents magnification in C. Scale bar 200µm (applies also to D). C. Representative labelling of retrogradely labelled POR somata following injections deposited directly into superficial layers of dorsolateral LEC through laterally drilled burr-holes showing distribution exclusively in superficial layers of PORv. Dashed line represents border between POR LII/III from deep layers. Injection site visible in upper left panel. D. High power image of the square box visible in A, demonstrating that many POR somata projecting to LEC colocalize with NeuN and Cb. White arrowheads indicate triple colocalization between CTB, NeuN and Cb (checked at multiple Z-levels, see method section for details). Scale bar 50µm. E. Number of RG labelled superficial POR cells (from CTB and FG injections in dorsolateral LEC) that express Cb (27.2%, or n=828/3044 cells; σ=1.1, n=5). σ, standard deviation; grey dots represent percentages from single animals. F. PER projections to LEC demonstrated with a WHS 3D model with black lines representing the three different coronal levels of sections in G and H. The red dot represents the location of the injection visible in G. G. Representative case of an iontophoretic injection deposited in PER as indicated by the red dot. H. Two coronal sections demonstrating the typical terminal pattern of PER projections in LEC. Upper and lower left panels represent the complete section and upper and lower right panels represent the corresponding areas indicated with the grey squares in left panels. In the higher power images, dashed lines indicate the main laminar delineations in EC. Scale bare in B equals 1mm (applies to G and upper and lower left panels in H). Scale bar in lower right panel of H equals 200µm (applies to both upper and lower right panels). I. Postsynaptic traces in LEC II cell following extracellular PER stimulation reflect synaptic transmission. Recorded postsynaptic potentials following extracellular PER activation were in all tested cases (n=8 from 3 rats) abolished by bath application of 1 μM TTX (lower panel) and therefore not evoked by direct volume conduction.

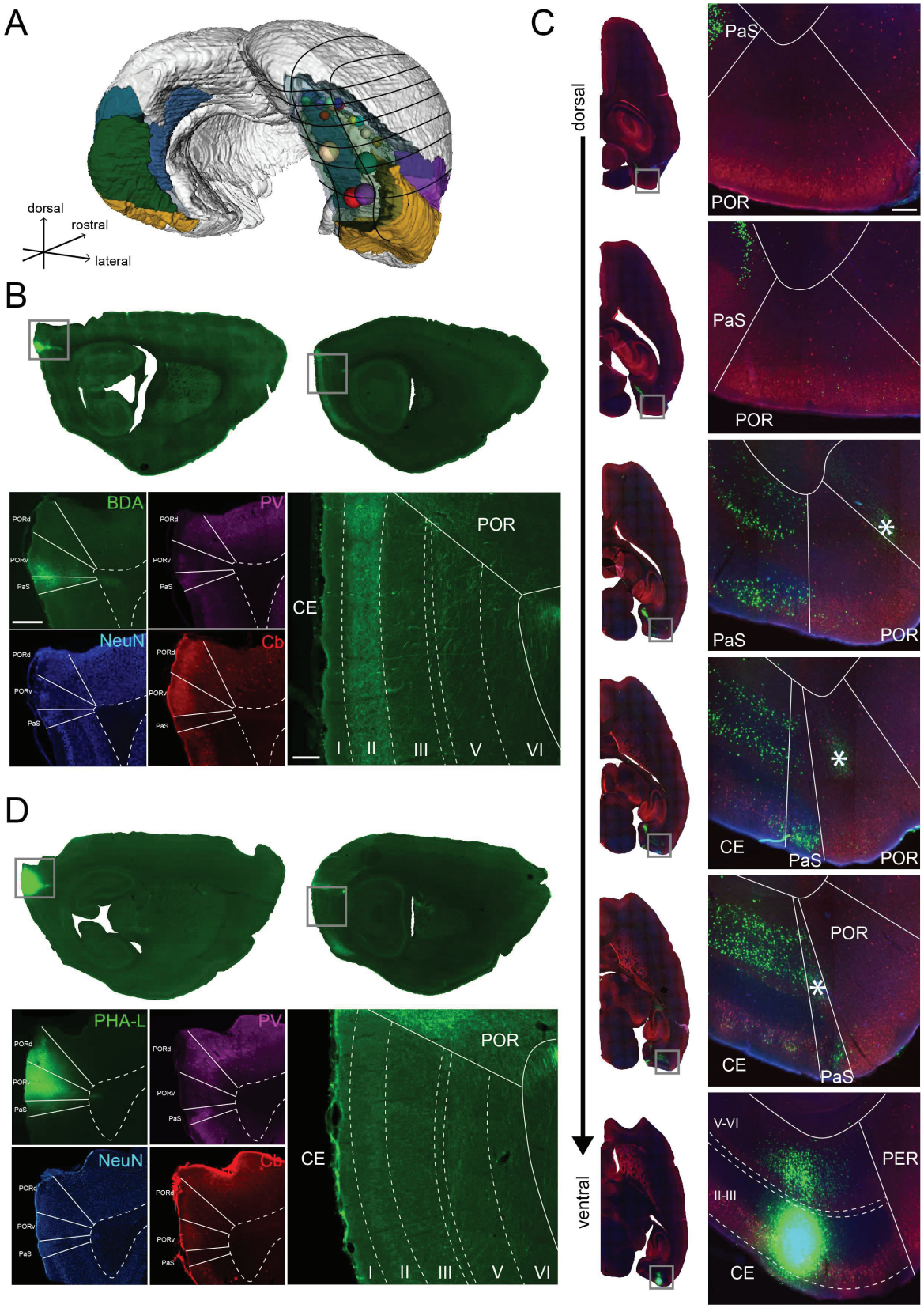
A
dorsal
rostral
lateral
B
BDA
PV
NeuN
Cb
PORd
PORv
PaS
POR
CE
I
II
III
V
VI
C
dorsal
ventral
PaS
POR
CE
V-VI
PER
II-III
D
PHA-L
PV
NeuN
Cb
POR
CE
I
II
III
V
VI

Supplementary figure 3. Superficial layers of MEC area CE are essentially devoid of POR inputs (Relates to fig. 3)

A. WHS 3D model representing all POR anterograde tracer injections that leaked in underlying PaS/CE and retrograde tracer injections in superficial layers of CE. The horizontal and vertical black lines represent the different dorsoventral levels in C and mediolateral levels in B-D respectively. B. Representative case of a POR anterograde tracer injection (BDA) that leaked in lateral PaS extension as delineated using triple NeuN, PV and Cb staining as in (Boccara et al., 2015). Upper left panel represents the mediolateral level of the injection with inset magnified for each staining in lower left panel. Scale bar 500µm. Upper right panel represents the mediolateral level with inset magnified in lower left panel to appreciate the fibers in superficial layers of CE. Scale bar 200 µm. C. Representative case of a retrograde tracer injection (FB) in green deposited in superficial layers of area CE demonstrating extensive retrogradely labelled somata in dorsal CE and PaS lateral extension but almost absent in adjacent POR. The asterisk represents the injection needle track. Scale bar 200 µm. D. Representative case of a pure POR anterograde tracer injection (PHA-L), delineated using triple NeuN, PV and Cb staining as in (Boccara et al., 2015). Upper left panel represents the mediolateral level of the injection with inset magnified for each staining in lower left panel. Upper right panel represents the mediolateral level with inset magnified in lower left panel to appreciate that modest amount of fibers are present only in deep layers of CE. Scale similar to that in B.

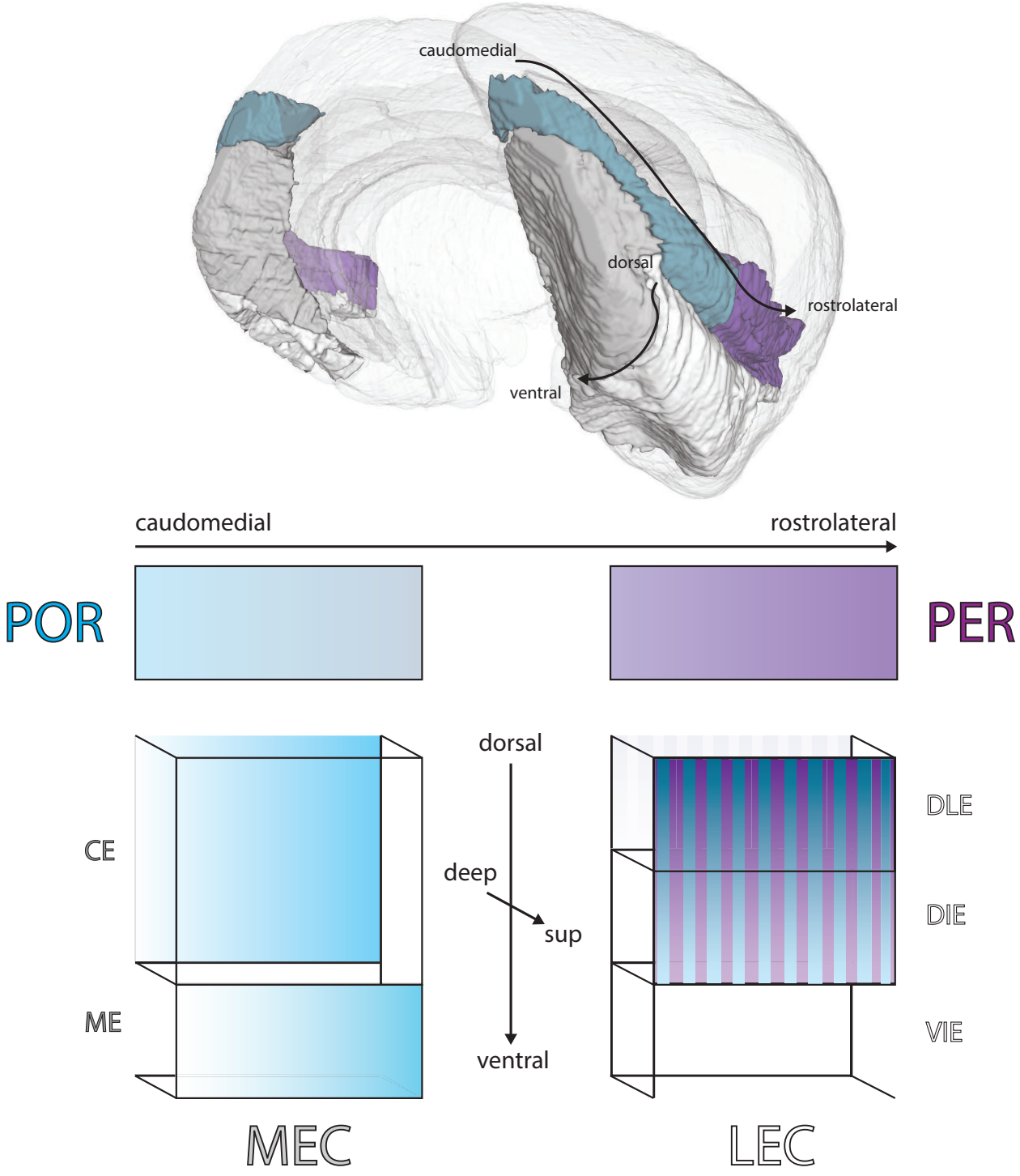

Supplementary figure 4. Summary diagram of POR and PER projections to EC (Relates to fig. 4).

Schematic representation of comparable POR (blue) and PER (purple) projection patterns to EC indicated by color gradients. A restricted caudomedial portion of POR projects to deep layers of area CE and superficial layers of area ME, whereas the entire POR projects to dorsolateral portions of LEC, mainly distributing in superficial layers of DIE and DLE (with a weak component in deep layers of DLE). Similarly, the entire PER also projects to the same two LEC areas in a comparable fashion. Purple/blue hatching in EC indicates the combination of complementary POR and PER inputs, whose densest axonal terminals overlap in superficial layers of DLE and DIE.

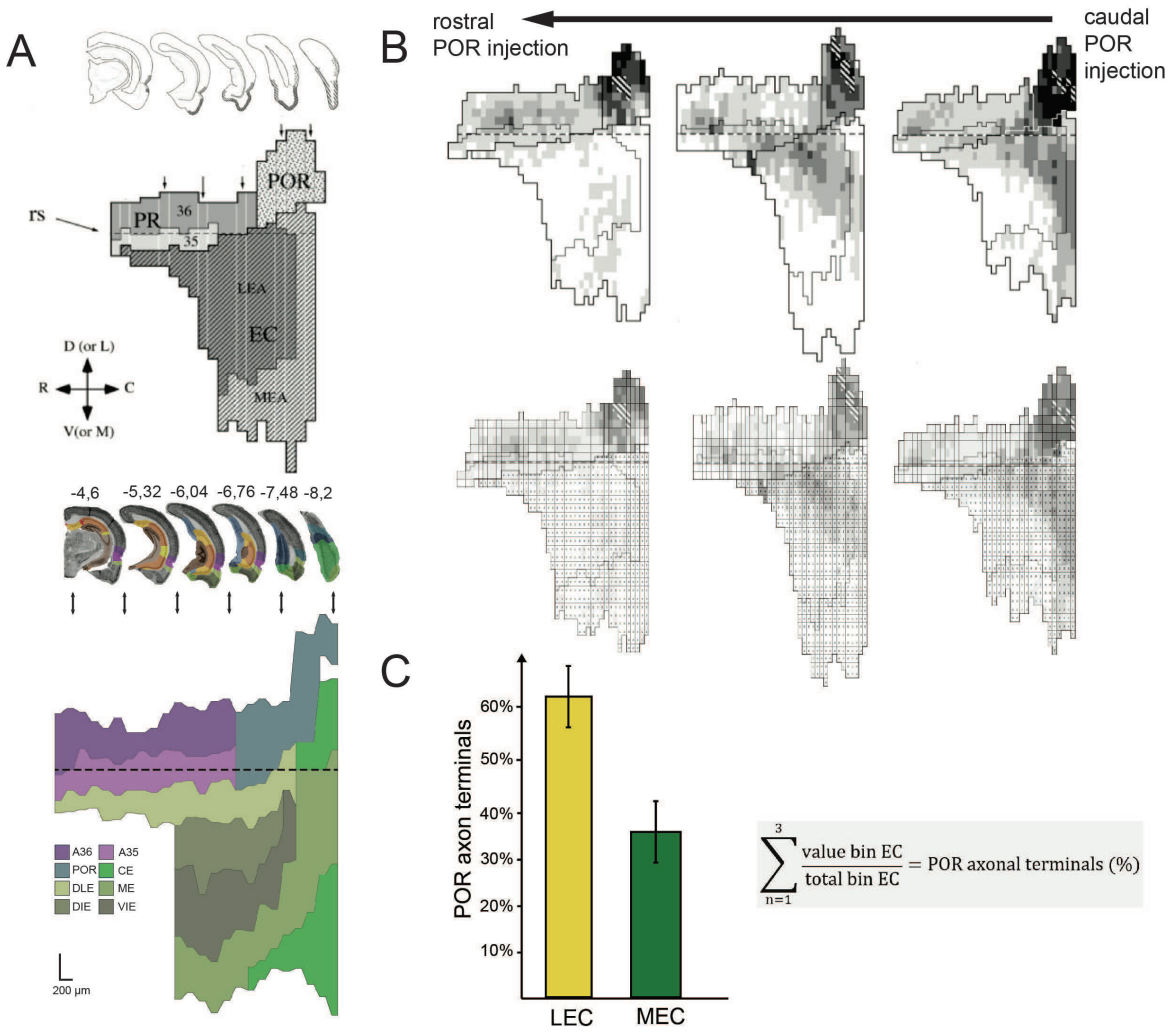

Supplementary figure 5. POR axon terminals in EC (modified with permission from Burwell and Amaral, 1998) (Relates to fig. 4 and Sup. Fig. 4)

A. PHR Flatmaps modified with permission (from Burwell and Amaral, 1998; upper panel) compared to flatmap constructed on similar coronal sections (lower panel) from dataset available at the Rat Hippocampus Atlas online (http://cmbn-navigator.uio.no/rat_hippocampus_atlas) which includes MEC and LEC subdivisions based on NeuN, Cb and PV stainings (Insausti et al., 1997, Boccara et al., 2015). The numbers above coronal sections in lower panel corresponds to distance from Bregma. B. 3 available POR flatmaps from (Burwell and Amaral, 1998b) with labelling in PHR. Upper panel shows the original figures indicating POR axons in each region from five-level set of standards designated from none (0) to very light (1), light (2), moderate (3), heavy (4) and very heavy (5) allowing a numerical representation of the same maps for MEC and LEC (lower panel). Note that POR injections organized caudorostrally follow projection pattern in EC as described in the present paper. C. Normalisation of POR axonal terminal densities, based on values in B lower panel, demonstrating a majority of fibers in LEC (64.5%, σ=13.1; n=3) and lower input density in MEC (35.5%, σ=13.1; n=3). The latter projection is mainly terminating in ventral MEC, presumably area ME (compare flatmaps B. upper panel with Rat Hippocampus Atlas constructed flatmap in A. lower panel).

animal	location site	WHS color	WHS coods (x, y ,z)	injection spread	cutting plane	thickness (μm)	series	species	sex
24142 F	caudomedial CE I-IV		418, 148, 318	-	horizontal	30	6	LE	F
24446 C	rostral DLE/DIE I-IV		492, 85, 227	-	horizontal	40	6	LE	M
24447 F	ventrolateral CE I-IV		415, 115, 281	-	horizontal	40	6	LE	F
24461 C	rostral DLE/DIE I-VI		488, 93, 239	negligible A35 V-VI	horizontal	40	6	LE	M
24617 C	mid rostrocaudal DIE I-V		458, 90, 235	negligible A35 V-VI	horizontal	50	6	LE	F
24617 F	ventrolateral CE I-IV		420, 127, 276	-	horizontal	50	6	LE	F
24630 F	lateral CE I-V		411, 112, 310	-	horizontal	50	6	LE	M
24000 F	rostral DLE I-III		505, 81, 231	-	coronal	40	4	W	M
24001 F	caudal DLE/DIE I-VI		441, 91, 267	-	coronal	40	4	W	M
24002 F	rostral DLE I-V		496, 79, 230	from lateral side	coronal	40	4	W	M
24003 F	mid rostrocaudal DLE/DIE I-III		466, 83, 225	from lateral side	horizontal	40	4	W	M
24004 F	caudal DLE/VIE I-III		441, 113, 238	from lateral side	horizontal	40	4	W	M
24005 F	mid rostrocaudal DLE/DIE I-III		482, 77, 239	from lateral side	coronal	40	4	W	M

Supplementary table 2. Retrograde tracer injections across LEC and MEC (Relates to figs. 1 and 3)

Letters following single animal numbers used for the present study indicate the retrograde tracer injected in each case ie. F stands for FB or FG, C for CTB 555. Long Evans (LE), Sprague Dawley (SD), Wistar (W). Male (M) and Female (F).

Convergence of cortical inputs in layer II of the lateral entorhinal cortex

Eirik S. Nilssen[1], Thanh P. Doan[1], Menno P. Witter[1]*

[1]Kavli Institute for Systems Neuroscience and Centre for Neural Computation, NTNU Norwegian University of Science and Technology, Trondheim, Norway.

*Corresponding author: Menno P. Witter, Kavli Institute for Systems Neuroscience and Centre for Neural Computation, The Faculty of Medicine and Health Sciences, NTNU,
Po. box 8905, 7491 Trondheim, menno.witter@ntnu.no

frontiers in Systems Neuroscience

ORIGINAL RESEARCH
published: 15 October 2019
doi: 10.3389/fnsys.2019.00054

Entorhinal Layer II Calbindin-Expressing Neurons Originate Widespread Telencephalic and Intrinsic Projections

*Shinya Ohara[1,2], Michele Gianatti[1†], Kazuki Itou[2], Christin H. Berndtsson[1], Thanh P. Doan[1], Takuma Kitanishi[3], Kenji Mizuseki[3], Toshio Iijima[2], Ken-Ichiro Tsutsui[2] and Menno P. Witter[1]**

[1] Kavli Institute for Systems Neuroscience, Center for Computational Neuroscience, Egil and Pauline Braathen and Fred Kavli Centre for Cortical Microcircuits, Norwegian University of Science and Technology (NTNU), Trondheim, Norway, [2] Laboratory of Systems Neuroscience, Graduate School of Life Sciences, Tohoku University, Sendai, Japan, [3] Department of Physiology, Graduate School of Medicine, Osaka City University, Osaka, Japan

OPEN ACCESS

Edited by:
Michael E. Hasselmo,
Boston University, United States

Reviewed by:
Prateep Beed,
Charité – Berlin University of Medicine, Germany
Andrea Burgalossi,
University of Tübingen, Germany
Patricia Preston-Ferrer, University of Tübingen, in collaboration with reviewer AB

***Correspondence:**
Menno P. Witter
menno.witter@ntnu.no

†Present address:
Michele Gianatti,
Faculty of Medicine, University of Oslo, Oslo, Norway

Received: 23 May 2019
Accepted: 30 September 2019
Published: 15 October 2019

Citation:
Ohara S, Gianatti M, Itou K, Berndtsson CH, Doan TP, Kitanishi T, Mizuseki K, Iijima T, Tsutsui K-I and Witter MP (2019) Entorhinal Layer II Calbindin-Expressing Neurons Originate Widespread Telencephalic and Intrinsic Projections. Front. Syst. Neurosci. 13:54. doi: 10.3389/fnsys.2019.00054

In the present study we provide the first systematic and quantitative hodological study of the calbindin-expressing (CB+) principal neurons in layer II of the entorhinal cortex and compared the respective projections of the lateral and medial subdivisions of the entorhinal cortex. Using elaborate quantitative retrograde tracing, complemented by anterograde tracing, we report that the layer II CB+ population comprises neurons with diverse, mainly excitatory projections. At least half of them originate local intrinsic and commissural projections which distribute mainly to layer I and II. We further show that long-range CB+ projections from the two entorhinal subdivisions differ substantially in that MEC projections mainly target field CA1 of the hippocampus, whereas LEC CB+ projections distribute much more widely to a substantial number of known forebrain targets. This connectional difference between the CB+ populations in LEC and MEC is reminiscent of the overall projection pattern of the two entorhinal subdivisions.

Keywords: medial entorhinal cortex, lateral entorhinal cortex, parahippocampus, connectivity, rodent, commissural projections, long-range intrinsic projections

INTRODUCTION

The entorhinal cortex (EC) is conceived as the nodal point in the cortico-hippocampal network that is critically involved in memory and spatial navigation (Schenk and Morris, 1985; Brun et al., 2002, 2008; Eichenbaum et al., 2007; Ji and Maren, 2008; Reagh and Yassa, 2014; Rodo et al., 2016). Anatomically, EC can be divided into two functionally distinct subdivisions, lateral and medial EC (LEC and MEC, respectively). A substantial proportion of neurons in MEC are spatially modulated, reflecting self-location relative to the geometry of the environment. In contrast, in LEC such spatial modulation is essentially absent, with activity correlating to odors or objects in context (Fyhn et al., 2004; Deshmukh and Knierim, 2011; Neunuebel et al., 2013; Tsao et al., 2013; Moser et al., 2014) or reflecting the temporal progression of the experimental event (Tsao et al., 2018; Montchal et al., 2019).

We previously showed that differences in morphological and physiological properties exist between MEC and LEC in layer II neurons, whereas differences in other layers are not evident (Canto and Witter, 2012a,b; Cappaert et al., 2015). Principal cells in EC layer II come in two chemical types, calbindin- and reelin-expressing cells (CB+ and RE+, respectively), and interestingly, these two neuron-types distribute differently in the two subdivisions. In the rodent MEC, the two types appear to be grouped in patches, while in LEC they form two separate sublayers, RE+ cells superficially (IIa) and CB+ cells deeper (IIb) (Tuñón et al., 1992; Fujimaru and Kosaka, 1996; Wouterlood, 2002; Ramos-Moreno et al., 2006; Kitamura et al., 2014; Ray et al., 2014; Leitner et al., 2016). Taken together, these data indicate that layer II principal neurons may contribute to the phenotypical differences between MEC and LEC. However, studies on the local networks of RE+ neurons show a striking similarity between LEC and MEC (Pastoll et al., 2012; Couey et al., 2013; Fuchs et al., 2016; Leitner et al., 2016; Nilssen et al., 2018), and in both subdivisions RE+ cells are the exclusive origin of the projections to dentate gyrus, and hippocampal fields CA2 and CA3 (Varga et al., 2010; Ray et al., 2014; Witter et al., 2017). Therefore, a difference in the connectional organization of CB+ layer II neurons might be relevant to explore.

Recent studies have proposed that MEC CB+ pyramidal cells play an important role in generating grid cell activity, which was related to their anatomical clustering, rhythmicity, cholinergic modulation (Ray et al., 2014), and spatial discharge properties (Tang et al., 2014). On the other hand, LEC CB+ pyramidal cells are proposed to have a functional role in top-down modulation of olfactory processing (Leitner et al., 2016).

The projections of CB+ neurons in MEC and LEC have only been described in incidental reports. In case of MEC CB+ neurons, projections to the hippocampus (Wouterlood, 2002), more specifically to stratum lacunosum of CA1 (Kitamura et al., 2014), to contralateral MEC (Varga et al., 2010), ipsilateral MEC (Zutshi et al., 2018), and the medial septum (MS) (Fuchs et al., 2016) have been described. For LEC CB+ neurons, projections to CA1 (Kitamura et al., 2014), to contralateral LEC, the olfactory bulb, and piriform cortex (Leitner et al., 2016) have been reported. Although these previous studies described the targets of the CB+ neurons, the proportion of the CB+ neurons contributing to each of these projections was not provided. Hence, it is unclear whether all CB+ neurons or only part of them project to the target regions. Furthermore, a systematic and quantitative comparison of the efferent connectivity of CB+ populations in LEC and MEC is lacking. In the present study, we used combinations of quantitative retrograde tracing and immunohistochemical approaches, supplemented with anterograde tracing, to assess projections of CB+ neurons in layer II of both MEC and LEC in rats. Our analysis included all known major EC projections and showed that the CB+ population in layer II is composed of diverse neurons having distinct projections. Most importantly, layer II CB+ neurons in both entorhinal subdivisions are a main source of an elaborate local excitatory projection within EC. We further demonstrated LEC CB+ neurons mediate widespread forebrain projections, whereas the projections of MEC CB+ neurons distribute axons almost exclusively within the hippocampus and the EC.

MATERIALS AND METHODS

Surgical Procedures and Tracer/Virus Injections

Either adult male Wistar rats weighing 200–230 g, adult female Sprague Dawley rats weighing 230–285 g, or adult female Long Evans rats 210–280 g were used in this study. All experiments using Wistar rats were performed at Tohoku University. The experiments were approved by the Center for Laboratory Animal Research, Tohoku University, and were conducted according to the Guidelines of the National Institutes of Health and the Tohoku University Guidelines for Animal Care and Use. All experiments using Sprague Dawley rats, Long Evans rats, and GAD67 transgenic mice expressing GFP (Tanaka et al., 2003) were performed at the Kavli Institute for Systems Neuroscience/Centre for Neural Computation at the Norwegian University of Science and Technology (NTNU), where animals were housed and handled according to the Norwegian laws and regulations concerning animal welfare and animal research. Experimental protocols were approved by the Norwegian Animal Research Authority and were in accordance with the European Convention for the Protection of Vertebrate Animals used for Experimental and Other Scientific Purposes.

Under deep anesthesia either with isoflurane or with ketamine (80.0 mg/kg, i.p.) and xylazine (0.8 mg/kg, i.p.), rats were mounted in a stereotaxic frame. The skull was exposed, and a small burr hole was drilled above the injection site. Retrograde tracers were injected into the target areas by pressure injection using a glass micropipette (tip diameter = 20–40 μm) either connected to a 1 μl Hamilton microsyringe or to an automated microinjection pump (WPI Nanoliter, 2010). Three fluorescent retrograde tracers were used in rats in the following parameter: 50–200 nl of fluorogold (FG; 2.5% in H_2O, Fluorochrome), 100–500 nl of Alexa Fluor 555 conjugated Cholera Toxin Subunit B (CTB-555; 1 mg/ml in phosphate-buffered saline (PBS), Thermo Fisher), 100 nl of Fast Blue (FB; 1% in PBS, EMS-Grivory). The coordinates of the injection sites and detailed information of each sample are shown in **Supplementary Table 1**. Some samples were also used in our previous study (Ohara et al., 2018). For retrograde tracing experiments in mice, red retrobeads (Lumafluor) and Fast Blue were used. After the injection, at 25 nl per minute, the pipette was left in place for another 15 minutes before it was withdrawn. The wound was sutured, and the animal was monitored for recovery from anesthesia before being returned to its home cage. The survival periods were 5–7 days for these retrograde tracing experiments.

For dual anterograde tracing experiments, 2.5% *Phaseolus vulgaris*-leucoagglutinin (PHA-L; Vector Laboratories) and 3.5% 10 kDa biotinylated dextran amine (BDA, Invitrogen, Molecular Probes) were injected iontophoretically with positive 5 μA current pulses (6 s on; 6 s off) for 15 min in the following coordinates (anterior to either bregma (APb) or transverse

sinus (APt), lateral to sagittal sinus (ML), ventral to dura (DV) in mm): MEC (layer II; APt + 0.5; ML 4.9, DV 2.9, angle 11 degrees in the sagittal plane with the glass micropipette pointing to rostral); MEC (layer III; APt + 1.0, ML 4.9, DV 2.9, angle 11 degrees in the sagittal plane with the glass micropipette pointing to rostral); LEC (layer II; APb -6.0, ML 6.8, DV 4.7); LEC (layer III; APb -8.3, ML 6.0, DV 4.0). The survival period for this anterograde tracing was 7 days.

For AAV double infection approach, 500 nl of retrograde-infecting AAV expressing Cre recombinase (AAV6-Cre; Aronoff et al., 2010) was injected into the border of LEC and MEC (APb -8.3, ML 6.0, DV 3.8) while 500 nl of Cre-dependent reporter AAV that expresses EYFP after recombination (AAV1/2-EF1α-DIO-EYFP) was injected into the rostral LEC (APb 6.0, ML 6.8, DV 4.7). The survival period was 3 weeks.

Immunohistochemistry and Analysis

Following an appropriate survival period for each experiment, the animals were deeply anaesthetized with sodium pentobarbital (100 mg/kg, i.p.) and perfused transcardially either with 10% sucrose in 0.1 M phosphate-buffer (PB) or with Ringer's solution (0.85% NaCl, 0.025% KCl, 0.02% NaHCO3) followed by 4% paraformaldehyde in 0.1M PB. The brains were removed from the skulls, postfixed in 4% paraformaldehyde in 0.1 M PB for 4 h at 4°C, and then cryoprotected either in PB containing 30% sucrose or in a mixture of 20% glycerol and 2% dimethyl sulfoxide (DMSO) for at least 48 h at 4°C. The brains were cut into 40–60 μm sections in either the coronal or horizontal plane on a freezing microtome.

For immunofluorescence staining, floating sections were washed in PBS, permeabilized with PBS containing 5% normal goat serum and 0.1% Triton-X 100 for an hour at room temperature, and then incubated overnight at 4°C with a rabbit anti-calbindin antibody (1:1000; Abcam), a rabbit anti-calbindin antibody (1:5000; Swant), or a mouse anti-reelin antibody (1:1000; Millipore) diluted in PBS containing 5% normal goat serum and 0.1% Triton-X 100. They were then washed PBS containing 0.1% Triton X-100 (PBT) and incubated for 2–6 h at room temperature in Cy5-conjugated goat anti-rabbit IgG (1:400; Jackson ImmunoResearch), Alexa 546-conjugated goat anti-rabbit IgG (1:800; Invitrogen Ltd.), or Alexa488-conjugated goat anti-mouse IgG (1:800; Invitrogen Ltd.) diluted in PBT. The sections were counterstained with either Hoechst 33258 (1:1000; Dojindo) or NeuroTrace 500/525 Green Fluorescent Nissl Stain (1:300; Invitrogen Ltd.), mounted on gelatin-coated slides, and coverslipped using Entellan new (Millipore). The brain sections were examined under a Zeiss Axiovert 200M microscope, and images were captured using an AxioCam MRm digital camera and Axiovision image processing software (Carl Zeiss). Degital images were also obtained using an automated scanner (Zeiss Axio Scan Z1). In order to precisely identify the location of the injection site in horizontally sectioned samples, we used the Waxholm space three-plane architectonic atlas of the rat hippocampal region (Papp et al., 2014; Boccara et al., 2015; Kjonigsen et al., 2015), and identified the corresponding location of the injection site in the coronal plane.

To quantify the colocalization of calbindin immunolabeling and retrograde labeling, confocal images of retrogradely labeled and immunohistochemically stained entorhinal neurons were acquired in sections taken at every 240 μm throughout EC, using a confocal microscope (LSM 5 Exciter and LSM 880, Carl Zeiss) with a 40× oil objective (Plan Apochromat 40× NA1.3 Oil, Carl Zeiss, **Supplementary Figure 1**). Since the signal of Calbindin immunolabeling decreases in the center of the sections in samples cut at a thickness of 60 μm, the confocal images were taken at the upper surface and lower surface of each section. We set the region of interest (ROI) as the area where there were a certain number of retrogradely labeled neurons in EC layer II, and quantified the number of retrogradely labeled neurons and immunohistochemically stained neurons in this ROI using ImageJ software[1]. Similar to previous studies (Varga et al., 2010; Kitamura et al., 2014; Fuchs et al., 2016; Leitner et al., 2016), the projection of CB+ neurons were analyzed by quantifying the percentage of double-labeled neurons among the retrogradely labeled neurons in layer II of MEC and LEC. This provided information of whether the projection to the targeted regions specifically originated from CB+ neurons. In addition, we examined the percentage of double-labeled neurons with respect to the total CB+ neuron population to examine the proportion of CB+ neurons that contributed to the targeted projections.

The data are shown as mean ± standard erros. Prism software was used for data analysis (Graphpad software), and the Wilcoxon signed rank test was used for the analysis of the hippocampal injection experiments. Friedman test followed with Dunn's multiple comparisons post-test was used to compare groups in case of the entorhinal injection experiments.

RESULTS

Distribution of Calbindin Neurons in LEC and MEC

We first examined the distribution of CB+ neurons together with the RE+ neurons in layer II of the EC in both rats and mice. In line with previous studies, the overall distribution of CB+ and RE+ neurons differed between MEC and LEC in both species: the two types appear to be grouped in patches in MEC, while they are more or less confined to two sublayers, RE+ cells superficially (IIa) and CB+ cells deeper (IIb) in LEC (**Figure 1A** and **Supplementary Figure 2**, Tuñón et al., 1992; Fujimaru and Kosaka, 1996; Wouterlood, 2002; Ramos-Moreno et al., 2006; Varga et al., 2010; Kitamura et al., 2014; Ray et al., 2014; Leitner et al., 2016; Witter et al., 2017).

In the rat MEC, RE+ neurons were intermingled with CB+ neurons in layer II (**Figure 1A** and **Supplementary Figures 2A,B**). The reported clustering of CB+ neurons (Ray et al., 2014) was particularly striking in the dorsal MEC but not in the ventral MEC. In LEC, RE+ neurons were located almost exclusively in layer IIa, whereas CB+ neurons tended to occupy almost exclusively layer IIb. We further noticed that in LEC, RE+ neurons were often organized in patches that were separated by

[1]http://rsb.info.nih.gov/ij

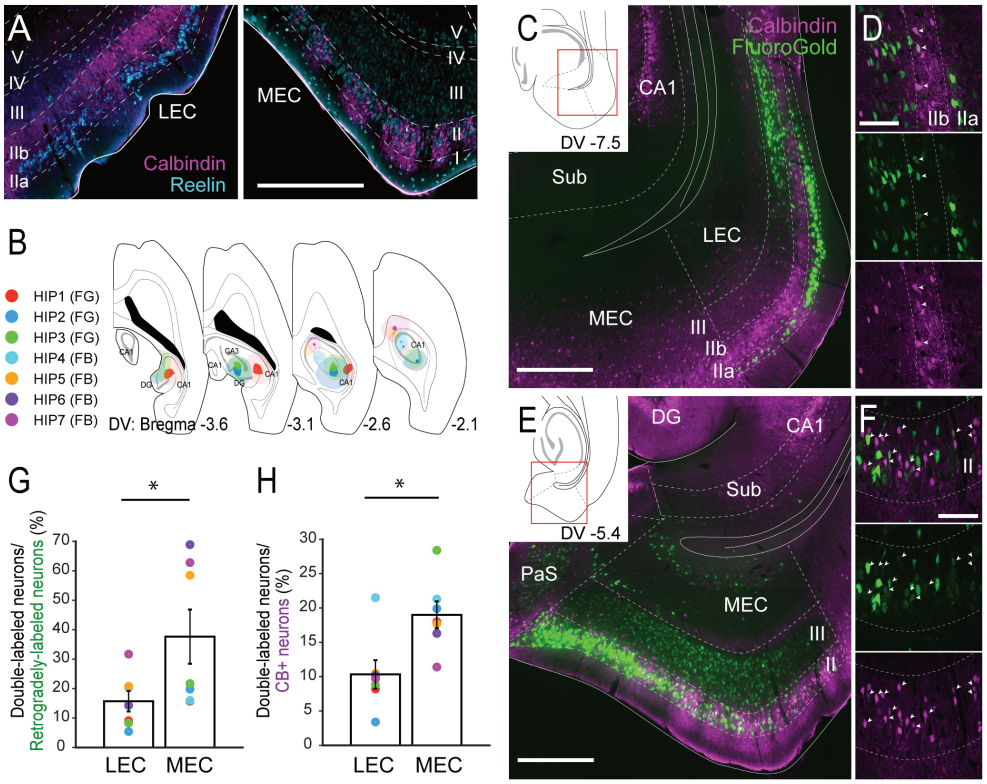

FIGURE 1 | Projections of CB+ neurons in LEC and MEC to the hippocampus. **(A)** Distribution of neurons immunoreactive for RE (cyan) and CB (magenta) in rat LEC and MEC. **(B)** The injection sites of retrograde tracers, either FG or FB, in samples with hippocampal injection. Each injection is illustrated with a different color. For all cases, the dark color shows the injection site whereas the light color shows the area of diffusion. **(C–F)** Distribution of retrogradely labeled neurons (green) in LEC at a dorsoventral (DV) level of –7.5 mm **(C)**, and in MEC at a DV level of –5.4 mm **(E)** in horizontal sections (case: HIP2). High magnification images of the superficial layers in LEC and MEC are shown in panels **(D,F)** respectively. White arrows indicate neurons that were double-labeled with FG and CB immunoreactivity. **(G,H)** The percentage of double-labeled neurons among retrogradely-labeled neurons **(G)**, and the percentage of double-labeled neurons among the CB+ neurons **(H)** are compared between LEC and MEC (mean ± standard errors, $N = 7$; $^*p < 0.05$; Wilcoxon signed rank test). Each colored dot corresponds to the value for the sample shown in panel **B**. Scale bars are 500 μm for panels **A,C,E**, and 100 μm for panels **D,F**. Sub, subiculum; DG, dentate gyrus; PaS, parasubiculum.

bundles of apical dendrites arising from CB+ neurons (**Figure 1A** and **Supplementary Figures 2C,D**).

The distribution of RE+ and CB+ neurons was different in layer II of the mouse dorsal MEC compared to that of the rat (**Supplementary Figures 2A',B'**). In this layer, RE+ neurons were located in the middle and deep portions. Moreover, they were located deeper in layer II compared to CB+ neurons, which were in turn distributed in clusters in the most superficial part of this layer. At more ventral levels of MEC and in LEC this species difference was absent (**Supplementary Figures 2C',D'**, Naumann et al., 2016).

Hippocampal Projections

We first set out to analyze the projections to the hippocampus in order to confirm the previously reported projection of layer II CB+ neurons to stratum lacunosum of CA1 (Kitamura et al., 2014). We focused on the dorsal hippocampus and injected retrograde tracers in the different subfields in various combinations ($n = 7$; **Figure 1B**, **Supplementary Figure 3**). Confirming previous results, injections that include the dentate gyrus and CA1, consistently labeled many neurons in layer II and III of both LEC and MEC (**Figures 1C,E**), whereas injections confined to the dentate gyrus and/or CA3 result in labeling largely restricted to layer II cells ($n = 3$; data not shown). In line with previous studies, some labeled neurons were also observed in the deep layers (Cappaert et al., 2015). In LEC, the majority of the retrogradely labeled neurons were observed in layer IIa and III, with only a few in layer IIb in all cases (**Figures 1C,D**). In MEC, retrograde neuronal labeling was apparent throughout the depth of layers II and III. The percentage of retrogradely labeled neurons that showed CB+ co-labeling varied considerably (between 5.4 and 68.9%; **Figure 1G**).

This large variation results from the difference of injection sites in the hippocampus. Samples which received an injection mainly in CA1 (HIP5–7) show higher percentages since retrogradely labeled neurons are preferentially located in layer III, whereas samples with an injection involving both CA1 and dentate gyrus show low percentage due to the strongly increased retrograde labeling of RE+ cells (HIP1–4). Irrespective of this substantial variation, the percentages of retrogradely labeled cells that co-labeled for CB+ were consistently lower in LEC than in MEC, 15.7 versus 37.6%, ($p < 0.05$, Wilcoxon signed rank test). In contrast, the percentage of CB+ neurons that were retrogradely labeled varied less (between 3.4 and 28.4%; **Figure 1H**). Yet again, the percentages in case of LEC were consistently lower than in MEC, 10.3% versus 19.0% ($p < 0.005$, Wilcoxon signed rank test). The observed consistent differences between LEC and MEC were not due to the injection position along the proximodistal axis of CA1 (Witter et al., 2000), since similar trends were observed in samples which received injections either in the proximal (HIP1) or distal CA1 (HIP2, **Supplementary Figure 3**). We conclude that EC projections to the hippocampus originate predominantly from neurons in layers II and III, in line with previous reports (Steward and Scoville, 1976; Witter et al., 1989a,b), with a moderate contribution of CB+ neurons in MEC, and a small contribution of CB+ neurons in LEC. These findings are thus in line with specific viral anterograde tracing data in transgenic mice that CB+ neurons in MEC and LEC project specifically to stratum lacunosum of CA1 (**Supplementary Figure 4**; Kitamura et al., 2014).

Entorhinal Projections

To confirm the claim that CB+ neurons in MEC and LEC are a specific source of crossed projections to the contralateral EC projections (Varga et al., 2010), we analyzed the distribution of labeled neurons following injections either in the MEC ($n = 3$; **Figures 2A–G**) or LEC ($n = 3$; **Figures 2H–N**). For MEC, we injected a small volume of retrograde tracer (FB) into layer I and II (**Figure 2A**), since MEC CB+ neurons are known to project their axons to layer I and II of the contralateral MEC (Fuchs et al., 2016). In all three samples, many labeled neurons were observed in layer II of the contralateral MEC, and a high percentage of the contralateral labeled cells were CB+ positive (**Figures 2B,C,F**). Note that in addition to the labeled CB+ neurons in layer II, a substantial number of commissurally projecting neurons are found in layer III, especially in dorsal sections close to the level of the injection site (Steward and Scoville, 1976; Wouterlood, 2002; Ray et al., 2014) (data not shown). In contrast to these samples, retrograde labeling of contralateral CB+ neurons was hardly observed when the injection was placed in the deep MEC (data not shown). In addition to retrograde neuronal labeling in the contralateral EC, we observed a high percentage of double-labeling in the ipsilateral MEC (**Figures 2D,E**). The percentage of double-labeled neurons among the CB+ neurons was substantially lower than that of double-labeled/retrogradely-labeled neurons, and it was higher in the ipsilateral than in the contralateral MEC (**Figure 2G**; 56.2 versus 31.0%). In two out of three samples, retrogradely labeled neurons were also observed in the superficial layers of the ipsilateral LEC but the percentage of double-labeled neurons was lower than that seen in ipsi- and contralateral MEC.

In case of LEC, we injected the retrograde tracer (FG) into the superficial layers of LEC (**Figure 2H**). In two out of three samples, many labeled neurons were observed in the contralateral EC, and a high percentage of the contralateral layer II cells were CB+ (**Figures 2I,J,M**). A high percentage of retrogradely labeled neurons were also double-labeled in ipsilateral LEC and MEC (**Figures 2K,L,M**). Similar to the case of MEC injection, the percentage of double-labeled neurons among the CB+ neurons was higher in the ipsilateral than in the contralateral LEC (**Figure 2N**; 81.1 versus 26.5%). The labeling originating from the ipsilateral interconnections between the LEC and MEC, however, was different between the MEC- and LEC-injection cases. For the projections of MEC CB+ neurons to LEC we noted a higher percentage of double-labeled neurons than the other way around (**Figures 2F,G, M,N**; 70.4 versus 28.2% for double-labeled/retrogradely-labeled neurons, 50.1 versus 13.8% for double-labeled/CB+ neurons). Note that all three injections aimed to target LEC leaked into the perirhinal cortex (PER), implying that labeled neurons in the contralateral LEC and ipsilateral EC could be due to this unintended leakage. However, retrograde injections confined to PER did not results in labeled neurons in contralateral LEC and ipsilateral MEC (**Figures 3M–O**, **Supplementary Figure 6L**), so we find it likely that the labeling in these areas is due to injecting in LEC. In contrast, the ipsilateral LEC retrograde labeling might be confounded by neurons that are retrogradely labeled due to PER involvement (see also below other telencephalic projections).

We also analyzed the distribution of labeled neurons following injections in the border region between LEC and MEC ($n = 8$; **Supplementary Figure 5A**). Relatively high percentages of the retrogradely labeled neurons were CB+ in ipsi- and contralateral of LEC and MEC, although the percentage was significantly higher in ipsilateral MEC than in LEC (**Supplementary Figures 5B–F**; 47.5 versus 31.3%; Friedman test $p = 0.0148$; Dunn's multiple comparisons post-test, $p < 0.05$). In contrast, similar to the results shown in **Figure 2**, the reverse percentage (percentage of the double-labeled neurons among the CB+ neurons) was significantly higher in ipsilateral than in contralateral EC (**Supplementary Figures 5B–E,G**; Friedman test $p = 0.0002$; Dunn's multiple comparisons post-test, $p < 0.05$ for ipsi-LEC vs. contra-LEC, $p < 0.01$ for ipsi-MEC vs. contra-MEC). In one case, we injected FG in the ipsilateral EC and CTB-555 into the contralateral EC (EC5), resulting in some double labeled CB+ neurons, indicating that some CB+ neurons have projection to both ipsi- and contralateral EC (**Supplementary Figure 5H**).

Other Telencephalic Projections

Neurons in the EC in rodents project to a number of telencephalic domains, other than the EC and hippocampus. These include projections to olfactory domains, multimodal cortical areas as well as subcortical areas (Swanson and Köhler, 1986; Insausti et al., 1997; Kerr et al., 2007; Cappaert et al., 2015). Although many of these entorhinal projections originate from neurons in layer Va (Insausti et al., 1997; Sürmeli et al., 2015; Ohara et al., 2018), contributions from superficial layers II and III have also

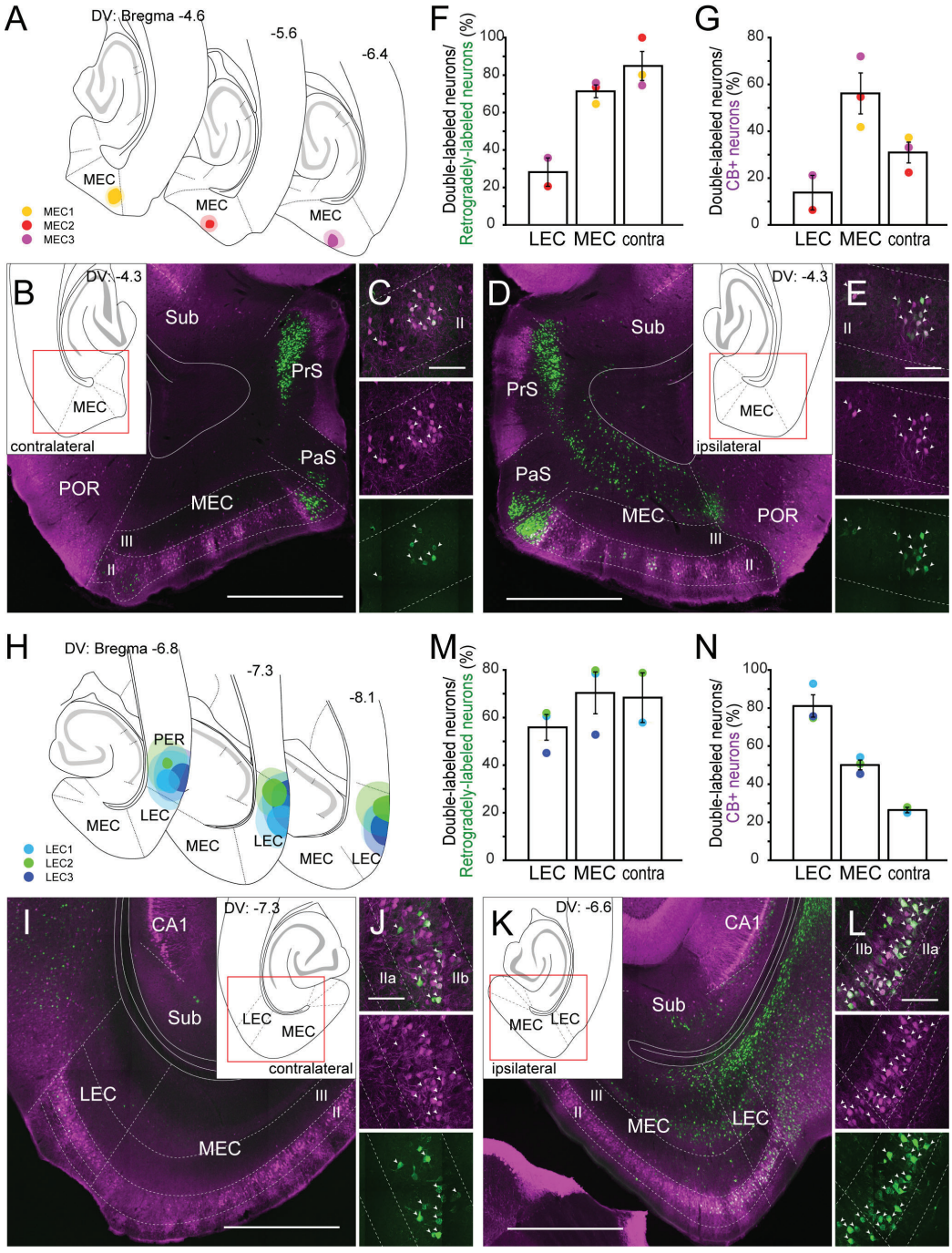

FIGURE 2 | Continued

FIGURE 2 | Projection of CB+ neurons to MEC **(A–E)** and LEC **(H–L)**. **(A,H)** The injection sites of retrograde tracer in samples with MEC **(A)** and LEC **(H)** injection. Each injection is illustrated with a different color. For each injection, the dark color shows the injection site while the light color shows the area of diffusion. **(B–E, I–L)** Distribution of retrogradely labeled neurons in contralateral EC **(B,I)**, and in ipsilateral EC **(D,K)** in horizontal sections (case: MEC3 for **B–E**, LEC2 for **I–L**). High magnification images of the superficial layers in contra- and ipsi-lateral EC are shown in panels **(C,J)** and **(E,L)** respectively. White arrows indicate neurons that were double-labeled with FG/FB and CB immunoreactivity. **(F,G,M,N)** The percentage of double-labeled neurons among retrogradely-labeled neurons (mean ± standard errors, **F,M**), and the percentage of double-labeled neurons among the CB+ neurons (mean ± standard errors, **G,N**) are compared between ipsilateral LEC, ipsilatarl MEC, and the contralateral counterpart. Each colored dot corresponds to the value for the sample shown in panels **(A,H)**. Scale bars are 1000 μm for panels **(B,D,I,K)**, and 100 μm for panels **(C,E,J,L)**.

been reported, in particular in case of projections to olfactory and medial prefrontal areas and the amygdaloid complex (Shipley and Adamek, 1984; Insausti et al., 1997; Cappaert et al., 2015). In recent studies in mice, projections from CB+ layer II neurons in LEC to olfactory cortex and olfactory bulb have been described (Leitner et al., 2016).

To examine the contribution of the EC CB+ layer II neurons to these potential telencephalic projections, retrograde tracers were injected into telencephalic targets of EC, and the distribution of the retrogradely labeled neurons was examined in LEC and MEC. We placed injections in prelimbic cortex (PrL; $n = 2$), anterior piriform cortex (APir; $n = 2$), ventral orbitofrontal cortex (OFC; $n = 3$), nucleus accumbens (NAc; $n = 2$), anterior insular cortex (AIC; $n = 2$), retrosplenial cortex (RSC; $n = 3$), postrhinal cortex (POR; $n = 2$), ventral medial prefrontal cortex (vmPFC; $n = 2$), amygdaloid complex (AMG; $n = 2$), anterior olfactory nucleus (AON; $n = 2$), posterior piriform cortex (pPir; $n = 2$), and PER ($n = 2$; **Supplementary Figure 6**). In all cases, retrogradely labeled neurons were present mainly in layer Va of EC. In a number of cases, we observed additional retrogradely labeled neurons in LEC layer IIb. These cases had injections in vmPFC including infralimbic and medial orbitofrontal and dorsal peduncular cortex (IL/DP/MO), AMG, AON, pPir, and PER (**Supplementary Figures 6H–L**). No superficially located MEC neurons were labeled following injections in any of these five areas. Therefore, we further examined the co-localization of retrograde-labeling and CB+ labeling only in LEC (**Figure 3**). In samples with an injection in AMG ($n = 2$; **Figures 3A–C**), vmPFC ($n = 2$; **Figures 3D–F**), pPir ($n = 2$; **Figures 3G–I**), and AON ($n = 2$; **Figures 3J–L**), the percentages of CB+ neurons among the retrogradely labeled LEC neurons were 29.7, 21.9, 43.4, and 40.9%, respectively (**Figure 3P**). The percentages of CB+ neurons that were retrogradely labeled were 31.0, 20.1, 33.5, and 28.5%, respectively (**Figure 3Q**). Massive retrograde labeling was also observed in LEC layer IIb after FG injection in PER ($n = 2$; **Figures 3M–O**). Although the percentage of double-labeled neurons was high in this case (**Figures 3P,Q**), the distribution of retrogradely labeled neurons was restricted to the very dorsal portion of LEC close to the border of PER (**Figure 3N**).

We subsequently assessed whether there are LEC CB+ neurons that send collateralized projections to two targets as previously reported in case of olfactory and contralateral projections (Leitner et al., 2016). Injections of two different fluorescent chemical tracers in vmPFC and ipsilateral EC resulted in a low number of double labeled neurons (**Supplementary Figure 7**). Such collateralization of the local projecting LEC superficial neurons was further examined by an AAV double infection approach. In this approach, retrograde-infecting AAV, expressing Cre recombinase (AAV6-Cre) was injected into the rostral LEC and a Cre-dependent reporter AAV that expresses EYFP after recombination (AAV1/2-EF1α-DIO-EYFP) was injected into the border of LEC and MEC ($n = 2$, **Supplementary Figures 8A,B,I**). EYFP-expressing somata were distributed within the superficial layer of LEC, mainly in layer IIb, and approximately 40% of them were CB+ (**Supplementary Figures 8C,J**). In addition to a massively labeled fiber plexus in ipsilateral LEC (LI–III) and MEC (LI), labeled fibers were observed in olfactory areas, including AON and pPir (LI), PER (LI), and vmPFC especially in dorsal peduncular cortex (LI–III, **Supplementary Figures 8D–H, K–P**). Massive labeling of passing fibers as well as terminal-like labeling was also observed in the endopiriform nucleus and AMG. Since our retrograde tracing experiments show that such extrinsic projections mainly originate from layer IIb and not from layer IIa/III, we conclude that local projecting LEC CB+ neurons also send collaterals to extrinsic regions. The data also indicate the endopiriform nucleus as a possible target of LEC CB+ neurons. We also tested whether CB+ neurons might contribute to projections to the medial septum, in view of a recent mouse study, in which it was reported that MEC CB+ neurons project to MS (Fuchs et al., 2016). In our rat study, injections in the septal complex did produce labeling in LII of EC but the retrogradely labeled neurons were sparsely observed only in ventral EC (**Supplementary Figures 9A–F**, Alonso and Köhler, 1984), and the colocalization with CB+ was also sparse. Finally, we placed retrograde tracer injections into the thalamic nucleus reuniens ($n = 3$), but these did not result in labeled neurons in either LEC or MEC (**Supplementary Figures 9G,H**). This is in line with a previous study showing that rostromedial or caudomedial reuniens hardly receive input from EC and that the few EC neurons projecting to the rostrolateral reuniens are mainly located in deep layers (McKenna and Vertes, 2004).

The CB+ population in EC comprise GABAergic neurons in addition to glutamatergic excitatory neurons (Wouterlood and Jasperse, 2001), and therefore, CB+ inhibitory neurons may contribute to the extrinsic and intrinsic projection shown above. To investigate this possibility, we injected retrograde tracers into the dorsal CA1 and contralateral MEC of GAD67 transgenic mouse line expressing GFP (Tanaka et al., 2003), and examined the distribution of retrogradely labeled neurons in EC layer II ($n = 2$, **Supplementary Figure 10**). Similar to the results observed in rats (**Figures 1**,**2**), CB+ neurons of both MEC and LEC were retrogradely labeled by the tracer injected into the dorsal CA1 and contralateral EC (**Supplementary Figures 10C–F**). CB+ entorhinal neurons, ipsilateral to the Fast Blue injection in MEC, were also

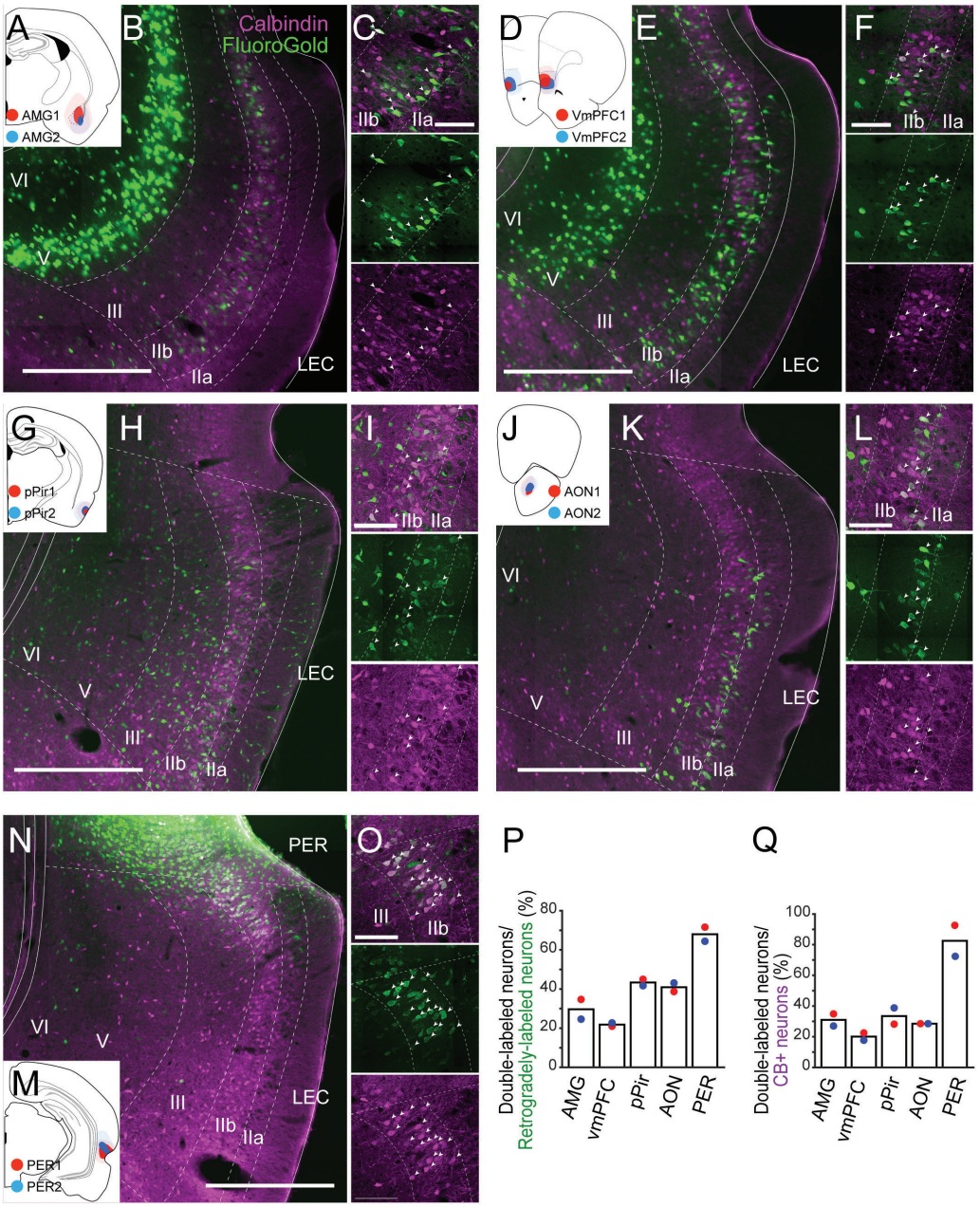

FIGURE 3 | Projections of LEC CB+ neurons to telencephalic structures. FG was injected either in AMG **(A)**, vmPFC **(D)**, pPir **(G)**, AON **(J)**, or PER **(M)**. Each injection is illustrated with a different color. For each injection, the dark color shows the injection site while the light color shows the area of diffusion. Distribution of retrogradely labeled neurons in LEC after FG injection in AMG (**B,C**, case: AMG1), vmPFC (**E,F**, case: vmPFC2), pPir (**H,I**, case: pPir2), AON (**K,L**, case: AON2), and PER (**N,O**, case: PER2) in coronal sections. White arrows indicate neurons that were double-labeled with FG and CB immunoreactivity. **(P,Q)** The percentage of double-labeled neurons among retrogradely-labeled neurons ($N = 2$ each, **P**), and the percentage of double-labeled neurons among the CB+ neurons ($N = 2$ each, **Q**) in LEC. Scale bars are 500 μm for panels **(B,E,H,K,N)**, and 100 μm for panels **(C,F,I,L,O)**.

retrogradely labeled (**Supplementary Figures 10G–I**). We further observed CB+ inhibitory neurons which are double-positive for CB and GAD67-GFP. These neurons tend to have high levels of CB immuno-labeling. We did not find any CB+ inhibitory neurons that were retrogradely labeled in contralateral MEC (**Supplementary Figure 10D**), contralateral LEC (**Supplementary Figure 10F**), and in ipsilateral LEC (**Supplementary Figure 10H**). We did find a very low presence of triple-labeled neurons only in MEC ipsilateral to the fast blue injection (**Supplementary Figure 10I**). Together, these results indicate that CB+ inhibitory neurons contribute to the intrinsic projections, but not to the long-range extrinsic projections. In other words, the long-range extrinsic projections of CB+ entorhinal neurons likely originate solely of the excitatory set of CB+ neurons.

This study provides the first systematic and quantitative analysis of efferent projections of CB+ neurons in layer II of both LEC and MEC (**Figure 4**). We conclude that CB+ neurons in both LEC and MEC are the source of widespread cortical and subcortical projections, partially mirroring the known projections of EC as well as the well-established differences between efferent projections of LEC and MEC. The majority of MEC layer II CB+ neurons are intrinsic projecting neurons targeting LEC (50.1% of the total population), MEC (56.2%), and contralateral MEC (31.0%), and the remainder contribute to hippocampal projections (19.0%). In LEC, these percentages are 81.1% to LEC, 13.8% to MEC, 26.5% to contralateral LEC, and 10.3% to hippocampus, additionally contributing substantially to projections to AMG (31.0% of the CB+ neurons), vmPFC (20.1% of the CB+ population), olfactory structures (28.5% to AON and 33.5% to pPir), and PER (82.5% of the CB+ population). We further report that EC efferents, originating exclusively from layer V neurons, are less commonly associated with a parallel CB+ layer II pathway. Most strikingly, our data point to CB+ neurons as key elements of local ipsi- and contralateral EC circuitry.

DISCUSSION

The connectivity and functional relevance of CB+ neurons became an issue of importance ever since it was described that in MEC layer II there is a substantial number of those neurons. The first report described that CB+ neurons are in majority excitatory pyramidal neurons contributing to extrinsic efferent projections of MEC to contralateral MEC by showing that 88.9% of the retrogradely labeled neurons were CB+ positive (Varga et al., 2010). This study, however, did not describe the proportion of the CB+ neurons contributing to this projection. This was also the case in the papers which later reported the projections from MEC CB+ neurons to the medial septum (Fuchs et al., 2016) and the projections of LEC CB+ neurons (Leitner et al., 2016). Further projections of MEC CB+ neurons to CA1 were revealed by using a transgenic mouse line (Kitamura et al., 2014) or to ipsilateral MEC (Zutshi et al., 2018). These studies also did not show the proportion of the CB+ neurons contributing to each of these projections. All these studies therefore lead to two potential misinterpretations: (i) that a very substantial percentage of CB+ neurons project to these targets and (ii) that the majority of CB+ neurons therefore project to all of these targets. Our results show that this is not the case. First of all, the large majority of crossed and commissural projections originate from CB- neurons in layer III of the EC, which is in line with previous reports (Steward and Scoville, 1976; Köhler et al., 1978). More significant is the fact that the CB+ neurons which project to the contralateral EC, the hippocampus, and the medial septum are only part of the total CB+ population (26.7, 10.3, and 4.2% respectively for LEC CB+ neurons, and 31.0, 19.0, and 2.1% respectively for MEC CB+ neurons). We further show that the LEC CB+ neurons, contribute to a number of additional long-range projections not reported previously. Essentially all of the long-range extrinsic projections originate from excitatory CB+ neurons. A substantial part of the CB+ population projects intrinsically (50.1% for LEC CB+ neurons, and 56.2% for MEC CB+ neurons). This intrinsic projection mainly originates from CB+ excitatory neurons though CB+ inhibitory neurons do contribute to this local innervation.

The present semiquantitative findings can only be revealed by the extensive retrograde tracing approach as applied in this study, and not by the use of CB-specific transgenic mice. Anterograde tracing experiments using transgenic mouse lines are indeed powerful to examine the detailed connectivity of specific cell types with homogeneous projections. However, this approach is not ideal when it comes to CB+ neurons which, as we show here, are a heterogenous population with diverse projections, since such an approach would simply label all projections originating in CB+ neurons. Of course, retrograde tracing approaches also have limitations, and the number of retrogradely labeled neurons vary regarding to the amount of the tracer injected, the size of the injection site, as well as the sensitivity of tracer detection. The retrograde tracer can be taken up not only by the axon terminal but also by passing fibers, which can result in false positive labeling (Schmued and Fallon, 1986). The estimates of the connectivity shown in this study are thus semi-quantitative, but still unequivocally show the unique projection system originating from CB+ neurons in both LEC and MEC.

We further show that CB+ neurons in both EC subdivisions contribute sparsely to a variety of projections outside EC, most, if not all of which have a shared origin in layer III and in some instances also in layer V. These include projections to mPFC, olfactory telencephalic structures, the amygdaloid complex, endopiriform nucleus and septal complex (Cappaert et al., 2015). Projections, known to originate almost exclusively from layer V, including those targeting the cingulate and retrosplenial cortex, the orbitofrontal and insular cortex, as well as the nucleus accumbens (Cappaert et al., 2015), do not seem to have much of an accompanying CB+ pathway. All these projections, irrespective of whether they originate in MEC or LEC, have their origin in a single layer of genetically defined neurons, generally referred to as layer Va (Sürmeli et al., 2015; Ohara et al., 2018). We recently reported that layer Va neurons contribute little to local connections, in contrast to layer Vb neurons (Ohara et al., 2018). Aside from showing that the LII CB+ excitatory population comprises neurons with diverse projections, the three main messages in this paper are: (i) the largest percentage of layer

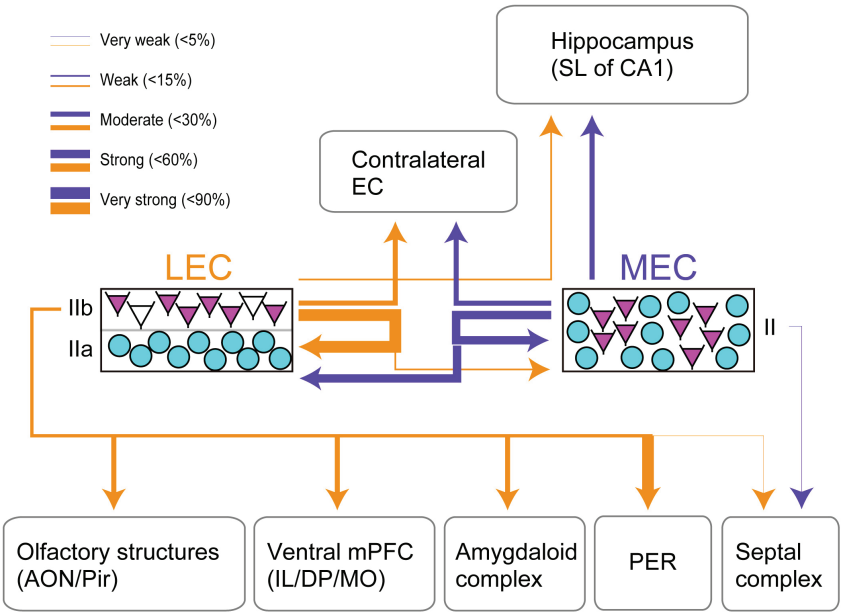

FIGURE 4 | Summary of the projection of CB+ neurons in LEC and MEC. EC Layer II neurons which comprise CB+ neurons (magenta) and RE+ neurons (cyan) are shown. The arrows indicate the projections originating from the LEC CB+ neurons (yellow) and the MEC CB+ neurons (purple). Note that the arrows do not show the laminar targets of the ipsi- and contralateral EC projections. The thickness of the lines is based on the percentage of double-labeled neurons/CB+ neurons. Note that although the projection from LEC CB+ cells to PER seems strong, this projection originates only from a restricted very dorsal portion of LEC.

II CB+ neurons contribute to intrinsic local projections, thus representing a yet not described group of excitatory interneurons, (ii) the CB+ neurons, including the local projecting population, tend to collateralize, targeting multiple targets, and (iii) CB+ neurons in LEC and MEC show strikingly different overall projection patterns, largely replicating the overall differences of efferent projections between the two entorhinal subdivisions.

CB+ Neurons Are Key Neuronal Intrinsic Network Elements

The intrinsic projections of CB+ neurons distribute bilaterally, within the area of origin and its commissural counterpart, but also contribute to unilateral interconnections between LEC and MEC. Although this is true in case of CB+ neurons in both LEC and MEC, there are striking differences in the numerical weight of these intrinsic projections (see below). This striking widespread intrinsic connectivity and sparse hippocampal CA1 connectivity makes layer II CB+ neurons very different from their counterparts, the RE+ neurons. The latter have strong and widespread projections to the dentate gyrus, CA2 and CA3 and based on *in vitro* studies, their local connectivity apparently is rather restricted to a small domain around the cell body (Pastoll et al., 2012; Couey et al., 2013; Schmidt et al., 2017; Nilssen et al., 2018). This notion is supported by the present retrograde data. Moreover, unlike CB+ neurons, the RE+ population does not seem to contribute substantially to any of the other extrinsic EC projection targets. It is of interest to note that in our hands, injections of retrograde tracers in EC, vmPFC and AMG resulted in many retrogradely labeled LIIb neurons, which seemed negative for CB+. Although we cannot exclude that this is an artifact of our immunohistochemical procedures, we suggest that these observations indicate that there might yet be another neuron type in LEC LII (reelin-negative/CB-negative pyramidal cell) of which the identity needs to be determined. A potential candidate might be the much sparser population of calretinin-positive pyramidal neurons, known to be present in layer IIb (Wouterlood et al., 2000), but we lack conclusive data on these neurons. It is presently unknown how the morphologically described cell types in layer II of both LEC and MEC (Canto and Witter, 2012a,b; Cappaert et al., 2015; Fuchs et al., 2016; Leitner et al., 2016) relates to the class of calretinin + neurons.

It is also well established that CB+ neurons have local connections different from RE+ neurons. Whereas RE+ neurons preferentially reciprocally connect with PV + interneurons, CB+ are connected to interneurons expressing the 5HT3a receptor in case of MEC, and these likely represent CCK expressing basket cells (Varga et al., 2010; Burgalossi and Brecht, 2014; Fuchs et al., 2016). Moreover, MEC CB+ neurons reportedly receive specific inputs from cholinergic neurons in the medial septal complex and also from parasubicular neurons that apparently avoid RE+ neurons (Ray et al., 2014; Tang et al., 2016). It also has been

reported that the MEC microcircuitry differs between the two cell types, such that layer II stellate cells receive more superficial input than layer II pyramidal cells, and pyramidal cells receive more deep layer input than stellate cells (Beed et al., 2010). Both cell types share however a dominant distribution of their axons to layer I and superficial layer II, be it that the range of these projections is very different, as mentioned above. The present data on the preferred termination of CB+ local intrinsic ipsilateral projections in layer I is in line with previous reports (Köhler, 1986, 1988; Ray et al., 2014; Fuchs et al., 2016; Leitner et al., 2016), and holds true for the contralateral projections in case of MEC as well (present data; Blackstad, 1956; Zheng et al., 2014; Fuchs et al., 2016). Our data further show that the long-range projections from CB+ neurons in LEC targeting MEC, show a similar laminar distribution. Own unpublished results indicate that the opposite projection from MEC to LEC shows a terminal preference for layer II (Doan et al., 2016). Finally, CB+ pyramidals are known to provide excitatory input to the RE+ stellate cells both directly (Winterer et al., 2017) and indirectly through the CB+ intermediate pyramidal cells (Fuchs et al., 2016). A comparable wiring scheme is likely applicable to LEC (Witter et al., 2017). Since CB+ neurons also provide feed-forward inhibition to the CA1 pyramidal cells (Kitamura et al., 2014), we propose that activity in the CB+ population might switch the information flow in the EC-hippocampal system from the EC layer III-CA1/subiculum direct pathway to the EC layer II-DG/CA3 indirect pathway.

Intrinsic connectivity in EC of the rat not only originates from layer II CB+ neurons but also from neurons in layers III –VI and distributes in layers I–V (Köhler, 1986, 1988; Dolorfo and Amaral, 1998). This seems to hold true in other species as well (Witter et al., 1986, 1989b; Chrobak and Amaral, 2007). Our data for both LEC and MEC, in line with previous reports (Köhler, 1986, 1988; Fuchs et al., 2016; Leitner et al., 2016), thus indicate an interesting differentiation between the two systems. Whereas layer II CB+ neurons originate projections that preferentially terminate in layer I and superficial layer II, the projections to the deeper layer seem to originate mainly from neurons in layers III and V.

CB+ Projections Collateralize

The percentages of CB+ neurons that project to the identified projection targets for both LEC and MEC add up to way over 100%. In case of MEC we identified over 150% of the population of CB+ neurons and in LEC we identified over 300% based on single tracing experiments. We take these numbers as an indication that CB+ neurons in EC give rise to strongly collateralized projections and corroborated that contention by showing that retrograde double labeling occurs in case of injections in two targets. This is in line with previous reports. Morphologically, the populations of CB+ neurons in both LEC and MEC comprise two different neuronal types, pyramidal neurons and oblique/intermediate pyramidals (Fuchs et al., 2016; Leitner et al., 2016). It might thus be the case that the two morphologically different CB+ neurons can be equated with two populations of projection-selective neurons, for example one bilaterally intrinsic and one extrinsic. This might seem a likely scenario since in MEC, CB+ projection neurons projecting to contralateral MEC and the medial septum are colocalized in the same cluster, but single cells do not seem to collateralize to both targets (Fuchs et al., 2016). Supporting but yet insufficient data have been obtained in LEC, where single CB+ neurons have been shown to project to the piriform cortex and the olfactory bulb, but no evidence was presented that these also project intrinsically, neither ipsi- nor contralaterally (Leitner et al., 2016), and our results showing that CB+ neurons collateralize to target both ipsilateral and contralateral LEC. Conflicting with this notion are our present observations that single CB+ neurons can project to vmPFC and ipsilateral LEC. It is therefore not possible to relate the two morphologically defined CB+ neurons to their projection patterns. Our data further indicate that the level of collateralization in LEC is higher than in MEC, likely reflecting the increased number of CB+ projecting targets in case of LEC.

CB+ Projections From LEC Are More Diverse Than the Ones From MEC

We report striking differences between LEC and MEC in that CB+ MEC projections mainly reach CA1 and bilaterally target MEC, as well as contributing substantially to projections to LEC. In contrast, CB+ projections from LEC to CA1 are less pronounced than their MEC counterpart, whereas commissural projections are comparable. Projections of LEC CB+ neurons to MEC are numerically much weaker than the other way around (13.8 versus 50.1%). Further, LEC CB+ neurons contribute substantially to projections to targets not reached by MEC CB+ neurons. These targets include the amygdala, the medial prefrontal cortex and the perirhinal cortex. In other words, MEC is more parahippocampal/hippocampal centric, whereas LEC prefers other telencephalic structures over parahippocampal and hippocampal projections. This is in line with the overall excitatory connectivity patterns of LEC and MEC (Witter et al., 2017; Nilssen et al., 2019). Interestingly a similar difference in connectivity patterns have been reported with respect to inputs to interneuron populations in MEC versus LEC as well (Jacobsen et al., 2018).

These results are of interest when combined with two additional features. First, MEC CB+ neurons receive inputs from deep layers, which likely convey information processed in the hippocampus (Beed et al., 2010). Second it has been reported, using the isolated guinea pig *ex vivo* brain preparation, that olfactory stimulation resulted in a sequential activation in LEC, hippocampus and MEC, followed by LEC (Biella and de Curtis, 2000). Since we here show that reciprocal connections of LEC and MEC are unequal in strength, in favor of the MEC to LEC ones, and that LEC CB+ neurons provide an additional preferential projection to telencephalic structures including the olfactory regions, we suggest that hippocampal information may be processed first in MEC and subsequently in LEC followed by telencephalic structures. In case this turns out to be a generalizable trait, inputs arriving in LEC will, after hippocampal processing, not be returned to LEC but will be processed hierarchically from MEC to LEC and further downstream.

CONCLUSION

In conclusion, CB+ neurons in MEC and LEC are the source of a widespread intrinsic excitatory projection, connecting ipsilateral LEC and MEC to contralateral LEC and MEC respectively, as well reciprocally connecting LEC and MEC within one hemisphere. Such local circuits of MEC LII pyramidal cells are critical for the precise firing location of grid cells (Zutshi et al., 2018). In addition to this main projection, we showed that the long-range projections of CB+ neurons outside EC differ between LEC and MEC. Although such extrinsic projections are numerically-weaker than the intrinsic ones, a high-degree of cellular specificity can still be present, such as the selective targeting of interneurons in CA1 stratum lacunosum which controls temporal association memory (Kitamura et al., 2014). Although plausible, whether the intrinsic and extrinsic projections of CB+ neurons specific for the two entorhinal subdivisions contribute to the functional difference between LEC and MEC require further investigation.

DATA AVAILABILITY STATEMENT

All datasets generated for this study are included in the manuscript/**Supplementary Files**.

ETHICS STATEMENT

The animal study was reviewed and approved by the Center for Laboratory Animal Research of Tohoku University and the Norwegian Animal Research Authority.

AUTHOR CONTRIBUTIONS

SO and MW conceived the study design. SO, MG, KI, CB, and TD collected and analyzed the experimental data. TK and KM produced AAV vectors. SO and MG carried out all the quantifications. All authors contributed to the discussions that resulted in this article, which was written by SO and MW, and approved the final version of the manuscript.

FUNDING

This work has been supported by the Kavli Foundation, the Centre of Excellence scheme – Centre for Neural Computation and research grant # 227769 of the Research Council of Norway, The Egil and Pauline Braathen and Fred Kavli Centre for Cortical Microcircuits, and the National Infrastructure scheme of the Research Council of Norway – NORBRAIN #197467. This work has also been supported by Grants-in-Aid for Scientific Research on Innovative Areas (#16H01495), and by Grant-in-Aid for Scientific Research (KAKENHI, #15K18358, #19K06917, and #16H04656) from the Ministry of Education, Culture, Sports, Science and Technology (MEXT) of Japan.

ACKNOWLEDGMENTS

We thank Grethe M. Olsen, Paulo JB. Girão, and Bruno Monterotti for help with histological preparations and digital microscopic imaging.

SUPPLEMENTARY MATERIAL

The Supplementary Material for this article can be found online at: https://www.frontiersin.org/articles/10.3389/fnsys.2019.00054/full#supplementary-material

REFERENCES

Alonso, A., and Köhler, C. (1984). A study of the reciprocal connections between the septum and the entorhinal area using anterograde and retrograde axonal transport methods in the rat brain. *J. Comp. Neurol.* 225, 327–343. doi: 10.1002/cne.902250303

Aronoff, R., Matyas, F., Mateo, C., Ciron, C., Schneider, B., and Petersen, C. C. (2010). Long-range connectivity of mouse primary somatosensory barrel cortex. *Eur. J. Neurosci.* 31, 2221–2233. doi: 10.1111/j.1460-9568.2010.07264.x

Beed, P., Bendels, M. H. K., Wiegand, H. F., Leibold, C., Johenning, F. W., and Schmitz, D. (2010). Analysis of excitatory microcircuitry in the medial entorhinal cortex reveals cell-type-specific differences. *Neuron* 68, 1059–1066. doi: 10.1016/j.neuron.2010.12.009

Biella, G., and de Curtis, M. (2000). Olfactory inputs activate the medial entorhinal cortex via the hippocampus. *J. Neurophysiol.* 83, 1924–1931. doi: 10.1152/jn.2000.83.4.1924

Blackstad, T. W. (1956). Commissural connections of the hippocampal region in the rat, with special reference to their mode of termination. *J. Comp. Neurol.* 105, 417–537. doi: 10.1002/cne.901050305

Boccara, C. N., Kjonigsen, L. J., Hammer, I. M., Bjaalie, J. G., Leergaard, T. B., and Witter, M. P. (2015). A three-plane architectonic atlas of the rat hippocampal region. *Hippocampus* 25, 838–857. doi: 10.1002/hipo.22407

Brun, V. H., Leutgeb, S., Wu, H. Q., Schwarcz, R., Witter, M. P., Moser, E. I., et al. (2008). Impaired spatial representation in CA1 after lesion of direct input from entorhinal cortex. *Neuron* 57, 290–302. doi: 10.1016/j.neuron.2007.11.034

Brun, V. H., Otnæss, M. K., Molden, S., Steffenach, H., Witter, M. P., Moser, M., et al. (2002). Place cells and place recognition maintained by direct entorhinal-hippocampal circuitry. *Science* 296, 2243–2246. doi: 10.1126/science.1071089

Burgalossi, A., and Brecht, M. (2014). Cellular, columnar and modular organization of spatial representations in medial entorhinal cortex. *Curr. Opin. Neurobiol.* 24, 47–54. doi: 10.1016/j.conb.2013.08.011

Canto, C. B., and Witter, M. P. (2012b). Cellular properties of principal neurons in the rat entorhinal cortex. II. The medial entorhinal cortex. *Hippocampus* 22, 1277–1299. doi: 10.1002/hipo.20993

Canto, C. B., and Witter, M. P. (2012a). Cellular properties of principal neurons in the rat entorhinal cortex. I. The lateral entorhinal cortex. *Hippocampus* 22, 1256–1276. doi: 10.1002/hipo.20997

Cappaert, N. L. M., Van Strien, N. M., and Witter, M. P. (2015). "Hippocampal formation," in *The Rat Nervous System*, 4th Edn, ed. G. Paxinos (Amsterdam: Elsevier), 511–573.

Chrobak, J. J., and Amaral, D. G. (2007). Entorhinal cortex of the monkey: VII. Intrinsic connections. *J. Comp. Neurol.* 500, 612–633. doi: 10.1002/cne.21200

Couey, J. J., Witoelar, A., Zhang, S. J., Zheng, K., Ye, J., Dunn, B., et al. (2013). Recurrent inhibitory circuitry as a mechanism for grid formation. *Nat. Neurosci.* 16, 318–324. doi: 10.1038/nn.3310

Deshmukh, S. S., and Knierim, J. J. (2011). Representation of non-spatial and spatial information in the lateral entorhinal cortex. *Front. Behav. Neurosci.* 5:69. doi: 10.3389/fnbeh.2011.00069

Doan, T., Nilsen, E., and Witter, M. (2016). *Postsynaptic Targets of Inputs to the Lateral Entorhinal Cortex. SfN Abstr. 183.16*. Høgskoleringen: Norwegian University of Science and Technology.

Dolorfo, C. L., and Amaral, D. G. (1998). Entorhinal cortex of the rat: organization of intrinsic connections. *J. Comp. Neurol.* 398, 49–82. doi: 10.1002/(sici)1096-9861(19980817)398:1<49::aid-cne4>3.0.co;2-9

Eichenbaum, H., Yonelinas, A. P., and Ranganath, C. (2007). The medial temporal lobe and recognition memory. *Annu. Rev. Neurosci.* 30, 123–152.

Fuchs, E. C., Neitz, A., Pinna, R., Melzer, S., Caputi, A., and Monyer, H. (2016). Local and distant input controlling excitation in layer II of the medial entorhinal cortex. *Neuron* 89, 194–208. doi: 10.1016/j.neuron.2015.11.029

Fujimaru, Y., and Kosaka, T. (1996). The distribution of two calcium binding proteins, calbindin D-28K and parvalbumin, in the entorhinal cortex of the adult mouse. *Neurosci. Res.* 24, 329–343. doi: 10.1016/0168-0102(95)01008-4

Fyhn, M., Molden, S., Witter, M. P., Moser, E. I., and Moser, M. B. (2004). Spatial representation in the entorhinal cortex. *Science* 305, 1258–1264. doi: 10.1126/science.1099901

Insausti, R., Herrero, M. T., and Witter, M. P. (1997). Entorhinal cortex of the rat: cytoarchitectonic subdivisions and the origin and distribution of cortical efferents. *Hippocampus* 7, 146–183. doi: 10.1002/(sici)1098-1063(1997)7:2<146::aid-hipo4>3.0.co;2-l

Jacobsen, B., Zheng, K., Nair, R. R., Meletis, K., and Witter, M. P. (2018). Monosynaptic inputs to somatostatin and parvalbumin interneurons in the entorhinal cortex of mice. *FENS Abstr.* 4274.

Ji, J., and Maren, S. (2008). Lesions of the entorhinal cortex or fornix disrupt the context-dependence of fear extinction in rats. *Behav. Brain Res.* 194, 201–206. doi: 10.1016/j.bbr.2008.07.011

Kerr, K. M., Agster, K. L., Furtak, S. C., and Burwell, R. D. (2007). Functional neuroanatomy of the parahippocampal region: the lateral and medial entorhinal areas. *Hippocampus* 17, 697–708. doi: 10.1002/hipo.20315

Kitamura, T., Pignatelli, M., Suh, J., Kohara, K., Yoshiki, A., Abe, K., et al. (2014). Island cells control temporal association memory. *Science* 343, 896–901. doi: 10.1126/science.1244634

Kjonigsen, L. J., Lillehaug, S., Bjaalie, J. G., Witter, M. P., and Leergaard, T. B. (2015). Waxholm Space atlas of the rat brain hippocampal region: three-dimensional delineations based on magnetic resonance and diffusion tensor imaging. *Neuroimage* 108, 441–449. doi: 10.1016/j.neuroimage.2014.12.080

Köhler, C. (1986). Intrinsic connections of the retrohippocampal region in the rat brain. II. The medial entorhinal area. *J. Comp. Neurol.* 246, 149–169. doi: 10.1002/cne.902460202

Köhler, C. (1988). Intrinsic connections of the retrohippocampal region in the rat brain: III. The lateral entorhinal area. *J. Comp. Neurol.* 271, 208–228. doi: 10.1002/cne.902710204

Köhler, C., Shipley, M., Srebro, B., and Harkmark, W. (1978). Some retrohippocampal afferents to the entorhinal cortex. Cells of origin as studied by HRP method in the rat and mouse. *Neurosci. Lett.* 10, 115–120. doi: 10.1016/0304-3940(78)90021-6

Leitner, F. C., Melzer, S., Lütcke, H., Pinna, R., Seeburg, P. H., Helmchen, F., et al. (2016). Spatially segregated feedforward and feedback neurons support differential odor processing in the lateral entorhinal cortex. *Nat. Neurosci.* 19, 935–944. doi: 10.1038/nn.4303

McKenna, J. T., and Vertes, R. P. (2004). Afferent projections to nucleus reuniens of the thalamus. *J. Comp. Neurol.* 480, 115–142. doi: 10.1002/cne.20342

Montchal, M. E., Reagh, Z. M., and Yassa, M. A. (2019). Precise temporal memories are supported by the lateral entorhinal cortex in humans. *Nat. Neurosci.* 22, 284–288. doi: 10.1038/s41593-018-0303-1

Moser, E. I., Roudi, Y., Witter, M. P., Kentros, C., Bonhoeffer, T., and Moser, M.-B. (2014). Grid cells and cortical representation. *Nat. Rev. Neurosci.* 15, 466–481. doi: 10.1038/nrn3766

Naumann, R. K., Ray, S., Prokop, S., Las, L., Heppner, F. L., and Brecht, M. (2016). Conserved size and periodicity of pyramidal patches in layer 2 of medial/caudal entorhinal cortex. *J. Comp. Neurol.* 524, 783–806. doi: 10.1002/cne.23865

Neunuebel, J. P., Yoganarasimha, D., Rao, G., and Knierim, J. J. (2013). Conflicts between local and global spatial frameworks dissociate neural representations of the lateral and medial entorhinal cortex. *J. Neurosci.* 33, 9246–9258. doi: 10.1523/JNEUROSCI.0946-13.2013

Nilssen, E. S., Doan, T. P., Nigro, M. J., Ohara, S., and Witter, M. P. (2019). A reappraisal of the lateral and medial entorhinal subdivisions mediating parallel cortical pathways. *Hippocampus* doi: 10.1002/hipo.23145 [Epub ahead of print].

Nilssen, E. S., Jacobsen, B., Fjeld, G., Nair, R. R., Blankvoort, S., Kentros, C., et al. (2018). Inhibitory connectivity dominates the fan cell network in layer II of lateral entorhinal cortex. *J. Neurosci.* 38, 9712–9727. doi: 10.1523/JNEUROSCI.1290-18.2018

Ohara, S., Onodera, M., Simonsen, Ø.W., Yoshino, R., Hioki, H., Iijima, T., et al. (2018). Intrinsic projections of layer vb neurons to layers va, III, and II in the lateral and medial entorhinal cortex of the rat. *Cell Rep.* 24, 107–116. doi: 10.1016/j.celrep.2018.06.014

Papp, E. A., Leergaard, T. B., Calabrese, E., Johnson, G. A., and Bjaalie, J. G. (2014). Waxholm space atlas of the sprague dawley rat brain. *Neuroimage* 97, 374–386. doi: 10.1016/j.neuroimage.2014.04.001

Pastoll, H., Ramsden, H. L., and Nolan, M. F. (2012). Intrinsic electrophysiological properties of entorhinal cortex stellate cells and their contribution to grid cell firing fields. *Front. Neural Circuits* 6:17. doi: 10.3389/fncir.2012.00017

Ramos-Moreno, T., Galazo, M. J., Porrero, C., Martínez-Cerdeño, V., and Clascá, F. (2006). Extracellular matrix molecules and synaptic plasticity: immunomapping of intracellular and secreted Reelin in the adult rat brain. *Eur. J. Neurosci.* 23, 401–422. doi: 10.1111/j.1460-9568.2005.04567.x

Ray, S., Naumann, R., Burgalossi, A., Tang, Q., Schmidt, H., and Brecht, M. (2014). Grid-layout and theta-modulation of layer 2 pyramidal neurons in medial entorhinal cortex. *Science* 13, 987–994. doi: 10.1126/science.1243028

Reagh, Z. M., and Yassa, M. A. (2014). Object and spatial mnemonic interference differentially engage lateral and medial entorhinal cortex in humans. *Proc. Natl. Acad. Sci. U.S.A.* 111, E4264–E4273. doi: 10.1073/pnas.1411250111

Rodo, C., Sargolini, F., and Save, E. (2016). Processing of spatial and non-spatial information in rats with lesions of the medial and lateral entorhinal cortex: environmental complexity matters. *Behav. Brain Res.* 320, 200–209. doi: 10.1016/j.bbr.2016.12.009

Schenk, F., and Morris, R. G. M. (1985). Dissociation between components of spatial memory in rats after recovery from the effects of retrohippocampal lesions. *Exp. Brain Res.* 58, 11–28.

Schmidt, H., Gour, A., Straehle, J., Boergens, K. M., Brecht, M., and Helmstaedter, M. (2017). Axonal synapse sorting in medial entorhinal cortex. *Nature* 549, 469–475. doi: 10.1038/nature24005

Schmued, L. C., and Fallon, J. H. (1986). Fluoro-gold: a new fluorescent retrograde axonal tracer with numerous unique properties. *Brain Res.* 377, 147–154. doi: 10.1016/0006-8993(86)91199-6

Shipley, M. T., and Adamek, G. D. (1984). The connections of the mouse olfactory bulb: a study using orthograde and retrograde transport of wheat germ agglutinin conjugated to horseradish peroxidase. *Brain Res. Bull.* 12, 669–688. doi: 10.1016/0361-9230(84)90148-5

Steward, O., and Scoville, S. A. (1976). Cells of origin of entorhinal cortical afferents to the hippocampus and fascia dentata of the rat. *J. Comp. Neurol.* 169, 347–370. doi: 10.1002/cne.901690306

Sürmeli, G., Marcu, D. C., McClure, C., Garden, D. L. F., Pastoll, H., and Nolan, M. F. (2015). Molecularly defined circuitry reveals input-output segregation in deep layers of the medial entorhinal cortex. *Neuron* 88, 1040–1053. doi: 10.1016/j.neuron.2015.10.041

Swanson, L. W., and Köhler, C. (1986). Anatomical evidence for direct projections from the entorhinal area to the entire cortical mantle in the rat. *J. Neurosci.* 6, 3010–3023. doi: 10.1523/jneurosci.06-10-03010.1986

Tanaka, D., Nakaya, Y., Yanagawa, Y., Obata, K., and Murakami, F. (2003). Multimodal tangential migration of neocortical GABAergic neurons independent of GPI-anchored proteins. *Development* 130, 5803–5813. doi: 10.1242/dev.00825

Tang, Q., Burgalossi, A., Ebbesen, C. L., Ray, S., Naumann, R., Schmidt, H., et al. (2014). Pyramidal and stellate cell specificity of grid and border representations in layer 2 of medial entorhinal cortex. *Neuron* 84, 1191–1197. doi: 10.1016/j.neuron.2014.11.009

Tang, Q., Burgalossi, A., Ebbesen, C. L., Sanguinetti-Scheck, J. I., Schmidt, H., Tukker, J. J., et al. (2016). Functional architecture of the rat parasubiculum. *J. Neurosci.* 36, 2289–2301. doi: 10.1523/JNEUROSCI.3749-15.2016

Tsao, A., Moser, M. B., and Moser, E. I. (2013). Traces of experience in the lateral entorhinal cortex. *Curr. Biol.* 23, 399–405. doi: 10.1016/j.cub.2013.01.036

Tsao, A., Sugar, J., Lu, L., Wang, C., Knierim, J. J., Moser, M.-B., et al. (2018). Integrating time from experience in the lateral entorhinal cortex. *Nature* 561, 57–62. doi: 10.1038/s41586-018-0459-6

Tuñón, T., Insausti, R., Ferrer, I., Sobreviela, T., and Soriano, E. (1992). Parvalbumin and calbindin D-28K in the human entorhinal cortex. An immunohistochemical study. *Brain Res.* 589, 24–32. doi: 10.1016/0006-8993(92)91157-a

Varga, C., Lee, S. Y., and Soltesz, I. (2010). Target-selective GABAergic control of entorhinal cortex output. *Nat. Neurosci.* 13, 822–824. doi: 10.1038/nn.2570

Winterer, J., Maier, N., Wozny, C., Beed, P., Breustedt, J., Evangelista, R., et al. (2017). Excitatory microcircuits within superficial layers of the medial entorhinal cortex. *Cell Rep.* 1247, 1110–1116. doi: 10.1016/j.celrep.2017.04.041

Witter, M. P., Chan-Palay, V., and Kohler, C. (1989a). "Connectivity of the rat hippocampus," in *The Hippocampus-New Vistas*, eds V. Chan-Palay, and C. Kohler (New York, NY: Allen R. Liss), 53–69.

Witter, M. P., Groenewegen, H. J., Lopes da Silva, F. H., and Lohman, A. H. M. (1989b). Functional organization of the extrinsic and intrinsic circuitry of the parahippocampal region. *Prog. Neurobiol.* 33, 161–253. doi: 10.1016/0301-0082(89)90009-9

Witter, M. P., Doan, T. P., Jacobsen, B., Nilssen, E. S., and Ohara, S. (2017). Architecture of the entorhinal cortex a review of entorhinal anatomy in rodents with some comparative notes. *Front. Syst. Neurosci.* 11:46. doi: 10.3389/fnsys.2017.00046

Witter, M. P., Naber, P. A., Van Haeften, T., Machielsen, W. C. M., Rombouts, S. A., Barkhof, F., et al. (2000). Cortico-hippocampal communication by way of parallel parahippocampal-subicular pathways. *Hippocampus* 10, 398–410. doi: 10.1002/1098-1063(2000)10:4<398::aid-hipo6>3.3.co;2-b

Witter, M. P., Room, P., Groenewegen, H. J., and Lohman, A. H. M. (1986). Connections of the parahippocampal cortex in the cat. V. Intrinsic connections; comments on input/output connections with the hippocampus. *J. Comp. Neurol.* 252, 78–94. doi: 10.1002/cne.902520105

Wouterlood, F. G. (2002). "Spotlight on the neurons (I): cell types, local connectivity, microcircuits, and distribution of markers," in *The Parahippocampal Region. Organization and Role in Cognitive Function*, eds M. P. Witter, and F. G. Wouterlood (Oxford: Oxford University Press), 61–88.

Wouterlood, F. G., and Jasperse, B. (2001). Co-expression of calbindin-d28k and gaba in the entorhinal cortex of the rat. *Soc. Neurosci. Abstr.* 27:1827.

Wouterlood, F. G., Van Denderen, J. C. M., Van Haeften, T., and Witter, M. P. (2000). Calretinin in the entorhinal cortex of the rat: distribution, morphology, ultrastructure of neurons, and co-localization with γ-aminobutyric acid and parvalbumin. *J. Comp. Neurol.* 425, 177–192. doi: 10.1002/1096-9861(20000918)425:2<177::aid-cne2>3.0.co;2-g

Zheng, K., Simonsen, Ø., and Witter, M. (2014). Interhemispheric connections between left and right medial entorhinal cortices. *FENS Abstr.* 1717.

Zutshi, I., Fu, M. L., Lilascharoen, V., Leutgeb, J. K., Lim, B. K., and Leutgeb, S. (2018). Recurrent circuits within medial entorhinal cortex superficial layers support grid cell firing. *Nat. Commun.* 9:3701. doi: 10.1038/s41467-018-06104-5

Conflict of Interest: The authors declare that the research was conducted in the absence of any commercial or financial relationships that could be construed as a potential conflict of interest.

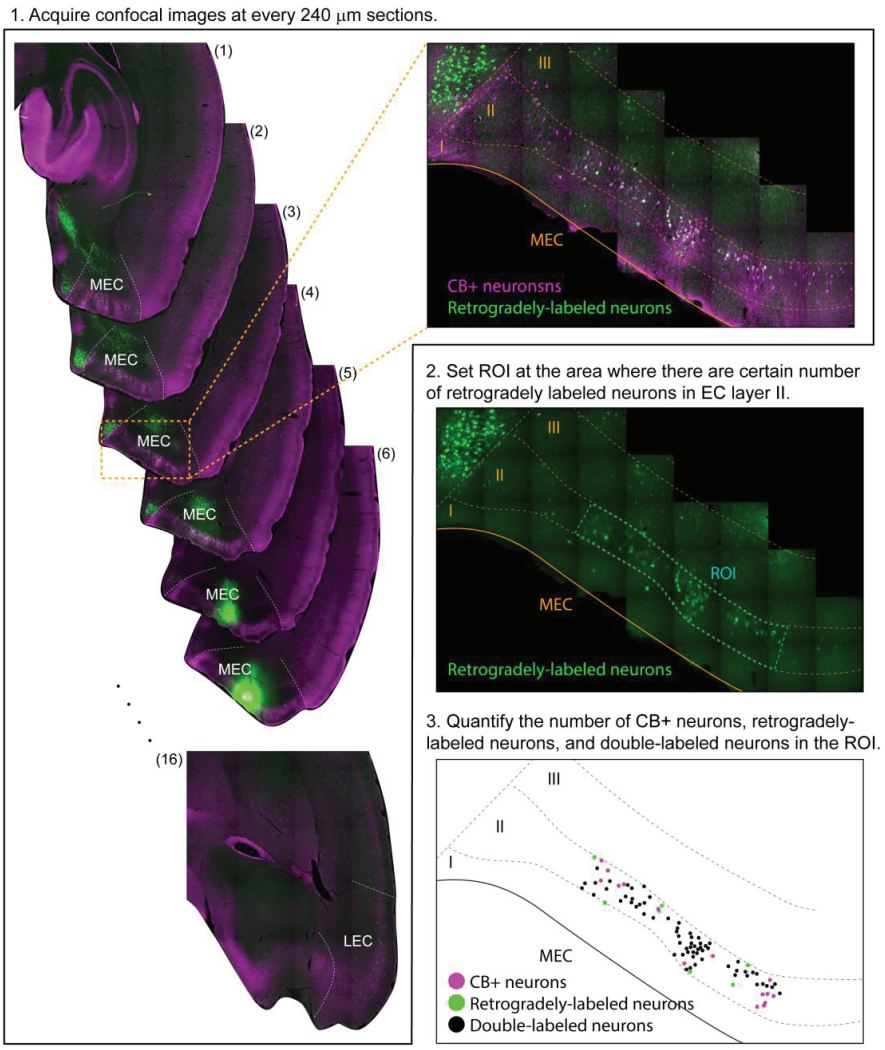

4. Calculate the percentage of "Double-labeled neurons/CB+ neurons" and "Double-labled neurons/ Retrogradely-labeled neurons".

CB+ neurons	Retrogradely-labeled neurons	Double-labeled neurons	Double-labeled neurons/ CB+ neurons (%)	Double-labeled neurons/ Retrogradely-labeled neurons (%)
97	71	64	65.98	90.14

Supplementary Figure 1. Schematic diagram illustrating the quantitative analysis of the colocalization of CB immunolabeling and retrograde labeling. Samples were analysed in sections that were 240 μm apart, using one z-level of the confocal image (Step 1). We selected a Region of Interest (ROI) where there were sufficient retrogradely labeled neurons in EC layer II (Step 2). Subsequently, the retrogradely labeled neurons and immunohistochemically stained CB+ neurons were counted in this ROI (Step 3). The percentage of "Double-labeled neurons/CB+ neurons" and "Double-labeled neurons/Retrogradely-labeled neurons" were calculated and compared between MEC and LEC (Step 4).

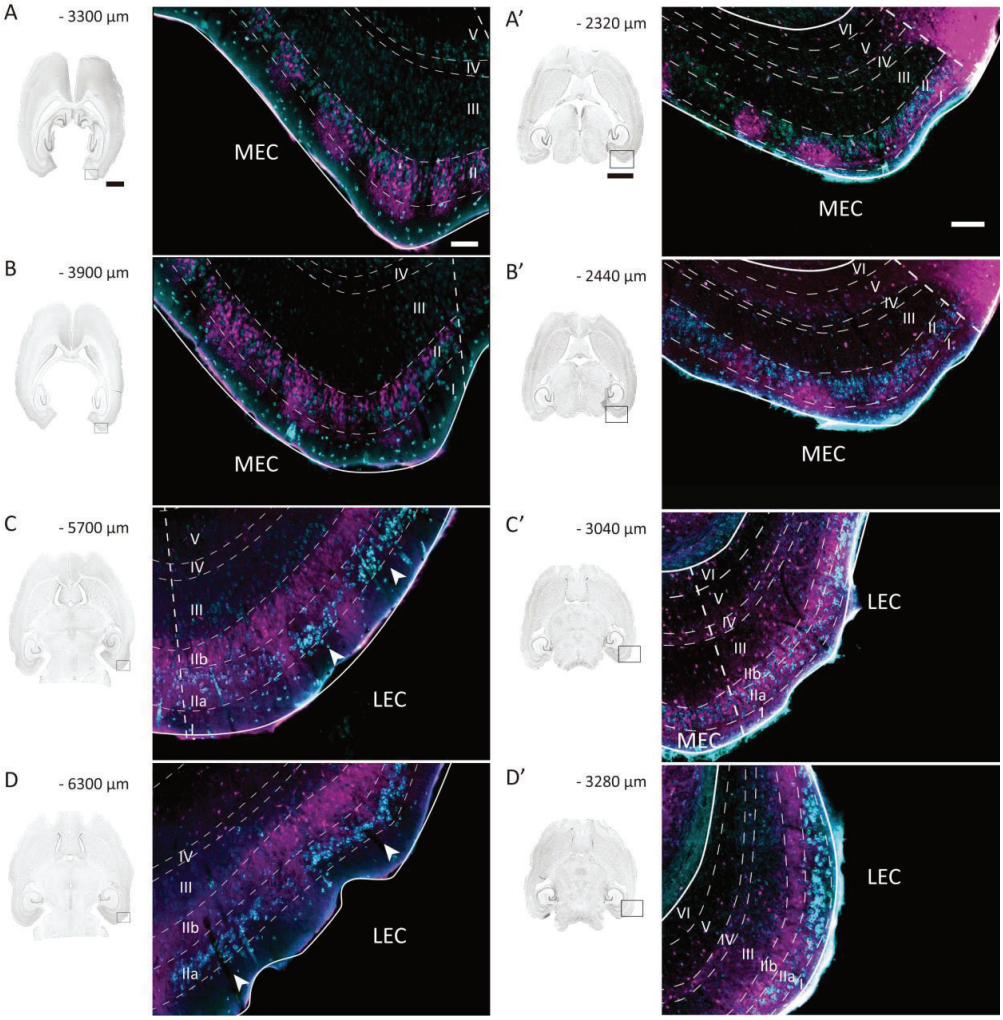

Supplementary Figure 2. Distribution of neurons immunoreactive for RE (cyan) and CB (magenta) in rat (A–D) and mouse (A'–D') EC at four different levels from dorsal to ventral. Left panel represents Nissl stained sections; right panel shows magnifications of parts of immunostained images corresponding with the boxed areas in the Nissl stained sections. Arrows in C–D: patches of reelin-positive neurons separated by bundles of dendrites arising from CB-positive neurons. Scale bars A and A' (apply to all sections in the same column): black scale bar equals 2000 µm; white scale bar equals 100 µm.

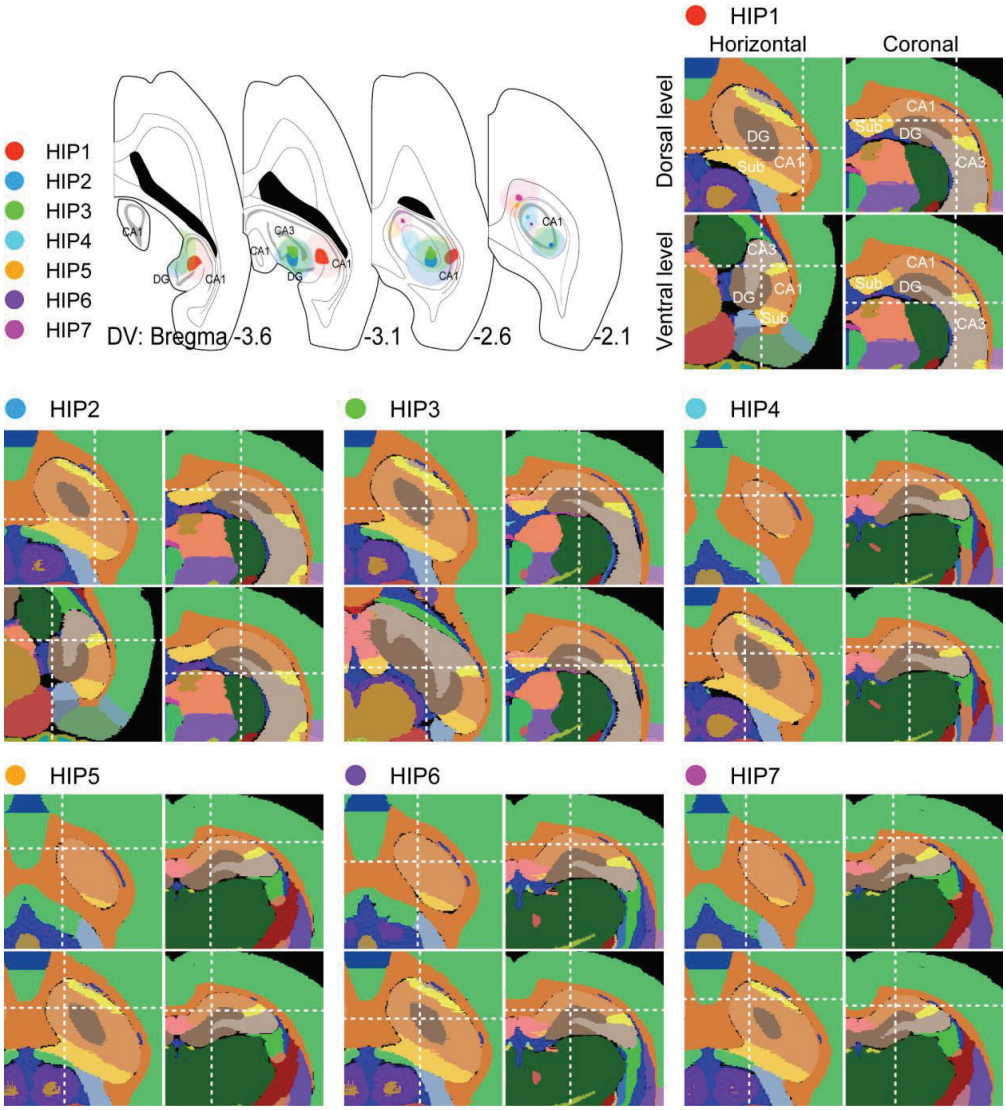

Supplementary Figure 3. The injection sites in the hippocampus were reconstructed in coronal sections using the Waxholm space based three-plane architectonic atlas of the rat hippocampal region (Boccara et al., 2015; Kjonigsen et al., 2015). Intersection of dotted lines represents the position of the injection site. Location of the injection sites are shown at the dorsal (top panel) and the ventral level (bottom panel) for each case. Left panels show the injection position in horizontal sections, whereas right panels show the corresponding location of the injection site in coronal sections.

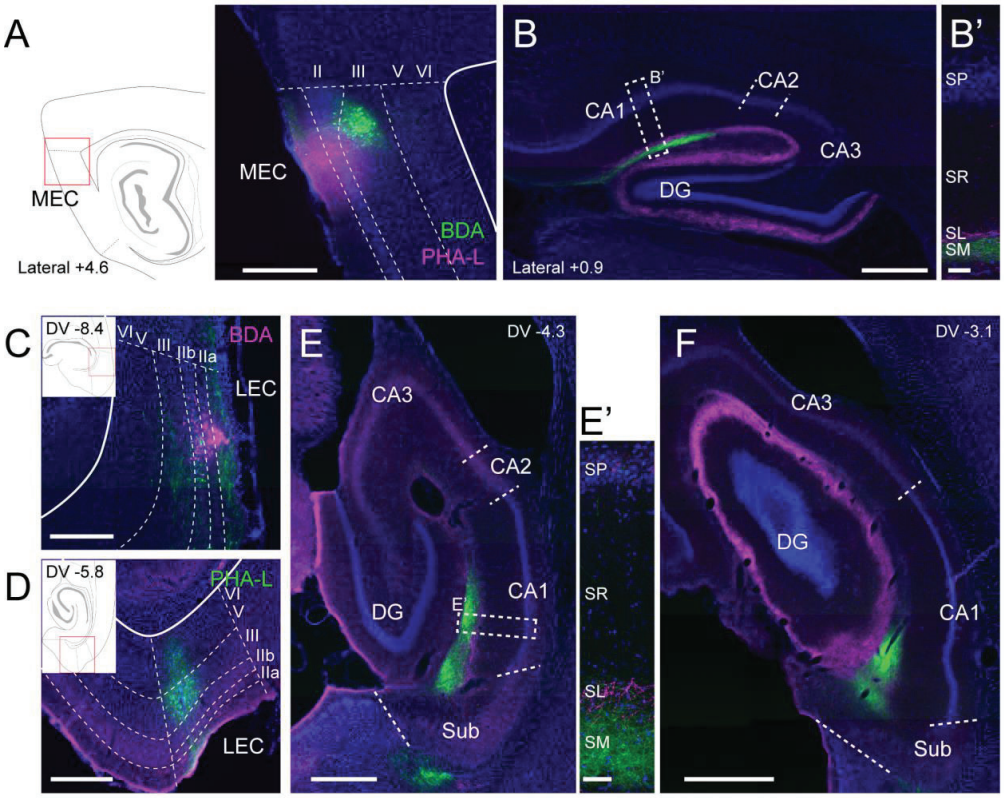

Supplementary Figure 4. Anterograde tracing from EC superficial layers to the hippocampus. (A, B) Line drawing of a sagittal sections indicating the position of the image showing the injection sites of the two anterograde tracers, PHA-L and BDA, in MEC layer II and III respectively (A). The distribution of labeled fibers (PHA-L: magenta , BDA: green) as seen in the hippocampus (B) in a sagittal section. (B') High power image of the boxed area indicated in B, showing the differential projections of layer III neurons to stratum moleculare (SM) and from layer II neurons to stratum lacunosum (SL). (C–F) Injection sites of BDA and PHA-L into LEC layer II and III respectively (inset shows a schematic line drawing of part of a horizontal section, indicating the position of the image; C, D) The distribution of labeled fibers (BDA: magenta, PHA-L: green) as seen in the hippocampus (E, F) in horizontal sections. (E') High power image of the boxed area indicated in E, showing the differential projections of layer III neurons to SM and from layer II neurons to SL. Scale bars are 1000 μm for (E) and (F), 500 μm for (A), (B), (C), and (D), and 50 μm for (B') and (E'). Abbreviations: SP, stratum pyramidale; SR, stratum radiatum.

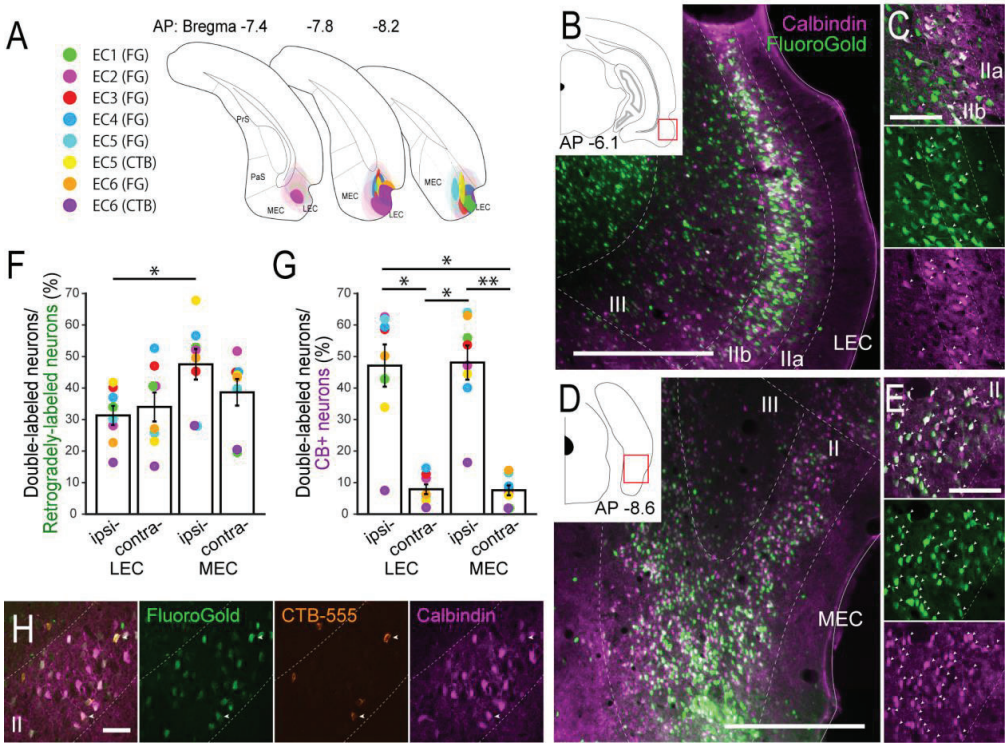

Supplementary Figure 5. Projection of CB+ neurons in LEC and MEC to the ipsi- and contralateral EC. (A) The injection sites of retrograde tracer injections in EC (n = 8 in 6 animals) are illustrated with a different color in three coronal sections taken at different anteroposterior (AP) levels from bregma. The dark color shows the injection site and the light color shows the area of tracer diffusion. CTB-555 was injected in the contralateral EC in case "EC5" and "EC6", but the injection sites are illustrated in the same hemisphere for simplicity. (B–E) Distribution of retrogradely labeled neurons in ipsilateral LEC at an AP level of -6.1 mm (B), and in ipsilateral MEC at an AP level of -8.6 mm (D) in coronal sections (case: EC2). High magnification images of the superficial layers in LEC and MEC are shown in (C) and (E) respectively. White arrows indicate neurons that were double-labeled with FG and CB immunoreactivity. (F, G) The percentage of double-labeled neurons among the retrogradely-labeled neurons (F), and the percentage of double-labeled neurons among the CB+ neurons (G) are compared between LEC and MEC in the ipsilateral and contralateral side of the injection (mean ± standard errors, N = 8; *p < 0.05, **p < 0.01, Friedman test followed with Dunn's multiple comparison post test). Each colored dot corresponds to the value for the sample shown in (A). (H) High magnification images of MEC in case "EC5", which received a FG injection in the ipsilateral EC and a CTB-555 injection into the contralateral EC. White arrows indicate neurons that were triple-labeled with FG, CTB-555, and CB immunoreactivity. Scale bars are 500 μm for (B) and (D), and 100 μm for (C), (E), and (H).

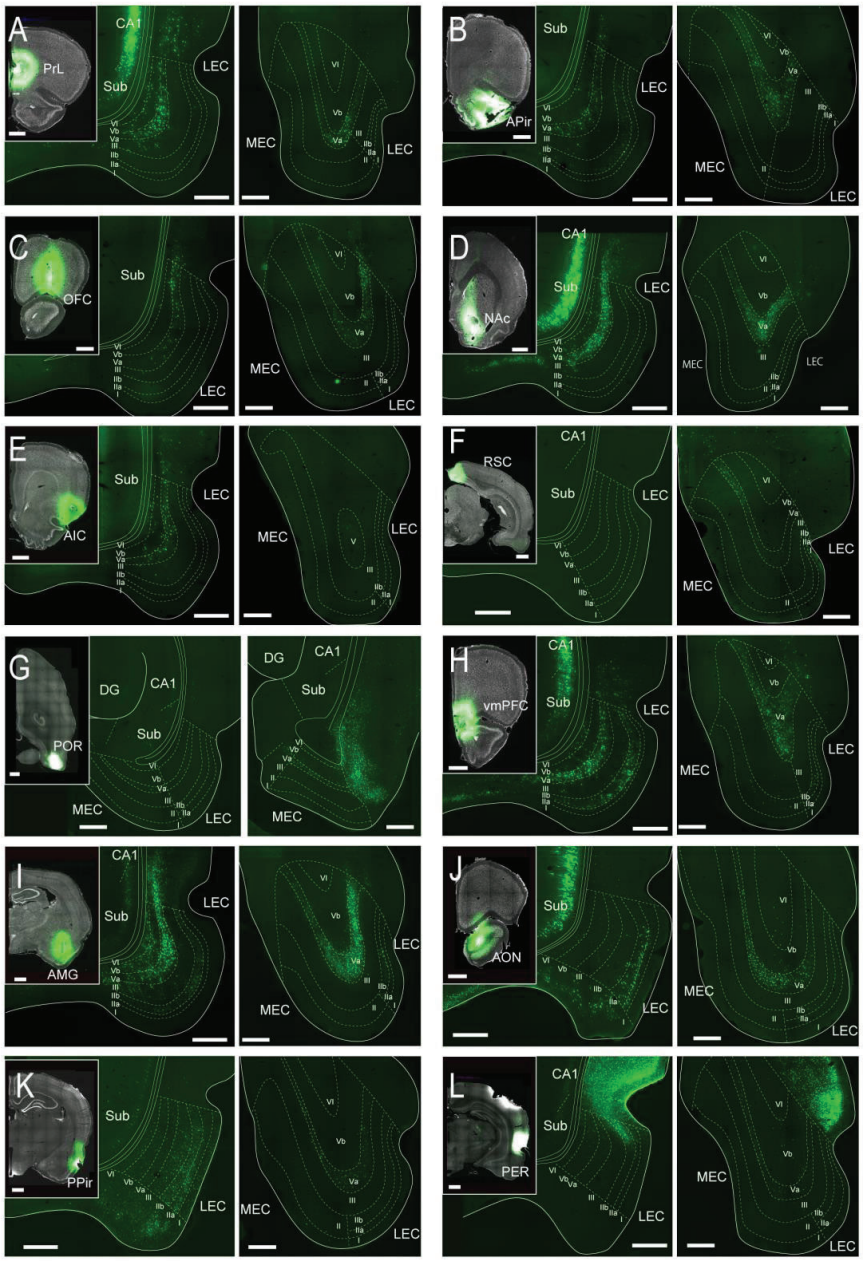

Supplementary Figure 6. Distribution of retrogradely labeled neurons in LEC and MEC after FG injection into telencephalic structures. The injection site is shown in the inset, and the distribution of retrogradely labeled neurons in the LEC and MEC are shown in the left and right panel, respectively, for each injection case. The images are from coronal sections except for (G), which shows horizontal sections. Scale bars are 1000 μm in the injection site (inset), and 500 μm in LEC and MEC images (left and right panel).

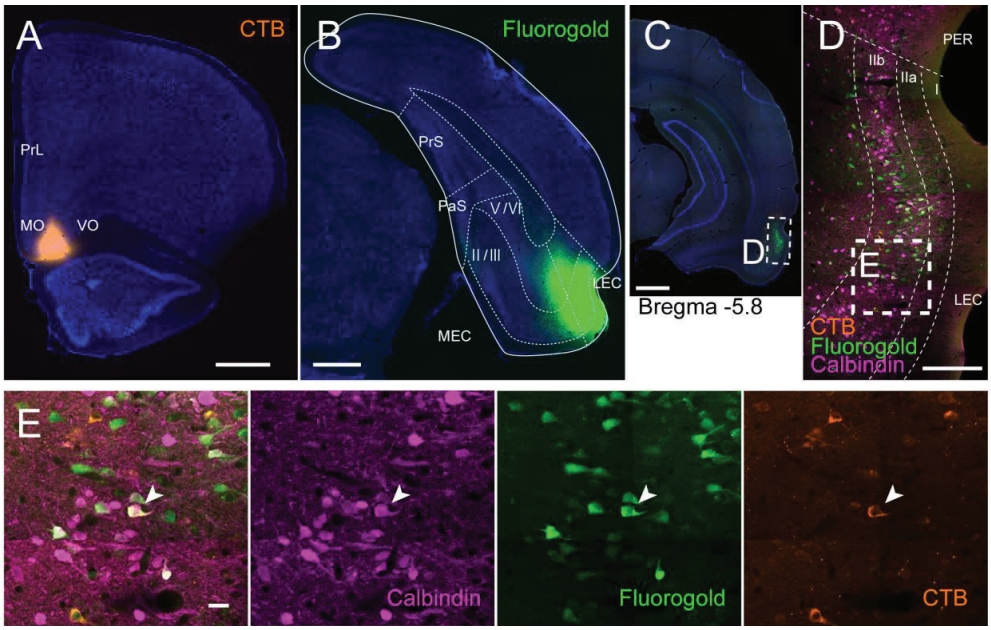

Supplementary Figure 7. Double labelling of retrogradely labelled neurons in LEC following an injection of CTB-555 in the ventral mPFC and FG in EC (A–B, case: EC1). (C–D) Distribution of retrogradely labeled neurons in ipsilateral LEC at an anteroposterior (AP) level of -5.8 mm in coronal sections. Boxed area in C is shown in D. (E) High magnification confocal images of the boxed area of LEC in (D). White arrows indicate neurons that were triple-labeled with FG, CTB-555, and CB immunoreactivity. Scale bars are 1000 μm for (A–C), 200 μm for (D), and 20 μm for (E).

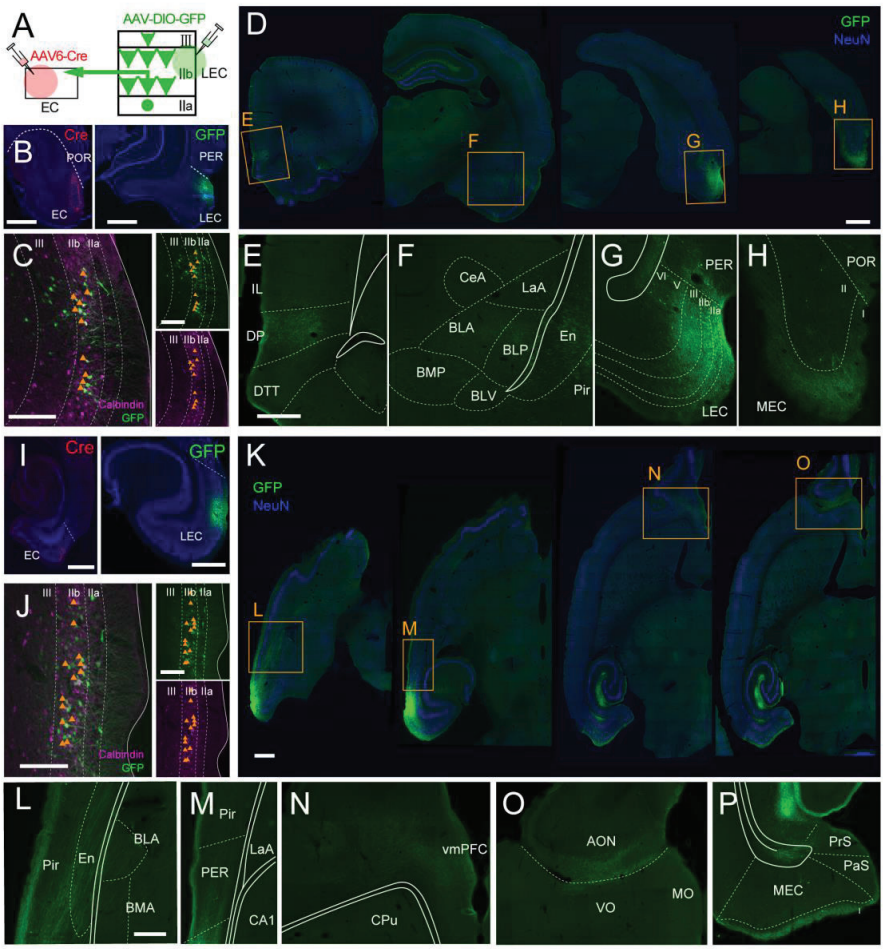

Supplementary Figure 8. Axon distribution of the local-projecting entorhinal neurons in the superficial layers. (A) Schematic diagram of the double infection approach to visualize local projecting LEC neurons in the superficial layers. (B, I) AAV6-Cre was injected in the border of LEC and MEC and AAV1/2-EF1α-DIO-EYFP was injected in LEC. The distributions of labeled fibers were examined either in coronal sections (D–H) or in horizontal sections (K–P). (C, J) High magnification image of the injection site of AAV1/2-EF1α-DIO-EYFP in LEC. Yellow arrows indicate double-labeled neurons with GFP (green) and CB (magenta). (D–H, K–O) Distribution of labeled fibers in low magnification images (D, K), and in high magnification images of boxed area in D (E–H) and in K (L–O). (P) High magnification image of MEC taken from a section ventral to the ones shown in K. Scale bars are 1000 μm for (B), (D), (I) and (K), 500 μm for (E) and (L), and 200 μm for (C) and (J). Abbreviations: BLA, basolateral amygdala; BLP, basolateral amygdala, posterior part; BLV, basolateral amygdala, ventral part; BMA, basomedial amygdala; BMP, basomedial amygdala, posterior part; CeA, central amygdala; CPu, caudate putatum; DP, dorsal peduncular cortex; DTT, dorsal tenia tecta; En, endopiriform nucleus; LaA, lateral amygdala; MO, medial orbital cortex; PaS, parasubiculum; PER, perirhinal cortex; POR, postrhinal cortex; PrS, presubiculum; VO, ventral orbital cortex.

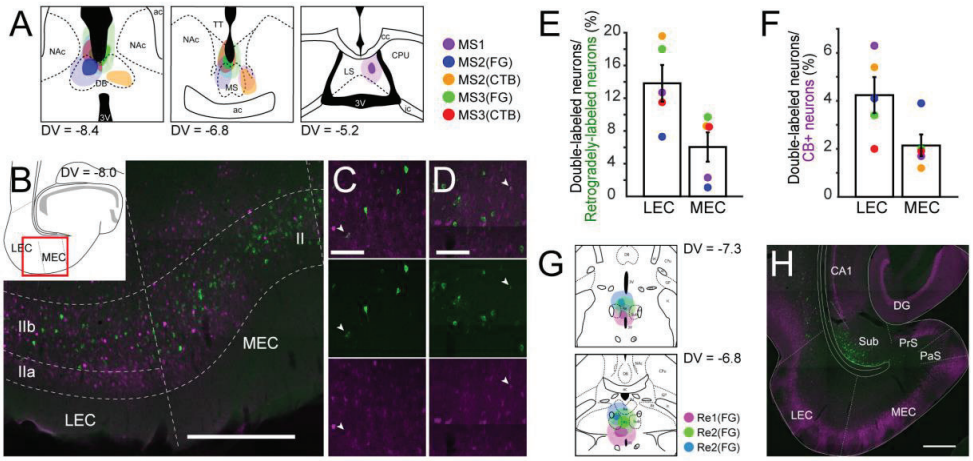

Supplementary Figure 9. Retrogradely-labeling in EC after retrograde tracer injection into septal complex (A–F) and thalamic nucleus reuniens (G–H). (A) The injection sites of retrograde tracers in samples with septal injection are shown in horizontal sections at three different dorsoventral level. Each injection is illustrated with a different color. The dark color shows the injection site and the light color shows the area of tracer diffusion. (B–D) Distribution of retrogradely labeled neurons (green) in ventral EC in horizontal section (case: MS2 (CTB)). High magnification images of the superficial layers in LEC and MEC are shown in (C) and (D) respectively. White arrows indicate neurons that were double-labeled with CTB-555 and CB immunoreactivity. (E, F) The percentage of double-labeled neurons among retrogradely-labeled neurons (E), and the percentage of double-labeled neurons among the CB+ neurons (F) are compared between LEC and MEC (mean ± standard errors, N = 5). (G) The injection sites of FG in samples with reuniens injection are shown in two horizontal sections at two different dorsoventral level. (H) Distribution of FG-labeled neurons in a horizontal section (case: Re1). Scale bars are 500 μm for (B) and (H), and 100 μm for (C) and (D).

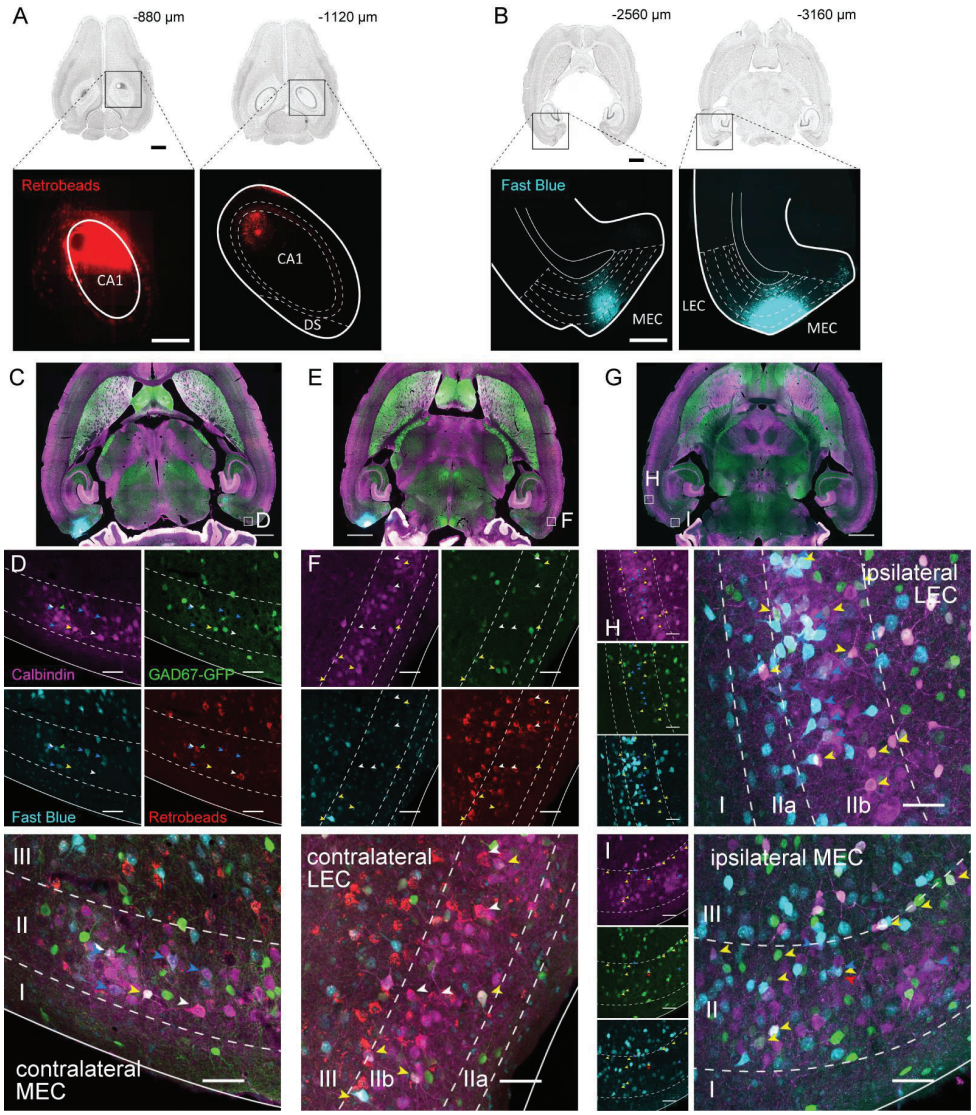

Supplementary Figure 10. Representative example of retrograde tracing in a GAD67 transgenic mouse expressing GFP, following injection of red retrobeads in dorsal CA1 (A), and Fast Blue in contralateral MEC (B). Colocalization between labeling for calbindin (magenta), GAD67-GFP (green), Fast Blue (cyan), and retrobeads (red) in MEC (C, D) and LEC (E, F) contralateral to Fast Blue injection, and LEC (G, H) and MEC (I) ipsilateral to fast blue injection. Retrogradely labeled CB+ positive neurons are common in LEC and MEC, both on the ipsilateral and contralateral side of the MEC injection. We rarely observed CB+/GAD+ retrogradely-labeled neurons and these were only present in MEC ipsilateral to the MEC injection (I). Blue arrows: Fast Blue labeled CB+ neurons. White arrows: retrobeads labeled CB+ neurons. Yellow arrows: GAD67-GFP expressing CB+ neurons. Green arrow: triple-labeled with Fast Blue, retrobeads, and CB (D). Red arrow: triple labeled with Fast Blue, GAD67-GFP, and CB (I). Scale bars are 1000 µm for (A–B black scale bars) and (C), (E), and (G), 500 µm for (A–B white bars), and 50 µm for (D, F, H, I).

Sample name	Species	sex	weight (g)	Injection location	Coordinates					Tracer	Volume (nl)	Cutting plane	Thickness (μm)	Reference in manuscript	Animal number
					APb	Apt	ML	DV	Angle						
HIP1	W	M	200-230	CA1, CA3	-5.1		3.4	-2.3/-2.8		FG	200	H	60	Fig.1B-H, Sfig.3	j2039
HIP2	W	M	200-230	CA1, DG	-5.1		3.4	-2.4/-2.9		FG	200	H	60	Fig.1B,G,H, Sfig.3	j2040
HIP3	W	M	200-230	CA1, DG	-3.7		4.3	3		FG	100	H	60	Fig.1B,G,H, Sfig.3	j1989
HIP4	SD	F	200-230	CA1, DG	-3.6		2	-2.4		FB	150	H	40	Fig.1B,G,H, Sfig.3	20218
HIP5	SD	F	200-230	CA1	-3.6		2	-2.1		FB	150	H	40	Fig.1B,G,H, Sfig.3	20187
HIP6	SD	F	200-230	CA1	-3.6		2	-2.1		FB	150	H	40	Fig.1B,G,H, Sfig.3	20188
HIP7	SD	F	200-230	CA1	-3.6		2	-2.1		FB	150	H	40	Fig.1B,G,H, Sfig.3	20350
MEC1	LE	F	213	MEC		0.9	5.1	3.3		FB	40	H	40	Fig. 2A-G	24448
MEC2	LE	F	237	MEC		0.9	5.3	3.3		FB	40	H	40	Fig. 2A-G	24447
MEC3	LE	M	281	MEC		0.9	5.3	3.3		FB	40	H	40	Fig. 2A-G	24461
LEC1	LE	M	242	LEC, (PER)	-6.0		7.0	4.8		FG	50	H	40	Fig. 2H-N	24360
LEC2	LE	F	250	LEC, (PER)	-6.0		7.0	4.8		FG	50	H	40	Fig. 2H-N	24362
LEC3	LE	F	233	LEC, (PER)	-6.0		7.05	4.8		FG	75	H	40	Fig. 2H-N	24139
EC1	W	M	200-230	EC	-8.3		6.0	-4.0		FG	100	C	60	Sfig. 5A, F, G, Sfig. 7	j1994
				vmPFC	3.5		0.6	-4.2		CTB	60				
EC2	W	M	200-230	EC	-8.3		6.0	-4.0		FG	100	C	60	Sfig. 5A-G	j1995
EC3	W	M	200-230	EC	-8.3		6.0	-3.8		FG	100	C	60	Sfig. 5A, F, G	j1944
EC4	W	M	200-230	EC	-8.3		6.0	-4.0		FG	100	C	60	Sfig. 5A, F, G	j1993
EC5	W	M	200-230	left EC	-8.3		6.0	-4.0		FG	100	H	40	Sfig. 5A, F-H	j2547
				right EC	-8.3		6.0	-4.0		CTB	100				
EC6	W	M	200-230	left EC	-8.3		6.0	-4.0		FG	200	H	40	Sfig. 5A, F, G	j2548
				right EC	-8.3		6.0	-4.0		CTB	250				
OFC1	W	M	200-230	ventral OFC	3.7		2.2	-2.7		FG	180	C	60	Sfig. 6C	j1748
OFC2	W	M	200-230	ventral OFC	3.7		2.2	-3.7		FG	100	C	60		j1749
OFC3	W	M	200-230	ventral OFC	3.7		2.2	-3.2		FG	100	C	60		j1821
aPir1	W	M	200-230	anterior Pir	3.7		2.2	-5.5		FG	150	C	60	Sfig. 6B	j1822
aPir2	W	M	200-230	anterior Pir	3.7		2.3	-5.5		FG		C	60		j2464
dmPFC1	W	M	200-230	PrL	3.5		0.6	-2.6		FG	100	C	60	Sfig. 6A Ohara et al., 2018	j1817
dmPFC2	W	M	200-230	PrL	3.5		0.6	-2.6		FG	100	C	60		j1818
AIC1	W	M	200-230	AIC	3.0		4.4	-4.2		FG	100	C	60		j1750
AIC2	W	M	200-230	AIC	3.0		4.4	-4.2		FG	80	C	60	Sfig. 6E	j1751
NAc1	W	M	200-230	NAc	2.5		1.6	-6.1		FG	120	C	60	Ohara et al., 2018	j1833
NAc2	W	M	200-230	NAc	2.5		1.6	-6.1		FG	100	C	60	Sfig. 6D	j1834
RSC1	W	M	200-230	RSC	-7.0		0.9	1.2		FG	50	C	60		j2334
RSC2	W	M	200-230	RSC	-7.0		0.9	1.2		FG	60	C	60	Sfig. 6F Ohara et al., 2018	j2335
RSC3	W	M	200-230	RSC	-7.7		0.8	1.5		FG	100	S	60		j2465
POR1	SD	F	270g	left POR		0.5	4.4	1.4		FG	50	H	40	Sfig. 6G	24585
				right POR		0.5	4.4	1.4		CTB	500				
vmPFC1	W	M	200-230	IL, DP, MO	3.5		0.6	4.2		FG	100	C	60	Fig. 3D	j1773
vmPFC2	W	M	200-230	IL, DP, MO	3.5		0.6	4.2		FG	125	C	60	Fig. 3D-F, Sfig. 6H	j1795
AMG1	W	M	200-230	AMG	-2.3		5.1	7.0		FG	100	C	60	Fig. 3A-C, Sfig. 6I Ohara et al., 2018	j1736
AMG2	W	M	200-230	AMG	-2.3		5.1	7.0		FG	100	C	60	Fig. 3A	j1737
AON1	SD	F	250	AON	5.5		1.2	-4.2		FG	150	C	40	Fig. 3J	25042
AON2	SD	F	280	AON	5.5		1.2	-4.2		FG	100	C	40	Fig. 3J-L, Sfig. 6J	25043
pPir1	SD	F	240	posterior Pir	-2.7		6.0	-6.7		FG	80	C	40	Fig. 3G	25040
pPir2	SD	F	240	posterior Pir	-2.7		6.1	-6.7		FG	100	C	40	Fig. 3G-I, Sfig. 6K	25041
PER1	SD	F	300	PER	-5.0		6.8	-4.5		FG	100	H	40	Fig. 3M	24801
PER2	SD	F	260	PER	-5.0		6.8	-4.5		FG	100	H	40	Fig. 3M-O, Sfig. 6L	25044
MS1	W	M	200-230	LS	0.5		0.6	-5.0		FG	120	H	40	Sfig. 9A, E-F	j2471
MS2	W	M	200-230	right MS/DB	0.5		0.6	-4.2/-4.0		FG	250	H	40	Sfig. 9A-F	j2549
	W			left MS/DB	-0.1		0.6	-4.0/-3.8		CTB	300				
MS3	W	M	200-230	left MS/DB	-0.1		0.6	-4.0/-3.8		FG	250	H	40	Sfig. 9A, E-F	j2550
	W			right MS/DB	0.5		0.6	-4.2/-4.0		CTB	200				
Re1	SD	F	250	Re	-2.5		2.8	7.3	22	FG	200	H	40	Sfig. 9G, H	24128
Re2	SD	F	240	Re	-2.2		2.8	7.3	22	FG	125	H	40	Sfig. 9G	24420
Re3	SD	F	230	Re	-2.3		2.8	7.3	22	FG	125	H	40	Sfig. 9G	24424

Supplementary Table 1. Injection parameters of retrograde tracing experiments. Either the Fluorogold (FG), Fast Blue (FB), or Alexa Fluor 555 conjugated Cholera Toxin Subunit B (CTB) was used. In the Coordinates column, APb stands for anterior to bregma, APt for anterior to transverse sinus, ML for lateral to sagittal sinus, and DV for ventral to dura. These coordinates are shown in mm. Angle shows the degree angle of the injection micropipette in the coronal plane with the tip pointing to the midline. Long Evans (LE), Sprague Dawley (SD), Wistar (W). Male (M) and Female (F). Horizontal plane (H), Coronal plane (C), Sagittal plane (S).